Alma Mater Studiorum – Università di Bologna

DOTTORATO DI RICERCA IN

SCIENZE DELLA TERRA, DELLA VITA E DELL'AMBIENTE

Ciclo 36

Settore concorsuale: 04/02 - GEOLOGIA STRUTTURALE, GEOLOGIA STRATIGRAFICA, SEDIMENTOLOGIA E PALEONTOLOGIA

Settore scientifico disciplinare: GEO/03 – GEOLOGIA STRUTTURALE

TECTONICS OF THE WEDGE-TOP EPILIGURIAN BASINS AND IMPLICATIONS FOR THE SYN-TO-POST OROGENIC EVOLUTION OF THE NORTHERN APENNINES FOLD-AND-THRUST BELT (ITALY)

Presentata da: Francesca Stendardi

Coordinatore dottorato

Prof.ssa Maria Giovanna Belcastro

Supervisore

Prof. Gianluca Vignaroli

Co-supervisore

Prof. Giulio Viola

Esame finale anno 2024

Acknowledgements

Giunta alla fine di questi tre anni non posso che spendere qualche parola per ringraziare tutte le persone che mi hanno accompagnato in questo percorso, tortuoso sì, ma allo stesso tempo bellissimo e ricco di soddisfazioni. Non posso che cominciare dalle persone che hanno reso possibile per me intraprendere questo percorso di dottorato, il Prof. Gianluca Vignaroli e il Prof. Giulio Viola. Grazie per avermi guidato lungo questi tre anni, per avermi insegnato a non arrendermi davanti alle difficoltà e per avermi aiutato a combattere la mia timidezza e ad essere più sicura di me. Grazie per tutte le critiche e le correzioni, a volte dure da accettare, ma necessarie per il raggiungimento di questo risultato, e grazie anche per tutti i momenti più spensierati e divertenti che siamo riusciti a condividere. Farò tesoro dei vostri insegnamenti.

Ringrazio Barbara e Gilby, che hanno reso il mio periodo all'estero più "leggero" e che mi hanno fatto scoprire altri lati belli della geologia. Da voi ho imparato davvero moltissimo e chissà, magari lavoreremo ancora insieme in futuro.

Grazie ad Irene, per essere stata il tecnico di laboratorio migliore del mondo, un'amica con cui confidarmi e una spalla preziosa a cui appoggiarmi nei momenti di sconforto. Grazie per l'immensa pazienza, per le risate e per non avermi mai fatto perdere d'animo quando pensavo che fosse tutto da rifare.

Ringrazio i “grandi” del dipartimento: Thomas, Riccardo e Francesco. Voi siete stati per me l’esempio da seguire, le persone da cui apprendere la dedizione, la tenacia e la pazienza che servono per fare questo lavoro. Siete stati sempre pronti a darmi consigli preziosi e a trasmettermi il meglio della vostra esperienza.

Grazie a tutti gli amici del terzo piano che ho avuto la fortuna di incontrare: Sabrina, Alessandro, Tommaso, Nicola, Matt, Rodolfo, Elena, Giacomo.. siete davvero tantissimi. Mi mancheranno i pranzi in balena, le partite a freccette post-pranzo, le serate insieme e le risate. Grazie per avermi sostenuta sempre e per aver ascoltato con pazienza tutti i miei sfoghi. Spero davvero di poter condividere ancora con voi esperienze bellissime e che questo sia solo l’inizio di una lunga amicizia.

Ringrazio la mia famiglia, mamma, papà e mia sorella Martina, senza i quali nulla di tutto questo sarebbe stato possibile. Grazie per tutto l’appoggio che mi avete dato, anche restando in silenzio, vostro malgrado, e per i sacrifici che avete fatto affinché potessi intraprendere la mia strada, senza farmi mai mancare niente. Siete i miei pilastri e le mie rocce. Grazie per essere la famiglia migliore che potessi desiderare.

In ultimo, ma non per importanza, devo ringraziare la persona che mi ha accompagnata dall’inizio della mia passione per la geologia; il mio sostegno e compagno di vita. Grazie a te, Costantino, per avermi reso fortunata nel condividere con te anche questo pezzo di strada.

Abstract

The PhD project at the core of this thesis aimed at the characterisation of the Epiligurian wedge-top basins, which are exposed in stratigraphic depressions along the axial domain of the Northern Apennines fold-and-thrust belt (Italy). The thesis presents the results of an integrated, multiscalar and multitechnique approach that relied on field and laboratory data to analyse the structural, architectural and thermal features that governed the deformation of the wedge-top basins through time and space during the evolutionary tectonics of the belt.

Wedge-top basins are essential for understanding the deformation history of an orogen, as their strategic structural position allows them to record the tectonic and sedimentary response to the complex dynamics of the governing tectonic regime.

To this end, I focused on the study of a representative example of wedge-top basin (the Marzabotto Basin), located immediately to the south of Bologna. I chose this basin because of its continuous exposure of the Epiligurian sedimentary succession and its easily recognisable contacts with the underlying Ligurian units and overlying Pliocene units

Firstly, the study started with the remote sensing analysis of lineaments aiming at the investigation of the dominant trends of the morphostructures which affect the Epiligurian units in the study area to obtain regional-scale information on the general

faulting pattern, as well as the stress conditions in the upper structural levels of the belt. The same lineaments have been also compared in term of strike distribution and kinematics to previously detected morphostructures in the other wedge-top basins, available in different databases on the Emilia-Romagna Region Geoportal. Then, I conducted fieldwork to characterise the main tectonic features of the study area at different scales. This included geological mapping and mesoscopic analysis of faults, with the aim to define their orientation, kinematics, mutual cross-cutting, and their genetic relationships with the deformed sedimentary succession.

A thermal study of the Epiligurian units has been done, with the goal to produce new thermochronometric data to better constrain the local exhumation history and correlate it with the large-scale tectonic evolution of the Northern Apennines. For this purpose, I applied low-temperature thermochronology (apatite fission-tracks and (U-Th)/He) analyses of detrital minerals and thermal modelling on the middle-upper Eocene siliciclastic deposits of the Marzabotto Basin.

Finally, I constrained the timing and kinematics of post-orogenic tectonic structures affecting the Epiligurian units by performing U-Th dating analysis on syn-kinematic mineralizations (calcite veins and slickenlines) decorating selected representative normal faults. The study aimed at the investigation of the propagating extensional deformation waves which affected the hinterland of the Northern Apennines fold-and-thrust belt as consequence of the opening the Tyrrhenian back-arc basin, to see if it is also recorded in the axial zone of the belt by the Epiligurian wedge-top basins.

The approach I used has shed new light on the tectonic evolution of the Epiligurian wedge-top basins and allowed me to refine conceptual models that account for the syn- to post-orogenic history of the Northern Apennines belt from the Oligocene onwards.

In general, the structural dataset obtained documents that the Marzabotto Basin was affected by: i) two sets of thrusts indicating a NE-SW and NW-SE shortening of the sedimentary succession; ii) NE-SW-left lateral transtensional faults related to a strike-slip tectonic phase which led the lateral juxtaposition of Ligurian units and Epiligurian units; iii) three main sets of extensional structures which are rather pervasive in the entire study area and formed in response to different deformation mechanism, which cut and displace the previous thrusts. The extensional structures are mainly related to the post-orogenic evolution of the belt. Specifically, I documented the occurrence of NNE-SSW-striking extensional tectonic structures that developed in response to the reactivation early syn-orogenic strike-slip faults. New U-Th ages from syn-kinematic mineralisation constrained the normal faulting activity to the Middle-Late Pleistocene.

The Marzabotto Basin experienced a complex burial-exhumation history during the syn-orogenic evolution of the Northern Apennines. Apatite fission-tracks analysis reveals that the Epiligurian sedimentary succession it characterised by different detrital populations, between ~71 and ~57.9 Ma, which have been interpreted as representative of Western Alps derived source rock cooling ages**.** The He ages show a more variable single grain age distribution ranging from 104 to 7 Ma indicating a significant degree of thermal resetting after the deposition. Based on these data, the inverse thermal modelling

performed on the ages obtained show that the study areas reached a maximum temperature of ca. 90°C and an Oligocene to Pliocene cooling consistent with deformation of the Northern Apennine.

In conclusion, it is possible to affirm that the study conducted during the present PhD project and exposed in this thesis was useful to add new constrains about the structural and thermal framework of the Epiligurian wedge-top basins. This study and its multiscale-multitechnique approach would shed new light on our knowledge of the poorly constrained, shallowest structural parts of fold-and-thrust belts.

Contents

Chapter 1

Introduction

1.1 Rationale of the study

1.1.1 Wedge-top basins within the dynamics of a foreland basin system

Wedge-top basins represent common features in fold-and-thrust belts worldwide and they are defined as sedimentary basins set on top of the tectonic units that build a fold-and-thrust belt (Beaumont, 1981; DeCelles and Giles, 1996). The formation of this kind of basin is related to the deformation of the original foredeep basin due to the migration of the thrust front of the belt (**Fig. 1.1**) (Ori and Friend, 1984; Allen et al., 1986; Ricci Lucchi, 1986; Allen and Allen, 1990; Mutti et al., 2003). Unlike other depozone types, wedge-top basins are in general characterized by a prismatic shape that tapers (in cross section) both inward and outward with respect to the belt overall vergence.

In the past, previous works distinguished the terms aimed to the definition of a wedge-top basin. In particular, they defined as "satellite" (Ricci Lucchi, 1986) or "piggy-back basins" (Ori and Friend, 1984) thrust based basins bounded by imbricated active thrusts associated with a main foredeep; "thrust-top basin" (Ricci Lucchi, 1990) as meso-allochthonous derived sediments basin filled formed in absence of a well-defined major foredeep.

Wedge-top basins can form up to 30-70% of volume of sedimentary budget of a foreland basin system; they develop in response to active crustal deformation and, as such, are readily prone to recording the dynamics of contractional systems (e.g., Ford, 2004). They represent the tectonic and sedimentary response to the complex dynamics induced by

the tectonic regime governing the evolution of the fold-and-thrust belt on which they are located (Ori and Friends, 1984).

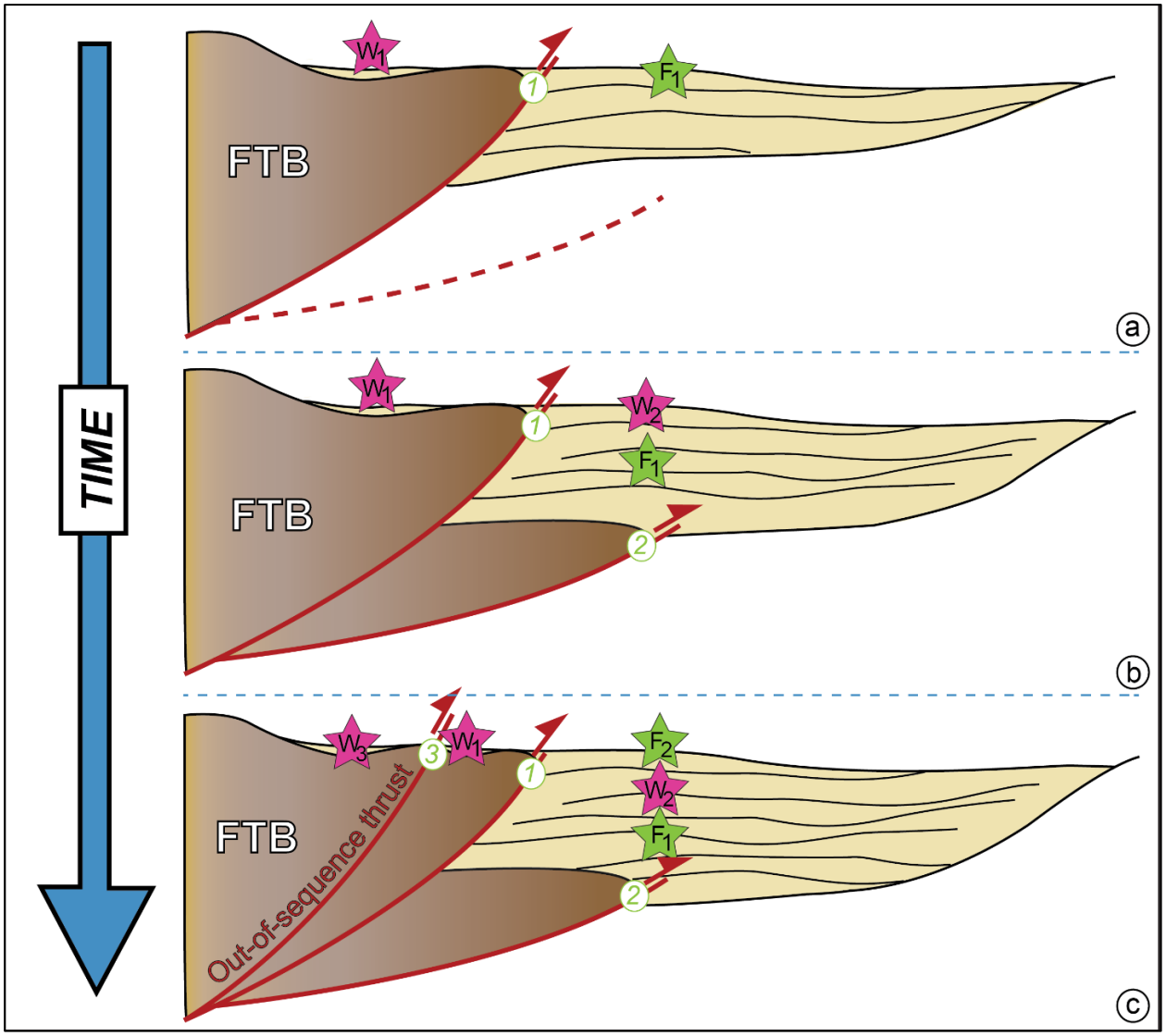

Figure 1.1- Schematic reconstruction showing the progressive deposition and burial of sediments in a foreland basin system. The numbers on each thrust surfaces represent the order of thrust development and propagation towards the foreland according to either an in- or out-of-sequence propagation style. Stars represent sediments according to their belonging to either wedge-top (dark pink) or foredeep (green) basins (Modified and redrawn after DeCelles and Giles, 1996).

Aiming at the correlation between the formation and development of a wedge-top basin over time and the propagation of the underlying fold-and-thrust belt, it is important to accept that, in the context of a foreland basin system, a depozone is better defined in terms of its position during the sedimentary cycle, rather than its location with respect to the thrust belt (De Celles and Giles, 1996).

Figure 1.1 illustrates how the deposition in wedge-top basins and foredeeps may occur in response to the propagation of the belt towards the undeformed foreland. In particular, a sedimentary succession is deposited in the foredeep under the effects of a number of processes that are indeed typical of foredeeps **(Fig. 1.1a)**. Although this succession is affected by the process of orogenic build-up by frontal imbrication, it will not become part of a wedge-top basin infill. Instead, it becomes part of an active orogen as remnant of a now fossil foredeep unless it is cannibalised and reincorporated into the active depositional regime **(Fig. 1.1b)**. A wedge-top deposit that was deposited into a foredeep remains part of it even if out-of-sequence thrusting transiently shifts the locus of active propagation of the fold-and-thrust belt again to the hinterland **(Fig. 1.1c)** (e.g., DeCelles and Giles, 1996; Ford, 2004).

Wedge-top basins can accommodate substantial volumes of sediments from emerged areas of the wedge. While they are being infilled, however, they may still be affected by multiple phases of intense tectonic deformation (Butler and Grasso, 1993; Butler et al., 1995) such that the interaction between syn-depositional structures and sedimentation over prolonged periods of time may lead to complex sedimentary thickness and facies

changes in the basins (e.g., Ford, 2004). In particular, sediment budget and accommodation is the net result of the competition between regional, load-driven subsidence and the local uplift of the fold-and-thrust belt (Ricci Lucchi, 1986; DeCelles and Giles, 1996; Covault and Graham, 2008), as also attested to by the occurrence of sedimentary bodies lateral interdigitations, thickness variations and erosional unconformities (e.g., Beaumont, 1981; Ori et al., 1986; Butler and Grasso, 1993; Posemantier and Allen, 1993; DeCelles, 1994; DeCelles and Giles, 1996; Cibin et al., 2001; Mutti et al., 2003; Ford, 2004; Artoni, 2007; Conti et al., 2008; DeCelles, 2012; Ogata et al., 2012).

Mutti et al. (2003) analysed wedge-top basins from a sedimentological perspective. They defined wedge-top basins as mixed depositional systems consisting of sand-rich deposits that share several features with basinal (foredeep) turbidites but differ from them because of a less mature facies development. Indeed, the depositional system occurring in wedge-top basins can be defined as an immature and little efficient turbidite-like system formed adjacent to feeder delta complexes.

The stratigraphic evolution of wedge-top basins over time appears to be sensitive to the dynamics of the underlying belt: whereas the older sedimentary successions mostly record the dynamics of the thrust sheets, the younger deposits tend to accumulate while the basins are relatively static while the thrust front is migrating foreland-ward (Ori and Friend, 1984). Several common stratigraphic and sedimentological features of wedge-top basins, such as unconformities (both local and regional), growth structures and the

general textural and compositional immaturity of their sedimentary infill, have been documented as sensitive gages of the overall belt dynamics (Beaumont, 1981; Ori and Friends, 1984; Ori et al., 1986; **Fig. 1.2**).

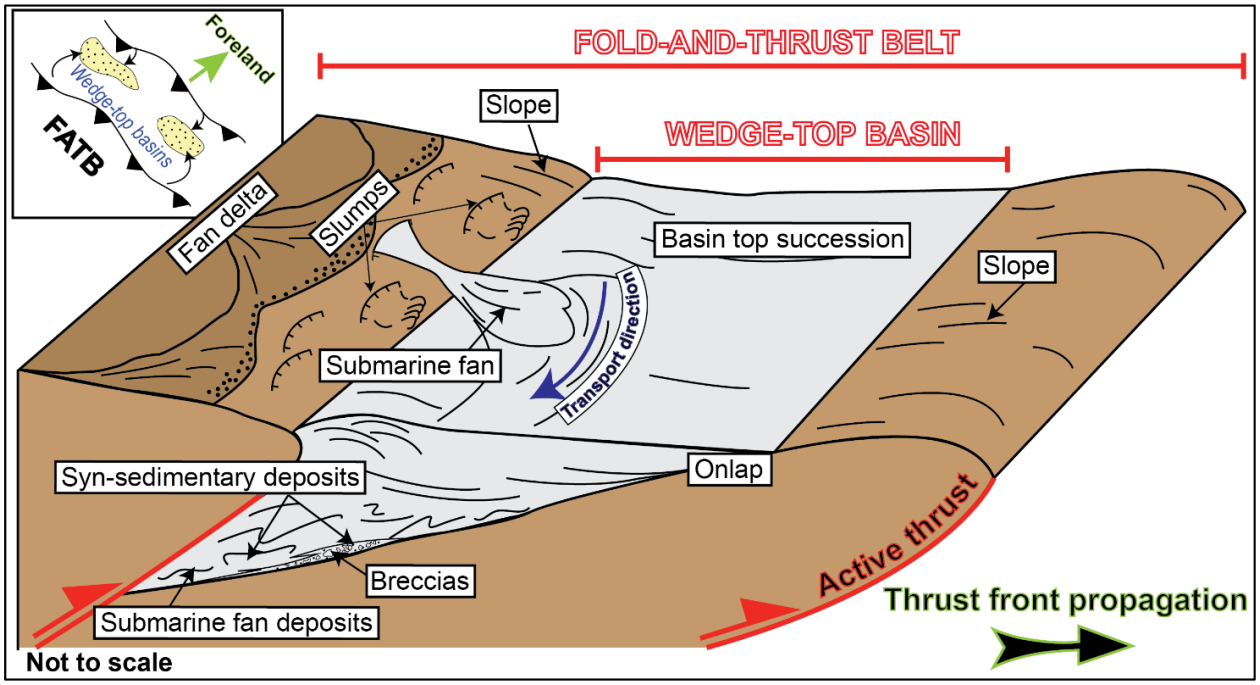

Figure 1.2 – Possible depositional environments associated with a wedge-top basin evolving in time and space in response to the evolution of an adjacent, actively shortening thrust sheet (modified and redrawn after Ori and Friend, 1984). FTB: fold-and-thrust belt

By considering the relationships between uplift and sedimentation in wedge-top basins, it is possible to define time intervals characterised by intense shortening of the belt and an increase of the basin subsidence rate, which allows for the deposition of coarse sediments adjacent to the zone of maximum tectonic loading. On the other hand, in more distal areas, fine-grained sediments are deposited together with the development of unconformities and bypassing erosion in the foredeep. In the case of less intense of shortening, however, erosion reduces the overburden and, consequently, the

accommodation space for sediment deposition in the proximal zones, thus allowing for the propagation of basal sediments towards the more distal and external zone of the basin (e.g., Ori and Friend, 1984; DeCelles, 1994; Mutti et al., 2003; Conti et al., 2008; Covault and Graham, 2008).

1.1.2 The wedge-top Epiligurian units of the Northern Apennines fold-and-thrust belt

This section provides a brief overview of the current state of knowledge on the Epiligurian wedge-top basins, the focus of this thesis. It also discusses the information acquired so far that designates these units as useful markers for understanding the tectonic evolution of the underlying Northern Apennines fold-and-thrust belt (Italy). The Epiligurian units serve as an emblematic example of wedge-top basins situated in the axial zone of the Northern Apennines fold-and-thrust belt and extending approximately 400 km along a NW-SE direction from the Ligurian Alps (NW) to the Romagna coastline (SE) **(Fig.1.3)**.

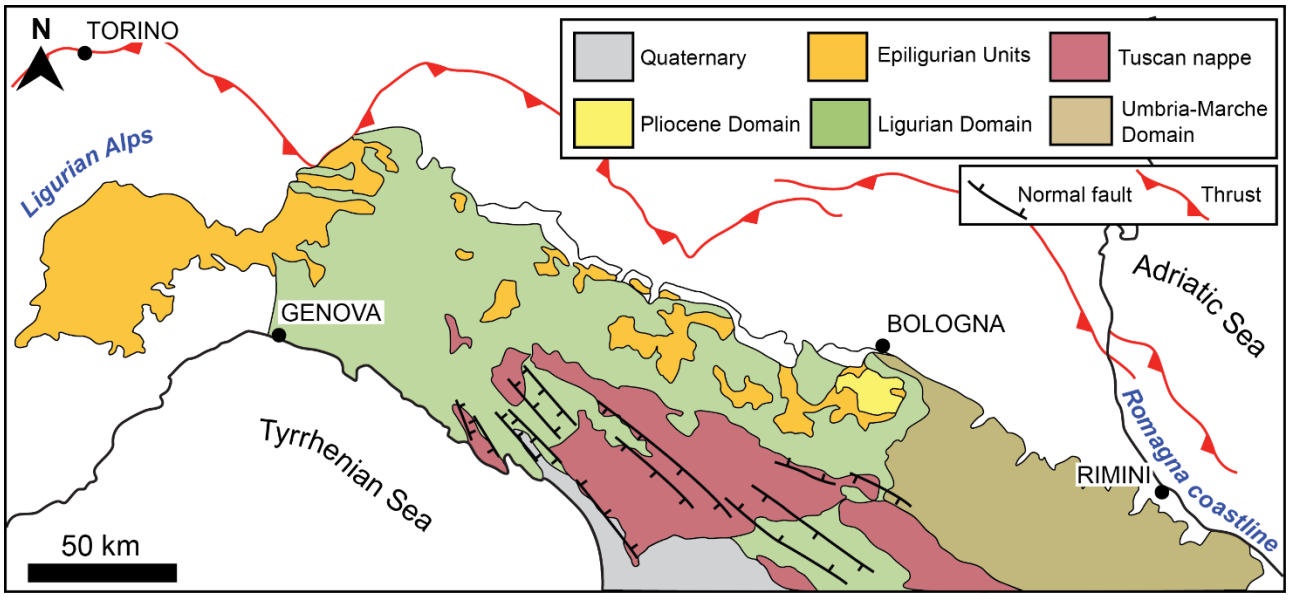

Figure 1.3- Simplified geological map of the Northern Apennines with the location of the different domains (modified and redrawn after Vai and Martini, 2001).

Previous studies have investigated the sedimentological and structural characteristics of the Epiligurian units. Sedimentological, petrographic and geochemical analyses have been carried out to explore the composition, spatial distribution and temporal relationships of these units aiming to better constrain paleogeographic reconstructions and provenance studies (e.g., Ricci Lucchi, 1986; Spadafora et al., 1998; Amorosi, 1995; Amorosi et al., 1996; Cibin et al., 2001; Zattin and Zuffa, 2004; Conti et al., 2008; Fontana et al., 2015; Conti et al., 2016; Barbero et al., 2017). Additionally, a few thermochronological investigations have been conducted on a range of formations within the Epiligurian sedimentary succession to provide insights into the thermal history of the Northern Apennines (Boettcher and McBride, 1993; Carlini et al., 2013). Chapter 4 of this thesis will provide details on the insights gained from these thermochronological studies.

Several studies have investigated the structural architecture of the Epiligurian units as exposed in several basins of the Northern Apennines (e.g., Catanzariti et al., 1999; Ottria, 2000; Antonellini and Mollema, 2002; Panini et al., 2002; Artoni et al., 2006; Balocchi, 2014; Piazza et al. 2016; Balocchi and Santagata, 2018; Del Sole and Antonellini, 2019; Del Sole et al., 2020). These studies mainly focus on the meso-to-outcrop scale characteristics (geometry and kinematics) of the tectonic structures affecting the Epiligurian units. Despite the progress made in understanding the structural architecture of these units,

however, our knowledge remains limited especially concerning how the basins are capable to respond to the orogenic history of the Northern Apennines at a broader scale. Specifically, we have a limited understanding of the structural patterns recorded by the Epiligurian basins and their burial/exhumation history, and how these relate to the syn-to-post-orogenic evolution of the Northern Apennines.

1.2 Terminology

This section provides the reader with a comprehensive overview of the complex and diverse terminology adopted in this thesis to describe the geological elements that characterise wedge-top basins and influence their structural and stratigraphic evolution. In particular, the geological elements that require clarity in the way they are referred to are: i) the accretionary wedge; ii) the fold-and-thrust belt; iii) the foreland basin system; iv) wedge-top basins. **Figure 1.4** presents a schematic representation of these tectonic and physiographic elements.

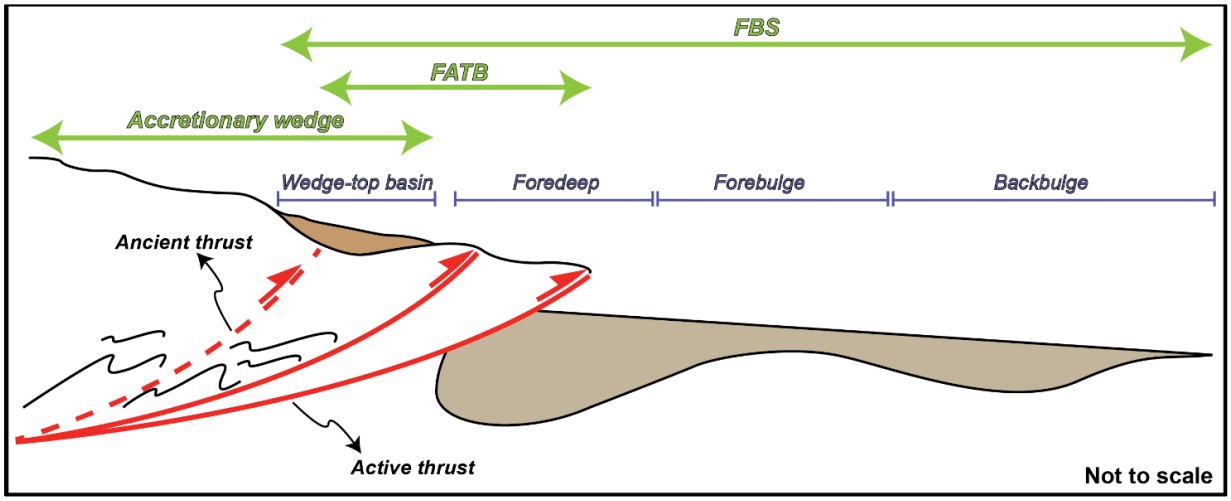

Figure 1.4- Schematic illustration of the general configuration of accretionary wedge, fold-and-thrust belt (FTB) and foreland basin system (FBS). Concerning this latter, its

main depozones are shown. Note that this configuration implies a spatial-temporal evolution of the entire system during continuous orogenic shortening.

i) An accretionary wedge is a dynamic object in a subduction zone and consists of a stack of intensely deformed tectonic slices located directly at the boundary between two converging plates. In particular, it forms by the mechanical off-scraping at the expense of the down going oceanic slab and parts of continental units, which leads to the accretion onto the seaward edge of the upper advancing plate of discrete thrust sheets (e.g., Davis et al., 1983; Cloos, 1984; Cloos and Shreve, 1988a; Dahlen et al., 1984; Platt, 1986; Shreve and Clooos, 1986; van der Pluijm, 2004; Mitra, 1997; Silver and Reed, 1987; Ford, 2004; Meschede, 2015; Lacombe et al., 2019). In general, accretionary wedges are usually composed by lithologically heterogeneous thrust sheets, with their geometry being strongly controlled by the thickness of the sedimentary cover atop the subducting plate. The wedge is underlain by a detachment that ramps up to progressively shallower levels towards the trench and propagates seaward decoupling oceanic sediments from the down going slab (e.g., Poblet and Lisle, 2011).

ii) A fold-and-thrust belt represents an advanced evolutionary stage of an accretionary wedge and consists of faulted and folded sedimentary rocks of a passive margin sequence emplaced above a basal decollement (Davis et al., 1983; Twiss and Moores, 1992; Morley et al., 2011; Lacombe et al., 2019). The latter separates the deformed rocks from an underlying basement that is not involved in the shallow thin-skinned

orogenic-related deformation, cutting up-section the stratigraphy towards the foreland (Chapple, 1978). Many thrusts root down into this basal decollement, featuring a typically ramp-flat geometry that cuts steeply up through competent layers (Boyer and Elliot, 1982; McClay, 1992; Twiss and Moores, 1992; Poblet and Lisle, 2011). The movement of such faults accommodates horizontal shortening and vertical thickening of the wedge and creates folds that are mostly asymmetric with a vergence toward the undeformed foreland. The evolution of a fold-and-thrust belt has been simulated most successfully by the critical taper model (Chapple, 1978; Davis et al., 1983; Dahlen et al., 1984; Platt, 1986; Dahlen, 1990; Boyer, 1995). According to this model a wedge-shaped prism under compression seeks to maintain a stable taper geometry configuration while material is accreted and the prism is translated above the under thrusting plate (Dahlen et al., 1984; Mitra, 1997; Ford, 2004). In particular, the critical taper model implies the dynamic equilibrium between the dip of the undergoing basal slip surface (β; dipping toward the hinterland) and the dip of the upper topographic surface (α; dipping towards the foreland) **(Fig. 1.5)**. The prism evolves continuously through time and in space and, if the taper is to be maintained at its critical configuration, it has to continuously and dynamically respond to changing physical conditions, surface processes and material property boundary conditions. It is controlled by the strength of both the accreted material and the basal detachment; consequently, the volume of the prism can increase by incorporating new material at the front or at the base of it (frontal or basal accretion, respectively), or decreased by thinning it by erosion and tectonic extensional faulting

at its upper parts (Dahlen, 1990; DeCelles and Mitra, 1995; Mitra, 1997; McClay 2012). In particular, if the prism is under critical, it reacts with shortening and thickening due to the propagation of out-of-sequence thrusts, back-thrusts or duplexes along decollement zones (Sinclair and Allen, 1992; DeCelles and Mitra, 1995). On the contrary, if the prism is overcritical, it reacts by increasing its length by extension or collapse at the top of the belt due to gravitational instabilities, coupled with erosion at the surface (Suppe and Connors, 1992; Nemčok et al., 2005).

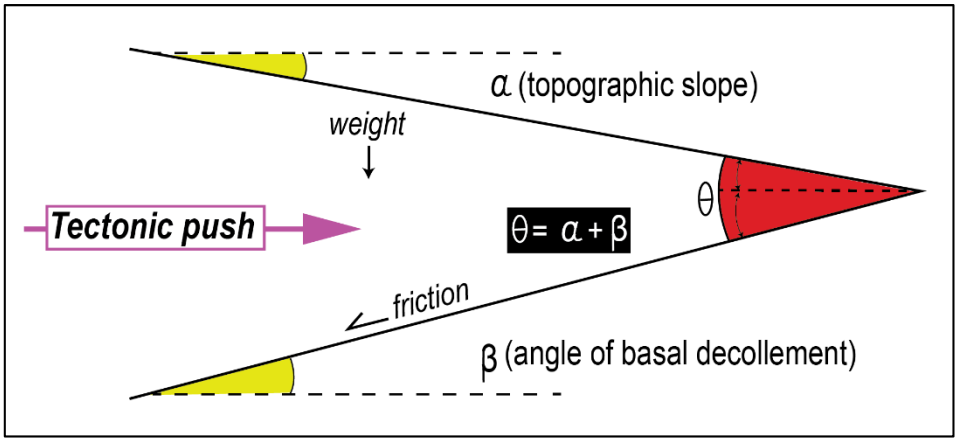

Figure 1.5- Simplified scheme representing the geometry of a wedge-shaped prism according to a critical taper model (modified and redrawn after Dahlen, 1990).

A foreland basin system is defined as an elongated region with high potential for sediment accommodation, situated between the developing orogenic belt in a hinterland position and an undeformed cratonic area (Price, 1973; DeCelles, 2012). Foreland basin systems typically originate from flexural subsidence mechanisms driven by loading resulting from the arrangement of tectonic units during the build-up of the orogenic belt

(Dickinson, 1974; Turcotte and Schubert, 1982; Allen et al., 1986; Stockmal et al., 1986, DeCelles and Giles, 1996, Ford, 2004; De Celles, 2012). During plate convergence, the vertical load exerted by the orogen gradually shifts toward the foreland, thus exerting pressure on the progressively more external portions of the subducting plate. This mechanism leads to the outward migration of the foreland system (Dickinson, 1974; Beaumont, 1981; Sinclair and Allen, 1992; Jordan, 1995). From a sedimentological perspective, a foreland basin system identifies a large and articulated area of sedimentation that can be further subdivided into four main depozones **(Fig. 1.4)**: a) the foredeep depozone, which is typically 100-300 km wide and capable of accommodating up to 2-8 km of sedimentary infill (e.g., DeCelles and Giles, 1996). The sediment therein can deposit in sub-aerial (fluvial and alluvial systems) and sub-aqueous environments typical of relatively shallow (deltaic or shelf sediments) or relatively deep-sea conditions (turbiditic sediments) (Covey, 1986; Sinclair and Allen, 1992; DeCelles and Giles, 1996, Ford, 2004, DeCelles, 2012); b) the forebulge depozone, which occurs along the outer margin of the foreland basin system where flexural-type bending dominates. Due to this, the forebulge is generally considered to be a zone of non-deposition and erosion, thus leading to the consequent formation of unconformities that are used for tracking its position through time (e.g., Stockmal et alii, 1986; Flemings and Jordan, 1990; Crampton and Allen, 1995; Chapman and DeCelles, 2015); c) the back-bulge depozone, which constitutes the depocenter where sediments accumulate between the forebulge depozone and the craton (DeCelles and Giles, 1996). Because of the relatively low rates of subsidence in this area, stratigraphic units are much thinner than those in the foredeep

depozone (e.g., Flemings and Jordan, 1989; DeCelles and Burden, 1992); d) the wedge-top basin, the focus of this dissertation. As explained above, wedge-top basins are considered and defined as syn-orogenic depozones that form on top of an accretionary wedge, which, in its dynamic form, acts as the source of their sedimentary infill. Then, the accretionary wedge and the wedge-top basin are together deformed by the thrusts activated during the formation of the fold-and-thrust belt, which controls the regional stress field and the subsidence/exhumation of wedge-top basins.

1.3 Aim of the thesis

This thesis aims to contribute to the understanding of the structural and thermal characteristics of the Epiligurian wedge-top basins in terms of tectonic regimes, exhumation and erosional rate through space and time. To do this, I adopted a multidisciplinary approach integrating meso-scale analyses of different kind of tectonic structures, microscopic examination of faults, remote sensing analyses of lineaments, geochronological and thermochronological investigations.

In particular, I focused my attention on a representative Epiligurian wedge-top basin (the Marzabotto Basin, located immediately to the south of the city of Bologna; see Chapter 3 for details), whose middle Eocene to upper Miocene stratigraphic succession spans the temporal range of the Northern Apennines building and uplift. I analysed different tectonic structures affecting the whole stratigraphic succession and I characterised them in terms of orientation, kinematic and cross-cutting relationships. I compared field structural data with data deriving from the remote sensing analysis of morpho structural lineaments. I derived structural and kinematic constraints on the deformation history recorded by the Marzabotto Basin and I proposed a conceptual model on the syn-to-post-orogenic evolution of this shallow depocenter. I also provided absolute chronological constraints on the long-lived tectonic evolution of this basin from its depositional formation to its exhumation within the dynamics of the underlying fold-and-thrust belt. In particular, I carried out a thermochronological study of the entire Epiligurian succession with the goal to better define the exhumation age and rates of the Marzabotto

Basin. Finally, I provided age constraints on the structural pattern controlling the post-orogenic evolution of this basin.

1.4 Structure of the thesis

Chapter 2 – *"Geological setting"* shortly describes the setting of the Northern Apennines fold-and-thrust belt with the aim to contextualise the structural data presented in the other chapters. The chapter focuses on the description of the evolution of the Northern Apennines from a paleogeographic, geodynamic, and tectonic point of view, with the description of the main tectono-stratigraphic units.

Chapter 3 – It is based on the paper *"Multiscale structural analysis of an Epiligurian wedge-top basin: insights into the syn-to post-orogenic evolution of the Northern Apennines accretionary wedge"* by Stendardi F., Viola G., and Vignaroli G., published in the International Journal of Earth Sciences. In this chapter, the main structural results of the thesis are presented. In particular, the chapter deals with the investigation at the meso-scale of the tectonic structures affecting the Marzabotto Basin, with an in-depth analysis and interpretation of its polyphasic tectonic evolution, based on field observations and remote sensing lineament analysis to correlate the local structural pattern with the regional picture.

Chapter 4- It is based on the paper *"Thermal history of the Epiligurian Marzabotto wedge-top basin records the tectonic development of the Northern Apennines fold-and-thrust belt (Italy)"* by Stendardi F., Vignaroli G., Carrapa B., Albino I., Viola G., submitted in the Terra Nova

journal. It presents the results of a thermochronological investigation of the Epiligurian units exposed in the Marzabotto Basin. The goal was to produce new thermochronometric data to better constrain the local exhumation history and correlate it with the large-scale tectonic evolution of the Northern Apennines.

Chapter 5 – *"Late Pleistocene deformation in the axial zone of the Northern Apennines, Italy: insights into the early stages of post-orogenic extension"* presents the results of the multidisciplinary study about the investigation of the pattern and kinematics characterisation of the extensional tectonic structures that affect the Epiligurian units. It combines detailed field structural observations with remote sensing lineament analysis and a geochronological study on syn-kinematic mineralisations. The latter was used to constrain the age of the post-orogenic evolution in the Epiligurian Marzabotto Basin.

Chapter 6 – It discusses the obtained results in a regional perspective and draws conclusions of general validity on the basis of the data described in the previous chapters.

Chapter 2

Geological background of the Northern Apennines

2.1 Geodynamic framework

The Northern Apennines (NA) of Italy are an arcuate shaped orogenic belt located between the Western Alps arc to the north and the Central Apennines to the south. Geographically, the belt comprehends almost the entirely the regions of Emilia-Romagna and Tuscany, while the offshore side comprehends the Tyrrhenian Sea to the SW (hinterland) and the Adriatic Sea to the NE (it is part of the present-day foredeep).

The NA are a prominent fold-and-thrust belt that formed due to the subduction of the Ligurian Ocean and the subsequent continental collision between the Adria and Europa plates (Boccaletti et al., 1971; Boccaletti et al., 1980; Carmignani and Kligfield, 1990; Carmignani et al., 1995; Castellarin, 2001; Faccenna et al., 2001; Bettelli et al., 2003; Rosenbaum and Lister, 2004; Faccenna et al., 2004; Doglioni, 2006; Carminati and Doglioni, 2012). In this geodynamic context, the Adria plate (pertaining to the Africa plate) is subducted underneath the European plate since the middle-upper Eocene (e.g., Carminati et al., 2012). The WNW- dipping slab composed of the Adria lithosphere, progressively moved towards the east due to the onset of the slab retreat (i.e., slab rollback process; e.g., Faccenna et al., 2001; Carminati et al., 2012). The main trench of the still ongoing subduction zone was (and it is) oriented sub-orthogonal with respect to the main convergence vectors, which steered the compression and the structuring of the Apennine fold-and-thrust belt (Dewey et al., 1989; Patacca et al., 1990). Several studies have aimed to reconstruct the kinematic evolution of the Apennine subduction zone from a seismic perspective, taking into account the main phases that occurred: i) low

subduction speed at the beginning. In this phase, the subducting slab is relatively thin and buoyant, and it subducts slowly beneath the overriding Europa plate; ii) slab development with an exponential increase of subduction speed as the subducting slab cools, thickens, and sinks more rapidly into the mantle, leading to the first opening of the Provencal back-arc basin; iii) slow-down of subduction due to the interaction with the transition zone, subsequent eastward roll-back of the subduction trench and opening of the Tyrrhenian back-arc basin (Faccenna et al., 2001). This latter velocity decreasing is permanent in the Northern Apennines due to the imbrication of continental material in the trench since the Oligocene (e.g., Faccenna et al., 2001; Carminati et al., 2012).

In general, the onset of the subduction along the Northern Apennines trench is characterised by several features including: i) the onset of siliciclastic deposition of a foredeep system which shows continuous sedimentation from the Upper-Cretaceous to the early Palaeocene (Marroni et al., 2010) and then moved towards the eastern quadrant (present-day Adriatic foredeep; e.g., Patacca et al., 1990); ii) the occurrence of large-scale angular unconformities due to the formation of wedge-top basins, filled by syn-tectonic clastic units, on the top of the growing fold-and-thrust belt, and to a rapid subsidence toward the trench that is filled by the dismantling of the chain; iii) the development of high pressure/low-temperature metamorphic conditions in both oceanic-derived and continental-derived units exposed along the NA belt (Jolivet et al., 1998, 2003; Vignaroli et al., 2009). Since the early Oligocene, extension occurred at the rear of a NW-dipping subducting lithosphere, with the age of the syn-rift deposits spanning from the Oligocene

to the Aquitanian. At that time, post-rift deposits unconformably overly the syn-rift sequence and the emplacement of the oceanic crust coincided with the 25-30° clockwise rotation of the Sardo-Corso block **(Fig.2.1a-c)** (e.g., Jolivet et al., 1998; 2003; Faccenna et al., 2001). Then, since the Middle Miocene, in response to the continuation of the slab retreat, the Tyrrhenian back-arc basin developed **(Fig.2.1d-e)**. In particular, the crustal thinning is marked by the development of shear zone system, sedimentary basins and magmatic activity that get younger from Corsica to the Apennines (eastward direction) with the formation of oceanic crust in the Tyrrhenian basin (Jolivet et al., 1994; Bartole, 1995; Faccenna et al., 1997).

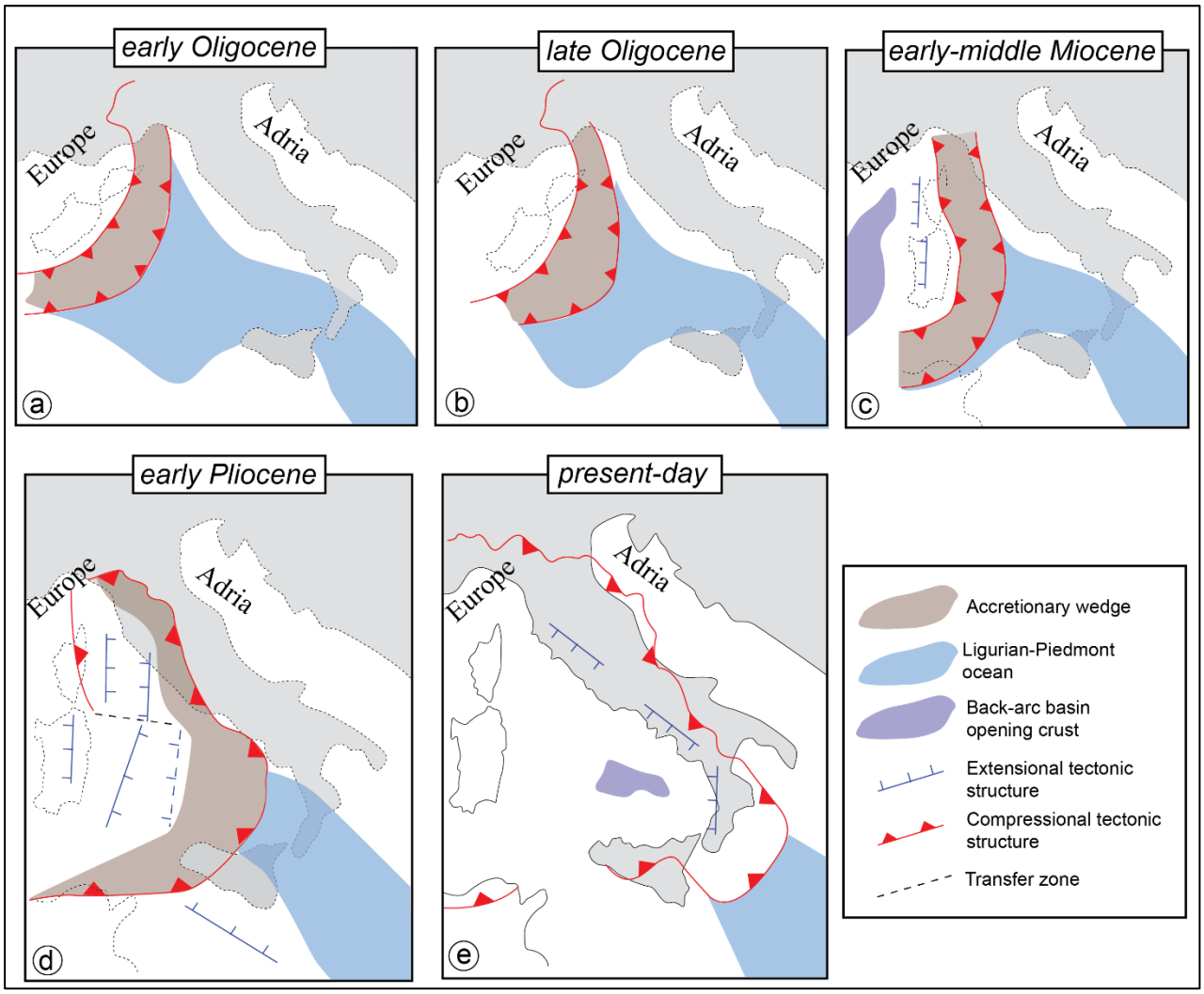

Figure 2.1- Paleogeographic reconstruction of the Central Mediterranean area (modified and redrawn after Faccenna et al., 1997; 2001) from 30 Ma to present-day. The polygons in sky-blue represents the deep basins in the African-Adriatic domains and the brown one refers to the developing orogenic belt. The propagation of the thrust front is represented by the red-line, followed by the onset of extensional which culminated with the opening of a back-arc basin, as consequence of the progressive slab retreat. The purple areas represent the sector where the formation of new oceanic crust occurs.

2.2 Anatomy and tectonics of the Northern Apennines

The stratigraphic-structural architecture of the NA is a stack of units from different paleogeographic domains that have been deformed during the orogenic shortening. From the innermost to the outermost and from top to bottom, these domains are (e.g., Elter, 1975; Ricci Lucchi, 1986; Vai and Martini, 2001; Carmignani et al., 1995; Barchi et al., 2001; Bortotti et al., 2001; Castellarin et al., 2001; Massoli et al. 2006; Conti et al. 2020; **Fig.2.2)**: i) the Ligurian Domain, composed by many elements all characterised by ophiolites and/or oceanic sediments of Jurassic to Eocene age, ultimately obducted over both the African and European continental margins of the former neo-Tethys during the mid-Eocene phase. ii) the Sub-Ligurian Domain, made of Paleocene-Eocene shales and limestones and early Oligocene siliciclastic turbidite rocks; iii) the Tuscan-Umbria-Marche Domain, characterised by Meso-Cenozoic evaporites and pelagic carbonates overlain by Miocene-Pliocene siliciclastic turbidites (Macigno and Cervarola fms.). The Tuscan Domain also includes metamorphosed rocks, exposed in the Alpi Apuane tectonic window, which are structurally juxtaposed against the non-metamorphic Tuscan Nappe along a major detachment fault (e.g., Carmignani and Kligfield, 1990; Fellin et al., 2007; Molli et al.,2010).

The Epiligurian units are the most surficial stratigraphic-structural domain of the Northern Apennines tectonic edifice. They are a sequence of siliciclastic deposits deposited in wedge-top basins during the middle Eocene to late Miocene and they

directly overly the Ligurian units (Ricci Lucchi, 1986; Cibin et al., 2001; see Chapter 3, Paragraph 3.2.2.1 for details).

The thin-skinned tectonics that characterised the understudy sector of the Apennines, is expressed by the development of regional NE-verging thrusts, which are oriented WNW-ESE. The propagation of these thrusts through time, allowed the progressive juxtaposition of the above-described tectono-stratigraphic units, which also testifies the former and the subsequent subduction and collision processes, respectively.

The complex architecture of the NA reflects the tectonic history that has affected the belt over time. Currently, it is characterised by the contemporaneous occurrence and eastward migration of coupled compression in the foreland and extension in the hinterland, with the direction of maximum extension disposed nearly parallel to the direction of the maximum shortening (e.g., Malinverno and Ryan 1986; Carmignani and Kligfield, 1990; Cavinato and DeCelles 1999; Barchi, 2010).

The coexisting of both compression and extension is clearly evidence by the eastward rejuvenation of the syn-tectonic basins, which represent important marker for the reconstruction of the tectonic history of the fold-and-thrust belt (Barchi et al., 2006; Barchi, 2010). The syn-tectonic basins usually evolve reflecting the different depositional zones of a foreland basin system (see Chapter 1) and the resultant sedimentary succession consist in forebulge/backbulge, foredeep and wedge-top basins deposits (De Celles and Giles, 1996) characterised by the occurrence of large-scale mass complexes consisting in

extrabasinal (i.e., olistostromes) and intrabasinal displaced sediments migrating from the west to the east (Lucente and Pini, 2008; Barchi, 2010; Ogata et al., 2019).

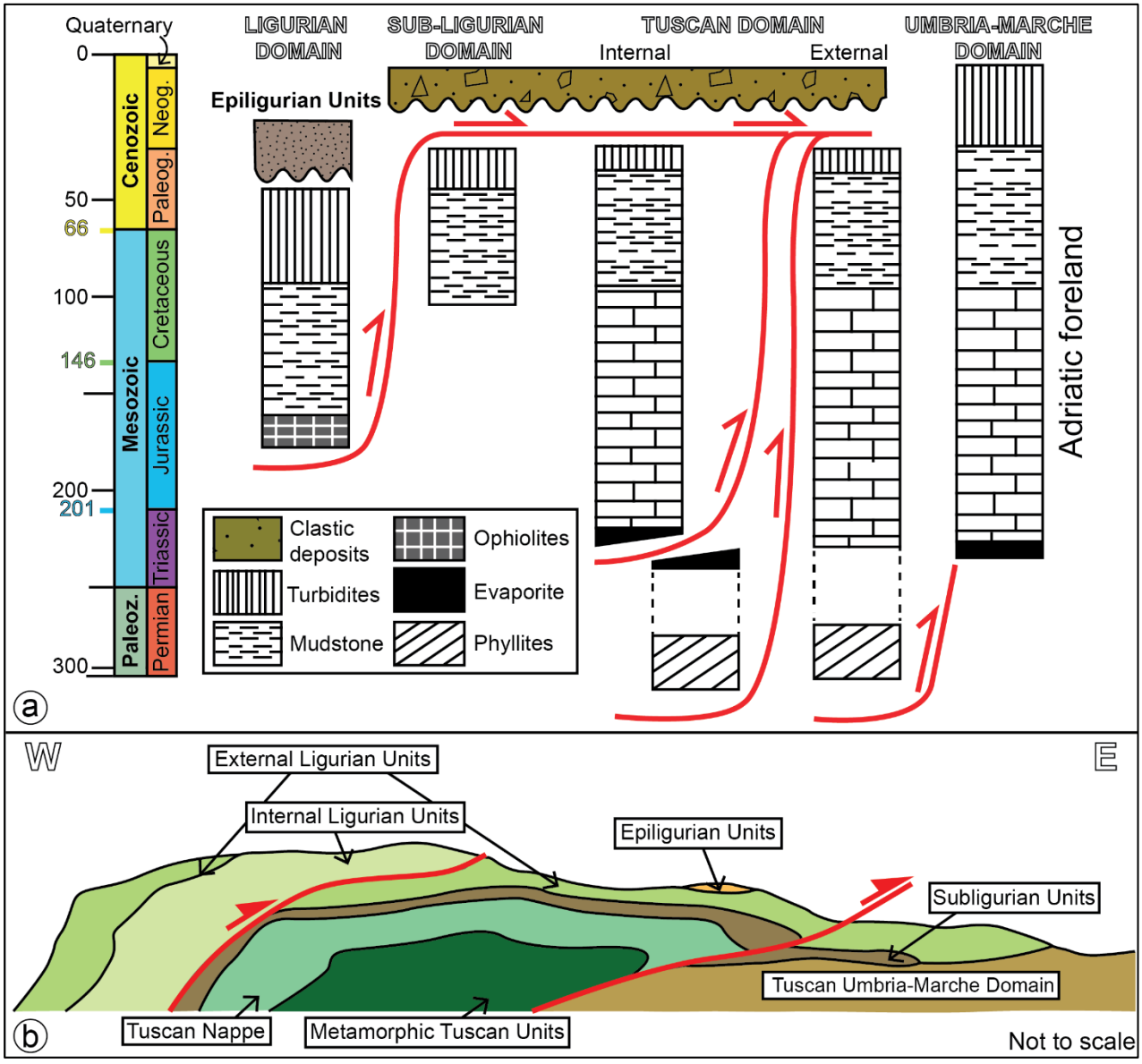

Figure 2.2- a) Schematic representation of the relationships between stratigraphic and tectonic units in the Northern Apennines fold-and-thrust belt (modified and redrawn after Carmignani et al., 1995); b) Schematic cross-section showing the general structure of the belt (from Elter, 1975).

As the compressional thrust front was propagating towards the foreland, since the early Pliocene the extensional tectonic phase started in the hinterland in response to the opening of the Tyrrhenian back-arc basin. The extensional deformation is strongly asymmetric and characterised by mostly east-dipping low-angle normal faults detached within the upper crust (e.g., Malinverno and Ryan 1986; Carmignani et al. 1990; Cavinato and De Celles, 1999; Decandia et al., 1998; Faccenna et al., 2001; Barchi, 2010). This post-orogenic phase led to the development of continental and shallow marine NW-SE basin-bounding faults that invariably reworked and cut through the earlier contractional features (e.g., Lavecchia et al., 1984; Bartole et al., 1991; Pialli and Alvarez., 1995; Jolivet et al., 1998; Barchi et al., 2006; Pauselli et al., 2006). Since the Pleistocene, the extensional tectonic regime then affected innermost part of the belt, causing uplift of the southwestern sector of the belt and subsidence in the north-eastern area (Bertotti et al., 1997).

2.3 Seismic and geophysical data

The NA fold-and-thrust belt is a tectonically and seismically active region, with the distribution of seismicity influenced by the rheology and structure of the lithosphere (e.g., Pauselli et al., 2006; Picotti and Pazzaglia, 2008; Barchi et al., 2010).

In general, the tectonic activity of the NA is driven by belt-perpendicular compression which is recognisable in the development of several arcs since the Messinian, followed by a rapid uplift since the Upper Miocene (e.g., Castellarin et al., 1982; Coltorti et al., 1991; Vai, and Martina, 2001; Boccaletti et al., 2010; Elter et al., 2012) **(Fig. 2.3)**.

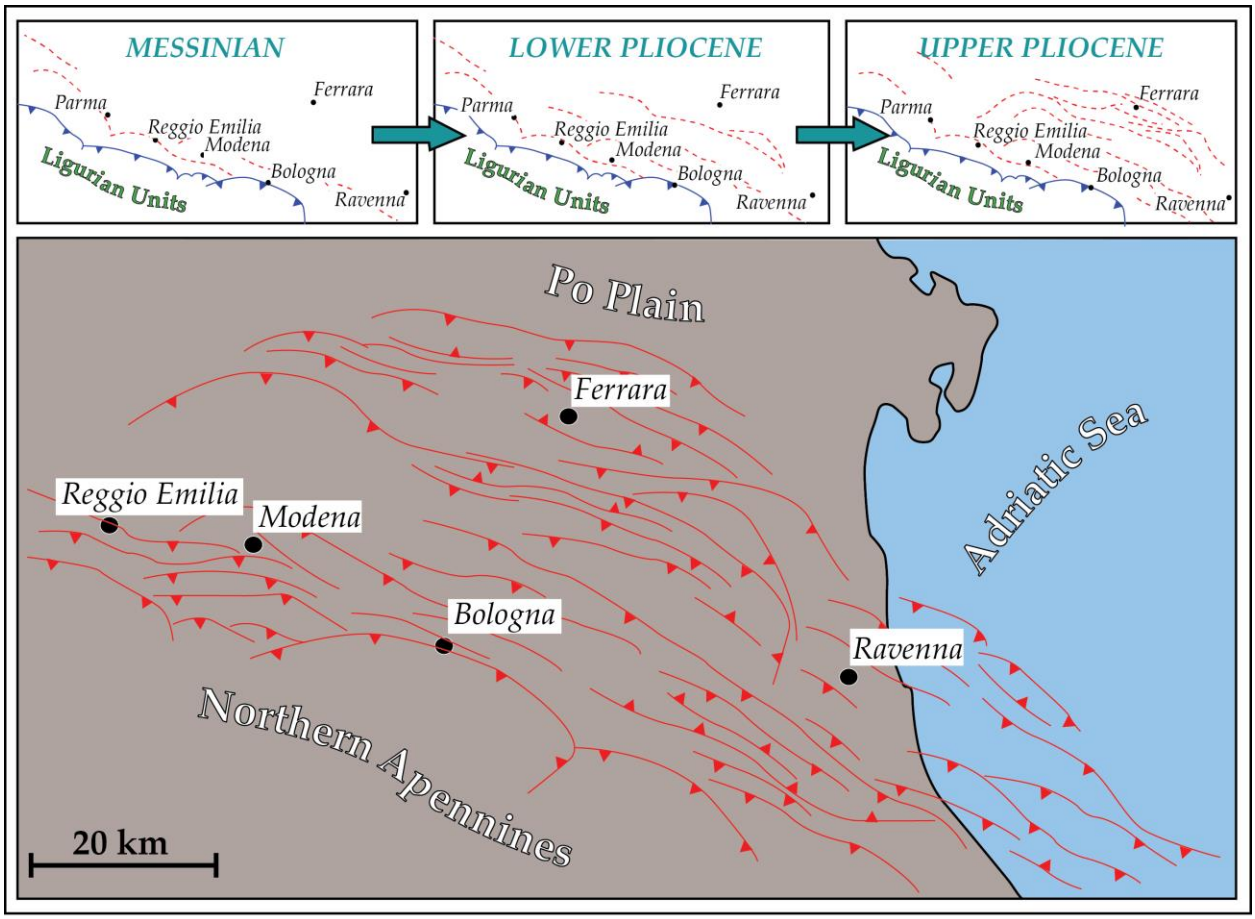

Figure 2.3- Representation of the propagation of the buried thrusts that constitute the building of the northern Apennines, since the Upper Miocene (modified and redrawn after Vai and Martini 2001 and Mantovani et al., 2013).

The compressional tectonic phase acting in the eastern side of the NA has led to the activation and propagation of arcuate tectonic structures, such as the Emilian and Ferrarese folds, which are buried beneath the Quaternary deposits of the Po Plain **(Fig. 2.4a)**. Here, the location of seismicity corresponds to the southern edge of the Po Plain (along the Pedeapenninic Front) and to the buried frontal arcs (Pieri and Groppi, 1981; Massoli et al., 2006; Pauselli et al., 2006; Picotti and Pazzaglia, 2008; Boccaletti et al., 2011; Mantovani et al., 2014; 2019) characterised by a maximum compression oriented

approximately NE-SW (e.g., Pizzi and Scisciani, 2012; Pondrelli et al., 2012). Seismogenic deformation is definitely associated with blind thrusts, and no structural evidence in the surface has yet been documented (e.g., Bartolini et al., 1983; Boccaletti et al., 1985). However, morphotectonic analysis has been carried out to identify the recent activity of these tectonic structures by characterising geomorphological features such as fault scarps, tectonic terraces, hydrographic network control, and dislocation and/or deformation of recent deposits and surfaces (Boccaletti et al., 2011).

The inner (Tyrrhenian) side of the belt is characterised by moderate to large (5<M<6) earthquakes that mostly occur on NW-striking, SW dipping, 5 to 10 km-long fault segments (Amato et al., 1998; Chiaraluce et al., 2003). The presence of this extensional zone is evidenced by the development of Plio-Quaternary intra-mountain basins, such as the Lunigiana, Garfagnana, and Mugello basins, which transect the entire fold-and-thrust belt longitudinally (e.g., Chiaraluce et al., 2003; Chiarabba et al., 2005; Barchi et al., 2006; 2010; **Fig. 2.4b)**. GPS data has contributed valuable constraints to the kinematic framework of the belt, revealing that the outer region of the NA experienced significantly faster movement, characterised by a greater eastward component compared to the inner part of the belt (e.g., Barchi, 2010; Cuffaro et al., 2010).

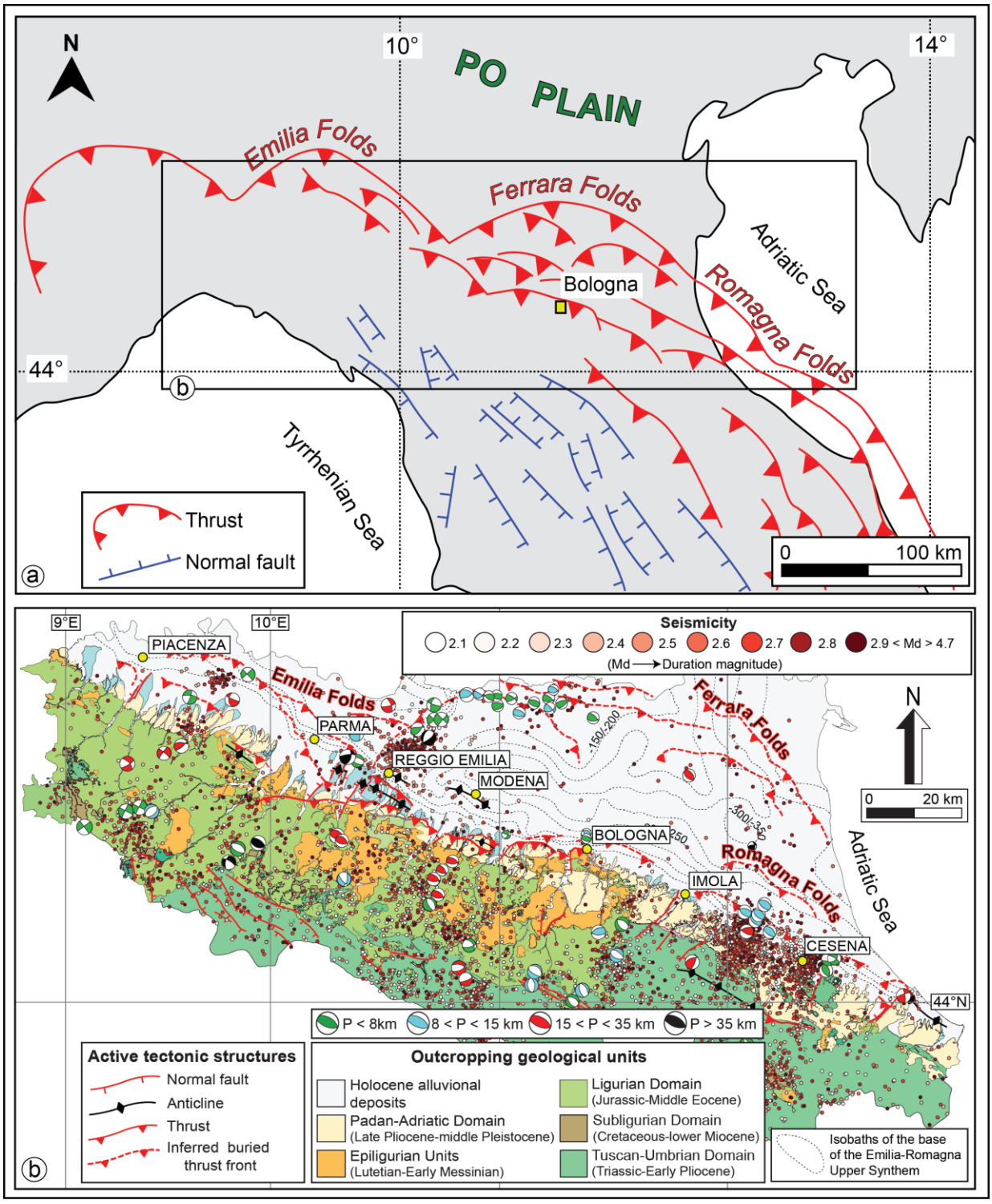

Figure 2.4- a) Structural map of the Northern Apennines fold-and-thrust belt which highlights recent and active structures (Modified and redrawn after Vai and Martini, 2001); b) Seismic data and focal mechanisms (reported from the Seismotectonic Map of the Emilia-Romagna and surrounding areas (Martelli et al., 2017)) for the Northern

Apennines sourced from the Italian Seismological Instrumental and Parametric Database (ISIDe) accessible at http://terremoti.ingv.it/en/iside.

Additionally, the analysis of the velocity field indicates active extension along the main ridge at an average rate of approximately 2.3-3 mm/yr, aligning well with seismicity data and other stress field indicators (D'Agostino et al., 2009; Barchi et al., 2010).

Chapter 3

Multiscale structural analysis of an Epiligurian wedge-top basin: insights into the syn-to-post orogenic evolution of the Northern Apennines accretionary wedge (Italy)

Stendardi F., Viola G. & Vignaroli G.

(Published in International Journal of Earth Sciences; doi: https://doi.org/10.1007/s00531-022-02286-y)

Dipartimento di Scienze Biologiche, Geologiche e Ambientali, Alma Mater Studiorum-Università degli Studi di Bologna, Italia

Abstract

Wedge-top basins represent useful tectonic elements for the characterization of the evolution of their underlying accretionary wedge in space and time, as their final state of deformation sums up the bulk shortening and structural instability conditions of the wedge. Here, we present the geometric and kinematic patterns of deformation structures deforming the wedge-top Epiligurian basins of the Northern Apennines (Italy). Our main goals are to generate an evolutionary model to account for the syn- to post-orogenic evolution of the Epiligurian basins and to infer the building style of the Northern Apennines wedge during continental collision. Mesoscale structural analysis shows that common and widely distributed thrust and normal fault arrays deform the entire Epiligurian stratigraphic succession infilling the broadly E-vergent wedge-top basins. Thrusts are invariably cut by later NW-SE and NE-SW-striking normal and oblique fault systems characterised by fault planes that mutually intersect at all scales to form polygonal patterns. Remote sensing analysis of the tectonic structures affecting the Epiligurian formations confirms the variable orientation of both thrusts and normal faults within the different studied stratigraphic successions. As a whole, results suggest a polyphase tectonic evolution of the Epiligurian wedge-top basins during the widening of the Northern Apennines accretionary wedge towards the foreland by frontal accretion. The recognised main phases are: i) syn-orogenic compression accommodating overall tectonic transport towards the eastern quadrants; ii) post-orogenic extension genetically related to the extension of the inner zone of the Northern Apennines; iii) more recent

extension forming collapse-induced normal faults spatially arranged in polygonal patterns.

Keywords: wedge-top basins; normal faulting; accretionary wedge; Epiligurian formations; Northern Apennines

3.1 Introduction

Wedge-top basins are dynamic stratigraphic and structural features located atop thrust sheet stacks imbricated during the contractional structuring of the underlying accretionary wedge (e.g., DeCelles and Giles 1996). They are filled by deposits deriving from the progressive dismantling of the growing wedge itself and may be involved in the build-up, uplift and evolution of actively shortening fold-and-thrust belts (e.g., Ori and Friend 1984; Ford 2004). The architecture of the underlying accretionary wedge and its kinematic evolution exert a significant influence upon the geometry and the stratigraphic evolution of wedge-top basins. From a structural point of view, their final state of deformation expresses and accommodates the i) bulk shortening and thickening of the wedge, at all scales, ii) propagation of in-sequence and out-of-sequence thrusts, iii) uplift and subsidence, iv) creation of accommodation space and potentially variable sedimentation rates and, finally, v) reworking of the thickened wedge under overall extension in post-orogenic conditions (Beaumont, 1981; Jordan, 1981; Ori and Friend, 1984; Bally et al., 1985; De Celles and Giles, 1996; Mutti et al., 2003, Ford, 2004). Wedge-top clastic deposits generally reflecting only limited transport and are characterised by immature textures controlled by different types of growth structures depending on the increasing proximity to the basin edges and according to the geometry of the thrust ramps upon which they develop (Beaumont, 1981; Ori and Friend, 1984; Peper and Boer, 1995). Previous studies have mostly focused on the sedimentological and stratigraphic features of wedge-top basins, aiming at defining the depositional environment of the

involved stratigraphic units and their mutual relationships in terms of stratigraphic gaps, lateral continuity, interdigitation and angular unconformities (e.g., DeCelles and Giles, 1996; Ricci Lucchi, 1986; 1990; Amorosi, 1995; Ambrosi et al., 1996; Amorosi et al., 1996; Horton, 1998; Sempere, 2000; Chiang et al., 2004; Ciarcia and Vitale, 2013). On the other hand, only little attention has instead been paid to the structural record of wedge-top basins, although a multidisciplinary structural perspective including the study of meso- to regional-scale structural features may indeed provide useful insights into the regional and local paleo-stress regime evolution, burial and thermal history and other far-field factors (shortening, exhumation and erosion rate, among others) influencing the space-time evolution of this type of basins (e.g., Hippolyte et al., 1994; Ferrière et al., 2004; Carrapa and DeCelles, 2008; Vera et al., 2015). In fact, wedge-top basins have been only seldomly used as structural-stratigraphic gauges to track down the tectonic style and orogenic evolution of accretionary wedges worldwide (e.g., Apennines and Calabrian Arc: Weltje, 1992; Hippolyte et al., 1994; Catanzariti et al., 1999; Piazza et al., 2016; Wyoming-Idaho-Utah thrust belt: Coogan et al., 1992; Mesohellenic Basin: Ferrièr et al., 2004).

The Epiligurian Basins of the Northern Apennines of Italy represent an iconic example of wedge-top basins formed atop an accretionary wedge progressively evolving into a fold-and-thrust belt (e.g., Conti et al., 2020). These middle Eocene-upper Miocene basins are characterised by a complex stratigraphic and sedimentological record (including highly variable lithological infill, composition and thickness, lateral interdigitation and

occurrence of regional and second-order unconformities) that was governed and modulated by the dynamic and continuously evolving tectonic regime and state of stress of the underlying Apennines wedge (e.g., Amorosi et al., 1995; Cibin et al., 2001). Therefore, the Epiligurian basins and their sedimentary successions can be used as powerful structural/stratigraphic markers to unravel the deformation history of the Northern Apennines wedge, with noteworthy implications upon its tectonic evolution since the middle Eocene.

In this paper, we describe the structural setting of the Marzabotto wedge-top basin of the Northern Apennines, which is an Epiligurian basin located immediately to the south of the city of Bologna **(Fig. 3.1)**. This basin is of particular interest because (i) it exposes the entire Epiligurian sedimentary succession, (ii) its contact to the underlying wedge units is easily accessible and is thus suitable for in-depth analysis, and (iii) its internal stratigraphic architecture is affected and deformed by multiple generations of deformation structures (e.g., Panini et al., 2002; see below), the study of which can reveal many insights into the local and regional deformation history. Through a multiscalar and multitechnique approach including geological mapping, mesoscopic structural analysis and remote sensing analysis of lineaments, we characterised different structural elements by defining their orientation, kinematics, mutual cross-cutting, and their genetic relationships with the deformed sedimentary succession. Results are used to support an evolutionary structural model that reflects the interaction between regional far-field and local tectonic stress conditions. We propose a polyphase tectonic evolution for the

Marzabotto basin that is representative for other wedge-top Epiligurian basins recording syn-orogenic compression and post-orogenic extension, with the latter accompanied by local instabilities during overall thinning of the transiently supercritical wedge.

3.1.1 Terminology used

In this work, we consider an accretionary wedge as the product of the first stage of orogen build-up, wherein sedimentary rocks belonging to passive margin sequences are involved in the trench dynamics, are reworked, accreted and imbricated and, eventually, displaced from the orogenic core towards the foreland (e.g., Dewey and Bird, 1970; Twiss and Moores, 1992; Cloos and Shreve, 1988; Cawood et al., 2009). Accretionary wedges are effectively conceptualised as a wedge-shaped geodynamic object (e.g., Davis et al., 1983; Dahlen et al., 1984; Platt, 1986), the evolution of which, in space and time, also depends on the combination of the flexure of the underthrusting lower plate and the mode of deformation of the wedge material itself (e.g., Mitra, 1997; Ford 2004). Wedge-top basin depozones may form on top of the frontal part of the accretionary wedge, which tapers towards the foreland (Davis et al., 1983; Dahlen, 1990; Ruh, 2020). On the other hand, fold-and-thrust belts represent the result of the more advanced evolutionary stages of an accretionary wedge (Morley et al., 2011). They tend to form in response to wedge uplift and the progressive involvement of foreland basin systems during progressive shortening (Davis et al., 1983). Folding and thrusting accommodate crustal shortening at shallow crustal levels and may variably affect the early stratigraphic setting of the wedge-top basins (Boyer and Elliot, 1982).

3.2. Geological setting

3.2.1 The Northern Apennines

The Northern Apennines (NA) are a fold-and-thrust belt that belongs to a retreating collisional foreland basin system (De Celles and Giles, 1996; Ford, 2004). The NA initially formed as part of an accretionary wedge in response to the Late Cretaceous-Eocene closure of the Ligurian-Piedmont Ocean, before later evolving into a NE-verging fold-and-thrust belt related to the W-vergent subduction of the Adria plate beneath Europe and their Oligo-Miocene collision (Carmignani and Kligfield, 1990; Carmignani et al., 1995; Bettelli et al., 2003; Elter et al., 2003; Rosembaum and Lister, 2004; Doglioni et al., 2006; Boccaletti et al., 2011; Carminati and Doglioni, 2012; Papeschi et al., 2022). The progressive development of the NA stems from the summation of both contractional and extensional deformation during syn- and post-orogenic tectonic phases (e.g., Malinverno and Ryan, 1986; Carmignani et al., 1990; Cavinato and DeCelles, 1999), with the former linked to the orogenic wedge structuring and the latter to the opening of the Tyrrhenian back-arc domain inducing the formation of extensional basins (e.g., Faccenna et al., 2001).

The syn-orogenic tectonic phase led to the stacking of tectonic units belonging to different paleogeographic domains along NW-SE-striking and NE-verging thrusts (Boccaletti et al., 1985; Carmignani et al., 1995; Pauselli et al., 2006). From the innermost to the outermost and from top to bottom, these domains are (e.g., Conti et al., 2020 and references therein): i) the Ligurian Domain, formed by Jurassic ophiolites and their Cretaceous-to-Palaeocene sedimentary cover; ii) the Sub-Ligurian Domain, formed by

Palaeocene-to-lower Miocene deep marine sediments and turbidites deposited on the Adria thinned continental crust; iii) the Tuscan-Umbria-Marche Domain, mostly including Triassic-to-Oligocene platform and basinal carbonate successions, overlain by Miocene-Pliocene turbidites.

Atop those domains occur the Epiligurian basins, the focus of this study, which unconformably overly the Ligurian Domain and consist of middle Eocene-upper Miocene siliciclastic successions deposited in an environmental domain that evolved in time from bathyal to shallow water conditions (e.g., Ricci Lucchi, 1986; 1990; Nirta et al., 2007). During the tectonic evolution of the NA accretionary wedge, shortening culminated with the Ligurian Domain being thrusted over the Tuscan Domain during the Oligo-Miocene collision (e.g., Boccaletti et al., 1990; Mantovani et al., 2019). Starting in the Late BurdigalianPliocene, contemporaneous to compression in the most external wedge, an extensional tectonic regime started to affect the most internal portion of the NA (Tyrrhenian side) and began to migrate eastwards in the wake of the NA advancing thrust front (e.g., Martini and Sagri, 1993; Barchi et al., 2006; **Fig. 3.1b).** This post-orogenic phase led to the development of NW-SE basin-bounding faults that invariably reworked and cut through the earlier contractional features (e.g., Lavecchia et al., 1984; Pialli and Alvarez., 1995; Barchi et al. ,2006; Pauselli et al., 2006). The extensional tectonic regime affected the northernmost exposed margin of the NA since the middle Pleistocene causing uplift of the southwestern sector of the belt and subsidence in the north-eastern area (Bertotti et al., 1997).

The present-day thrust front of the NA mainly formed in the Pliocene-lower Pleistocene. It is defined by concentric arcuate thrusts that are associated with the WNW-ESE-striking Emilian and Ferrarese fold systems, buried beneath the middle Pleistocene-Holocene Padan-Adriatic foredeep deposits (Boccaletti et al. ,1985; 2011; **Fig. 3.1a**).

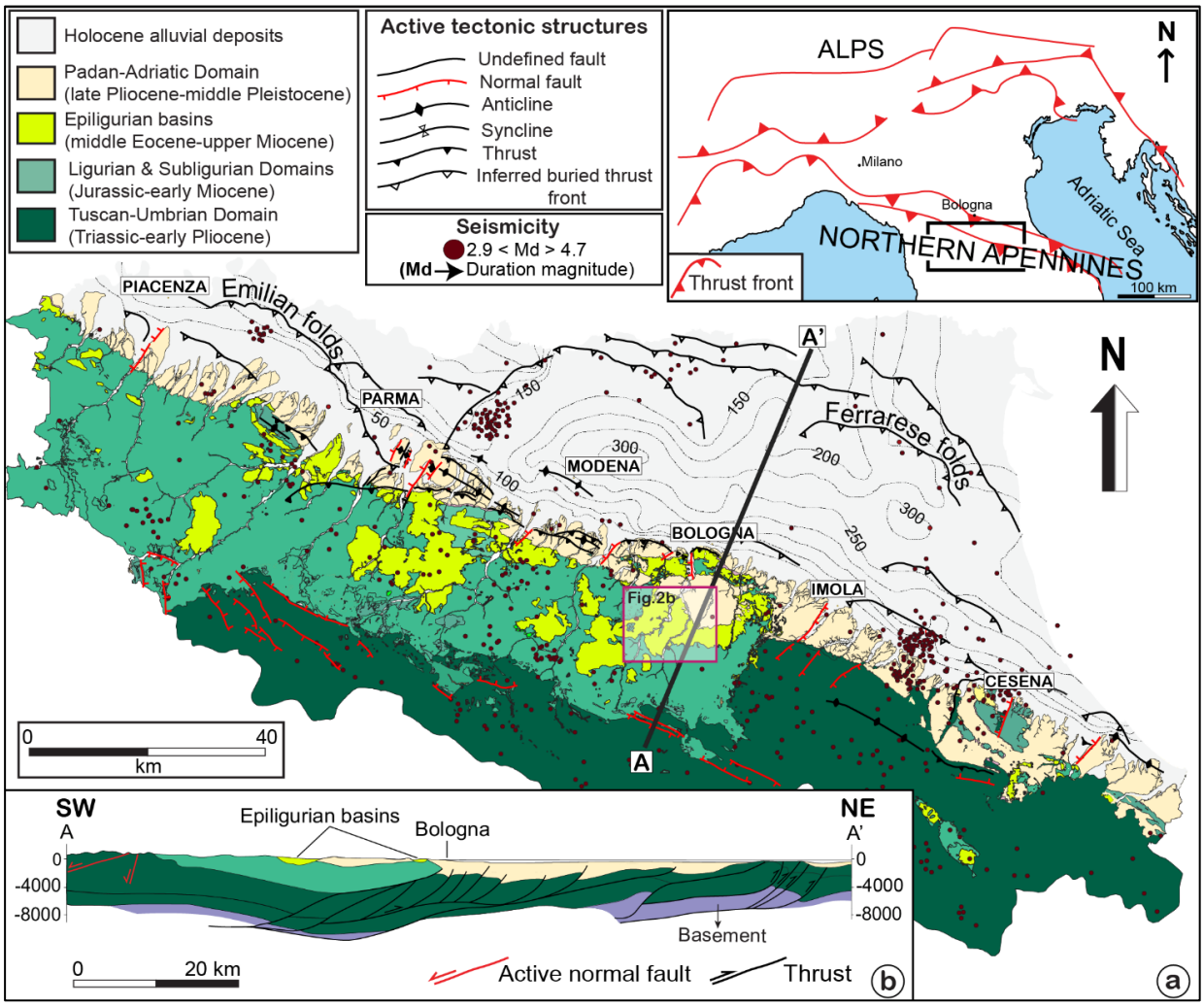

Figure 3.1 - a) Geological-structural map of the Northern Apennines (modified and redrawn after Conti et al. 2020). Seismicity data were taken from the Italian Seismological Instrumental and Parametric Database (ISIDe) at: http://terremoti.ingv.it/en/iside. b) Geological cross-section of the external Northern Apennines (modified and redrawn after Boccaletti et al. 2011).

The NA complex orogenic architecture fits well the seismotectonic framework of the belt **(Fig. 3.1a)**. Seismicity linked to the compressional tectonic regime is presently distributed both along the thrust front of the exposed belt and the frontal arcs (Emilian and Ferrarese fold systems) buried below the Holocene alluvial deposits (Pieri and Groppi, 1981; Massoli et al., 2006; Pauselli et al., 2006; Picotti and Pazzaglia, 2008; Mantovani et al., 2014; 2019). The latter are genetically associated with blind thrusts (e.g., Bartolini et al., 1983; Boccaletti et al., 1985; 2011), which are the seismogenic source of the 2012 Emilia seismic sequence and accommodate a maximum compressive stress oriented approximately N-S (e.g., Pizzi and Scisciani, 2012; Pondrelli et al., 2012). The recent to current activity of these contractional structures is also documented by the differential uplift of the Padan foredeep deposits and river terraces (Boccaletti et al., 2011), with the NE side systematically affected by higher uplift that the SW side. Seismicity linked to the extensional tectonic regime, on the other hand, is attributed to the NW-SE-striking, SW-dipping basin-boundary normal faults cited above that affect the most internal (southwestern) part of the belt (Mantovani et al., 2014).

3.2.2 The Epiligurian formations

3.2.2.1 Stratigraphic setting

The internal succession of the Epiligurian Basins **(Fig. 3.2a)** reflects a complex geological evolution and is characterised by regional unconformities that directly track the evolution of the underlying wedge (Ricci Lucchi, 1986; Amorosi et al., 1995; Amorosi et al., 1996; Cibin et al., 2001).

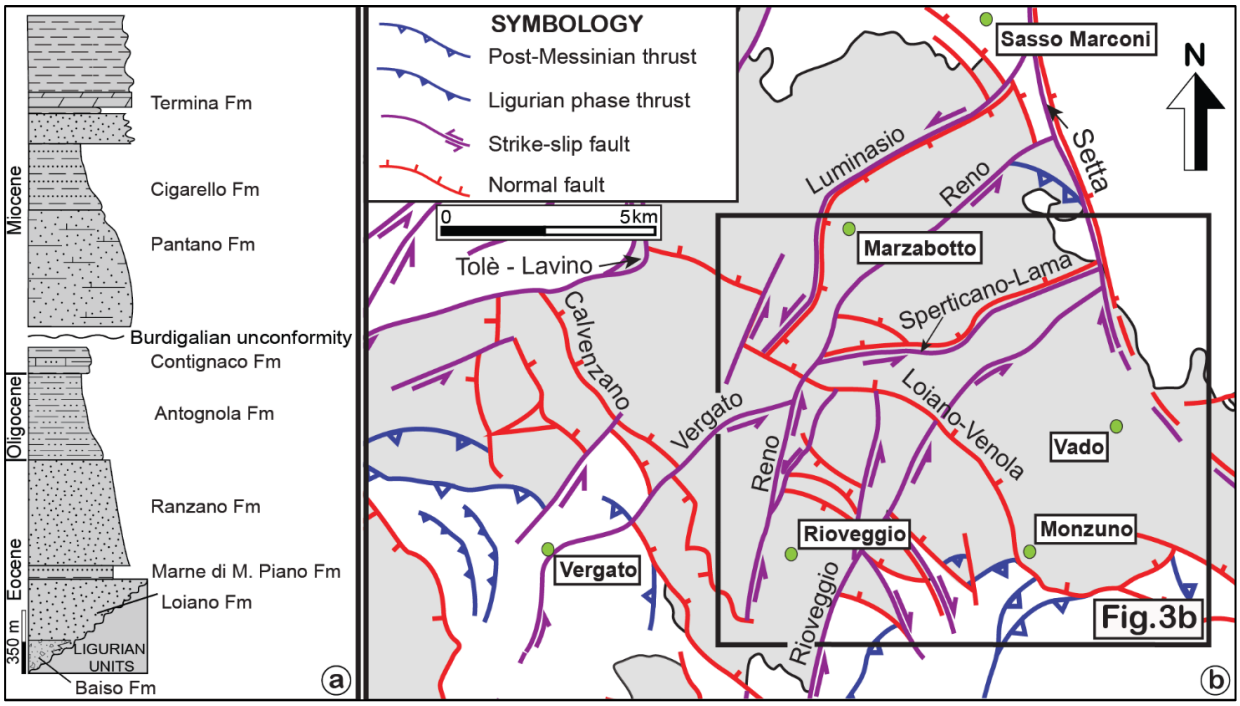

Figure 3.2 - a) Schematic Epiligurian sedimentary succession; b) Structural-tectonic scheme of the Marzabotto Basin and surroundings, which illustrates the main fault systems affecting the Marzabotto Basin in the study area (modified after Panini et al., 2002). Faults marked by double red and purple lines represent earlier strike-slip faults that were later reactivated as normal faults.

As an example, a major Burdigalian unconformity represents a key regional element marking an abrupt shift from a deep marine (pre-Burdigalian) to platform (post-Burdigalian) depositional environment during the progressive uplift of the wedge. Furthermore, the deposits of the pre- and post-Burdigalian sequences are characterised (even internally) by remarkable lateral thickness variations and local interdigitations and are in contact with each other along second-order angular erosive unconformities at the basin margins that tend to progressively disappear moving towards the depocenter (e.g., Amorosi et al., 1995). The Epiligurian sedimentary succession is also characterised by

basal erosive unconformities **(Fig. 3.2a)** marking the beginning of mass-transport processes during the uplift of the underlying wedge (Barbero et al., 2017).

The base of the Epiligurian succession **(Fig. 3.2a)** is represented by the Baiso Fm. (upper Lutetian-Bathonian), which consists of mudflow and debris flow deposits. The Baiso Fm. is overlain by the Loiano Fm. (upper Lutetian), a turbiditic sequence of resedimented course- to fine-grained arkosic sandstone with channel-fill facies. Upwards, the Marne di Monte Piano Fm. (Bathonian-Priabonian), consists of greenish-reddish clayey marl and marly clay commonly poorly or not stratified. Above, the Ranzano Fm. (middle-upper Rupelian) is characterised by sandstone interlayered with shale related to a slope-basin depositional environment. Moving up, the Antognola Fm. (Chattian-Aquitanian) consists of hemipelagic marl and pelite, intercalated with turbiditic arenaceous beds deposited in a slope depositional environment. Higher up, the Contignaco Fm. (lower Burdigalian) consists of dark grey marl mixed with turbiditic terrigenous currents deposited in a slope depositional environment transitional to hemipelagic conditions.

Above the major Burdigalian unconformity **(Fig. 3.2a)**, the Pantano Fm. (upper Burdigalian-lower Langhian) is characterised by very fine calcarenite and greyish siltstone, with poorly developed or even locally absent bedding, intercalated by coarse arenaceous resedimented beds typical of a slope depositional facies.

The upward transition to the Cigarello Fm. (lower Langhian-Serravallian) is the expression of a complex palaeogeographical evolution with the drowning of the

Burdigalian platform and the sedimentation of a pelitic marly-sandy and poorly sorted, locally cemented, arenaceous sequence.

The top of the Epiligurian sedimentary succession is formed by the Termina Fm. (upper Serravallian-lower Messinian), which consists of poorly stratified clayey marl interspersed with fine arenaceous intercalations typical of a transitional-to-outer shelf depositional environment. The Epiligurian formations are overlain by deposits of the Intra-Apenninic Pliocene basinal sequence, which is composed of conglomeratic-arenaceous deposits related to a distal coastal plain- to deltaic plain depositional environment (e.g., Amorosi et al., 2002).

3.2.2.2 Structural setting

Different deformation structures, styles and stress regimes have been documented for the Epiligurian formations of the NA (e.g., Capitani and Sasso, 1994; Ottria, 2000; Antonellini and Mollema, 2002; Panini et al., 2002; Artoni et al., 2006; Balocchi, 2014; Piazza et al., 2016; Balocchi and Santagata, 2018; Del Sole et al., 2020; **Fig. 3.2b)**. Two main compressional phases affected the Marzabotto Epiligurian Basin during the early Oligocene and the early Aquitanian to produce N-S and NW-SE-striking and NE- and SW-dipping thrusts (e.g., Catanzariti et al., 1999; Panini et al., 2002). Ottria (2000) even documented SW-vergent thrusts and associated km-scale recumbent folds deforming the Epiligurian formations during the late Eocene-Oligocene. During the Rupelian to Serravallian, sedimentation in the area was strongly controlled by the development of a major NE-SW left-lateral transpressive deformation zone that exerted a long-term control

on the local syn-shortening Epiligurian sedimentation (Piazza et al., 2016). Subsequently, a stress field dominated by N-S compression ensued, leading to the formation of major left- and right-lateral conjugated fault systems-oriented NNE-SSW and NNW-SSE, respectively (Panini et al., 2002; Balocchi, 2014). The NNE-SSW-striking left-lateral faults controlled the lateral juxtaposition of the Ligurian units against the Epiligurian formations (Reno, Rioveggio and Vergato Faults in **Fig. 3.2b**). Some of these strike-slip structures (e.g., Grizzana Morandi and Loiano-Venola Faults in **Fig. 3.2b**) were later reactivated as normal faults in response to N-S extension during the Pleistocene (Balocchi, 2014). Meso-to-micro-scale subsidiary structures, such as deformation bands within the highly porous sandstone of the Loiano Fm., have been reported to occur in proximity to the main normal faults dissecting the area, thus providing evidence of structural control on fluid flow atop the wedge units (Antonellini and Mollema, 2002; Del Sole and Antonellini, 2019; Del Sole et al. 2020).

3.3 Methods

A cartographic review of the study area was first carried out by consulting the geological maps available at the 1:50,000 and 1:25,000 scales that are freely available from the link https://datacatalog.regione.emilia-romagna.it/catalogCTA/. Then, we performed detailed structural mapping at the 1:10,000 and 1:5,000 scale in the Marzabotto Basin, to the south of the Bologna foothills, where the complete Epiligurian succession is well exposed over an area of about 200 km^2. We collected more than 500 orientations for bedding and tectonic structures (faults and associated structures) at 27 representative structural sites

from the pre- and post-Burdigalian formations, with the aim to constrain the local structural framework. The kinematics of the studied fault segments were determined by classical field criteria such as fault offset, growth fibres and secondary structures associated with faults (e.g., Petit, 1987; Doblas, 1998). The results of our structural investigations are synthesised in geological-structural maps and representative geological cross-sections (Figs. 3.3 and 3.4).

Finally, a remote sensing analysis of lineaments was carried out with the aim to define their geometry at the scale of the entire NA belt where the Epiligurian formations are exposed. We used the geo-referenced vectorial database of linear structural elements (WMS, WFS and WCS layers) provided by the Progetto CARG (CARtografia Geologica) and made available at the *minERva* portal (https://datacatalog.regione.emiliaromagna.it/(PortaleminERVA); *last access March 2022).* The remote sensing analysis was carried out for structures affecting both the pre- and post-Burdigalian formations through the Structural Data Integrated System Analyser provided within the DAISY 3 (v5.40) software (Salvini, 2002).

3.4 Structural data

3.4.1 General structural setting

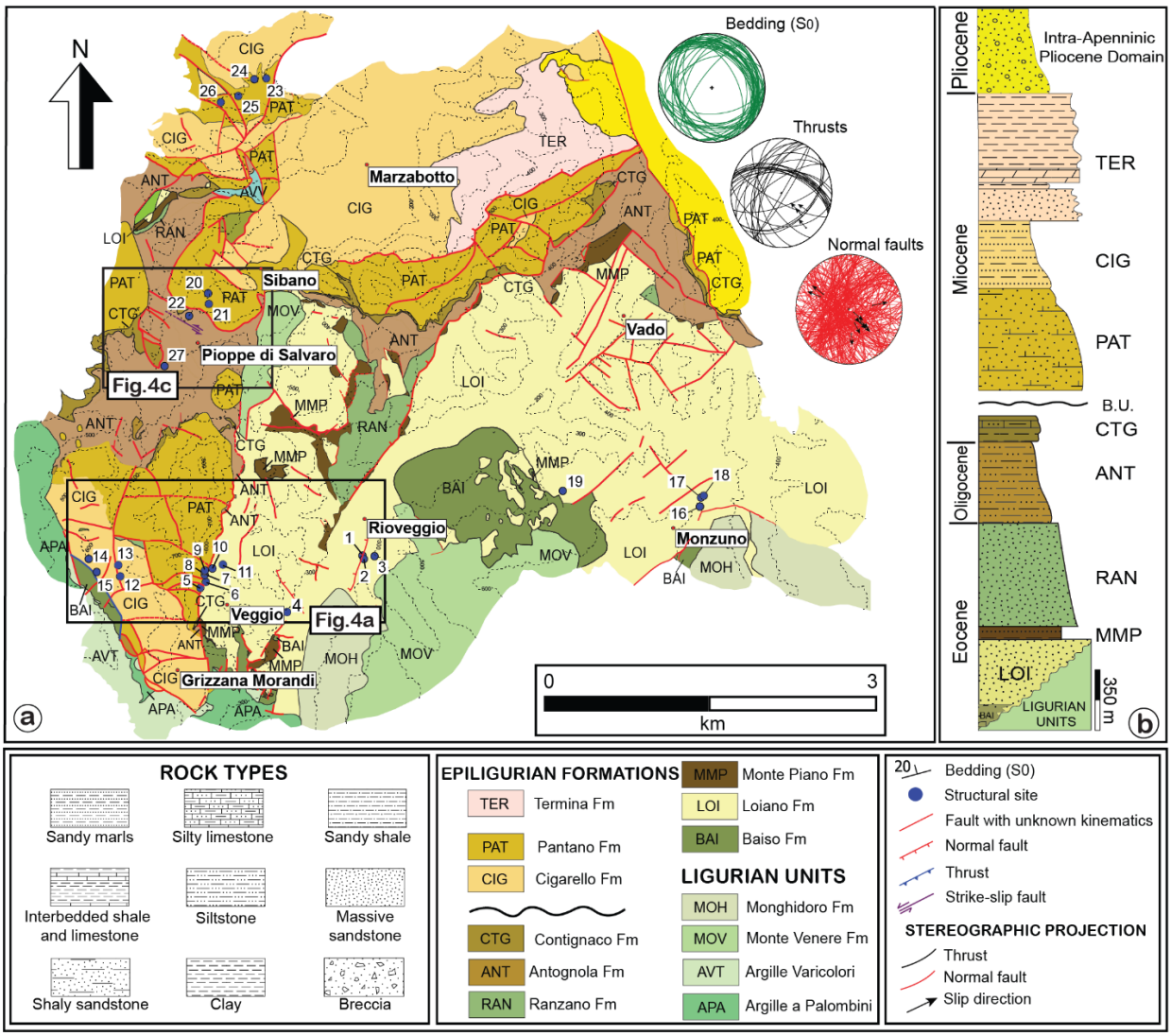

Figure 3.3 - a) Structural map of the study area based on the geological map of the Emilia-Romagna Region website (https://datacatalog.regione.emilia-romagna.it/(PortaleminERva)). The inserts report the cumulative stereographic projections (Schmidt net, lower hemisphere projection) of the main structural features (bedding, thrusts and normal faults). The area covered by the figure is shown in **Fig. 3.2**; b) Stratigraphic column illustrating the Epiligurian formations defining the sedimentary succession in the Marzabotto Basin.

The Marzabotto Basin **(Fig. 3.3a)** is a geographically isolated basin that well preserves the entire Epiligurian succession between the underlying Ligurian units and the overlying Intra-Apenninic Pliocene Domain **(Fig. 3.3b).** The Epiligurian formations are evenly distributed in the Marzabotto Basin, although they exhibit clear lateral variations of thickness across it.

The entire stratigraphy in the Marzabotto Basin dips between 20° to 40° monoclinally towards the NE, although the bedding locally dips to the WSW at low-to-very low angle **(Fig. 3.3a)**. To the south of the basin, the pre-Burdigalian Epiligurian formations (e.g., the Baiso Fm. and Loiano Fm.) rest above the Ligurian units through an erosional angular unconformity or through tectonic contacts. To the north, the post-Burdigalian units (e.g., Pantano Fm., Cigarello Fm. and Termina Fm.) dip below the Pliocene Domain. In the central portion of the basin, the Ligurian Domain crops out as inliers between the Epiligurian formations, the boundaries between them being commonly controlled by high-angle faults showing variable orientations. Tectonic structures directly influence the distribution of the Ligurian and Epiligurian sedimentary successions across the entire Marzabotto Basin. In particular, the stratigraphic-structural architecture of the basin suggests the presence of a transfer zone at basin scale with a general transport towards the NNE. This is also reflected in the lateral continuity of the lithological units, which commonly crop out as relics and isolated bodies (e.g., Baiso Fm., Marne di Monte Piano Fm. and Ranzano Fm. in **Fig. 3.3**), especially in the south and northeastern sectors of the area. In particular, the pre-Burdigalian Epiligurian formations exhibit a greater

stratigraphic complexity and poor outcropping lateral continuity than the post-Burdigalian fms. In addition, also the contact to the upper Pliocene Domain, which crops out only in the north-eastern portion of the Marzabotto Basin, reflects both a stratigraphic and tectonic component, with the former represented by an erosive angular unconformity and the latter connected with faulting along a right-lateral transfer zone, which caused the displacement of the Monte Rumici Fm. to the SE **(Fig. 3.3a)**.

The tectono-stratigraphic relationships between the pre-and post-Burdigalian Epiligurian formations within the Marzabotto Basin are analysed in detail in two representative areas both in plain and cross-section view **(Fig. 3.4)**.

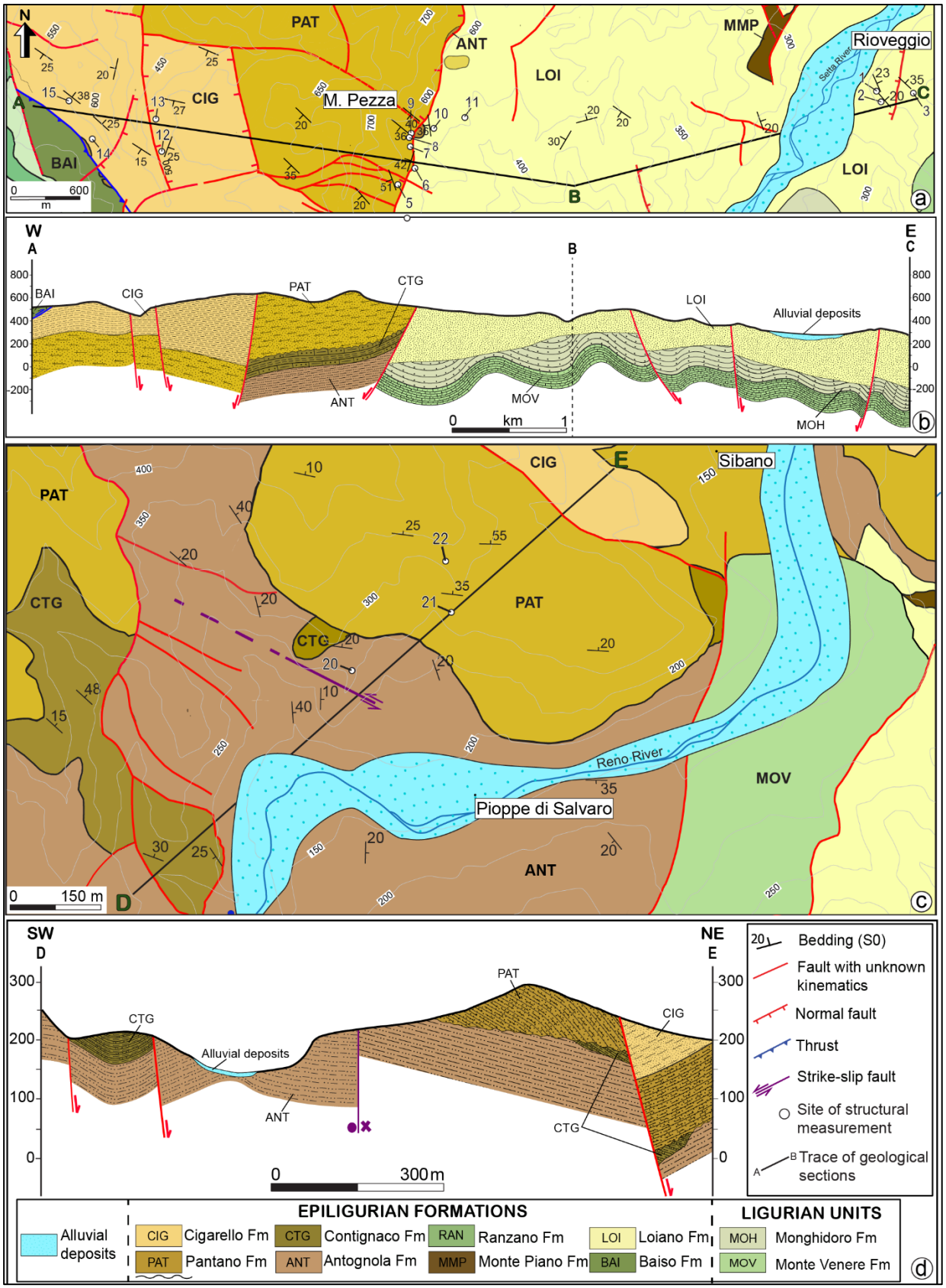

Figure 3.4 - a,c) Zoom onto the central/southern and northwestern areas of the Marzabotto Basin; b,d) Geological cross-sections representing the main structural

relationships between pre- and post-Burdigalian Epiligurian formations.

The Epiligurian formations contain the mutual intersection between variably oriented faults (striking from NNE-SSW to NNW-SSE, to WNW-ESE) to form a polygonal geometry in plain view. For example, a low angle NW-SE-striking and SW-dipping thrust juxtaposes the Baiso Fm. against the Cigarello Fm. in the western part of the investigated area (**Fig. 3.4b)**. Moving to the E, the Epiligurian formations are affected by NNW-SSE and N-S-striking normal faults that dip either to the E or W, which cut and variably downthrow the basin infill with throws from a few decametres up to several hundred metres. The most significant extensional structure analysed in that area is a N-S-striking, W-dipping normal fault that juxtaposes the Pantano Fm. against the Loiano Fm. along the southeastern slope of Monte Pezza **(Fig. 3.4a)**.

The eastern part of the geological section of **Figure 4b** illustrates the hybrid nature of the contact between the Epiligurian formations and the Ligurian Domain below, which stems from both a stratigraphic and tectonic origin. In particular, the stratigraphic component is represented by an erosional unconformity between the Loiano Fm. and the Monghidoro and Monte Venere Fm., while the structural aspect thereof relates to the contact between the Ranzano and Antognola fms. and the underlying Monte Venere Fm. through a normal fault **(Fig. 3.4b)**.

Figure 3.4c illustrates how high-angle faults control the lateral juxtaposition of pre-Burdigalian (Antognola and Contignaco fms.) and post-Burdigalian (Pantano and

Cigarello fms). In particular, from the SW to the NE, the Antognola Fm. Is affected by NW-SE-striking and NE-dipping high angle normal faults while, moving to the NE, it is cut by a NE-SW-striking left-lateral fault that displaces the pre-Burdigalian Epiligurian formations towards the north-western sectors of the basin **(Fig. 3.4d)**. In the north-eastern part of the basin, the Epiligurian succession is affected by a NW-SE and NE-dipping normal fault, which puts in contact the Cigarello Fm. in the hanging wall with the Pantano Fm. in the footwall **(Fig. 4d)**, thus down-throwing the succession towards the NE **(Fig. 3.4c)**.

The Contignaco Fm. crops out as lensoidal bodies, with a significant lateral variation of thickness below the Pantano Fm. due to the presence of the erosional Burdigalian unconformity as shown in the geological section of **Figure 3.4d**. Between Pioppe di Salvaro to the south and Sibano to the north **(Fig. 3.4c)**, the tectonic contact between the pre-Burdigalian Antognola Fm. and the Ligurian Monte Venere Fm. (**Figs. 3.3a** and **3.4c**) reflects the NNE-SSW-striking Reno Line, which is ascribable to the left-lateral transcurrent tectonic event mentioned above.

All the mentioned different tectonic structures have been studied and characterised according to their position with the Epiligurian stratigraphy and are reported accordingly **(Fig. 3.5)**. They have been sorted in homogeneous and presumably coeval kinematic/faulting classes and are described below.

3.4.2 *Tectonic structures analysed in pre-Burdigalian Epiligurian formations*

Within the pre-Burdigalian formations (e.g., Loiano andAntognola Fm.; structural stops n° 1-3, 16-18, 20-23 in **Fig. 3.3a**) we observed: i) reverse, ii) normal and iii) strike-slip faults **(Figs. 3.5-3.7)**. Due to the granular and porous character of the deformed rock types, deformation bands (DBs) are very common and, as such, have also been systematically investigated **(Fig. 3.7)**.

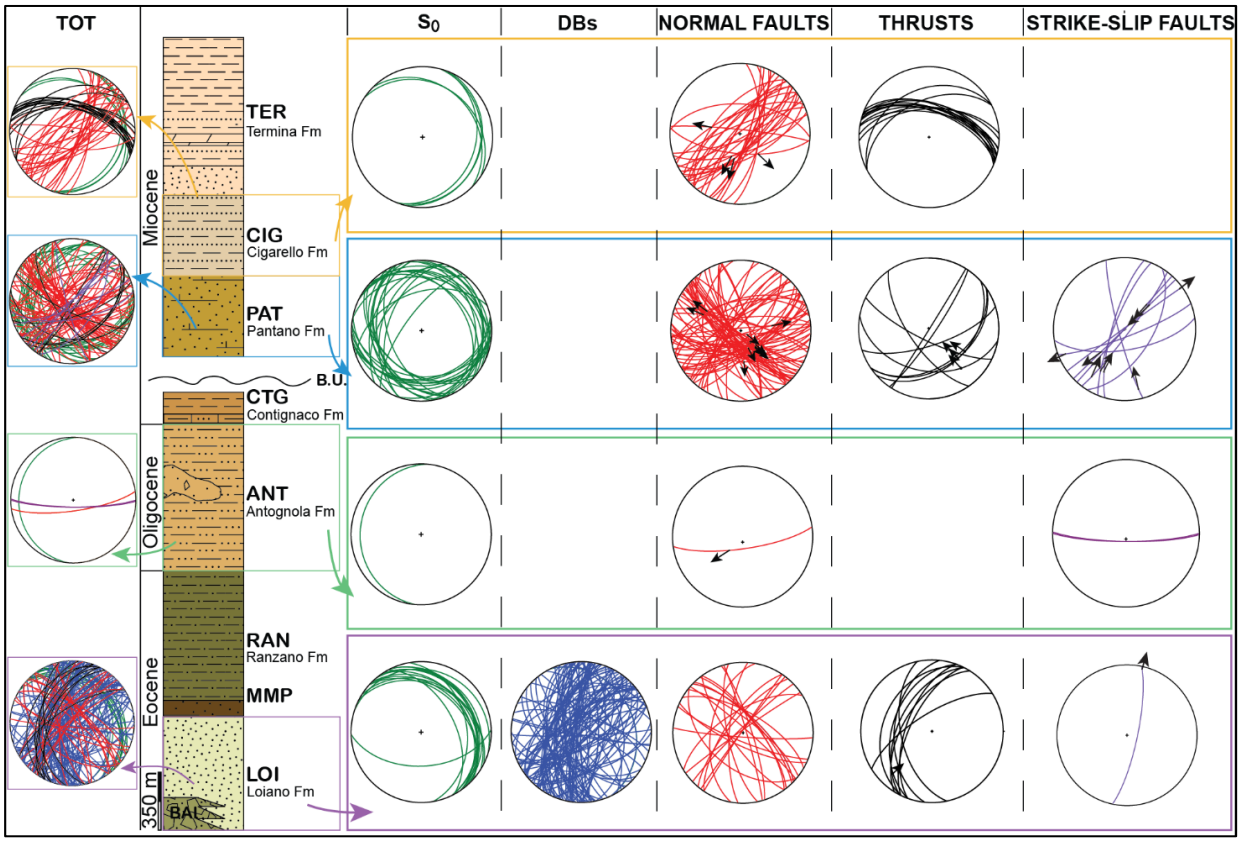

Figure 3.5 - Stereographic projections (Schmidt net, lower hemisphere projection) of bedding and faults sorted according to their kinematics and stratigraphic position.

It is not uncommon to find both reverse and normal faults at the same outcrop, which makes it possible to study in detail their cross-cutting relationships **(Fig. 3.6a)**. Thrusts

consist of NNE-SSW-striking and moderately WNW-dipping single slip surfaces associated with cataclastic layers and fractured damage zones **(Fig. 3.6b)**. Fault surfaces have a general planar morphology and decametre persistence at the outcrop. They locally contain preserved slickensided surfaces, mostly with abrasion striae **(Fig. 3.6c)**. Slickenlines exhibit pitch values of c. 30°, indicating an oblique component of slip **(Fig. 3.5 and 3.6a)**. The analysis of kinematic indicators such as stratigraphic offset, dragging of bedding into fault surfaces and Riedel shears, indicate top-to-the NE thrusting **(Fig. 3.6 b-c).**

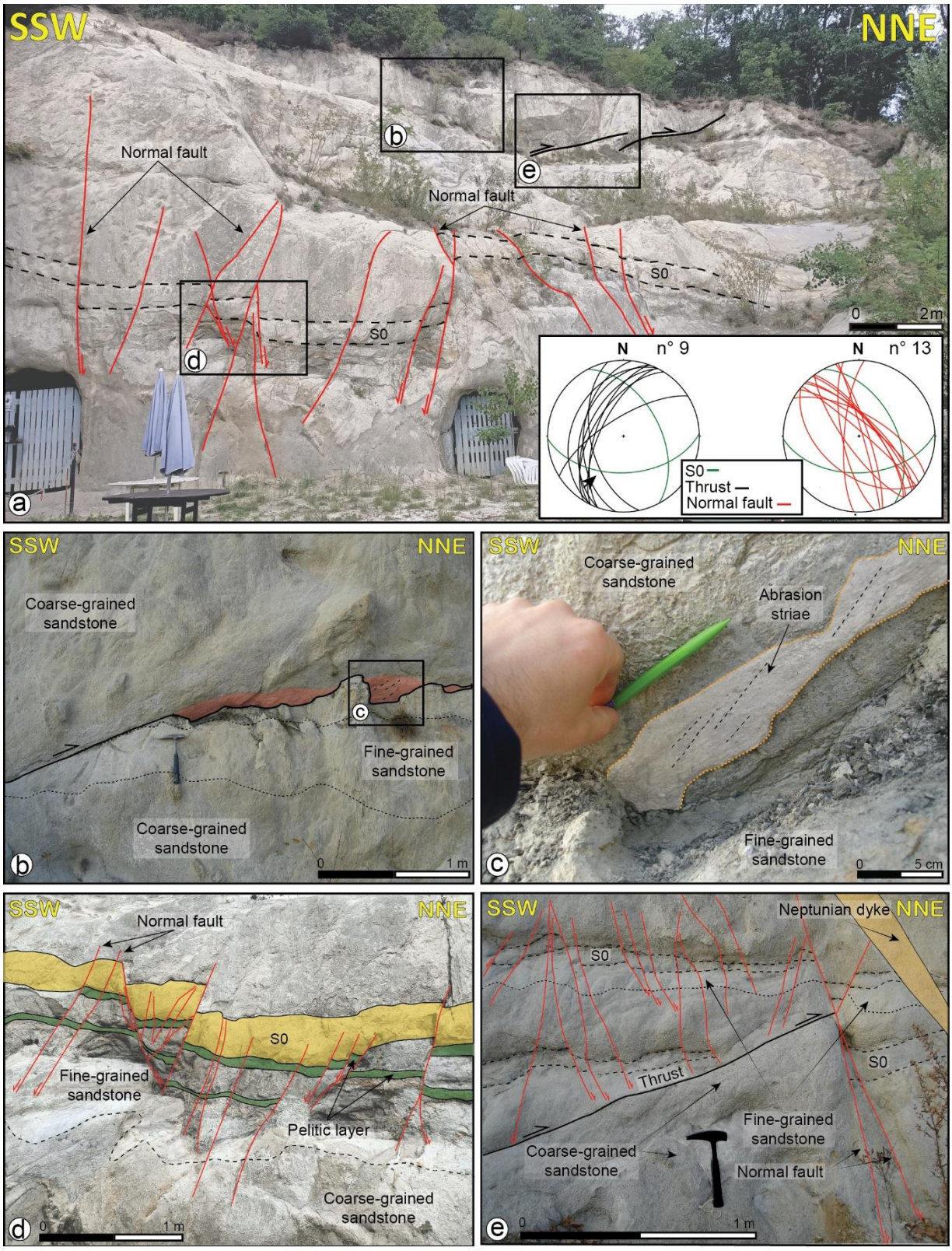

Figure 3.6 - a) Loiano Fm. outcrop located in the central/southern part of the study area. b) SSW-dipping reverse fault plane with a gently dipping planar morphology decorated by abrasion striae (c), indicating top-to-the NNE tectonic transport; d) Normal faults cut

across coarse-grained sandstone beds (S0) with a centimetric to decametric offset; e) SSW-dipping reverse fault with an oblique component (black solid line) cut by a NNE-dipping normal fault.

Normal faults strike either NE-SW or NW-SE and dip to the SW, NE or NW at a relatively high angle (average dip: 73°) or even vertically (Figs. 3.5 and 3.6a). They consist of decametric isolated slip segments without appreciable damage zones. At the outcrop, NW-SE normal faults have a general planar to gently curvilinear geometry, cross-cut bedding at high angle and accommodate centimetric to decametric offsets **(Fig. 3.6d)**. The analysis of the stratigraphic offset, together with the occurrence of synthetic shear fractures, attests to a normal-sense kinematics **(Fig. 3.6d and e)**. Cross-cutting relationships document that normal faults systematically cut and displace the aforementioned thrusts **(Fig. 3.6a, e)**, thus providing evidence for a relative chronology of faulting.

In the southern part of the Marzabotto Basin, the resedimented course- to fine-grained arkosic Loiano Fm. are affected by normal faults with a complex structural architecture represented by the occurrence of deformation bands (see also Antonellini, 2002; Del Sole et al., 2020; **Fig. 3.7a, b**).

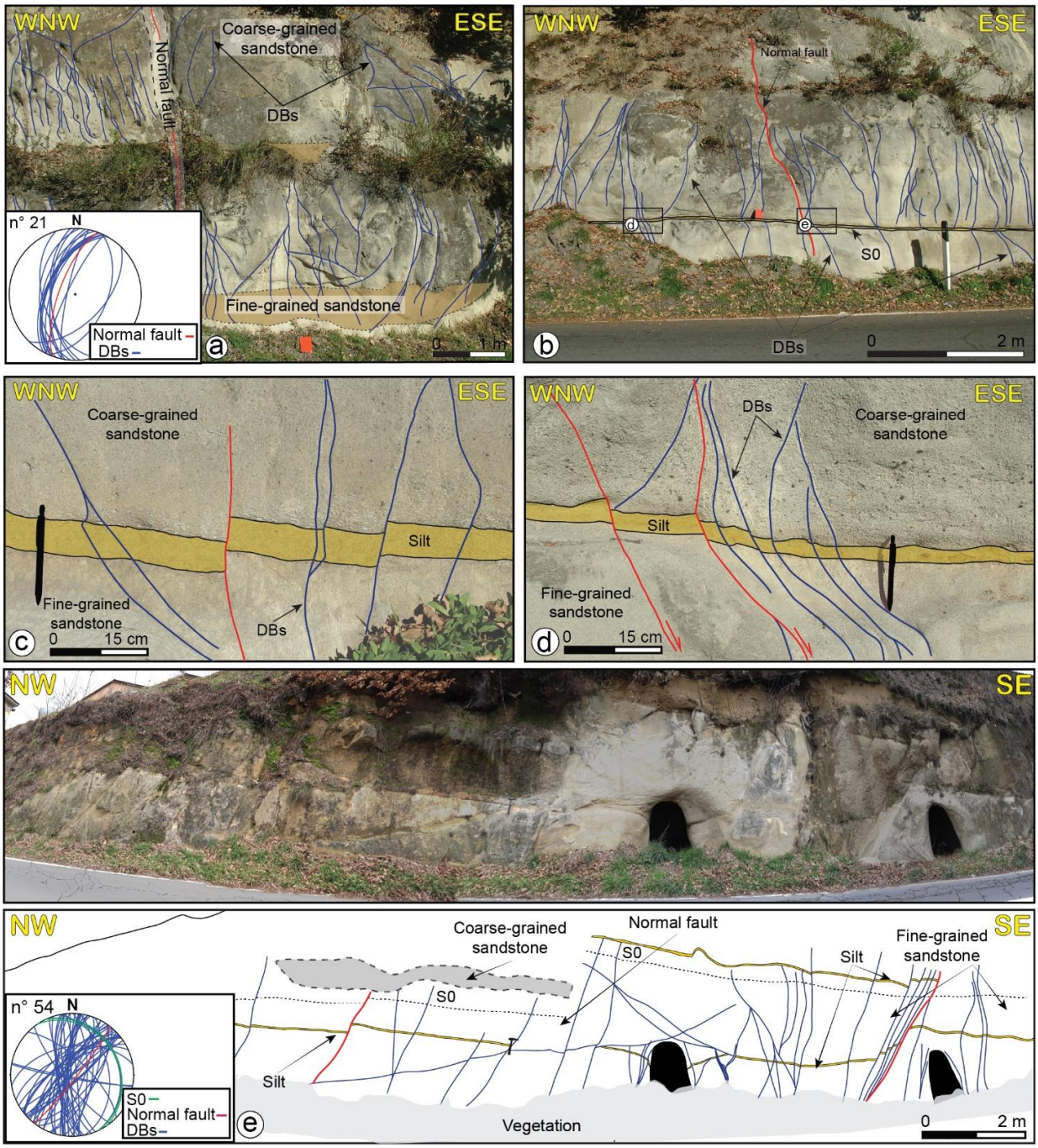

Figure 3.7 - a, b, e) Loiano Fm. outcrops located in the central part of the study area where WNW and ESE-dipping DBs (blue solid lines) occur as both single bands and clusters. The coalescence of DBs develops fault zones with a well-defined main slip surface (red solid lines); c, d) DBs deform and cut the bedding represented by a silty-sandy level of about 3-5 cm thick, accommodating variable offsets (from a few mm to 1 m).

Deformation bands occur as either single structures or in clusters. They mainly strike NNE-SSW (average attitude: 225°), and, subordinately, WNW-ESE (average attitude: 334°; see stereographic projection in **Fig. 3.5**). The dip angle of the deformation bands is generally medium-high (average 70°). They deform and cut across the bedding accommodating offsets between a few mm to 1 m **(Fig. 3.7c-d).** When approaching the main fault surfaces from an undeformed block, one can appreciate how deformation bands (i) tend to group into metre-thick deformation zones, (ii) systematically have their spacing decreasing from 1 m to 1-5 cm, and (iii) accommodate increasing cumulative offset from a few millimetres to half a metre **(Fig. 3.7a-e)**.

Strike-slip faults consist of single structures having generally a planar geometry and decametric persistence. They mostly strike NNE-SSW (strike attitude: 026°) and dip at high angle (average dip~77°) to the ESE **(Fig. 3.5)**. Kinematic criteria were defined based on the persistence of associated second-order fractures (pitch: 010°) and shears (R, R' and T fractures) and they indicate dominant right-lateral kinematics for the WNW-ESE-striking segments.

3.4.3 Tectonic structures analysed in post-Burdigalian Epiligurian formations

Reverse, normal and strike-slip faults cut across the post-Burdigalian formations (e.g., Pantano and Cigarello fms.; structural sites n° 5-15, 20-27 in **Fig. 3.3a**).

Thrusts **(Figs. 3.8a, b and 3.9a)** include both WNW-ESE and NE-SW-striking slip surfaces dipping either to the NE or SE, respectively, at a relatively high angle (average dip~64°).

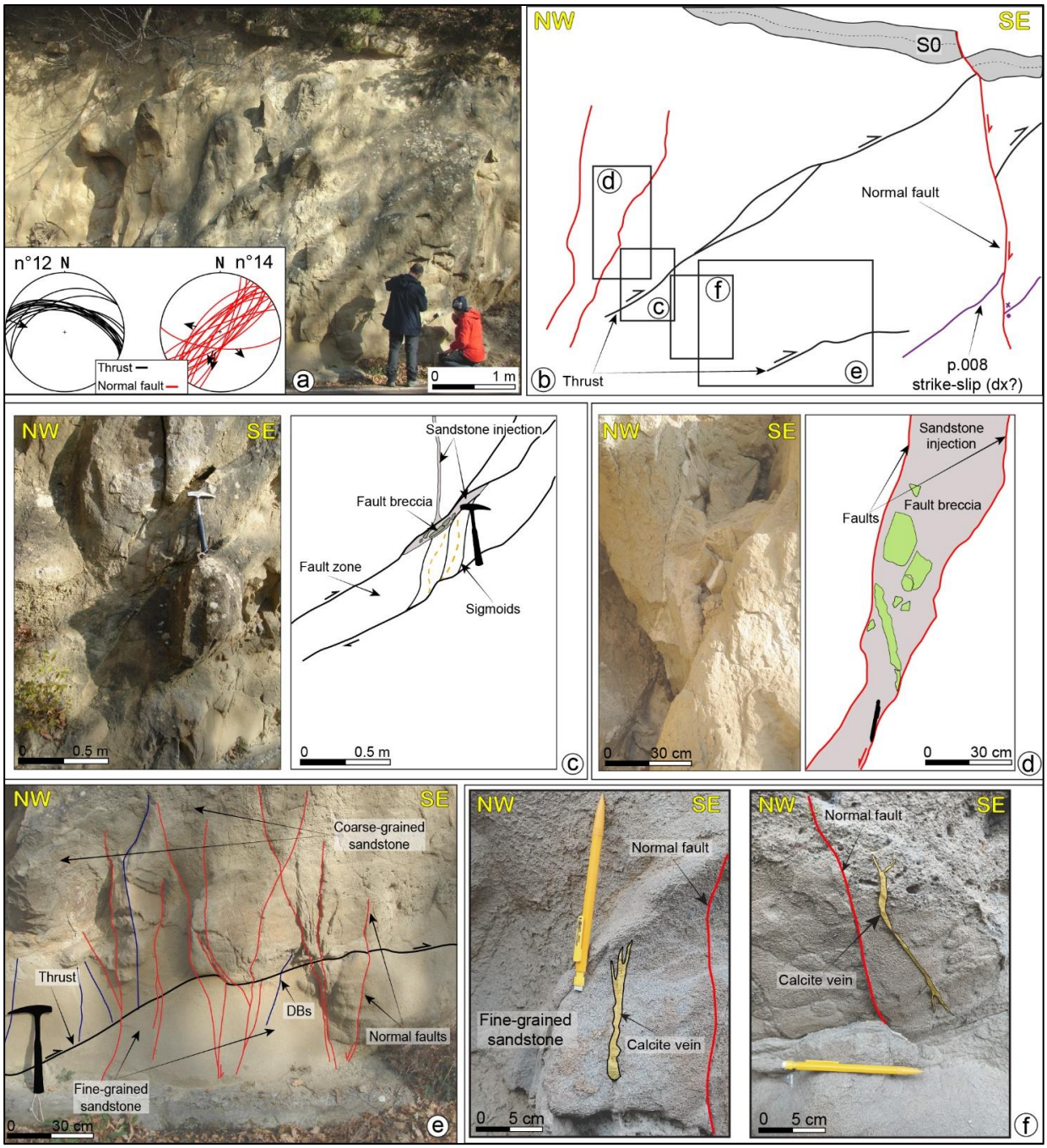

Figure 3.8 - a) Cigarello Fm. outcrop located in the south-eastern part of the study area. b) NW-dipping thrusts cut by a SE-dipping normal fault, characterised by a sigmoidal lens shape damage zone; c) Zoom of the NW-dipping reverse fault with a white-coloured sandstone injection; d) Fault breccia and sandstone injection in the damage zone of a NW-dipping normal fault; e) Cross-cutting relationship between reverse and normal faults viewed at a smaller scale; f) Calcite veins associated with extension.

Those dipping to the NE consists of a main slip surface, with a gently curvilinear morphology associated with a well-developed damage zone, with a thickness of 20-30 cm **(Fig. 3.8c)** that is instead missing along fault planes dipping to the SE. Within the damage zones, there occur sigmoidal lithons of dismembered finer arenaceous beds, the asymmetry of which has been used to constrain an overall top-to-the NW sense of shear **(Fig. 3.8c)**. Reverse fault planes are commonly associated with slickensides and slickenlines **(Fig. 3.9b)** with pitch values between 48° and 82° (see stereographic projections in Fig. 5). Within the damage zones, there locally occur white, altered sandy injections parallel to and along the slip surfaces, side by side with cm-thick fault breccia **(Fig. 3.8c)**.

Normal faults dip steeply (average dip ~ 68°) to vertical and strike from NW-SE to NE-SW (average attitude: 284° and 42° see stereographic projections in **Fig. 3.5**). At the outcrop, fault surfaces are generally several meter long, have a smooth to planar morphology and bear slickenlines with pitch between 70° to 85° **(Fig. 3.5)**. These normal faults cut across and displace with decametric to metric offset the thrusts described above **(Figs. 3.8b, e)**. These faults are locally characterised by decimetre-thick damage zones filled by altered white sandy injections and lenses of fault breccia **(Fig. 3.8d)**. Normal faults are locally associated with vertical, NE-SW-striking calcite veins formed during extension **(Fig. 3.8f)**. Finally, NNE-SSW-striking (average attitude: 202°) strike-slip fault planes, dipping either to WNW or ESE, are associated with WNW-ESE-striking normal faults **(Fig. 3.9c)**.

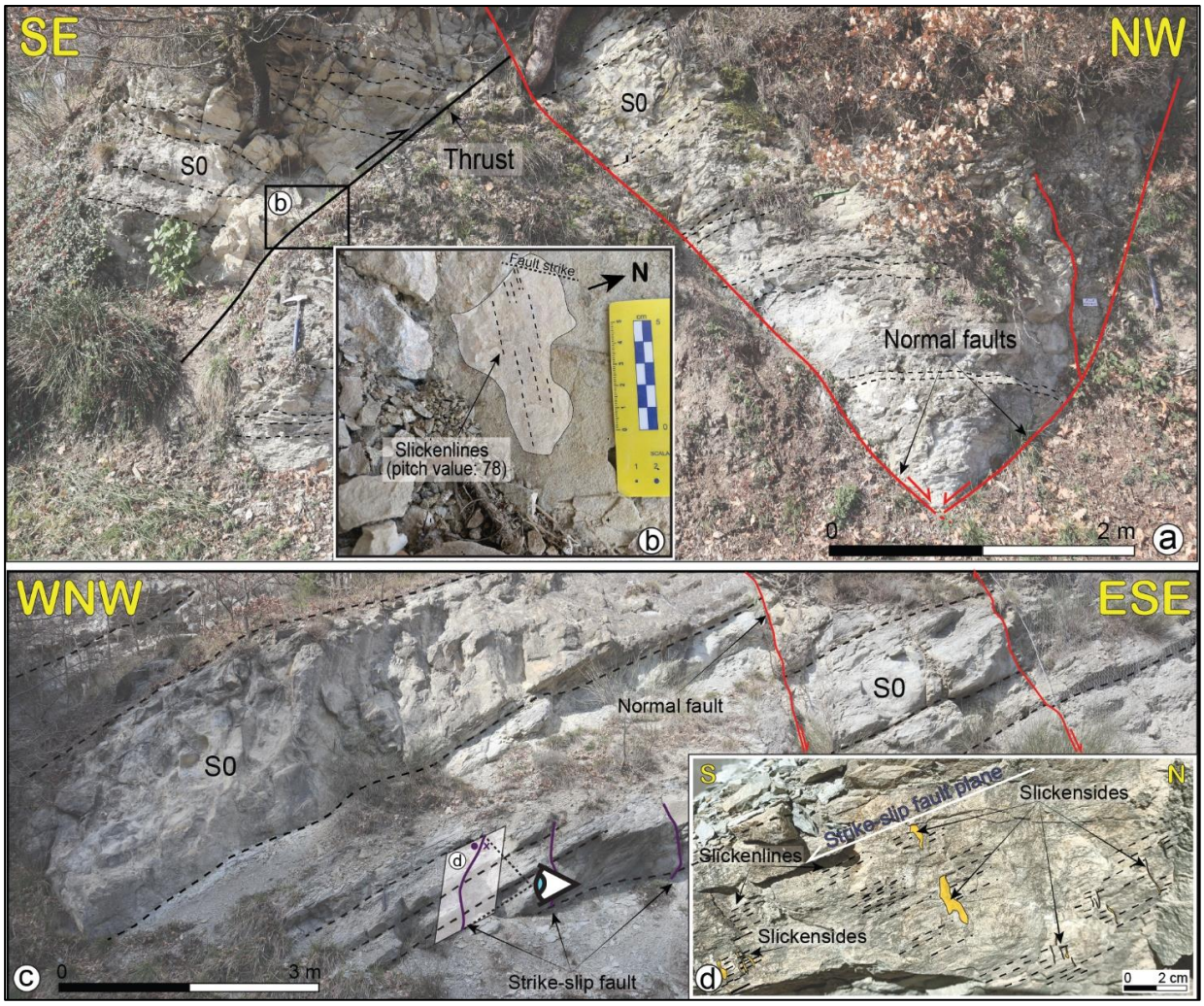

Figure 3.9 - a) Pantano Fm. in the central part of the study area deformed by a SE-dipping, top-to-the NW reverse fault and by NW and SE-dipping normal faults; b) The reverse fault plane hosts clear slickenlines; c) Pantano Fm. cut and deformed by an ESE-dipping normal fault that cuts the bedding with a metric offset, associated with NNE-SSW-striking and WNW and ESE-dipping strike-slip fault planes characterised by almost planar slip surfaces bearing slickenlines and slickensides (d).

These minor structures are characterised by planar slip surfaces bearing slickenlines and slickensides **(Fig. 3.9d)** with pitch values between 15° and 35° (see stereographic projection in **Fig. 3.5**). Criteria kinematic analysis based on R-shears and T fractures suggests a dominant left-lateral kinematics for the NNE-SSW-striking strike-slip faults.

3.5 Lineament analysis

Lineaments affecting all the Epiligurian Basins in the area between Bologna and Parma (Figs. 3.1a and 3.10) have been remotely sensed and classified in terms of pre- or post-Burdigalian age in relation to the mapped stratigraphic units. We acknowledge that the lineaments mapped within the either pre- or post-Burdigalian Epiligurian formations do not necessarily have an age corresponding to these periods of time. However, we use them to discriminate the structural patterns that affect only part of the whole Epiligurian sedimentary succession. Structures affecting the oldest formations (e.g., pre-Burdigalian) and not occurring in the youngest ones (e.g., post-Burdigalian) can be considered a threshold for constraining the variation of orientation and density of tectonic lineaments as a function of the affected Epiligurian sedimentary succession. This allows us to individuate temporal constraints on changes in faulting regime at the scale of the distribution of the Epiligurian basins along the Northern Apennines.

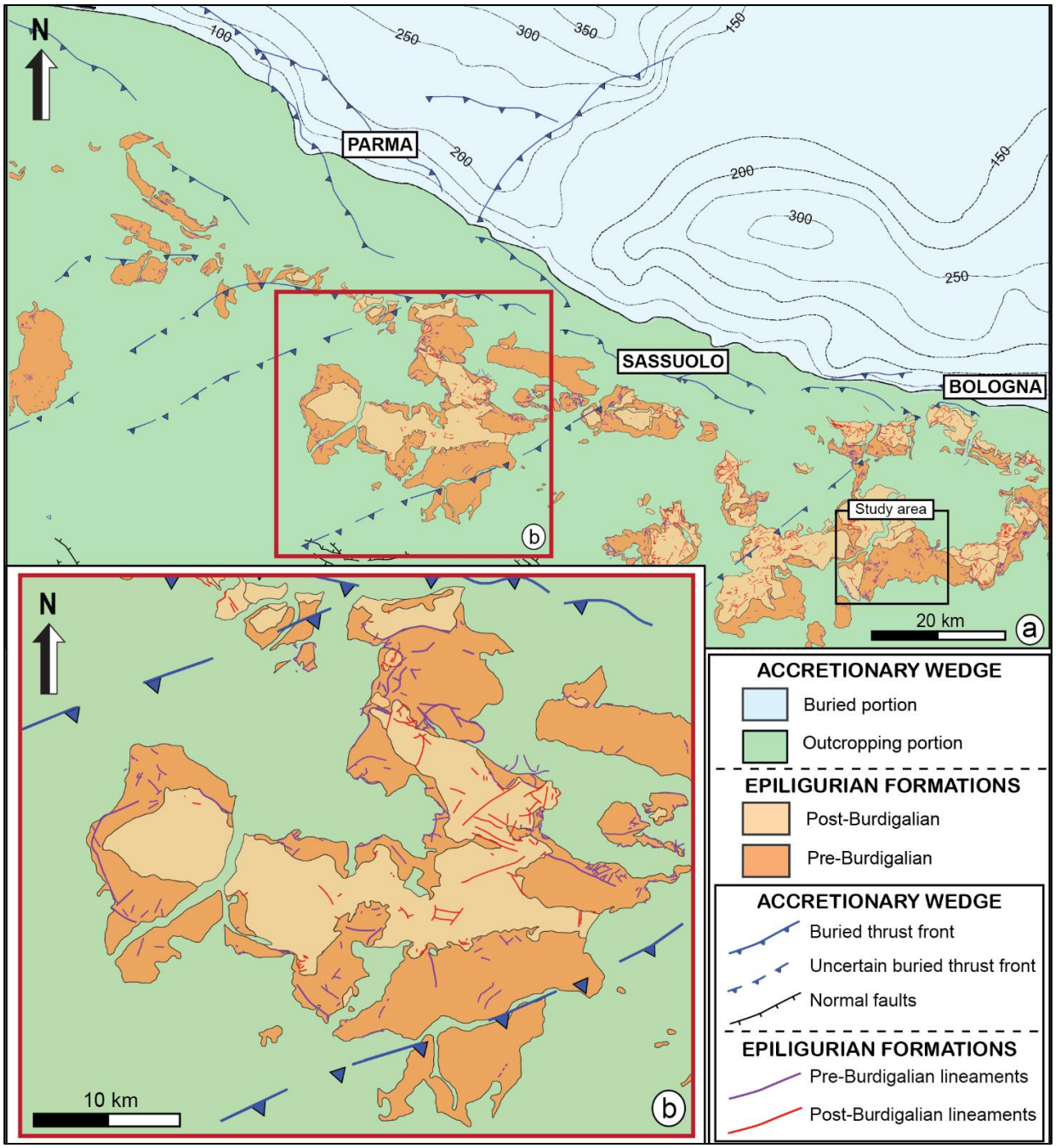

Figure 3.10 – a) Simplified geological map cantered on the structural lineaments cropping out in either pre- or post- Burdigalian Epiligurian Basins located in the area between Bologna to the SE and Parma to the NW. The study area is represented by the black square in the south-eastern portion of the map; b) Zoom of an example of an Epiligurian Basin located in the NW sector respect to the study area.

Our database was then additionally sorted according to the kinematics of the lineaments into i) normal faults, ii) thrusts, iii) strike-slip faults (without a defined sense of movement) and iv) undefined faults, i.e., faults without a clear kinematics **(Table 1)**.

Occurrence	Kinematics	n°
Pre-Burdigalian formations	Normal faults	21
	Thrusts	358
	Strike-slip faults	30
	Undefined faults	3989
Post-Burdigalian formations	Normal faults	81
	Thrusts	121
	Strike-slip faults	18
	Undefined faults	2735

Tab.1- Summary of the tectonic structures considered by the remote sensing analysis subdivided according to their kinematics and their occurrence in either pre- or post-Burdigalian Epiligurian formations (see **Fig. 3.10**). Kinematics is according to the fault attributes reported in the geo-referenced vectorial database of linear structural elements (WMS, WFS and WCS layers) provided by the Progetto CARG (CARtografia Geologica) and available at the *minERva* portal (https://datacatalog.regione.emiliaromagna.it/(PortaleminERVA)*; last access March 2022).*

To better understand the implications of the analysis of those lineaments, results are reported in here by describing separately lineaments occurring in pre- or post-Burdigalian units belonging to: i) the Marzabotto Basin; ii) other Epiligurian basins (remote and fieldwork data). For the comparison between structural elements, only normal faults and thrusts have been considered. A comparison is also made between lineaments mapped remotely in all Epiligurian Basins and fieldwork data from the Marzabotto Basin **(Fig. 3.11).**

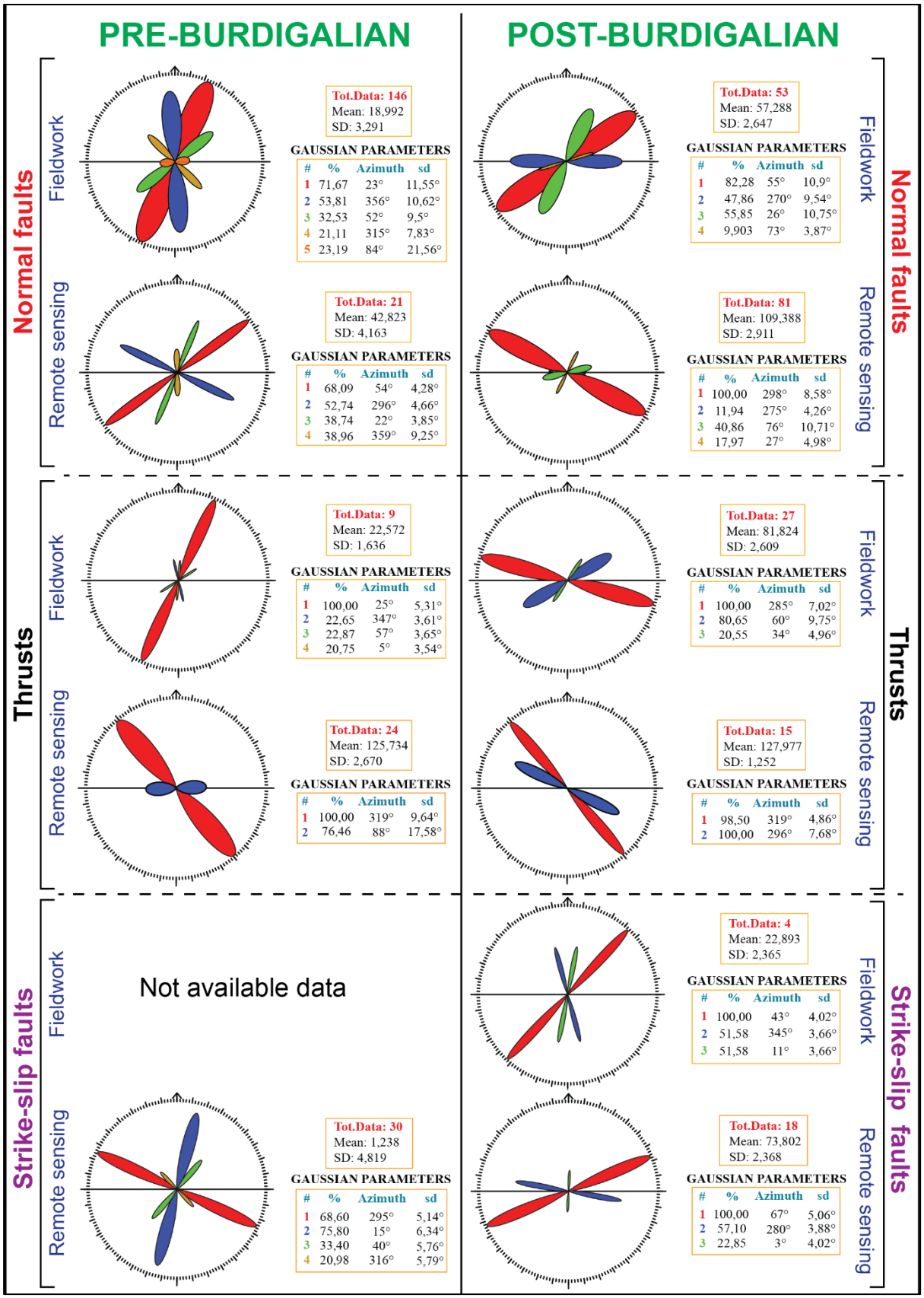

Figure 3.11 - Rose diagrams (Daisy 3 version 5.40; Salvini, 2002) reporting the strike values of the normal, reverse and strike-slip faults mapped in pre- or post-Burdigalian

Epiligurian formations. The red field represents the dominant trend while the brown field is the least representative. The tectonic readings include both field data (within the Marzabotto Basin) and remote sensing data (over all the Epiligurian Basin shown in **Fig. 3.10**).

3.5.1 Lineaments mapped in pre-Burdigalian Epiligurian formations

Normal faults are characterised by a preferred NE-SW strike for both the field data and remote sensing data, while thrusts strike NE-SW when constrained in the field and NW-SE when remotely sensed **(Fig. 3.11)**.

The analysis of strike-slip faults is not complete because of the lack of field data in the pre-Burdigalian succession. However, these tectonic structures are characterised by a dominant NW-SE direction in the remote sensing dataset.

3.5.2 Lineaments mapped in post- Burdigalian Epiligurian formations

Normal faults are characterised by a different orientation for the different analysed datasets (NE-SW for the fieldwork data and NW-SE for the remote sensing data), while thrusts show a preferred NW-SE orientation for both datasets **(Fig. 3.11)**.

Remotely mapped sinistral strike-slip faults strike NE-SW, in agreement with what has been mapped in the field but in contrast with the same faults mapped in the pre-Burdigalian units.

3.6 Discussion

3.6.1 Structural synthesis

The structural constraints derived from the Marzabotto Basin, integrated with other published data from field studies (Ottria, 2000; Antonellini and Mollema, 2002; Balocchi and Santagata, 2018), a re-interpretation of the available geological maps (Panini et al., 2002; Balocchi, 2014; Piazza et al., 2016), and results from our remote lineaments analysis, are used here to propose a model accounting for the local tectonic history as recorded by the Epiligurian basins during the syn- to post-orogenic evolution of the Northern Apennines (e.g., Boccaletti et al., 1985; Carmignani et al., 1995; Conti et al., 2020; Mantovani et al., 2019). Both the pre- and post-Burdigalian Epiligurian successions exhibit a tectonic history characterised by similar structural features and structural style, despite an important change of structure orientation that will be discussed farther down in this chapter.

Thrusts strike heterogeneously in the mapped area and they indicate both NE-SW and NW-SE shortening of the entire Epiligurian succession, as we could conclude also by lineament remote sensing analysis. This combined approach shows that the NW-SE-striking set is well recognisable for both the pre- and the post-Burdigalian succession. When discriminating the thrusts on the basis of their development with respect to the Burdigalian unconformity, we can say that the tectonic structures affecting the upper Lutetian Loiano Fm. may probably be ascribed to the lower Oligocene to lower Miocene tectonic phase documented in two other Epiligurian basins located in the axial and in the

frontal portion of the outcropping NA belt, where contractional deformation structures have been recognised within the sediments of Bartonian-Aquitanian age (Ottria, 2000; Balocchi and Santagata, 2018). However, lineament analysis shows that there is no correspondence between the orientations from the remote sensing analysis and those measured in the field. This is probably due to the different number of faults measured in the field compared to those in the regional dataset, the latter stemming from all the Epiligurian Basins and not only to the Marzabotto Basin. On the other hand, the NE-SW thrusts mapped within the post-Burdigalian units can be tentatively correlated with the post-Messinian compressional tectonic phase that controlled the juxtaposition of tectonic slices of Ligurian units on top of Epiligurian formations (Panini et al., 2002; **Figs. 3.3a and 3.4a, b**). In a northwestern side of the Northern Apennines (Val Secchia), the same tectonic framework has been identified with the Canossa-San Romano fault (Balocchi and Little, 2020), which was probably originated as a reverse fault and later, during the Messinian to Lower Pliocene, reactivated as a normal fault along the same surface. This caused the lowering of the lower part of the Epiligurian Succession and placing it in lateral contact with the Cassio Tectonic Unit (Ligurian Domain). During this time interval, a segment of the Canossa-San Romano system underwent a counter-clockwise rotation, developing a geometry with an anti-Apennine direction, which is interpreted as a left-lateral transpressive ramp (Bettelli et al., 1987a, 1987b; Balocchi and Santagata, 2018).

A strike-slip tectonic phase affected the Epiligurian formations after the shortening phase. The associated structures consist of NE-SW-striking, left-lateral faults that run

through the entire sedimentary succession, leading to the lateral juxtaposition of Ligurian and Epiligurian formations along the Rioveggio, Reno and Luminasio Faults (Panini et al., 2002; **Fig. 3.2b**). A comparison between the lineaments mapped remotely and field data is not possible because we do not have sufficient structural data to generate a statistically meaningful picture.

Extensional structures are rather pervasive in the entire Epiligurian succession, cutting and displacing the thrusts described above. We recognised three main sets of extensional structures as a function of their main strike and geometrical-structural properties (length, offset, thickness of damage zone, associated features):

a) Longitudinal (i.e., Apennines-oriented) normal faults consisting of high angle structures characterised by small (intraformational or intra-Epiligurian) stratigraphic offset. At the outcrop, they exhibit a curvilinear geometry, metre-to-decametre persistence and whitish alteration surfaces. They are barren of mineralised shear planes or thick damage zones. At the Marzabotto Basin scale, these mapped normal faults resemble the orientation and the kinematics of the Loiano-Venola and Calvenzano Faults that systematically determine the lowering of the succession towards the north-eastern sectors of the outcropping belt (Panini et al., 2002; Figs. 3.2b and 3a). Concerning their relationship with the remote sensing analysis of lineaments, these longitudinal normal faults correspond to the second-order class of structures reported on the rose diagrams shown in **Fig. 3.11**, showing a strike orientation of about NNW-SSE and WNW-ESE.

b) Transverse normal faults oriented approximately NNE-SSW (i.e., antiapennines) and that can be mapped both at the outcrop (metric persistence) and basin-scale (length greater than 1 km). These are tectonic structures recognised in the entire Marzabotto Basin that cause significant offsets within the Epiligurian formations of up to several kilometres and rework the early juxtaposition between the Ligurian and the Epiligurian formations. The structures consist of architecturally complex faults, with fairly planar morphologies and mineralised shear planes characterised by calcite veins from a few millimetres to a few centimetres thick. Within pre-Burdigalian deposits (i.e., the Loiano Fm.), normal fault planes are commonly associated with deformation bands that developed either as single, isolated planes or resulted from the progressive localisation of slip after clustering of these brittle structures. This set of normal faults corresponds to the structures that reactivated the Rioveggio, Reno, Vergato Faults **(Fig. 3.2)** in the Marzabotto Basin and, at the scale of the other Epiligurian basins, the Rupelian-Serravallian left-lateral faults. At the regional scale, these extensional tectonic structures might be correlated with the NNE-SSW-striking normal faults that affect the frontal part of the outcropping belt (i.e., at the southern edge of the Po Plain) deformed by fold systems with WNW-ESE axis (Martelli et al. 2017). Lineament remote analysis indicates that these tectonic structures are characterised by strike values compatible with the main and most statistically significant class shown in the rose diagrams in **Fig. 3.11**. Moreover, the membership classes of the tectonic structures mapped in the field described above and the lineaments extracted from the remote

sensing analysis are confirmed by the cross-cutting relationship between them, which can be compared to the existing intersection between the Rioveggio, Reno and Vergato Faults with the Loiano-Venola and Grizzana Morandi Faults.

c) The third group of normal faults is characterised by a wide range of strike values and mutual intersection relationships. These normal faults are common along the eastern and western edges of the Marzabotto Basin **(Fig. 3.3a and 3.4)**. They show a greater spacing than the NE-SW-striking faults with deformation bands but are also more closely spaced with respect to faults with antiapenninic trends. Faults of this third group are also characterised by a planar geometry, short trace lengths and, at times, negligible offsets (they are mostly intraformational). In map view, these normal faults define a non-systematic, polygonal architecture (e.g., Cartwright et al., 2003; Petracchini et al., 2015), suggesting a shallow, gravity-driven tectonic origin. We tentatively connect the formation of these structures with a stress field variation through time that would have occurred in response to a local change in slope gradient, faulting along active tectonic structures or the influence of local tectonic stresses (e.g., Cartwright et al., 2003) triggering gravity-driven deformation mostly within the shallower portions of the Marzabotto Basin. The relationships between these faults and the lineaments mapped by remote sensing analysis remain rather uncertain. This could be due to the different scale of data acquisition, which is smaller for field structural analysis. However, this group of normal faults could be related to the less representative classes of the rose

diagram reported in **Fig. 3.11**, which are arranged orthogonally to each other, confirming the highly variable trend distribution of these structures.

3.6.2. The significance of the Epiligurian formations within the evolution of the Northern Apennines accretionary wedge

Previous tectonic models relate the formation of wedge-top basins, the accommodation of sediments therein, and the development of unconformities to the interplay between subsidence (as due to the regional load) and the regional-to-local uplift of the accretionary wedge due to underplating and crustal thickening in the framework of its dynamic evolution (e.g., Beaumont, 1981; Jordan, 1981; Ori and Friend, 1984; Bally et al., 1985; De Celles and Giles, 1996; Mutti et al., 2003). In this perspective, the Epiligurian wedge-top basins are key geological elements to refine conceptual models that account for the syn- to post-orogenic history of the Northern Apennines accretionary wedge since the middle-late Eocene. Our structural dataset documents the structuring of the Epiligurian formations during the evolution of the entire foreland basin system framed within the dynamics of a critically tapered orogenic wedge, where the activation, geometry, and cross-cutting relationships of both thrusts and extensional faults, concomitant with sedimentation and erosion, are key to the unravelling of the internal architecture of the growing wedge (e.g., Dahlen, 1990; Willet, 1992; Zoetemeijer et al., 1993).

The starting configuration is represented by the Late Cretaceous-Palaeocene growth of the NA accretionary wedge by bulk shortening, thickening and piling of tectonic slices scraped off from the subducting Ligurian-Piedmont Ocean plate and underplated at the

bottom of the wedge (e.g., Marroni et al., 2002; Remitti et al., 2011; Vannucchi et al., 2012; Papeschi et al., 2022). The nappe stack of the Ligurian Domain represents the most internal (i.e., westernmost) paleoenvironment of the entire foreland basin system accommodating heterogeneous subsidence and sedimentation. Since the late Eocene (stage I in **Fig. 3.12a**), the depozones atop the Ligurian Domain were filled by sediments accumulated on top of inactive thrusts, leading to the formation of the Epiligurian wedge-top basins. At this stage, lateral thickness variations and local interdigitations within the Epiligurian basins occurred in response to alternating phases of turbiditic deposition and cessation of sedimentation, marked by the occurrence of second-order angular unconformities within the basal stratigraphic succession (e.g., Cibin et al., 2001; Barbero et al., 2017).

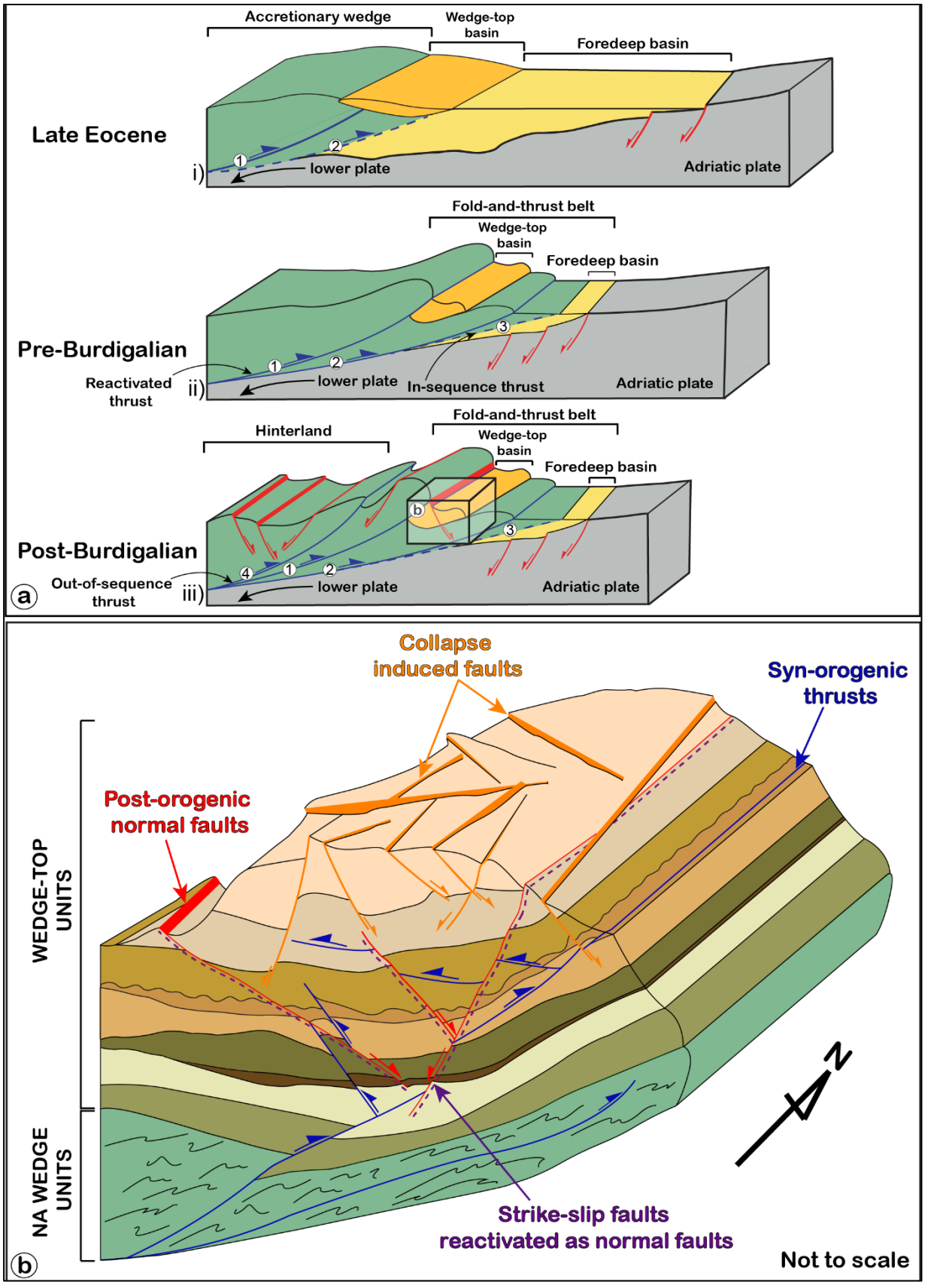

Figure 3.12 - a) Schematic evolution of wedge-top basins through time and space in relation to the propagation of the underlying Northern Apennines accretionary wedge

(modified and redrawn from Mutti et al., 2003); b) representative conceptual deformation model illustrating the tectonic structures affecting both the Ligurian and Epiligurian formations and their cross-cutting relationships.

During the pre-Burdigalian Epiligurian deposition (stage II in **Fig. 3.12a**), the accretionary wedge and the wedge top basins became progressively involved in the build-up and uplift of the evolving fold-and-thrust belt. We attribute this evolutionary stage of shortening from accretionary wedge to fold-and-thrust belt in NA to the progression of the Europe-Adria continental collision (e.g., Faccenna et al. 2001; Doglioni et al., 2006). At this stage, active compressional deformation induced both foreland-ward propagation of thrust fronts and reactivation of internal (and deeper) thrusts at the wedge toe to produce a stable wedge configuration. The development of syn-orogenic thrusts since the upper Lutetian affected the base of the sedimentary succession. This tectonic phase was interrupted by a marine regression documented by the presence of the regional Burdigalian angular unconformity, which developed in response to the uplift of the wedge concomitant with an abrupt change in the sedimentation pattern (e.g., Amorosi et al., 1995).

After the Burdigalian (stage III in **Fig. 3.12a**), the evolving fold-and-thrust belt was being deformed by folding and general tilting toward the hinterland and was affected by in-sequence and out-of-sequence thrusting. Wedge-top basins were thus deformed by active thrust sheets and were eroded and/or uplifted in response to thrusting. Our structural data, coupled with insights from published works (Catanzariti et al., 1999;

Ottria, 2000; Panini et al., 2002; Balocchi and Santagata, 2018) document that the shortening direction fluctuated from NE-SW to NW-SE in the entire Epiligurian succession. Since the upper Burdigalian, the former syn-orogenic thrusts activated with different trend distribution, probably reflecting the concomitant activity of in-sequence and out-of-sequence thrusts. We thus propose that the post-Burdigalian Epiligurian formations probably started to form under supercritical taper conditions before thrusts nucleated and propagated toward the foreland to restore a critical taper (e.g., DeCelles and Mitra,1995; Mitra, 1997).

The post-orogenic extensional phase that started to affect the Tyrrhenian side of the NA and then migrated to its northernmost uplifted margin (e.g., Martini and Sagri, 1993; Bertotti et al., 1997; Barchi et al., 2006), led to the normal-sense reactivation of inherited (mostly strike-slip) structures and the activation of newly formed normal faults. These post-orogenic normal faults cut and down-throw the earlier thrusts, affecting the whole sedimentary succession. The activation of normal fault systems adjusted the structural architecture of the upper portion of the belt and operated to reduce the taper angle to finally achieve the critical configuration. This tectonic phase included widespread gravity-driven deformation, which is documented by short, non-systematic, polygonal faults developed within the uppermost sequence of the Epiligurian formations and probably reflecting structural adjustments to local taper instability conditions **(Fig. 3.12b)**. In conclusion, our results suggest that a polyphase tectonic evolution has affected the Epiligurian formations during the progressive growth of the NA accretionary wedge

by frontal accretion, its progressive involvement in the fold-and-thrust belt and the successive switch from a syn- to a post-orogenic phase. Within this evolutionary scenario, three distinct types of tectonic structures have been recognised in the Marzabotto Basin as being characterised by different kinematic and geometric properties and timing **(Fig. 3.12b)**: i) syn-orogenic, NNE-SSW and WNW-ESE-striking thrusts with a transport direction towards the north-eastern quadrants; ii) post-orogenic, NW-SE-striking normal faults connected with an extensional tectonic regime affecting the inner and the axial zone of the NA and partly reactivating earlier left-lateral strike-slip structures connected with the thrust zones; iii) post-orogenic, collapse-induced faults that are related to the local variation of the wedge configuration and that connect, and partly cut, the early normal faults to form a polygonal architecture.

3.7 Conclusions

The wedge-top Epiligurian basins of the Apennines in northern Italy allow us to document the progressive deformation that steered the evolution of the shallowest structural levels of the Northern Apennines accretionary wedge during its syn-to-post-orogenic evolution. The Epiligurian formations record a polyphasic tectonic history accommodating significant changes in stress field orientation and faulting regime in the pre- and post-Burdigalian period. The kinematics, geometry and cross-cutting relationships of the main tectonic structures reflect the interaction between regional and local tectonic stress conditions that steered the stratigraphic configuration of the

Epiligurian formations through time and space. In particular, the mesostructural characteristics of these wedge-top basins suggest that the axial domain of the Northern Apennines belt started to experience an extensional tectonic phase within the complex configuration of an orogenic wedge, here driven by the NE propagation of the thrust fronts.

Chapter 4

Thermal history of the Epiligurian Marzabotto wedge-top basin records the tectonic development of the Northern Apennines fold-and-thrust belt (Italy)

Stendardi F.*[1,3], Vignaroli G.*[1], Carrapa B.[2], Albino I.[1], Viola G.[1]

(Submitted to Terra Nova)

1* Dipartimento di Scienze Biologiche, Geologiche e Ambientali, Alma Mater Studiorum Università di Bologna, Via Zamboni 67, 40126, Bologna, Italy

2 Department of Geosciences, University of Arizona, 1040 E 4th Street, Tucson, Arizona 85721, USA

3* Dipartimento di Scienze della Terra, Università di Pavia, Via Ferrata, 1, 27100, Pavia, Italy

Abstract

Apatite fission-track (AFT) and U-Th/He analysis (AHe) of detrital minerals from siliciclastic deposits is here applied to constrain the tectono-thermal history of the Epiligurian Marzabotto Basin (EMB). The Eocene to Pliocene EMB represents a key example of wedge-top basin within the Northern Apennines. Detrital AFT age populations from Eocene to Miocene strata cluster between ~71 and ~58 Ma**.** AHe ages show a quite variable single grain age distribution ranging from ~104 to ~7 Ma indicating a significant degree of post depositional thermal resetting. Thermal modelling of AFT and AHe ages indicates that the EMB experienced a maximum temperature of ~90° prior to Oligocene-to-Pliocene cooling. We interpret the Oligocene-Miocene cooling signal to represent rock uplift during the growth of the Apennines orogenic wedge and the late Miocene-Pliocene cooling to track accretion in the orogenic wedge concomitant with rollback-driven extension.

Significance statement

In this contribution, we present new thermochronological data (apatite fission-track (AFT) and U-Th/He data (AHe)) from a representative example of wedge-top basin, the Epiligurian Marzabotto basin (EMB) belonging to the Northern Apennines fold-and-thrust belt (Italy), aiming to constrain its cooling and exhumation history. We generated a tectono-thermal model with the purpose to constrain the time and maximum

temperature reached during the vertical movements of the EMB. This informs on the tectonics of the Northern Apennines during the Oligocene-Pliocene at a time of important processes related to the growth of the orogenic belt.

4.1 Introduction

The Northern Apennines (NA) are the archetypical example of a fold-and-thrust belt associated with a retreating subduction boundary during slab rollback (e.g., Malinverno and Ryan, 1986; Royden, 1993). Underplating (e.g., Platt, 1986; Jolivet et al., 1998) and delamination of the lower crust (e.g., Faccenna et al., 2004; Chiarabba et al., 2015), however, have also been considered as plausible mechanisms to explain the spatial-temporal migration of deformation across the belt. However, the geological record of such processes remains elusive. Detrital thermochronology provides useful information on cooling associated with rock uplift and exhumation of foreland basin deposits and can be used to understand orogenic processes (e.g., Painter et al., 2014; Zattin et al., 2002; Fügenschuh et al., 2003; Bernet et al., 2004; DeCelles et al., 2004; Carrapa et al., 2003; 2011; 2016). Whereas low-T thermochronology has been successfully applied to studying similar processes within the Alpine foreland basin system (e.g., Bernet et al., 2009; Carrapa, 2009; Carrapa et al., 2016; Hülscher et al., 2021), its application to wedge-top basins of the NA remains underutilised, mostly because those basins escaped significant burial, thermal resetting and exhumation (Thomson et al., 2010). The Epiligurian Marzabotto basin (EMB) represents a key example of wedge-top basin within the NA and its tectono-thermal history informs on the timing of the NA development in response to subduction and subsequent slab rollback.

We here apply AFT and AHe thermochronology and thermal modelling to the EMB, which records marine deposition from the Eocene to the Pliocene on top of the growing

NA fold-and-thrust belt. The reconstructed tectono-thermal history of the EMB is characterized by initial post-depositional heating to a maximum temperature of ~90°C and subsequent cooling starting in the late Oligocene. Our data, integrated with published thermochronological constraints, suggest cooling driven rock-uplift in the Oligo-Miocene during significant crustal shortening of the NA and moderate exhumation in the late Miocene to Pliocene during rollback and delamination of Adria continental crust.

4.2 Geological setting and low-T thermochronology constraints

The tectonic evolution of the NA reflects the westward subduction of Adria below Europe following the Late Cretaceous-Eocene closure of the Ligurian-Piedmont Ocean. Tectonic convergence culminated in the Oligo-Miocene leading to crustal shortening and progressive accretion of different lithotectonic units within the developing NA (e.g., Doglioni, 1991; Carmignani et al., 1995; Elter et al., 2003; Rosenbaum & Lister, 2004; Boccaletti et al., 2011). From the Miocene the NA experienced an extensional regime in its hinterland and the continuous foreland-ward migration of compression in response to the eastward rollback of the Adria slab (Malinverno and Ryan, 1986; Cavinato and De Celles, 1999; Faccenna et al., 2004; Carminati et al., 2012).

The tectonic edifice of the NA includes, from top to bottom (Conti et al., 2020**; Fig. 4.1a, b**): i) Ligurian and Sub Ligurian Units made of Jurassic ophiolites and Jurassic-to-

Paleogene shale and limestone; ii) Tuscan Domain made of a metamorphic basement, Triassic evaporite, Jurassic-to-early Oligocene limestone and marl, and late Oligocene-early Miocene turbidites (Macigno and Cervarola Fms.); iii) Umbria-Marche Domain made of Triassic evaporite, Jurassic-to-early Oligocene limestone and marl, and Miocene turbidites (Marnoso-Arenacea Fm.). Atop the tectonic edifice rest the Epiligurian Units, which contain middle Eocene-late Miocene bathyal to shallow-water siliciclastic deposits filling wedge-top basins (e.g., Amorosi, 1995; Cibin et al., 2001; Stendardi et al., 2023).

The age of continental accretion is constrained to approximately 30 Ma for the internal Tuscan units (Apuan Alps) and it becomes progressively younger to the east, as documented by the involvement of the Oligo-Miocene Tuscan and Umbria-Marche turbidites (Abbate and Bruni, 1987; Tinterri and Muzzi Magalhaes, 2011). Published thermochronological data show that the deepest and most internal units of the NA recorded higher T conditions than the more external units, which experienced lower magnitude and younger exhumation (e.g., Zattin et al., 2002; Corrado et al., 2010; **Fig. 1c**). For the Umbria-Marche Domain, the youngest documented cooling ages are recorded in the Marnoso Arenacea turbidites, constraining cooling and exhumation of the NA to ~ 6-4 Ma (e.g., Balestrieri et al., 1996; Zattin et al., 2000; 2002). For the Tuscan Domain, data from Oligo-Miocene turbidites constrain episodic exhumation of the NA hinterland ~ 12 - 5 Ma (Macigno Fm.) at ~ 10-3 Ma (Falterona Fm.) and ~ 7 - 2 Ma (Cervarola Fm.) (e.g., Abbate et al., 1994; Zattin et al., 2002; Ventura et al., 2001; Fellin et al., 2007; Thompson et

al., 2010). AFT data from the Ligurian Units indicate continuous cooling between ~ 20 Ma and ~ 5 Ma (Balestrieri et al., 1996; Carlini et al., 2013).

AFT data from the Epiligurian Units indicate either unreset or only partially reset ages (Boettcher and McBride, 1993). These units are located geographically to the east of the conceptual boundary separating complete AFT and AHe resetting in the most internal sector of the NA from areas from partial resetting (Thomson et al. 2010; Fig. 1a). To date, only one AFT cooling age (4.7 ± 1.0 Ma) is available for the upper Eocene Epiligurian fms. (Carlini et al., 2013; **Fig. 4.1b).**

The NA orogenic system experienced significant cooling and exhumation over the past 20 Myr at an average exhumation rate between ca. 0.3 and 1 mm/yr (Balestrieri et al., 2003; Thomson et al., 2010; Erlanger et al., 2022). Faster exhumation has generally occurred since the Pliocene in the northeastern side of the belt in response to continuous tectonic exhumation.

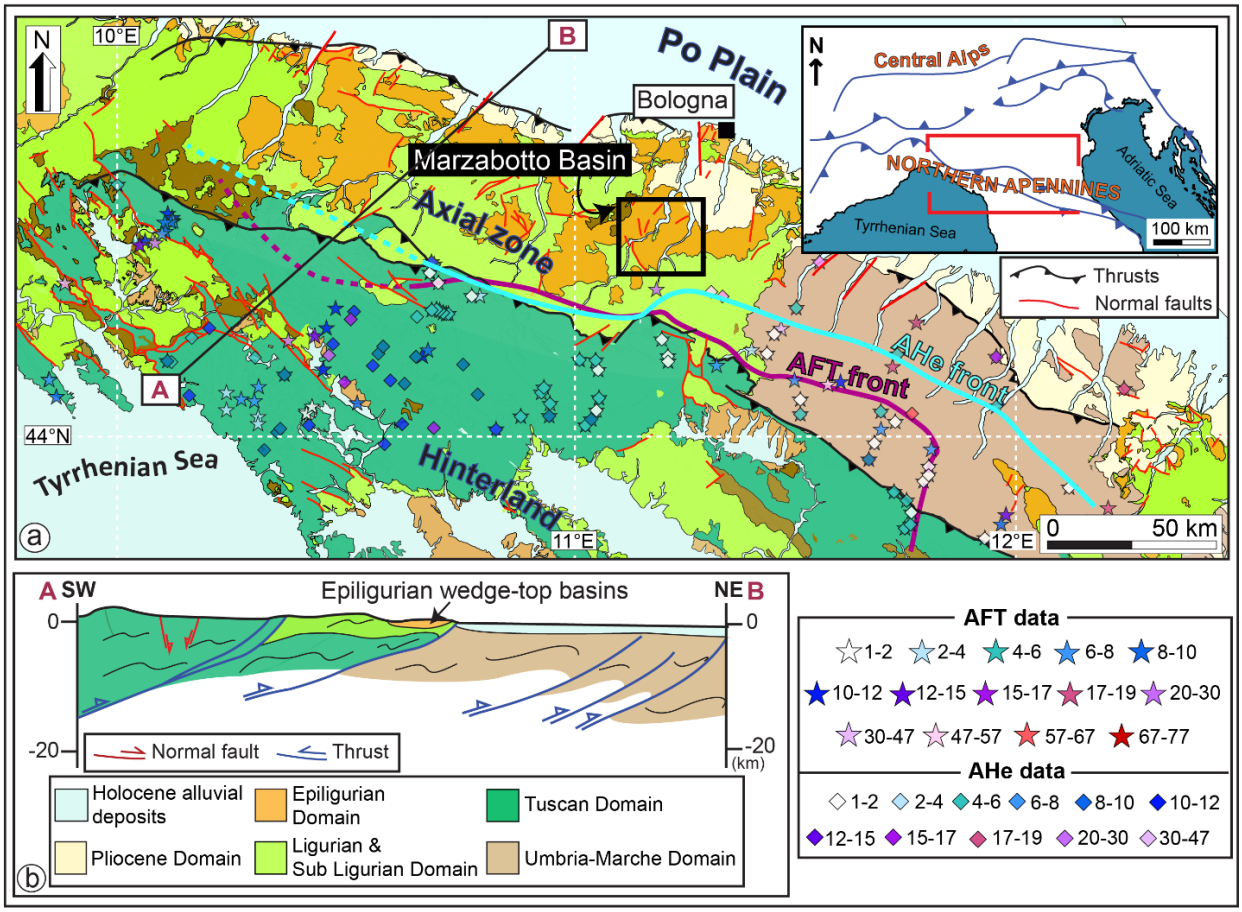
N
10°E
B
Po Plain
Bologna
Marzabotto Basin
Axial zone
A
44°N
Tyrrhenian Sea
Hinterland
AFT front
AHe front
11°E
12°E
0
50 km
Central Alps
NORTHERN APENNINES
Adriatic Sea
Tyrrhenian Sea
100 km
Thrusts
Normal faults
a
A SW
Epiligurian wedge-top basins
NE B
0
-20
Normal fault
Thrust
-20
(km)
Holocene alluvial deposits
Epiligurian Domain
Tuscan Domain
Pliocene Domain
Ligurian & Sub Ligurian Domain
Umbria-Marche Domain
b
AFT data
1-2
2-4
4-6
6-8
8-10
10-12
12-15
15-17
17-19
20-30
30-47
47-57
57-67
67-77
AHe data
1-2
2-4
4-6
6-8
8-10
10-12
12-15
15-17
17-19
20-30
30-47

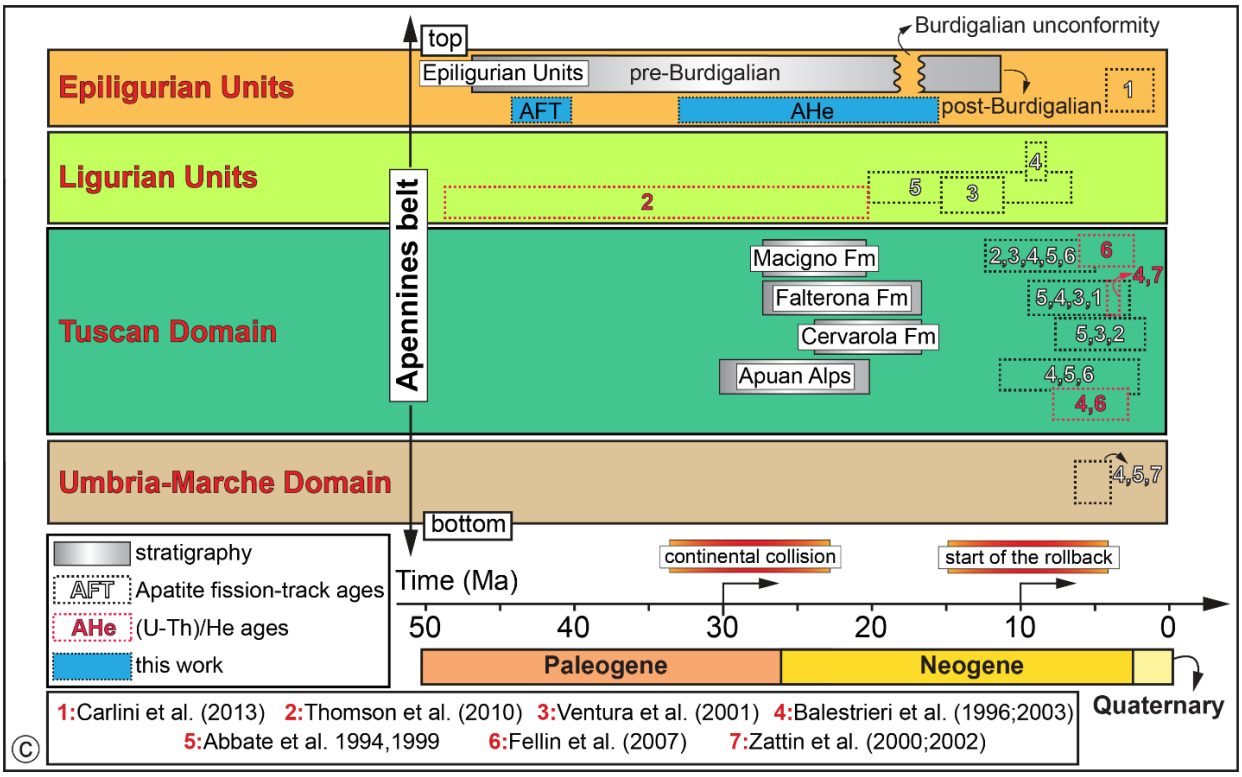
top
Burdigalian unconformity
Epiligurian Units
Epiligurian Units
pre-Burdigalian
AFT
AHe
post-Burdigalian
1
Ligurian Units
4
5
3
2
Apennines belt
Tuscan Domain
Macigno Fm
Falterona Fm
Cervarola Fm
Apuan Alps
2,3,4,5,6
6
4,7
5,4,3,1
5,3,2
4,5,6
4,6
Umbria-Marche Domain
4,5,7
bottom
stratigraphy
AFT
Apatite fission-track ages
AHe
(U-Th)/He ages
this work
continental collision
start of the rollback
Time (Ma)
50
40
30
20
10
0
Paleogene
Neogene
Quaternary
1:Carlini et al. (2013) 2:Thomson et al. (2010) 3:Ventura et al. (2001) 4:Balestrieri et al. (1996;2003)
5:Abbate et al. 1994,1999 6:Fellin et al. (2007) 7:Zattin et al. (2000;2002)
c

Figure 4.1- a) Simplified geological map of the NA (modified after Conti et al., 2020) with location of the published thermochronological data. The EMB is shown. Stars represent AFT ages (Ma) from Abbate et al. (1994), Balestrieri et al. (2003), Fellin et al. (2007); Thomson et al. (2010), Bonini et al. (2013) and Carlini et al. (2013). Rhombs represent AHe ages (Ma) from Fellin et al. (2007) and Thomson et al. (2010); b) Schematic geological cross-section highlighting the main structural relationships between the NA units (redrawn and modified after Molli, 2008); c) Summary of published thermochronology data combined with the new thermochronological results from this work (blue bars) and compiled for the different lithotectonic domains of the NA.

4.3 Methods and Results

4.3.1 Study area and sampling strategy

The EMB **(Fig. 1a)** is filled by a ~3.5 km thick, middle Eocene-upper Miocene marine siliciclastic strata. A major Burdigalian unconformity therein marks an abrupt shift from a deep marine (pre-Burdigalian) to a platform (post-Burdigalian) depositional environment during the progressive uplift of the underlying fold-and-thrust belt (Amorosi et al., 1996). Its complex stratigraphy **(Fig. 2a)** reflects the interplay between: i) NNE-SSW and WNW-ESE-striking reverse faults related to syn-orogenic tectonic shortening and ii) NW-SE-striking normal faults developed as consequence of the Middle-Late Pleistocene extension (Stendardi et al., 2023).

We collected thirteen samples for thermochronological analysis, targeting the coarsest clastic levels. We analysed four AFT samples and six AHe samples from the pre-Burdigalian Loiano (~47.8-41.2 Ma) and Antognola (~27.8-23 Ma) formations and from the post-Burdigalian Pantano (~19-16 Ma) and Cigarello. (~15-12 Ma) formations **(Fig. 4.2)**. By collecting samples that cover the entire stratigraphic succession across the EMB, we aimed to capture a comprehensive tectono-thermal record of the wedge top basin. While individual sample cooling ages may reflect localized tectonics related to local fault throws (in all cases not exceeding 1 km; Stendardi et al., 2023), the dataset provides a unique opportunity to examine the regional thermal response of the EMB to the growing belt.

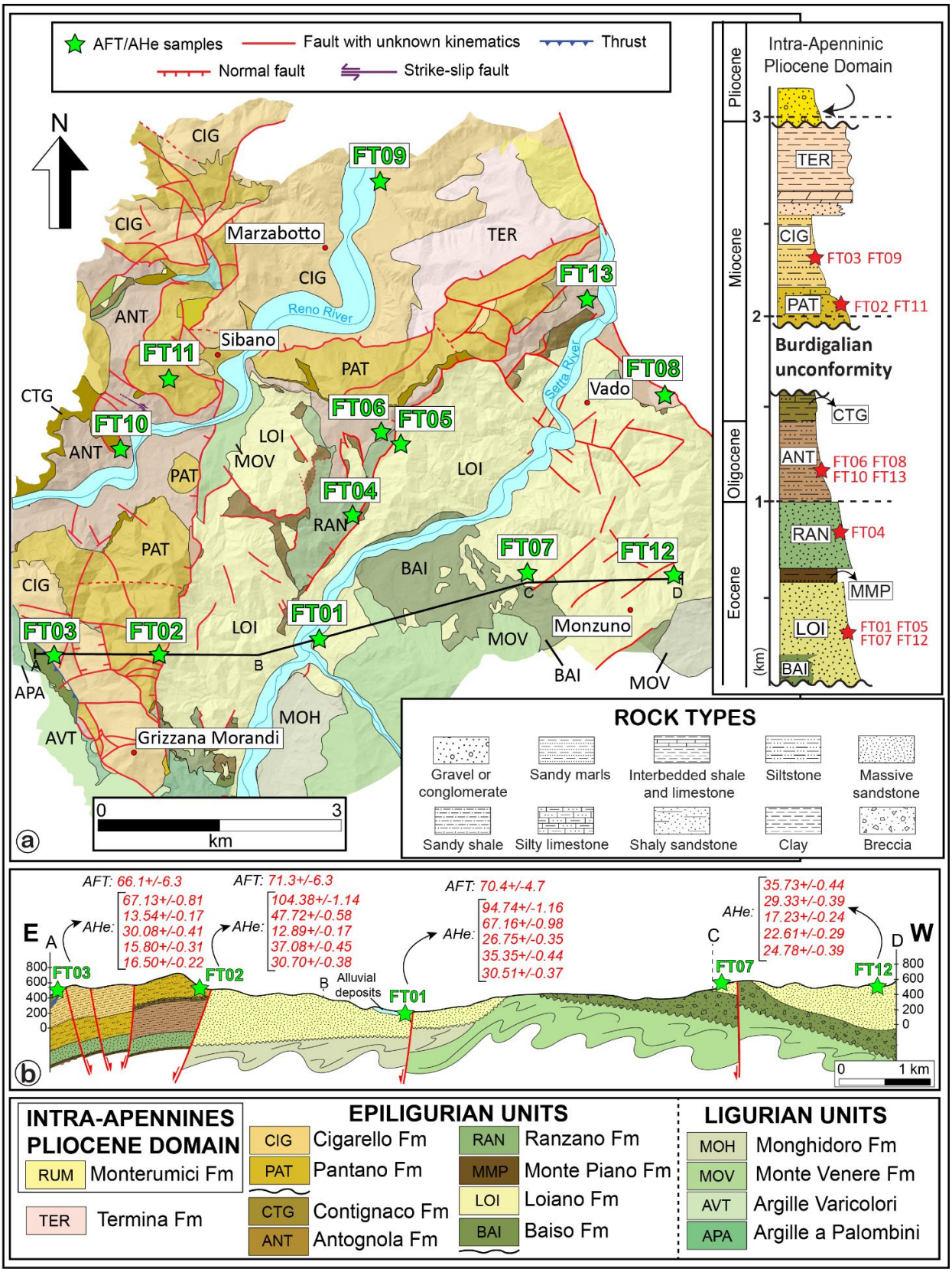

Figure 4.2- a) Structural map of the EMB showing the location of the AFT and AHe samples. The collected samples are also plotted in the stratigraphic column of the Epiligurian sedimentary succession of the EMB; b) Representative geological cross-

section for the southern part of the EMB reporting projection of the collected samples ad AFT and AHe ages.

4.3.2 AFT data

We targeted 100 grains for each detrital sample but, unfortunately, mineral separation only yielded <50 AFT grains (and ages) per sample. The four dated samples **(Table 1)** yielded AFT central ages older than or similar (within error) to the depositional ages of the hosting strata and range between 71.3 ± 6.3 and 57.9 ± 4.3 Ma (Late Cretaceous-Paleocene; **Figs. 4.3** and **4.4**).

Table 1- AFT data for the detrital units from the Marzabotto Basin. The counting and the elaboration of the AFT data have been performed at the Department of Geosciences of the University of Arizona.

Sample	Dep. Age	Formation	Latitude	Longitude	Mount	n° grains	ϱ_d	N_d	ϱ_s	N_s	ϱ_i	N_i	Central age	$P_{(\chi 2)}$
FT03	Miocene	Cigarello	44°16′20.4″ N	11°08′29.9″E	2	20	1.3	6055	7	533	2.9	2171	59.94+/-5.56	0
FT03	Miocene	Cigarello	44°16′20.4″ N	11°08′29.9″E	1	20	1.3	6091	1.3	1015	3.9	3063	74.98+/10.23	0
FT02	Miocene	Pantano	44°16′27.8″ N	11°09′51.4″E	2	28	1.3	6127	1.2	1359	3.8	4191	69.87+/-7.55	0
FT02	Miocene	Pantano	44°16′27.8″ N	11°09′51.4″E	1	17	1.3	6164	6.8	458	2.5	1679	61.15+/-2.43	0
FT06	Oligocene	Antognola	44°18′40.8″ N	11°12′03.6″E	2	23	1.2	5983	2	918	8.8	3994	48.38+/-4.10	0
FT06	Oligocene	Antognola	44°18′40.8″ N	11°12′03.6″E	1	27	1.2	6019	1.5	1579	4.5	4860	67.29+/-8.37	0
FT01	Eocene	Loiano	44°16′34.5″ N	11°12′03.5″E	2	27	1.3	6200	1.6	1640	3.5	3544	108.3+/10.72	0
FT01	Eocene	Loiano	44°16′34.5″ N	11°12′03.5″E	1	48	1.3	5911	9.4	1666	4.1	7330	52.21+/-3.24	0

Sample	Formation	N° grains	N_s	N_i	N_d	ϱ_d	Mean age	Central age	$P_{(\chi 2)}$
FT01pop1	Loiano	18	677	3682	1666	1.332E+06	41.2+/-1.1	41.8+/-2.3	0

ϱ_s: spontaneous track density; ϱ_i: induced track density in external detector; ϱ_d: induced track density in external detector adjacent to dosimeter glass (ϱ_s; ϱ_i; ϱ_d are densities expressed in 10^6 cm^{-2}); N_i number of counted induced tracks; N_s: number of counted spontaneous tracks.

All samples fail the χ^2 statistical test indicating the presence of multiple detrital populations. D_{par} values range between 1.26 μm to 2.95 μm (except for one grain of sample FT01 showing an unusual D_{par} value of 4.41) with no correlation with individual grain age. Confined track length histograms for all samples are reported in the Support Material **(Fig. S1)** together with radial plots with D_{par} values for all samples **(Fig. S2)** and details about the applied method.

For thermal modelling analysis we selected sample FT01 from the lowermost formation of the EMB (the Loiano Fm.) whose crystal ages are equal to or younger than the stratigraphic age (48-41 Ma; **Table S1** and **Fig. S3**). We obtained a subpopulation $FT01_{pop1}$ that passes the χ^2 test (96.58 %), indicating that its grains belong to one population, and yielded a 41.8 ± 2.3 Ma AFT central age **(Fig. 3)**. We measured confined track lengths and D_{par} for the grains belonging to $FT01_{pop1}$ **(Table S2)** and, together with AHe data (discussed below), we modelled the thermal history of the Loiano Fm.

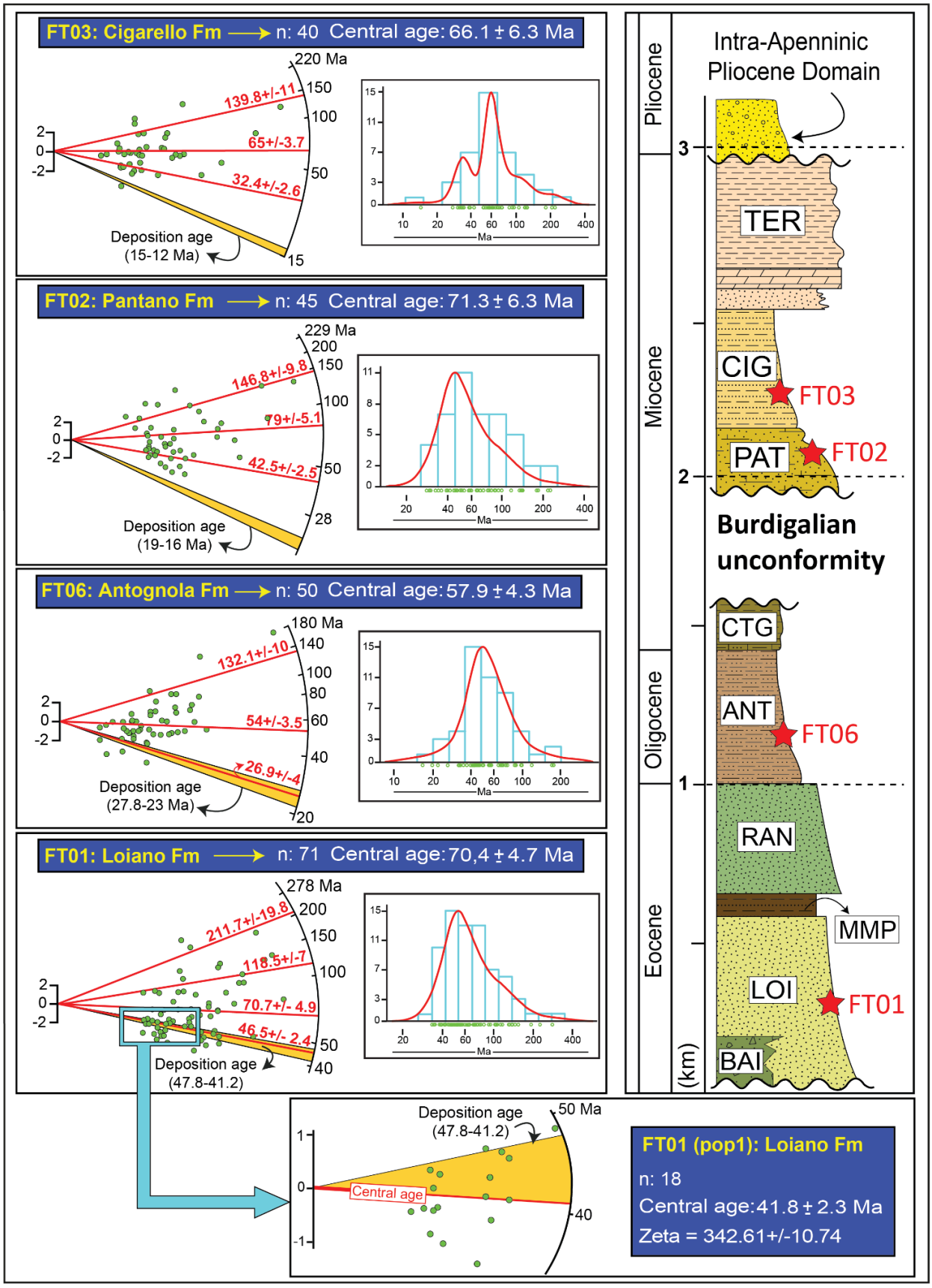
FT03: Cigarello Fm → n: 40 Central age: 66.1 ± 6.3 Ma
220 Ma
150
100
50
15
139.8+/-11
65+/-3.7
32.4+/-2.6
Deposition age
(15-12 Ma)
FT02: Pantano Fm → n: 45 Central age: 71.3 ± 6.3 Ma
229 Ma
200
150
100
50
28
146.8+/-9.8
79+/-5.1
42.5+/-2.5
Deposition age
(19-16 Ma)
FT06: Antognola Fm → n: 50 Central age: 57.9 ± 4.3 Ma
180 Ma
140
100
80
60
40
20
132.1+/-10
54+/-3.5
26.9+/-4
Deposition age
(27.8-23 Ma)
FT01: Loiano Fm → n: 71 Central age: 70,4 ± 4.7 Ma
278 Ma
200
150
100
50
40
211.7+/-19.8
118.5+/-7
70.7+/- 4.9
46.5+/- 2.4
Deposition age
(47.8-41.2)
Ma
Deposition age
(47.8-41.2)
50 Ma
Central age
40
FT01 (pop1): Loiano Fm
n: 18
Central age: 41.8 ± 2.3 Ma
Zeta = 342.61+/-10.74
Pliocene
Miocene
Oligocene
Eocene
Intra-Apenninic
Pliocene Domain
TER
CIG
FT03
PAT
FT02
Burdigalian
unconformity
CTG
ANT
FT06
RAN
MMP
LOI
FT01
BAI
(km)

Figure 4.3- AFT radial plots for the dated Epiligurian formations and probability density plots of fission-track single-grain age distribution. The red lines represent the different peak ages (or populations) obtained for each sample and the yellow fields indicate the depositional ages; n: number of dated apatite grains. The labels of the Epiligurian formations are as in **Figure 4.2**. At the bottom, the radial plot for the $FT01_{pop1}$ subpopulation is reported (see text and the Support Material for details).

4.3.3 AHe data

Six samples containing the most suitable apatite grains (euhedral, width > 60 μm and inclusion-free) were selected for AHe analyses. For each sample, five single grain apatite crystals were hand-picked, photographed and their dimensions measured. The concentration of U, Th and Sm were determined using a coupled plasma spectrometer and the alpha ejection correction was applied to the obtained He ages (Farley et al., 1996; Farley, 2002). Details about the method applied are reported in the Support Material.

Corrected ages exhibit high dispersion between 104 ± 1.14 Ma and 7.16 ± 0.10 Ma **(Table 2)**, indicating partial to full resetting. As expected, most measured AHe ages are younger than the AFT youngest populations for each sample **(Fig. 4.4)**.

Table 2 - AHe data for the detrital units from the Marzabotto Basin. The counting and the elaboration of the AHe data have been performed at the Department of Geosciences of the University of Arizona.

Sample	Formation		Rs	Age corr (Ma)	1s±date (Ma)	U (ppm)	Th (ppm)	Sm (ppm)
FT03_Ap1	Cigarello		36.45	67.13	0.81	56.40	68.95	233.86
FT03_Ap2	Cigarello		42.86	13.54	0.17	18.12	92.33	104.42
FT03_Ap3	Cigarello	Miocene	33.39	30.08	0.41	18.61	78.37	62.65
FT03_Ap4	Cigarello		34.43	15.80	0.31	11.99	17.80	49.50
FT03_Ap5	Cigarello		32.10	16.50	0.22	108.76	91.14	696.68
FT02_Ap1	Pantano		46.60	104.38	1.14	35.58	71.54	55.10
FT02_Ap2	Pantano		43.17	47.72	0.58	14.53	23.75	226.07
FT02_Ap3	Pantano	Miocene	40.27	12.89	0.17	30.63	21.22	288.32
FT02_Ap4	Pantano		47.49	37.08	0.45	48.74	39.89	208.85
FT02_Ap5	Pantano		38.99	30.70	0.38	21.83	32.74	216.83
FT06_Ap1	Antognola		39.36	55.81	0.64	10.13	22.77	134.90
FT06_Ap2	Antognola		44.89	20.95	0.23	43.61	75.26	421.29
FT06_Ap3	Antognola	Oligocene	36.26	35.95	0.45	40.04	29.50	398.33
FT06_Ap4	Antognola		41.46	21.60	0.24	20.93	162.76	116.26
FT06_Ap5	Antognola		34.74	22.41	0.27	13.42	36.65	229.77
FT10_Ap1	Antognola		38.37	7.16	0.10	21.44	78.39	418.31
FT10_Ap2	Antognola		38.82	11.80	0.14	38.87	126.59	485.74
FT10_Ap3	Antognola	Oligocene	41.43	15.57	0.17	21.88	136.58	193.95
FT10_Ap4	Antognola		52.31	7.25	0.08	52.24	97.78	320.69
FT10_Ap5	Antognola		36.98	19.39	0.22	50.93	96.87	476.73
FT12_Ap1	Loiano		31.33	35.73	0.44	44.46	60.47	65.77
FT12_Ap2	Loiano		32.03	29.33	0.39	18.16	27.36	235.45
FT12_Ap3	Loiano	Eocene	25.27	17.23	0.24	23.57	337.88	561.52
FT12_Ap4	Loiano		26.87	22.61	0.29	84.92	105.73	190.00
FT12_Ap5	Loiano		29.98	24.78	0.39	20.48	70.20	493.40
FT01_Ap1	Loiano		52.68	94.74	1.16	11.36	10.58	80.38
FT01_Ap2	Loiano		37.18	67.16	0.98	23.94	6.22	319.01
FT01_Ap3	Loiano	Eocene	36.85	26.75	0.35	71.65	36.48	215.59
FT01_Ap4	Loiano		32.79	35.35	0.44	23.38	53.14	289.92
FT01_Ap5	Loiano		52.70	30.51	0.37	28.19	24.52	148.48

All grains have moderate to high effective U contents (eU= U+ (0.24 x Th)) ranging between 6.9 and 141.4 ppm. Most samples show inverse relationship between eU and age **(Figs. S4-S9)**; however, sample FT12 (Loiano Fm.) and FT10 (Antognola Fm.) show a few grains with positive Age-eU correlations **(Figs. S4-S9)**. We selected these grains for inverse thermal modelling **(Table 3; Fig. 4.5)**.

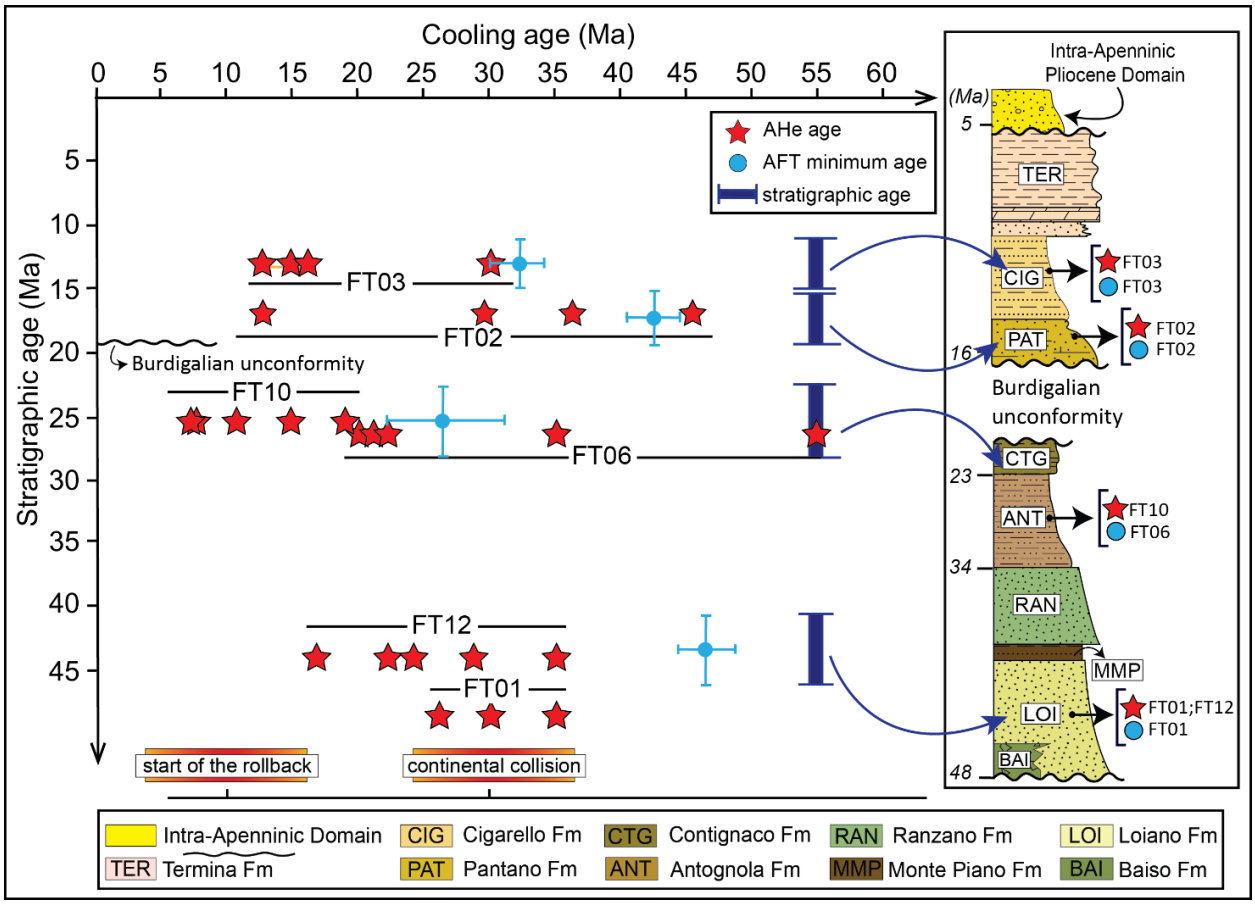

Figure 4.4- Cooling age (AHe and AFT) against stratigraphic age for the Loiano, Antognola, Pantano and Cigarello Fms. (FT01, FT02, FT03 and FT06, respectively). The sky-blue dots represent the youngest AFT population for each sample of **Fig. 4.3**

4.3.4 Thermal modelling

Inverse thermal modelling (Ketcham et al., 2007) for sub-population $FT01_{pop1}$ (with an age within error from the depositional age of the sample) and for AHe ages from the FT12 (Loiano Fm.) allows us to explore the time-temperature history of the EMB **(Fig. 4.5)**. We used the HeFTy software (version 2.1.4) (Ketcham, 2005) with track length, D_{par} (Ketcham et al., 2000; Sobel and Seward, 2010) and age data indicated in **Tables 1** and **2** as input parameters. The inversion parameters for HeFTy modelling are reported in **Table 3**.

Table 3- Inversion parameters for HeFTy modelling.

Thermochronological data	
Samples and data used	***AFT FT01pop1***
Data treatment	
Annealing model	Kinetic: Ketcham et al. (2007)
C-axis projection	Ketcham et al. (2007) (5.5M)
Kinetic parameters	D_{par}
Search method	Monte Carlo
Additional geological information and constraints	
Depositional age	47.8-41.2 Ma
Depositional temperature	15±15°C
Number of iterations in HeFTy	1000
Path between constraints	Monotonic variable
Halve	2 times
Randomizer style	Intermediate
GOF	0.95
Samples and data used	***AHe FT12 (ap1_5)***
Data treatment	
Calibration	Flowers et al. (2009), RDAAM
Precision	Better
Stopping distances	Ketcham et al. (2011)
α- calculation	Ejection
Search method	Monte Carlo
Additional geological information and constraints	
Depositional age	47.8-41.2 Ma
Depositional temperature	15±15°C
Number of iterations in HeFTy	1000
Path between constraints	Monotonic variable
Halve	2
Randomizer style	Intermediate
GOF	0.83-0.98

The mean path obtained for sub-population $FT01_{pop1}$ constrains a relatively rapid syn-depositional heating (burial) to a maximum T of ~90 °C between ~47 Ma and ~31 Ma (middle Eocene to lower Oligocene), followed by Oligocene-Miocene cooling, which accelerates starting at ca. 10 Ma **(Fig. 4.5)**. Inverse thermal modelling of AHe ages for FT12 (see average path in **Fig. 4.5)** shows a relatively rapid syn-depositional heating to a maximum T of ~60 °C between ~40 Ma and ~25 Ma (middle Eocene to late Oligocene), followed by cooling during the Miocene-Pliocene **(Fig. S10)**.

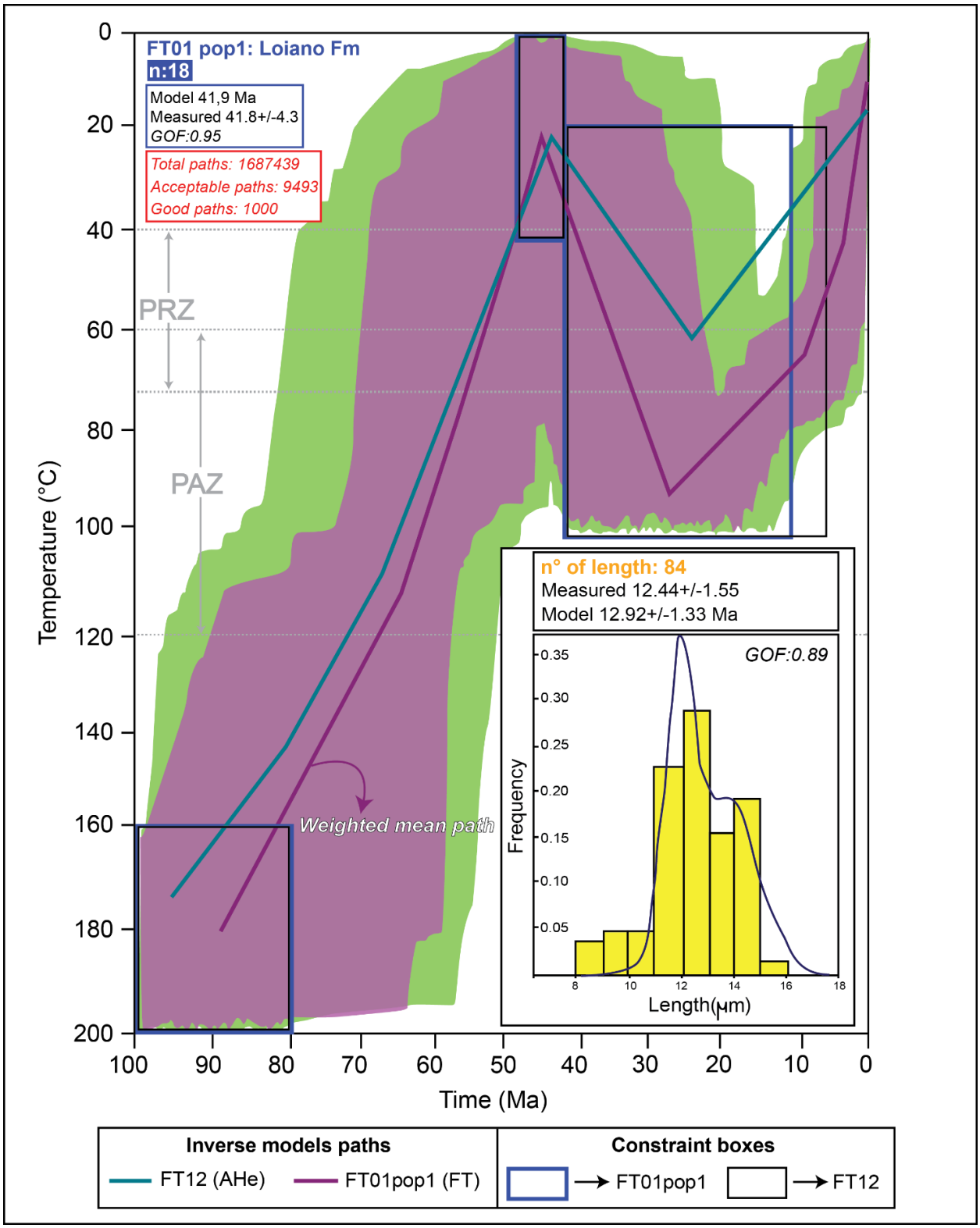

Figure 4.5- Inverse model of AFT of the Loiano Fm. subpopulation $FT01_{pop1}$ combined with AHe data of the same geologic formation (FT12) (its average path is indicated with the blue line) ~~and Antognola Fm. (FT10) (pink line).~~ The confined lengths distribution of the subpopulation $FT01_{pop1}$ is reported in the insert.

4.4 Discussion and Conclusions

4.4.1 Thermal history of the EMB

Our Paleogene and Cretaceous AFT detrital populations are a function of source cooling histories and are consistent with Western Alps cooling signature (e.g., Carrapa et al., 2003). Our thermochronological results suggest that the EMB has been exposed to a maximum temperature of ~ 90°C after deposition and a cooling history from the early Oligocene onward**.** Whereas AHe ages reflect significant resetting after deposition, the AFT detrital populations only show partial resetting. This is supported by the fact that the youngest detrital AFT age for the oldest samples is older than those of the younger samples. In case of significant or full resetting during burial the opposite situation should be expected as the deepest sample would have experienced the highest degree of resetting, which would result in younger ages. AHe ages for FT03 and FT10 are dispersed but as young as ~ 17 Ma, indicating partial resetting and temperature in the basin between 60° C and 90° C.

Overall, the Oligocene-Early Miocene thermal history of the EMB units indicates that although they were deposited under marine conditions, they experienced cooling driven rock uplift related to the development of the belt. This is consistent with the abrupt change of the depositional environment that affected the Epiligurian stratigraphy in the Burdigalian, when a shallowing upward trend from silica-rich marlstone to shelf and slope-basin facies occurred (Amorosi et al., 1995; Papani, 2002).

Thermal modelling of the EMB indicates that the lowermost Epiligurian Units experienced significant Oligocene through Pliocene cooling. The late Miocene-Pliocene thermal history is consistent with that recorded by the Ligurian Units (Abbate et al., 1999; Carlini et al., 2013), which indicates rock uplift of the NA axial domain starting in the Early Miocene. Oligocene cooling of the Epiligurian/Ligurian system (ca. 30 Ma) was coeval with continental accretion in the Apuan Alps of Tuscan Domain (Kligfield et al., 1986; Abbate and Bruni, 1987). This suggests that rock uplift was concomitant with deep crustal shortening and growth of the NA belt without significant erosion at the surface (England and Molnar, 1990; ter Voorde et al., 2004).

4.4.2 Implication for the Cenozoic tectonic evolution of the Northern Apennines

We show a simplified geodynamic evolutionary model for the tectonic evolution of the NA belt **(Fig. 6)** from initial contraction during the late Eocene-Early Miocene to a phase dominated by the Middle Miocene-Quaternary retreat of the margin, following the eastward Adria slab rollback (e.g., Faccenna et al., 2001; Rosenbaum & Lister, 2004; Carminati and Doglioni, 2012). This model is supported by published thermochronological data, which indicate an eastward younging of exhumation in the NA from the Ligurian to the Tuscan and Umbria-Marche domains during the early Miocene-Quaternary **(Fig. 1b)**. In the first (Oligo-Miocene) stage **(Fig. 4.6a)**, Adria margin deformation accommodated by overthrusting of the Ligurian wedge (Ligurian Units and the Epiligurian wedge-top basins) on top of Adria-related units, while shortening at

greater depth deformed the internal Tuscan Domain (Apuan Alps). Thermal maturity studies have constrained the maximum thickness of the Ligurian overburden to ca. 3 km and its progressive decrease towards the belt front, i.e. to the east (Botti et al., 2004; Caricchi et al., 2015, Zattin et al., 2002). We attribute the early cooling experienced by the Epiligurian and Ligurian units to rock uplift (e.g. ter Voorde et al., 2004) during this shortening stage.

In a second stage **(Fig. 4.6b)**, crustal shortening affected the external Tuscan Units (and the Umbria-Marche Domain through dominant frontal accretion, while extension dominated in the hinterland. Tuscan and Umbria-Marche turbidites exhumed at a rate of ~ 0.7-1.2 mm/yr during the last 10 Ma (e.g., Abbate et al., 1994; Ventura et al., 2001; Zattin et al., 2002; Balestrieri et al., 2003; Botti et al., 2004; Thompson et al., 2010; Erlanger et al., 2022; Lanari et al., 2023). We speculate that the second phase of cooling recorded by our study in the late Miocene-Pliocene corresponds to increased erosion related to accretion of tectonic units at the collisional front, while extension migrated from the hinterland to the axial domain. Delamination of the lower crust into the lithospheric mantle provides an efficient mechanism to accommodate continental subduction and forelandward accretion during the transition from shortening to rollback-related extension in the NA hinterland (e.g., Faccenna et al., 2004; Vignaroli et al., 2009; Chiarabba et al., 2015).

In summary, this study shows that cooling recorded by the uppermost structural levels of the NA was not steady-state but rather punctuated and mainly linked to the dynamics of the belt as controlled by (i) overthrusting during the Eocene-early Miocene and (ii)

frontal accretion during the middle Miocene-Quaternary. This switch in the overall mode of crustal shortening at the NA front seems to have played a major role in controlling the rate of rock uplift and exhumation concomitant with the eastward slab rollback.

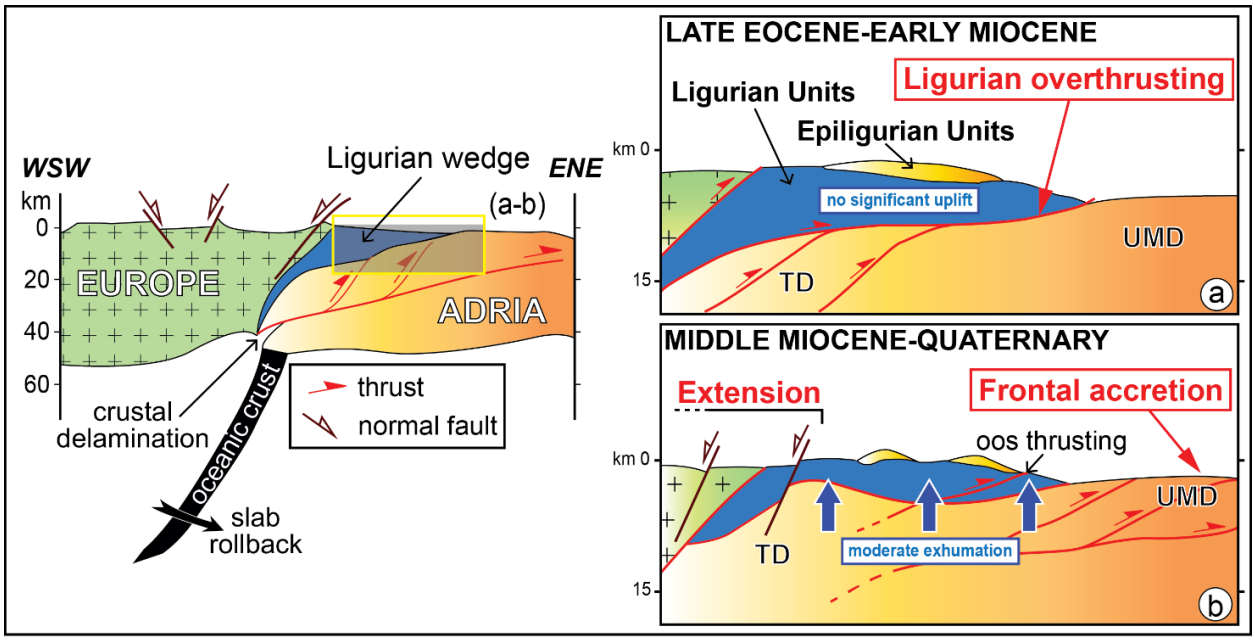

Figure 4.6- Possible two-stage tectonic scenario for the NA build-up phase during (a) the Eocene-early Miocene Ligurian overthrusting and (b) the middle Miocene-Quaternary frontal accretion concomitant with extension in the hinterland (TD= Tuscan Domain; UMD= Umbria-Marche Domain; oos thrusting= out-of-sequence thrusting).

Acknowledgement

We thank Gilby Jepson for help with AFT training and data reduction. We thank Uttam Chowdhury for AHe sample preparation and laboratory activity. William Cavazza is thanked for the fruitful discussion about the thermochronological data. Thomas Gusmeo

is thanked for his support during data processing. This work benefited from the fruitful and constructive reviews of P. Ballato and an anonymous reviewer. We thank the Editor (M. Coleman) for the editorial handling and for useful comments.

Addendum to Chapter 4

This paragraph, which was not included in the paper submitted to Terra Nova, discusses the lag time diagram to provide insights into the source provenance of the Marzabotto Basin. It also presents a possible paleogeographic evolution, based mainly on insights from published works.

4.1 Lag time

The lag time is defined as the difference between the cooling age and the depositional age (Garver et al. 1999) taking into account the erosion at the surface, transport (fluvial or glacial) and deposition of the rocks into the sedimentary basin. In summary, the lag time can be explained as the time needed for exhuming rocks from the closure temperature to the surface. When the peak ages change with the same rate as the depositional ages the lag rime is constant indicating a continuous exhumation of the mountain belt (e.g., Glotzbach et al. 2011) It also can vary in response to changes in exhumation rates depending from the variation of the geothermal gradient.

The lag time usually shows different paths tendency which are related to the variation of the exhumation rates of the rock and these relationships are used to infer if an accretionary wedge is under a constructional, steady-state or decay stage of evolution (Spotila, 2005) and to provide indication about the dynamic of the wedge (Carrapa, 2009). In particular, i) a decreasing lag-time values up section suggests an increasing of the exhumation rate; ii) constant lag time values indicate a steady-state exhumation rate;

iii) an increasing value of lag time means a decreasing of the exhumation rate. The width of the variation of the lag time can also be a good indicator for the presence of a simple or multi-step exhumation (short lag time: single pulse exhumation; long lag time: polyphase exhumation).

4.2 Source provenance

It is possible to affirm that the source rock that fed the Epiligurian Units have been characterised by a complex evolution through time and space (e.g., Cibin et al., 2001).

To reconstruct the thermal history of the Epiligurian Units I built a lag time plot **(Figure 4.7)** in which the single fission-track peak ages and the stratigraphic ages have been considered for each sample. In this case, these units have been characterised by a peculiar thermal history which reflect the complexity of the evolution of these wedge-top basins through time and space. The lag time plot suggests that the samples are characterised by approximately linear trends covering lag time values of 20, 60 and 120, respectively (within the error) and it means that the source area is exhumed and eroded producing sediments with progressively lower cooling age values. Furthermore, the samples are characterised by an increasing lag time up-section indicating a decreasing of the exhumation rate over time.

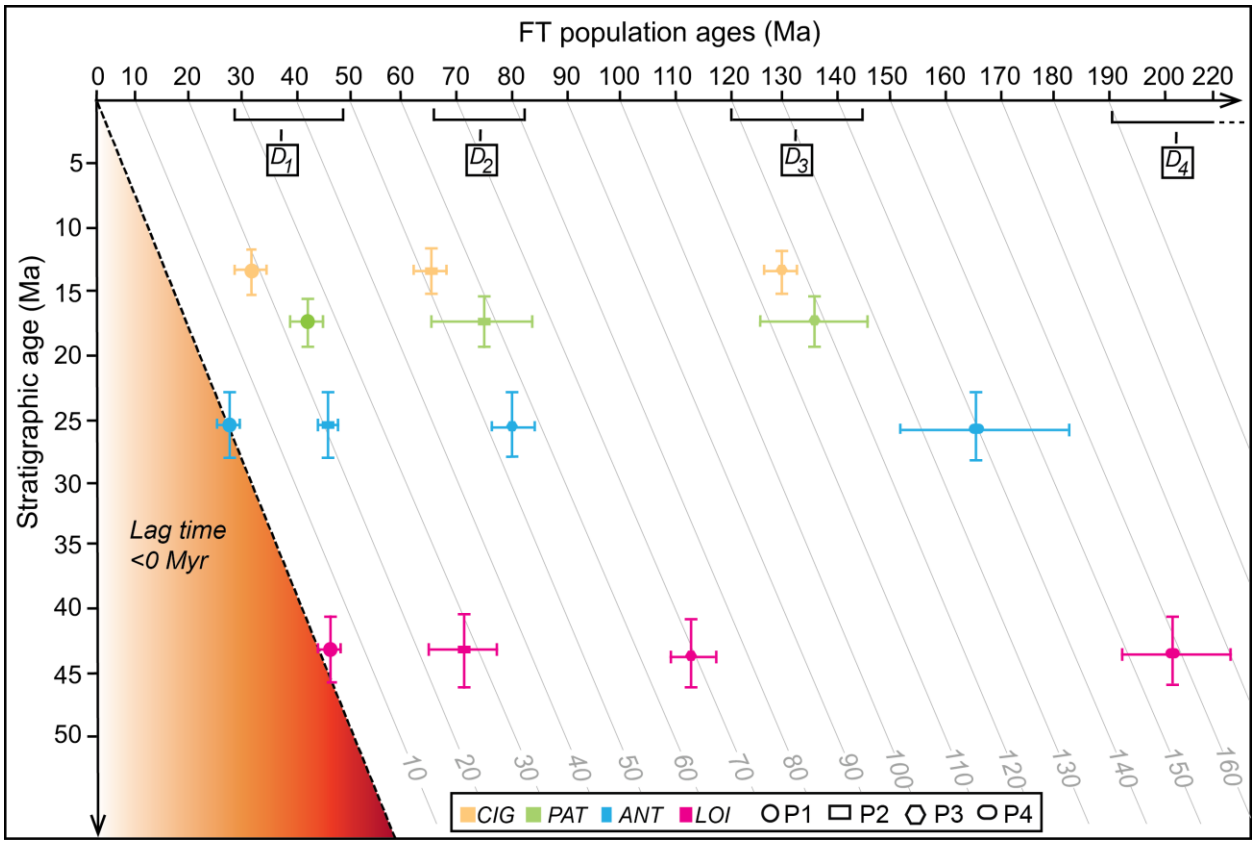

Figure 4.7 - Lag time plot representing the evolution of the detrital paths (D1-D4) through the stratigraphic record. Symbols indicate binomial peak-fit ages extracted from the mixed grain age distribution (P1-P4). Grey lines indicate the iso-lag time lines; the area right to the 1/1 correlation line corresponds to the resetting zone (Lg=tc-td<0).

In **Figure 4.8**, different steps of the evolution of the Northern Apennines after the continental collision referred to the provenance of the source rocks is shown, covering a lap of time between 41 and 7 Ma (middle Eocene-Upper Miocene). As shown in previous published papers, during the building of the Epiligurian wedge-top basins, the source is strongly influenced by the structural setting of the NA fold-and-thrust belt, in which the Ligurian Domain plays a fundamental role (Cibin et al., 2001).

In particular, the Epiligurian Units are fed by double source provenanced deposits. In the middle Eocene they are characterised by Pennidic-derived channels into the north

(**Fig. 4.8**; step 1) while, since the Oligocene, the Epiligurian Units are fed by both the underlying Ligurian Units and the lower part of the Epiligurian sedimentary succession itself (**Fig. 4.8**; step2 and 3) and the depositional environment of the Epiligurian Units shifted from a deep marine setting, dominated by sand-rich turbidite lobes (Loiano Fm) to an outer-shelf and slope setting, dominated by hemipelagites with terrigenous sands (Antognola and Contignaco Formations). The change of the depositional environment is due the occurring of a new compressional step in the accretionary wedge coupled with the late Oligocene global sea-level drop (Cibin et al., 2001). Then, the Lower Miocene (late Burdigalian) is characterised by the deposition of the Pantano and Cigarello Fms, which are characterised by a deepening trend (from nearshore to outershelf) after Sardo-Corso block rotation. The general deepening trend of the succession over time suggests deposition in extensional basins on top of the Ligurian nappe, which was advancing on the Apennines foreland thrust systems.

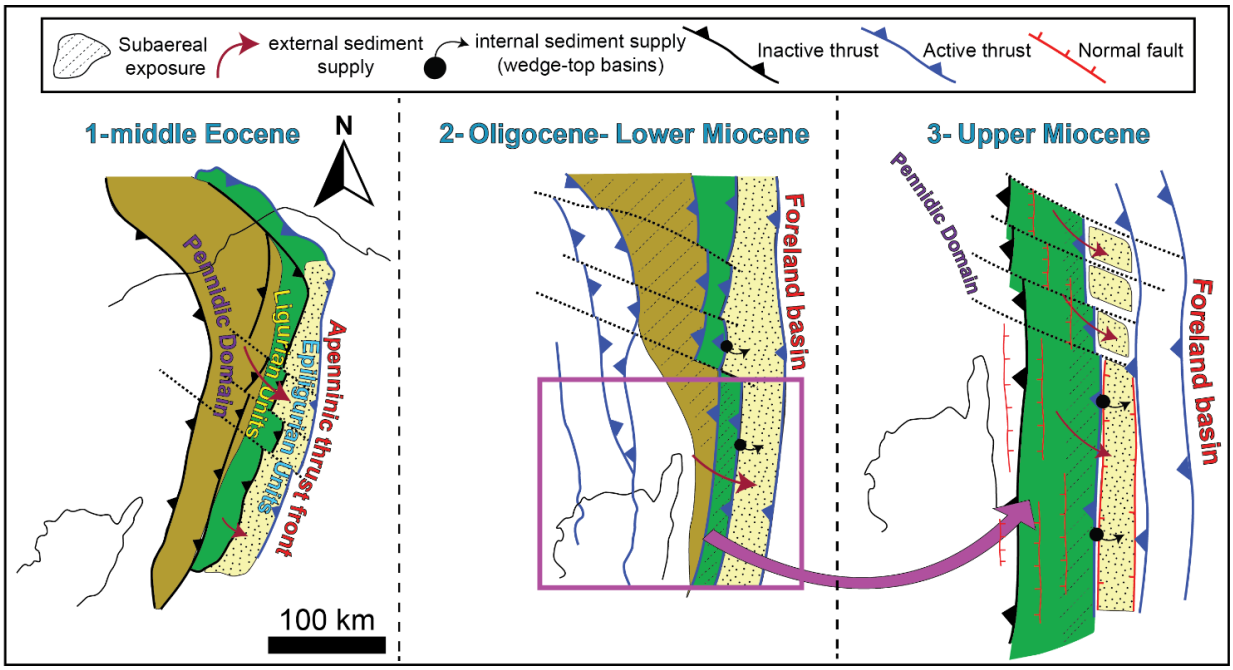

Figure 4.8- Sketch illustrating possible source provenance for the Epiligurian Basins framed within the evolution of the Western Alps-Northern Apennines tectonic junction. (Modified and redrawn after Cibin et al., 2001).

Supplementary Material

(Chapter 4)

This file contains: i) one figure **(Figure S1)** in which the length histograms obtained for all the Epiligurian formations analysed; ii) two tables showing the length data measured for the thermochronological analysis (**Table S1** and **Table S2**); iii) a brief explanation about the fission-track length measurement and the methodology applied for the individuation of the AFT population modelled for the Loiano Fm. (FT01); iv) two figures reporting plots of the main population individuated for the Loiano Fm. (FT01) **(Fig.S3_I and S3_II)**; v) six figures **(S4-S9)** representing graphs related to the correlation between Age-eU, Age-U, Age-Th, Age Rs, Rs-eU and Age-Th/U for all the AHe samples analysed; vi) two figures **(S10-S11)** showing the inverse AHe models realised for the Epiligurian units mentioned in Chapter 4;

Details about AFT method

All the 13 samples shown in Fig.2 of the Main Text were crushed and processed through hydrodynamic, magnetic and heavy-liquid separation. The obtained apatite grains were embedded in epoxy resin and polished to expose the internal surfaces within the grains. Spontaneous fission-tracks were revealed by etching the samples with 5N HNO_3 at 20°C for 20 seconds (e.g., Donelick et al., 2005, for details). The mounts have been then coupled with low-uranium fission-track-free muscovite mica sheet (external detector method) and sent for irradiation with thermal neutrons to Oregon State University. Nominal fluence of 9×10^{15} n cm^{-2} was monitored with a CN5 uranium-doped silicate dosimeter glass. Induced fission-tracks were revealed by etching the mica sheets, after irradiation, in 40% HF for 45 min. at 20 °C.

Fission-track counting (spontaneous and induced track density ρ_s and ρ_I), confined apatite fission track-lengths and D_{par} etch-pit parameters were measured using an Olympus microscope (BX51) at x1,250 magnification, equipped with a computer-automated stage and tablet system with the FTstage software (Dumitru 1993). Then D_{par} values were measured under reflected light approximately at the centre of the apatite grain in order to minimize problems of optical distortion. Etch pits were measured by placing the centre of the measuring LED (mounted on the tablet mouse) over each end of the pit.

Central ages were calculated using the zeta calibration method (Hurford & Green 1983) measuring 10 Durango (31.3 ± 0.3 Ma) age standards within grains exposing c-axis parallel crystallographic planes. Ages were calculated and analysed using the software Trackkey (Dunkl 2002) and RadialPlotter TM (Vermeesch 2009). The age-spectrum (probability density diagrams) are calculated according to (Hurford et al. 1984).

Length data

The histograms representing the length distribution obtained after the measuring for the four samples cited in the main text are shown in **Fig. S1**.

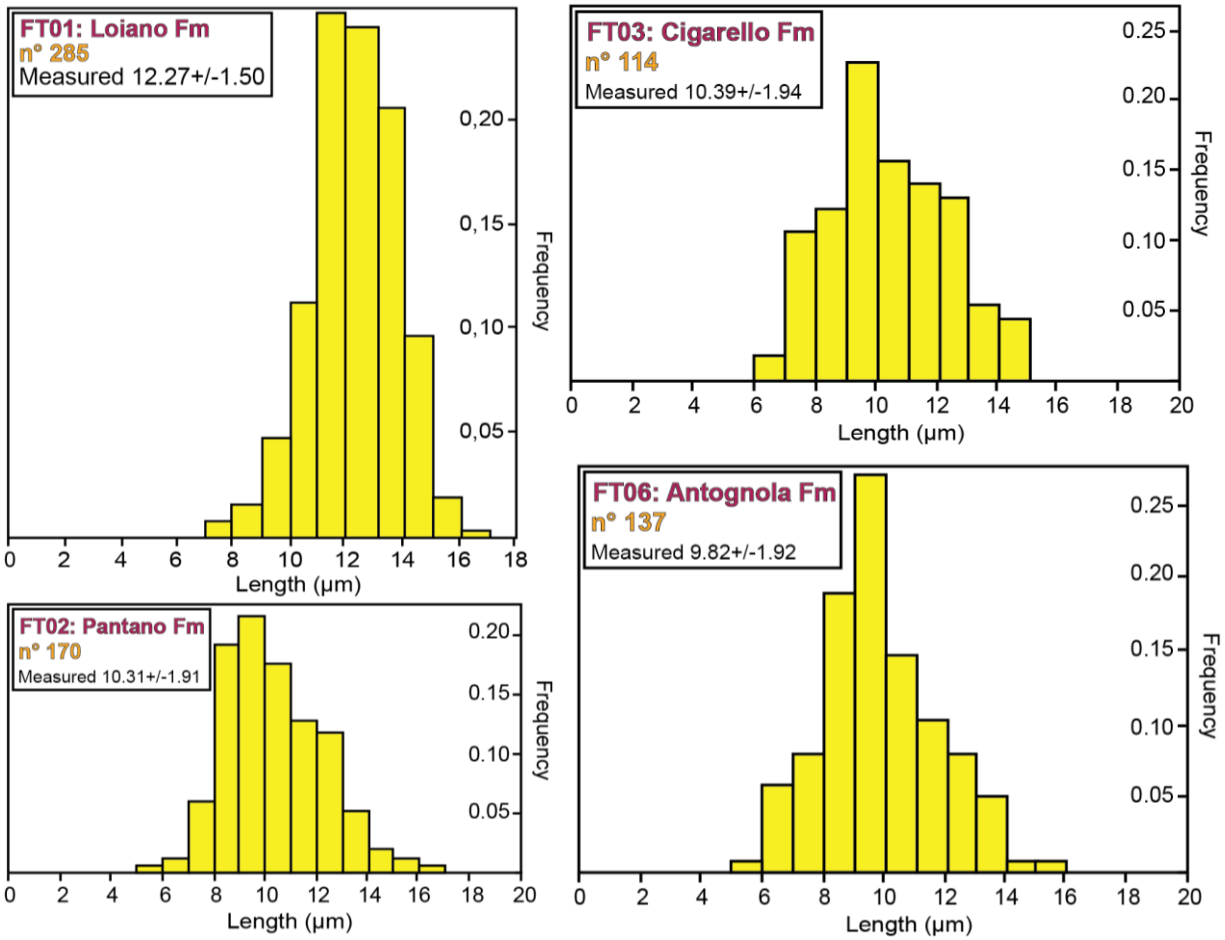

Figure S1- Lengths histogram for each AFT sample. The number of lengths refers to the total measured for all populations.

Confined track length data were measured for sample FT01 from the Loiano Fm. Only grains belonging to the youngest detrital population (FT01_pop1) (with an age within error from the depositional age of the sample) were selected in order to model this population and explore its thermal history. For each confined track length measured, the angle to the c-axis (<C) was also measured. In **Table S1** all the confined track length data for the Loiano Fm. (FT01) are shown.

#	Length	MDpar	MDprp	NDpar	X	Y	<C	<V	#in Gn
1	11.9	2.2	0.48	1	135191	199879	24.75	13.969	1
2	8.473	2.2	0.48	1	134826	199517	65.224	-76.057	2
3	8.761	2.2	0.48	1	134832	199492	89.479	-51.801	3
4	12.528	2.2	0.48	1	134630	200049	84.454	-45.735	4
5	9.71	2.2	0.48	1	134615	200078	83.855	-57.426	5
6	11.88	2.2	0.48	1	135250	199898	23.27	15.45	6
7	10.044	2.2	0.48	1	135466	200331	7.666	46.386	7
8	10.225	2.2	0.48	1	134552	200184	47.076	-8.357	8
9	13.061	1.926	4.321	1	97889	179587	85.095	-6.506	1
10	9.857	1.926	4.321	1	98028	180590	27.326	61.074	2
11	7.42	1.926	4.321	1	97844	180489	37.596	-54.005	3
12	11.151	1.926	4.321	1	97990	180487	55.117	33.283	4
13	8.022	2.118	0.549	1	181216	182253	25.278	20.746	1
14	11.635	2.118	0.549	1	180643	182616	47.435	-1.411	2
15	13.381	2.118	0.549	1	181196	182277	25.384	71.409	3
16	9.985	2.118	0.549	1	180678	182990	71.415	-62.56	4
17	7.491	2.118	0.549	1	181329	182640	76.093	-30.069	5
18	12.932	1.991	0.57	1	169957	168431	80.098	-59.761	1
19	14.324	1.991	0.57	1	169956	168492	41.966	-1.826	2
20	9.074	1.991	0.57	1	170209	168734	33.368	73.508	3
21	12.904	1.991	0.57	1	170719	168762	66.138	-25.998	4
22	12.758	1.991	0.57	1	170165	168356	80.299	-59.56	5
23	9.706	1.991	0.57	1	170550	168608	34.191	74.332	6
24	9.694	1.991	0.57	1	170968	168377	74.015	-33.875	7
25	10.771	2.297	1.016	1	84927	154808	31.234	-71.471	1
26	10.455	2.297	1.016	1	85344	155364	77.171	62.592	2
27	10.017	2.297	1.016	1	85465	154788	29.757	-10.48	3
28	7.741	2.297	1.016	1	85613	154872	68.469	71.295	4
29	11.169	2.297	1.016	1	84953	154781	19.199	-21.038	5
30	12.197	1.877	0.461	1	119996	152904	60.206	52.645	1
31	12.419	1.877	0.461	1	120430	152827	68.733	1.584	2
32	8.263	1.877	0.461	1	120612	152623	67.851	45	3
33	12.236	1.877	0.461	1	120914	152927	85.331	18.182	4
34	13.567	1.877	0.461	1	119936	153310	45.284	67.567	5
35	11.306	1.877	0.461	1	120170	152908	62.1	50.751	6
36	12.14	2.246	0.581	1	157402	132839	71.241	-53.076	1
37	11.46	2.246	0.581	1	157061	133048	85.127	-39.19	2
38	9.744	2.246	0.581	1	157617	133582	36.075	19.608	3
39	13.205	2.246	0.581	1	158675	132455	59.544	-64.772	4
40	12.93	2.246	0.581	1	158664	132204	61.219	-63.097	5
41	10.425	2.195	0.657	1	176715	134342	11.169	48.34	1
42	9.416	2.195	0.657	1	177378	134160	33.729	25.78	2
43	8.55	2.195	0.657	1	176672	133383	65.598	-6.089	3
44	12.748	2.195	0.657	1	176353	133546	42.518	16.991	4
45	13.441	1.728	0.768	1	137496	104047	51.953	23.671	1
48	12.492	1.728	0.768	1	138065	104678	19.653	-47.936	4
49	10.33	1.728	0.768	1	137978	104969	74.212	77.506	5

50	15.077	1.728	0.768	1	137547	104900	16.506	-11.777	6
51	9.532	1.728	0.768	1	137525	105097	52.841	24.558	7
52	11.084	1.728	0.768	1	137320	104889	51.016	22.733	8
53	12.588	1.728	0.768	1	136408	104693	70.503	81.215	9
54	13.408	1.77	0.579	2	126806	80023	44.891	10.305	1
55	10.713	1.77	0.579	2	126568	80294	71.152	36.565	2
56	12.581	1.77	0.579	2	126960	80021	42.422	7.836	3
57	10.465	1.77	0.579	2	126408	79544	70.269	35.683	4
58	13.799	1.77	0.579	2	126571	79532	36.725	2.139	5
59	11.24	1.77	0.579	2	127266	80618	56.279	21.692	6
60	10.494	1.77	0.579	2	126929	80370	27.115	-7.472	7
61	10.858	1.77	0.579	2	127446	79595	62.765	28.179	8
62	11.587	1.77	0.579	2	126455	79906	82.729	62.684	9
63	10.436	2.239	0.607	1	149246	83309	74.62	42.53	1
64	9.476	2.239	0.607	1	148044	82376	51.405	-11.445	2
65	8.744	2.239	0.607	1	148342	83297	56.425	60.725	3
66	11.633	1.547	0.761	1	208784	65396	35.752	-23.199	1
67	9.799	1.547	0.761	1	208644	65842	68.679	-56.125	2
68	9.266	1.547	0.761	1	209246	66236	66.319	-53.765	3
69	11.302	1.547	0.761	1	209815	65758	14.022	-1.469	4
70	11.436	1.547	0.761	1	209696	65424	31.835	44.388	5
71	8.59	2.062	0.506	1	225473	115696	30.06	-47.675	1
72	8.581	2.062	0.506	1	225928	115872	0.939	-18.555	2
73	12.114	2.062	0.506	1	225753	115472	83.105	65.489	3
74	13.856	2.062	0.506	1	225631	115621	38.5	-56.116	4
75	12.96	2.062	0.506	1	225553	114711	77.148	85.236	5
76	10.6	1.906	0.48	1	178172	129417	54.762	-20.194	1
77	14.598	2.124	0.646	1	81916	138274	64.908	64.956	1
78	11.612	2.124	0.646	1	81336	137937	70.904	-70.856	2
79	10.513	2.124	0.646	1	80930	137918	64.173	-64.125	3
80	12.314	2.124	0.646	1	81333	138331	71.528	-71.48	4
81	11.022	1.745	0.612	1	173644	141079	61.854	27.496	1
82	13.617	1.745	0.612	1	172403	140790	78.737	-11.913	2
83	12.473	1.745	0.612	1	172765	142192	43.605	45.744	3
84	9.92	1.745	0.612	1	172487	142235	85.69	3.659	4
85	7.812	1.745	0.612	1	172244	140660	36.378	-54.273	5
86	10.752	1.745	0.612	1	173151	141703	37.099	-53.552	6
87	11.094	1.961	0.814	1	126160	158092	73.885	-55.491	1
88	11.087	1.961	0.814	1	125563	158082	32.855	51.248	2
89	12.449	1.961	0.814	1	125416	158140	56.769	-38.376	3
90	11.727	1.961	0.814	1	125600	157722	62.145	80.538	4
91	9.315	1.961	0.814	1	125905	158105	38.165	-19.772	5
92	10.372	1.668	0.499	1	144554	179208	50.343	-25.731	1
93	10.529	1.668	0.499	1	144547	179207	51.149	-24.925	2
94	7.754	1.668	0.499	1	144589	179187	50.061	-26.012	3
95	11.217	1.668	0.499	1	144007	179728	79.27	3.196	4
96	12.508	1.668	0.499	1	143863	180207	63.183	40.743	5
97	12.444	1.668	0.499	1	143705	180099	83.831	20.095	6

98	9.727	1.668	0.499	1	143711	180512	57.033	46.893	7
99	9.902	1.668	0.499	1	144440	180368	58.481	-17.592	8
100	10.69	1.668	0.499	1	144234	179809	40.001	-36.072	9
101	10.831	1.668	0.499	1	144741	180195	80.332	23.595	10
102	12.707	1.668	0.499	1	144755	180132	24.783	79.144	11
103	10.228	1.668	0.499	1	144499	180401	55.48	-20.594	12
104	9.384	2.247	0.399	1	85337	154947	26.903	-10.833	1
105	9.938	2.247	0.399	1	85141	155486	79.271	62.993	2
106	9.826	2.247	0.399	1	84773	154904	16.747	-20.989	3
107	7.509	2.247	0.399	1	85506	155096	19.555	-57.291	4
108	8.919	2.154	0.764	1	124176	141769	65.224	-6.219	1
109	10.328	2.154	0.764	1	123198	142700	48.654	59.903	2
110	13.619	2.154	0.764	1	123904	142421	79.914	8.471	3
111	9.812	2.154	0.764	1	123639	142115	46.668	-24.775	4
112	11.849	1.846	0.579	1	137185	148780	50.74	25.084	1
113	10.87	1.846	0.579	1	137195	148745	29.893	4.236	2
114	9.108	1.846	0.579	1	137690	148293	59.312	-84.968	3
115	10.789	1.846	0.579	1	138030	148854	78.978	75.366	4
116	10.474	1.846	0.579	1	137216	149508	81.606	72.738	5
117	12.705	2.068	0.346	1	166784	213476	36.358	-39.181	1
118	9.993	2.104	0.579	1	84983	154811	33.597	-72.181	1
119	10.152	2.104	0.579	1	85490	154707	83.49	57.926	2
120	10.197	2.104	0.579	1	85344	155394	79.717	61.699	3
121	7.125	2.104	0.579	1	85607	154951	71.756	69.661	4
122	10.363	2.104	0.579	1	85473	154867	27.829	-10.755	5
123	11.012	1.556	0.36	1	82149	137594	32.242	-38.057	1
124	12.337	1.556	0.36	1	82276	138117	69.847	64.032	2
125	12.709	1.556	0.36	1	81698	138194	66.49	-72.305	3
126	11.686	1.556	0.36	1	81255	137694	59.101	-64.916	4
127	12.824	1.556	0.36	1	82254	137966	87.03	81.215	5
128	9.009	1.742	0.546	1	90772	50252	87.5	-26.405	1
129	9.573	1.742	0.546	1	90477	50111	87.661	-26.565	2
130	11.683	1.742	0.546	1	91023	48856	89.882	-28.787	3
131	11.55	1.931	0.472	1	97635	128626	86.541	-80.631	1
132	8.158	1.931	0.472	1	97513	128178	21.477	-15.566	2
133	9.151	2.377	0.689	1	98097	120228	42.104	-21.342	1
134	13.461	1.701	0.768	1	98526	87814	61.903	-11.023	1
135	11.004	1.701	0.768	1	98360	87996	65.818	-63.303	2
136	11.288	2.306	0.56	1	105822	49552	68.536	3.521	1
137	12.379	1.721	0.303	1	107602	54960	70.825	73.729	1
138	9.302	1.721	0.303	1	106956	55370	55.218	19.772	2
139	9.552	1.721	0.303	1	107511	54538	13.4	-48.846	3
141	9.19	1.941	0.852	1	104992	73735	34.788	12.645	2
142	8.245	1.941	0.852	1	103918	72916	85.756	63.613	3
143	7.888	1.875	0.663	1	108077	133284	75.913	28.048	1
144	9.611	1.875	0.663	1	108077	134393	29.57	-46.469	2
145	8.122	1.875	0.663	1	107497	134021	63.86	-12.179	3
146	9.093	1.723	0.796	1	112795	97752	42.076	38.884	1

147	9.355	1.723	0.796	1	112090	97874	35.42	32.229	2
148	8.282	1.987	0.353	1	120744	150231	62.038	-82.875	1
149	7.7	1.987	0.353	1	120319	150039	49.109	28.272	2
150	10.874	1.987	0.353	1	120894	152734	87.834	19.191	1
151	11.795	1.987	0.353	1	120018	152677	57.446	53.911	2
152	8.537	2.174	0.499	1	122809	116234	88.305	34.43	1
153	10.145	2.174	0.499	1	121951	116700	38.421	-15.455	2
154	8.651	2.174	0.499	1	121979	116662	60.718	6.843	3
155	11.802	1.864	0.448	1	131406	90131	74.352	-65.397	1
156	9.73	1.864	0.448	1	131293	90390	67.416	-27.165	2
157	7.102	1.864	0.448	1	131870	90822	30.484	9.767	3
158	9.555	1.864	0.448	1	131327	90305	61.166	-20.915	4
159	10.159	2.038	0.507	1	131561	83175	40.555	70.953	1
160	9.121	1.708	0.636	2	135773	48036	57.451	22.004	1
161	9.983	1.708	0.636	2	134580	47903	47.026	-53.519	2
162	12.101	1.905	0.645	1	137263	148498	52.214	26.806	1
163	10.846	1.905	0.645	1	137278	148466	27.806	2.398	2
164	10.414	1.905	0.645	1	137337	148479	36.229	-61.636	3
165	9.434	1.905	0.645	1	137238	148927	41.841	-67.249	4
166	6.788	1.7	0.721	1	146798	149035	4.586	21.801	1
167	11.904	1.826	0.54	1	145415	57372	72.206	-45.579	1
168	11.373	1.826	0.54	1	145041	58296	76.653	-41.132	2
169	10.555	1.826	0.54	1	145165	57367	53.381	-64.404	3
170	8.518	2.244	0.498	1	146933	149015	11.245	19.784	1
171	8.165	2.244	0.498	1	147035	148454	1.975	29.055	2
172	8.281	2.244	0.498	1	147034	148451	1.479	29.55	3
173	7.088	1.656	0.75	1	147542	149366	53.134	-64.458	1
174	8.033	1.656	0.75	1	147685	150847	87.675	-25.267	2
175	8.669	1.946	0.392	1	157009	171234	50.793	67.148	1
176	6.678	1.946	0.392	1	156751	171178	82.63	35.311	2
177	11.536	2.084	0.76	1	160182	74194	72.105	35.108	1
178	9.559	2.084	0.76	1	160709	73916	50.533	13.536	2
179	11.059	2.084	0.76	1	160937	73756	77.966	65.037	3
180	10.577	2.084	0.76	1	161012	73447	66.963	76.04	4
181	12.076	2.084	0.76	1	160964	73215	48.667	-85.664	5
182	12.037	1.527	0.708	1	157161	132626	62.878	-55.052	1
183	11.32	1.527	0.708	1	157785	132150	73.748	-44.182	2
184	9.583	1.527	0.708	1	157528	132193	77.067	-40.862	3
185	8.601	1.527	0.708	1	157271	132035	50.726	-67.203	4
186	11.739	1.867	0.835	1	179843	77274	54.098	-31.443	1
187	9.499	1.867	0.835	1	178718	76922	32.96	-10.305	2
188	8.974	1.867	0.835	1	179098	76506	70.722	-48.066	3
189	12.475	1.548	0.586	1	180115	86663	63.026	16.775	1
190	9.543	1.548	0.586	1	179723	86407	89.495	-10.704	2
191	10.449	1.548	0.586	1	179536	86818	85.511	-5.711	3
192	9.046	1.548	0.586	1	179898	86778	69.203	10.597	4
193	12.647	1.664	0.843	1	181983	149962	87.634	89.479	1
194	7.412	1.664	0.843	1	181641	149914	45.516	-48.403	2

195	8.192	1.856	0.649	1	181572	182542	75.722	-26.745	1
196	8.526	1.856	0.649	1	181347	182139	29.092	19.885	2
197	11.136	1.856	0.649	1	180632	182616	49.567	-0.591	3
198	9.412	1.856	0.649	1	180967	183029	49.675	-0.699	4
199	14.01	2.417	0.765	1	188571	32098	46.073	-64.159	1
200	8.069	2.417	0.765	1	188549	32146	89.107	-21.125	2
201	13.338	2.417	0.765	1	188772	31911	60.754	-49.478	3
202	12.067	2.417	0.765	1	188429	32200	83.181	-27.051	4
203	11.565	2.417	0.765	1	188108	32360	56.989	-53.243	5
204	11.761	2.417	0.765	1	188042	32454	44.195	-66.038	6
205	7.136	2.417	0.765	1	188294	31768	59.092	10.676	7
206	13.285	2.021	0.543	1	129436	184480	74.288	-15.341	1
207	10.356	2.021	0.543	1	129493	184485	53.247	37.124	2
208	9.565	2.021	0.543	1	129627	184417	87.257	-2.372	3
209	12.778	2.021	0.543	1	129482	183920	59.355	-30.275	4
210	10.917	2.021	0.543	1	129765	184036	55.77	34.601	5
211	10.204	2.021	0.543	1	129786	184126	58.971	31.399	6
212	10.921	2.021	0.543	1	129671	184920	79.12	11.251	7
213	12.902	2.021	0.543	1	128413	184337	56.189	34.182	8
214	8.742	2.021	0.543	1	128523	184631	85.89	-3.74	9
215	10.534	2.021	0.543	1	128532	184780	51.211	-38.418	10
216	10.431	2.021	0.543	1	128884	184305	81.84	8.531	11
217	9.51	1.699	0.53	1	200364	183971	84	18.981	1
218	11.851	1.699	0.53	1	199340	183959	31.853	71.128	2
219	13.574	2.316	0.698	1	224168	182796	56.166	-85.965	1
220	13.449	2.323	0.737	1	84906	154499	51.717	-34.16	1
221	8.617	2.323	0.737	1	86088	153784	26.332	-8.775	2
222	8.474	1.683	0.464	1	84125	148371	53.531	39.207	1
223	9.258	1.683	0.464	1	84639	148666	83.052	-4.21	2
224	8.379	1.683	0.464	1	84195	148331	34.037	58.7	3
225	11.251	1.734	0.558	1	194025	151733	35.964	48.318	1
226	8.003	1.734	0.558	1	194533	151341	48.982	-46.736	2
227	9.113	1.734	0.558	1	192899	151295	33.722	50.56	3
228	10.401	1.734	0.558	1	193009	151807	68.64	15.642	4
229	14.967	1.794	0.319	1	137143	147529	63.801	-42.55	1
230	9.481	1.794	0.319	1	137370	147670	70.576	-49.325	2
231	11.197	1.794	0.319	1	137045	147927	89.233	-67.983	3
232	11.017	2.419	0.63	1	102537	138552	54.543	-79.616	1
233	12.318	2.419	0.63	1	102144	138425	61.996	36.923	2
234	14.488	2.419	0.63	1	102425	139048	86.68	61.607	3
235	12.468	2.419	0.63	1	102410	138633	62.478	37.405	4
236	7.904	2.07	0.607	1	132809	143975	29.94	-6.973	1
237	8.592	2.07	0.607	1	133618	143553	41.487	4.574	2
238	8.655	2.07	0.607	1	132963	143191	37.503	-74.416	3
239	7.594	2.07	0.607	1	133341	142858	72.624	70.463	4
240	8.812	2.018	0.733	1	226090	136824	23.474	48.428	1
241	12.684	2.018	0.733	1	226578	137419	67.636	-87.409	2
242	14.851	2.018	0.733	1	225869	137568	70.74	-45.785	3

243	10.682	2.018	0.733	1	226251	137312	64.426	89.381	4
244	10.91	1.99	0.638	1	154799	132869	71.765	-70.527	1
245	8.34	1.99	0.638	1	154156	133033	40.982	42.221	2
246	12.659	1.99	0.638	1	153953	133076	69.279	70.518	3
247	12.005	1.624	0.531	1	94343	129143	36.95	4.336	1
248	7.731	1.624	0.531	1	94963	129059	5.483	-27.13	2
249	9.428	1.624	0.531	1	94725	129427	30.531	-2.083	3
250	9.754	2.245	0.51	1	193202	121761	85.509	-27.309	1
251	8.918	2.245	0.51	1	193288	122257	72.674	-5.492	2
252	12.169	2.245	0.51	1	193007	122551	29.07	38.112	3
253	10.791	2.245	0.51	1	193269	122972	78.793	-34.026	4
254	13.422	2.245	0.51	1	193062	122997	84.732	-28.087	5
255	9.446	1.831	0.779	1	153419	123820	62.683	-47.68	1
256	9.121	1.831	0.779	1	153299	123911	54.568	15.068	2
257	12.385	1.831	0.779	1	152829	124265	55.792	13.844	3
258	11.311	1.831	0.779	1	152490	124209	58.889	-51.474	4
259	12.11	1.831	0.779	1	152427	123730	31.103	38.534	5
260	12.497	1.831	0.779	1	152587	123839	81.968	-12.331	6
261	13.18	1.831	0.779	1	152279	124550	83.028	-27.335	7
262	15.417	1.604	0.653	1	192660	122455	58.872	-53.13	1
263	10.848	1.604	0.653	1	192978	122609	78.838	-10.84	2
264	12.686	1.604	0.653	1	193176	122913	81.524	-30.479	3
265	11.383	1.604	0.653	1	193375	122856	78.787	-33.215	4
266	8.111	1.604	0.653	1	193126	122243	57.477	10.521	5
267	9.849	1.604	0.653	1	193183	121688	87.204	-24.798	6
268	13.184	1.604	0.653	1	193653	121609	71.666	-3.668	7
269	11.172	1.604	0.653	1	192782	121712	49.655	18.343	8
270	11.18	1.604	0.653	1	192470	121626	45.994	-66.008	9
271	10.801	1.975	0.541	1	164734	116555	71.528	73.474	1
272	8.036	1.975	0.541	1	164069	117382	10.622	-24.376	2
273	11.796	1.883	0.731	1	155021	108502	51.834	20.428	1
274	12.607	1.883	0.731	1	154593	108982	50.719	-57.019	2
275	11.001	1.883	0.731	1	154470	109079	4.059	76.321	3
276	16.615	1.883	0.731	1	155719	109624	3.942	76.204	4
277	10.066	1.883	0.731	1	156176	109613	52.062	-55.676	5
278	12.052	1.883	0.731	1	155084	108574	50.913	21.349	6
279	6.672	2.114	0.557	1	141445	107718	40.541	-23.767	1
280	9.105	2.114	0.557	1	141906	108114	9.151	25.925	2
281	9.943	2.114	0.557	1	141442	108808	66.844	-50.069	3
282	14.191	1.562	0.406	1	110844	109539	51.823	-29.717	1
283	13.048	1.562	0.406	1	110783	109703	81.832	16.628	2
284	8.481	1.804	0.198	1	168643	104657	23.056	-40.054	1
285	8.582	1.804	0.198	1	168361	104785	42.015	25.017	2
286	10.179	2.043	0.495	1	77138	93437	78.275	-7.282	1
287	8.724	2.043	0.495	1	76743	93720	26.785	44.208	2
288	10.906	2.043	0.495	1	76585	94549	56.812	14.181	3
289	9.633	1.76	0.768	2	77189	93444	82.166	-9.407	1

290	10.454	1.76	0.768	2	76754	94615	58.798	13.96	2
291	10.086	1.822	0.869	1	127826	72796	18.325	43.377	1
292	9.995	1.822	0.869	1	128222	72178	7.469	32.521	2
293	11.51	1.822	0.869	1	127493	72988	30.706	-5.654	3
294	12.311	1.822	0.869	1	127988	73203	72.206	-82.742	4
295	9.387	2.37	1.054	1	173660	70523	83.224	0.699	1
296	12.489	2.37	1.054	1	173233	70302	69.051	-27.026	2
297	12.007	2.018	0.675	1	108616	67723	65.41	27.417	1
298	12.363	2.018	0.675	1	109193	67693	89.834	52.172	2
299	10.028	2.018	0.675	1	109186	67829	56.945	18.951	3
300	12.837	2.445	0.804	1	148391	53976	56.518	-40.876	1
301	12.441	2.445	0.804	1	147315	53228	47.099	35.507	2
302	9.588	2.445	0.804	1	148552	52892	52.568	30.038	3
303	9.796	2.445	0.804	1	148790	53234	6.4	76.206	4

Table S1- Length data belonging to the Loiano Fm

For the selection of the length values of the subpopulation of Loiano Fm (FT01pop1), an inverse procedure was performed. In particular, using the software Radial Plotter, we realised one radialplot for each sample analysed in this work based on the D_{par} values belonging to each crystal measured during the counting procedure **(Fig.S2)**. Then, we focused on the Loiano Fm, and correlated the number of each crystal with length values reported in **Table S2**.

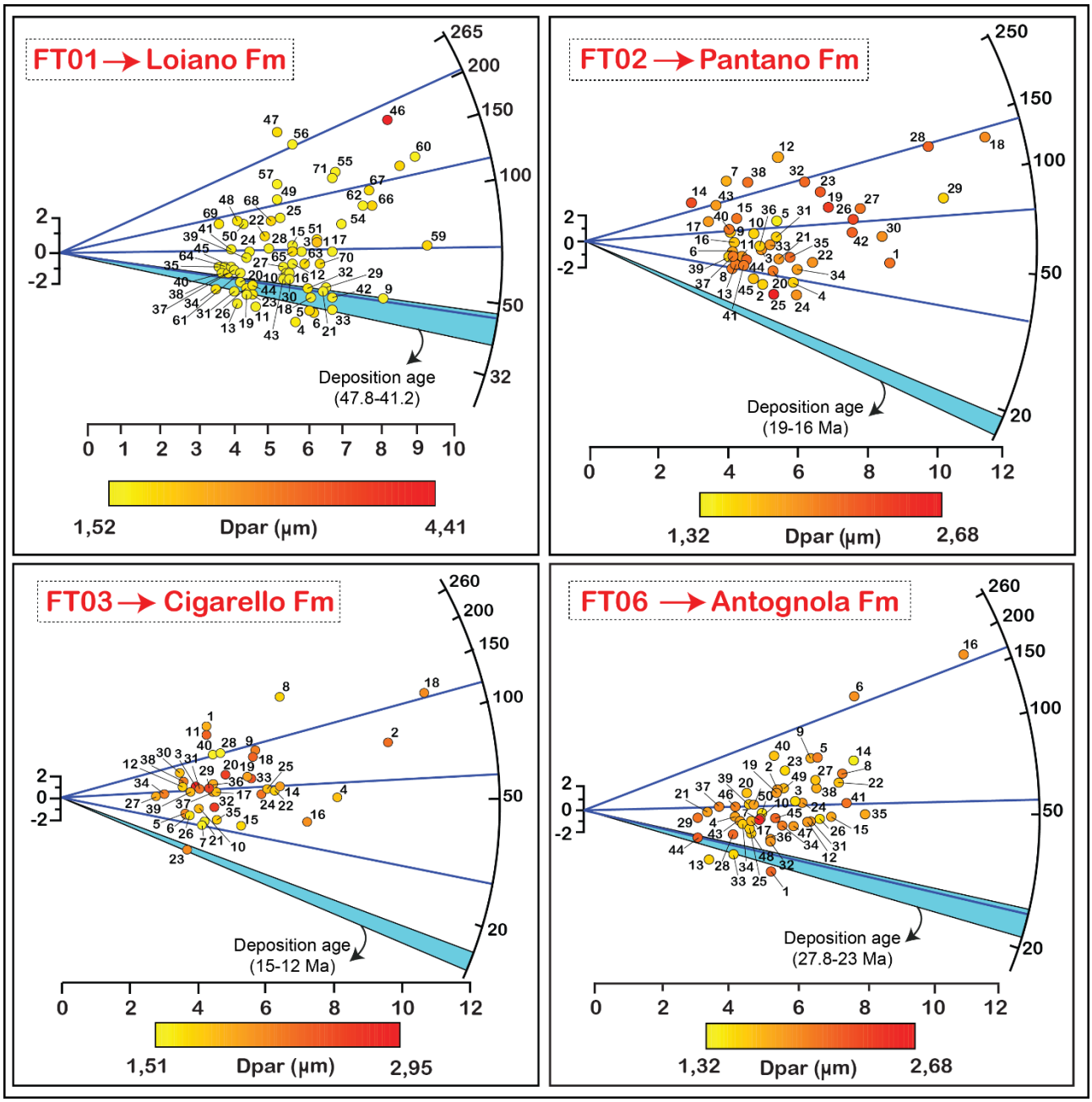

Figure S2- Radial plot calculated using Radial Plotter program, which show the Dpar values for each grain of the analysed samples.

Age data were analysed using BinomFit and Trackkey softwares (Ehlers et al., 2005; Dunkl, 2002), which provide tools for the analysis and interpretation of fission-track grain-age data. BinomFit calculated detrital populations or peaks (P) for mixed fission-

track grain-age distributions **(Fig. S3)** using the binomial peak-fitting algorithm of Galbraith and Green (1990) and Galbraith and Laslett (1993). The program supports both automatic and manual modes for searching and identifying the optimal number of significant P and can handle up to 1000 grain ages and solve for as many as 10 P. Trackkey calculates ages, main statistical parameters and tests and presents single-grain-data on different plots according to published algorithms.

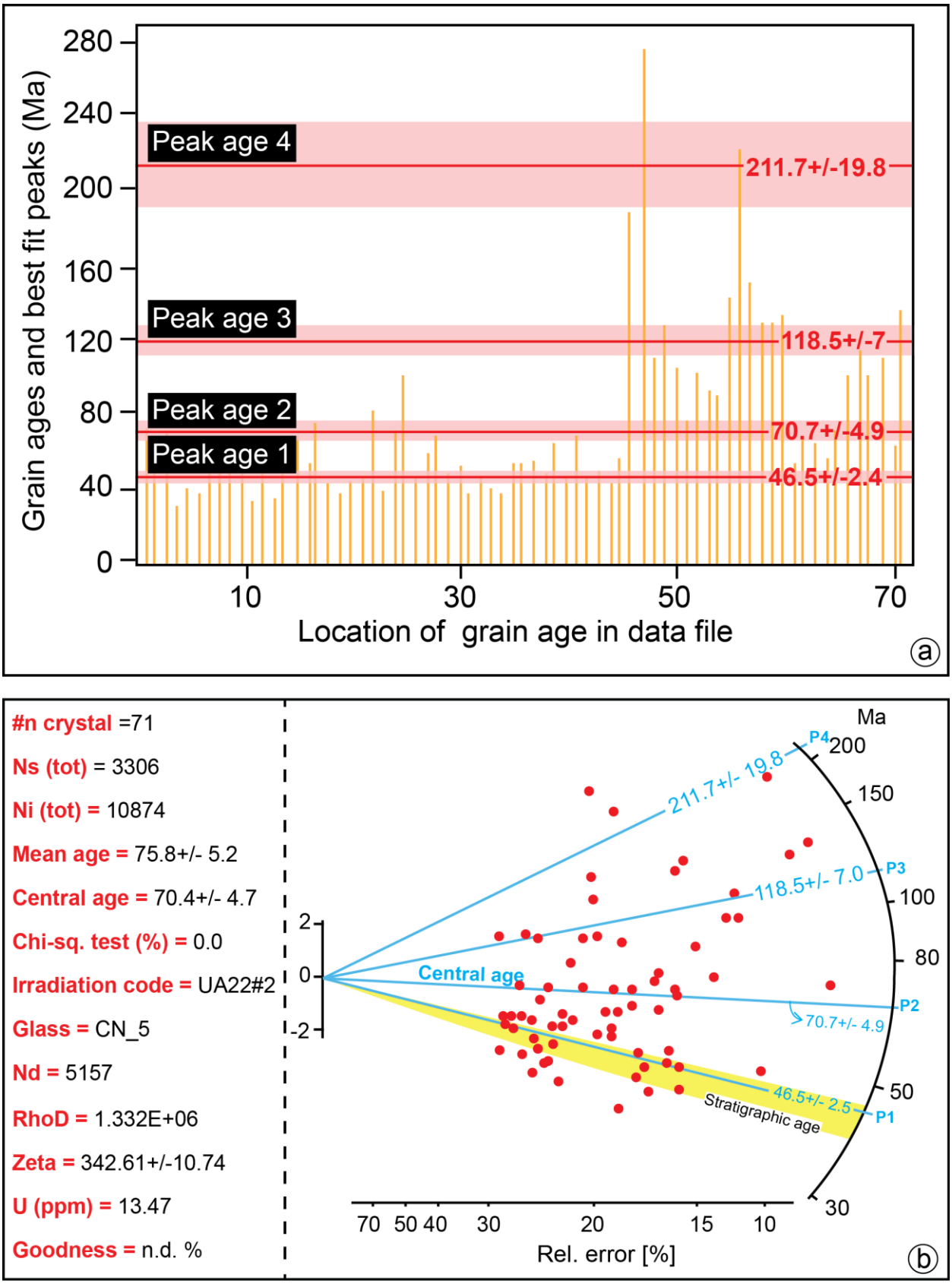

Figure S3_I- Detrital distribution and radioplot for the Loiano Fm. calculated using by BinomFit (a) and Trackkey (b) programs.

#	Length	MDpar	MDprp	NDpar	X	Y	<C	V	#in Gn
18	12.932	1.991	0.57	1	169957	168431	80.098	-59.761	1
19	14.324	1.991	0.57	1	169956	168492	41.966	-1.826	2
20	9.074	1.991	0.57	1	170209	168734	33.368	73.508	3
21	12.904	1.991	0.57	1	170719	168762	66.138	-25.998	4
22	12.758	1.991	0.57	1	170165	168356	80.299	-59.56	5
23	9.706	1.991	0.57	1	170550	168608	34.191	74.332	6
24	9.694	1.991	0.57	1	170968	168377	74.015	-33.875	7
25	10.771	2.297	1.016	1	84927	154808	31.234	-71.471	1
26	10.455	2.297	1.016	1	85344	155364	77.171	62.592	2
27	10.017	2.297	1.016	1	85465	154788	29.757	-10.48	3
28	7.741	2.297	1.016	1	85613	154872	68.469	71.295	4
29	11.169	2.297	1.016	1	84953	154781	19.199	-21.038	5
30	12.197	1.877	0.461	1	119996	152904	60.206	52.645	1
31	12.419	1.877	0.461	1	120430	152827	68.733	1.584	2
32	8.263	1.877	0.461	1	120612	152623	67.851	45	3
33	12.236	1.877	0.461	1	120914	152927	85.331	18.182	4
34	13.567	1.877	0.461	1	119936	153310	45.284	67.567	5
35	11.306	1.877	0.461	1	120170	152908	62.1	50.751	6
45	13.441	1.728	0.768	1	137496	104047	51.953	23.671	1
46	13.255	1.728	0.768	1	137572	104321	42.378	14.096	2
47	11.986	1.728	0.768	1	138189	104262	41.129	-69.412	3
48	12.492	1.728	0.768	1	138065	104678	19.653	-47.936	4
49	10.33	1.728	0.768	1	137978	104969	74.212	77.506	5
50	15.077	1.728	0.768	1	137547	104900	16.506	-11.777	6
51	9.532	1.728	0.768	1	137525	105097	52.841	24.558	7
52	11.084	1.728	0.768	1	137320	104889	51.016	22.733	8
53	12.588	1.728	0.768	1	136408	104693	70.503	81.215	9
63	10.436	2.239	0.607	1	149246	83309	74.62	42.53	1
64	9.476	2.239	0.607	1	148044	82376	51.405	-11.445	2
65	8.744	2.239	0.607	1	148342	83297	56.425	60.725	3
71	8.59	2.062	0.506	1	225473	115696	30.06	-47.675	1
72	8.581	2.062	0.506	1	225928	115872	0.939	-18.555	2
73	12.114	2.062	0.506	1	225753	115472	83.105	65.489	3
74	13.856	2.062	0.506	1	225631	115621	38.5	-56.116	4
75	12.96	2.062	0.506	1	225553	114711	77.148	85.236	5
92	10.372	1.668	0.499	1	144554	179208	50.343	-25.731	1
93	10.529	1.668	0.499	1	144547	179207	51.149	-24.925	2
94	7.754	1.668	0.499	1	144589	179187	50.061	-26.012	3
95	11.217	1.668	0.499	1	144007	179728	79.27	3.196	4
96	12.508	1.668	0.499	1	143863	180207	63.183	40.743	5
97	12.444	1.668	0.499	1	143705	180099	83.831	20.095	6
98	9.727	1.668	0.499	1	143711	180512	57.033	46.893	7
99	9.902	1.668	0.499	1	144440	180368	58.481	-17.592	8
100	10.69	1.668	0.499	1	144234	179809	40.001	-36.072	9

#	Length	MDpar	MDprp	NDpar	X	Y	<C	< V	#in Gn
101	10.831	1.668	0.499	1	144741	180195	80.332	23.595	10
102	12.707	1.668	0.499	1	144755	180132	24.783	79.144	11
103	10.228	1.668	0.499	1	144499	180401	55.48	-20.594	12
118	9.993	2.104	0.579	1	84983	154811	33.597	-72.181	1
119	10.152	2.104	0.579	1	85490	154707	83.49	57.926	2
120	10.197	2.104	0.579	1	85344	155394	79.717	61.699	3
121	7.125	2.104	0.579	1	85607	154951	71.756	69.661	4
122	10.363	2.104	0.579	1	85473	154867	27.829	-10.755	5
131	11.55	1.931	0.472	1	97635	128626	86.541	-80.631	1
132	8.158	1.931	0.472	1	97513	128178	21.477	-15.566	2
140	7.833	1.941	0.852	1	104125	74168	24.038	-46.181	1
141	9.19	1.941	0.852	1	104992	73735	34.788	12.645	2
142	8.245	1.941	0.852	1	103918	72916	85.756	63.613	3
143	7.888	1.875	0.663	1	108077	133284	75.913	28.048	1
144	9.611	1.875	0.663	1	108077	134393	29.57	-46.469	2
145	8.122	1.875	0.663	1	107497	134021	63.86	-12.179	3
146	9.093	1.723	0.796	1	112795	97752	42.076	38.884	1
147	9.355	1.723	0.796	1	112090	97874	35.42	32.229	2
148	8.282	1.987	0.353	1	120744	150231	62.038	-82.875	1
149	7.7	1.987	0.353	1	120319	150039	49.109	28.272	2
150	10.874	1.987	0.353	1	120894	152734	87.834	19.191	1
151	11.795	1.987	0.353	1	120018	152677	57.446	53.911	2
166	6.788	1.7	0.721	1	146798	149035	4.586	21.801	1
170	8.518	2.244	0.498	1	146933	149015	11.245	19.784	1
171	8.165	2.244	0.498	1	147035	148454	1.975	29.055	2
172	8.281	2.244	0.498	1	147034	148451	1.479	29.55	3
175	8.669	1.946	0.392	1	157009	171234	50.793	67.148	1
176	6.678	1.946	0.392	1	156751	171178	82.63	35.311	2

Table S2- Length data belonging to the youngest population of the Loiano Fm.

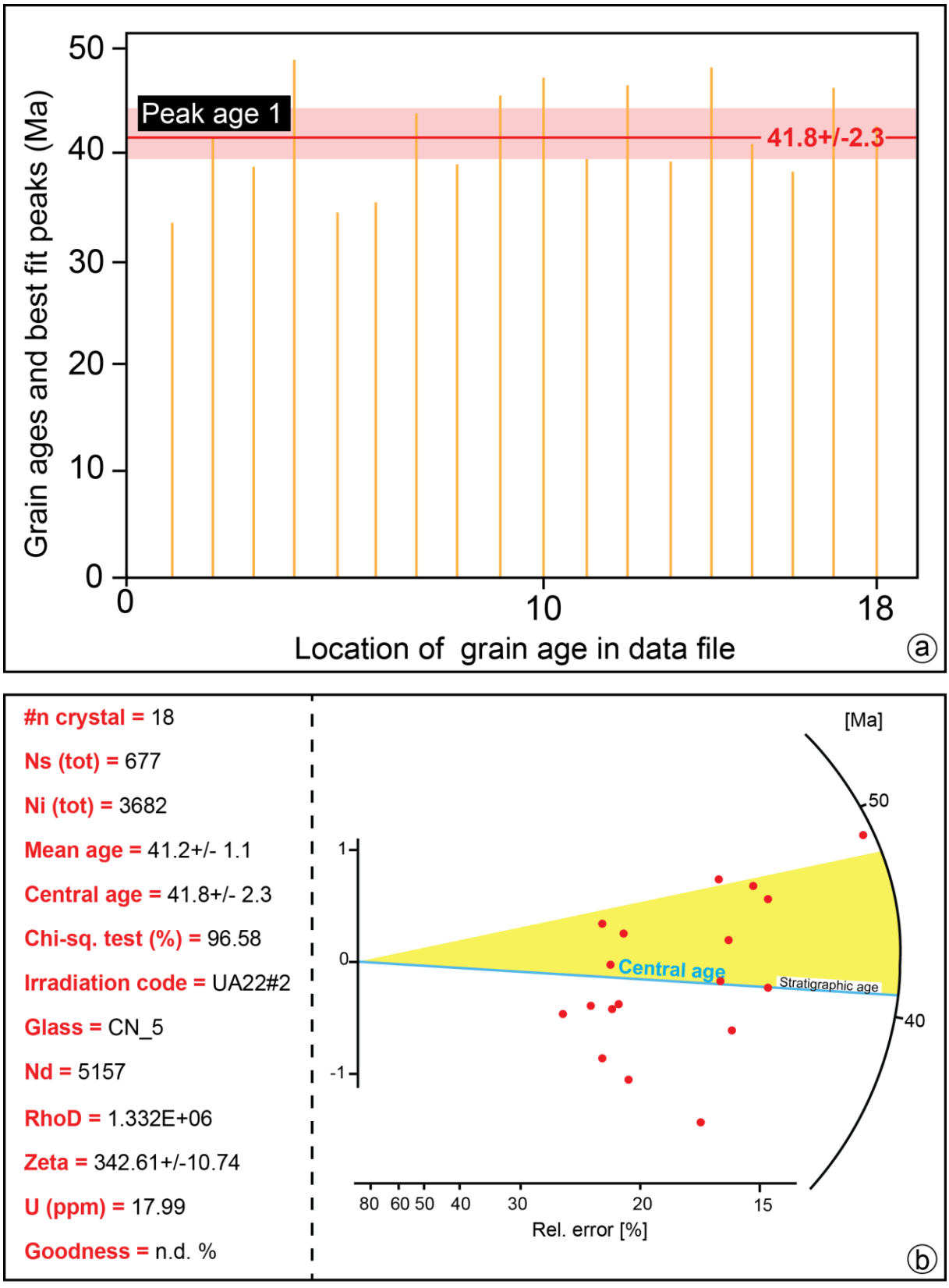

Figure S3_II- Graphic view of the data belonging to the subpopulation FT01_pop1 (Loiano Fm.) elaborated by BinomFit (a) and Trackkey (b) programs.

Details about AHe method

Five samples containing the best apatite grains (euhedral, widths > 60 μm and inclusion-free) were selected for AHe analyses. For each sample, five apatite crystal were hand-picked, measured and photographed and packed into 0.8 mm Nb tubes. The grains were degassed with a Nd-YAG laser and ^{4}He was measured by a quadruple mass spectrometer. The concentration of U, Th and Sm were calculated using a coupled plasma spectrometer and the alpha ejection correction was applied to the measured He ages (see Farley et al. 1996; Farley 2002 for details).

Figure S4- Plots related to apatite (U-Th)/He results of sample FT01

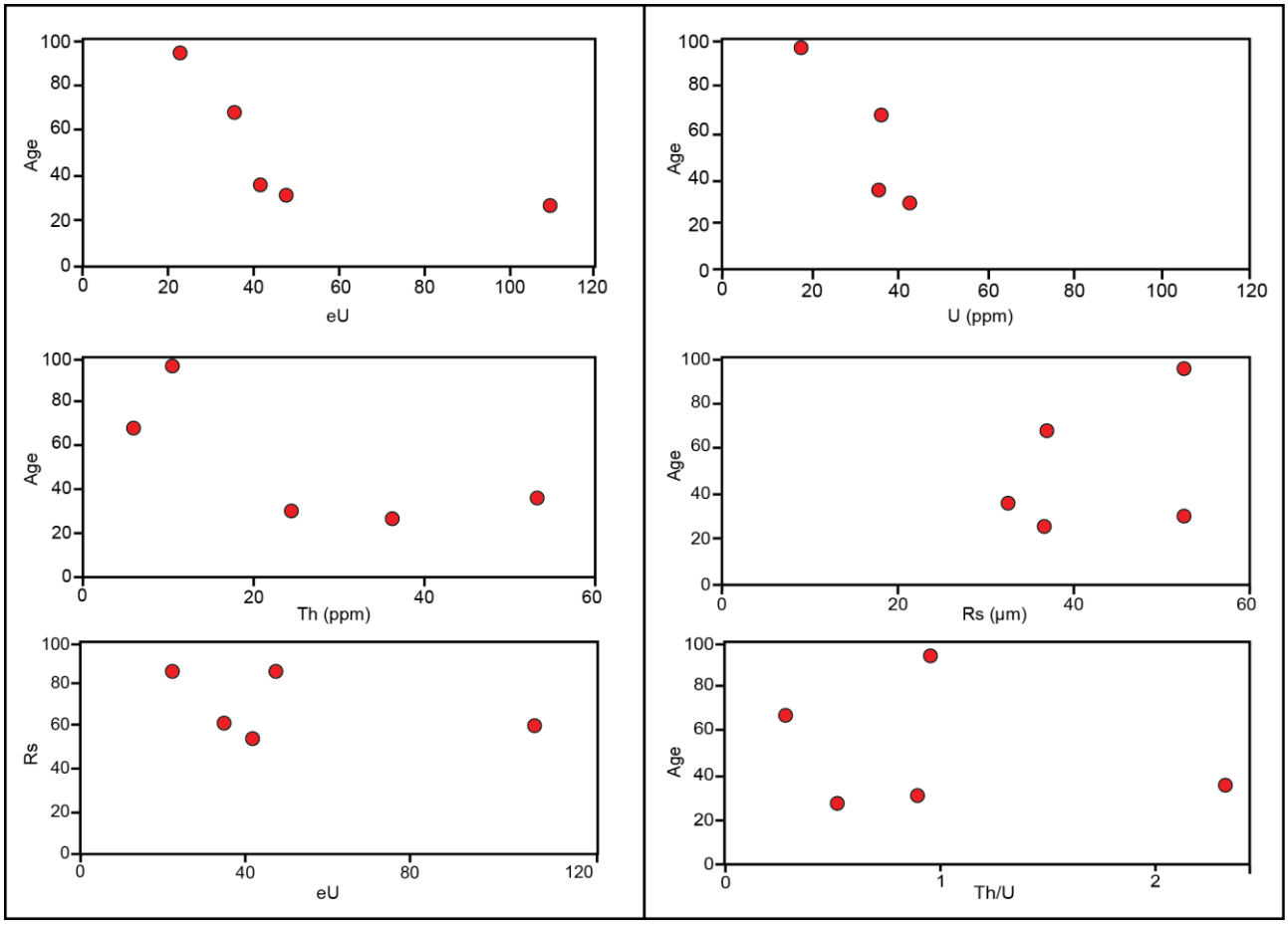

Figure S5- Plots related to apatite (U-Th)/He results of sample FT02

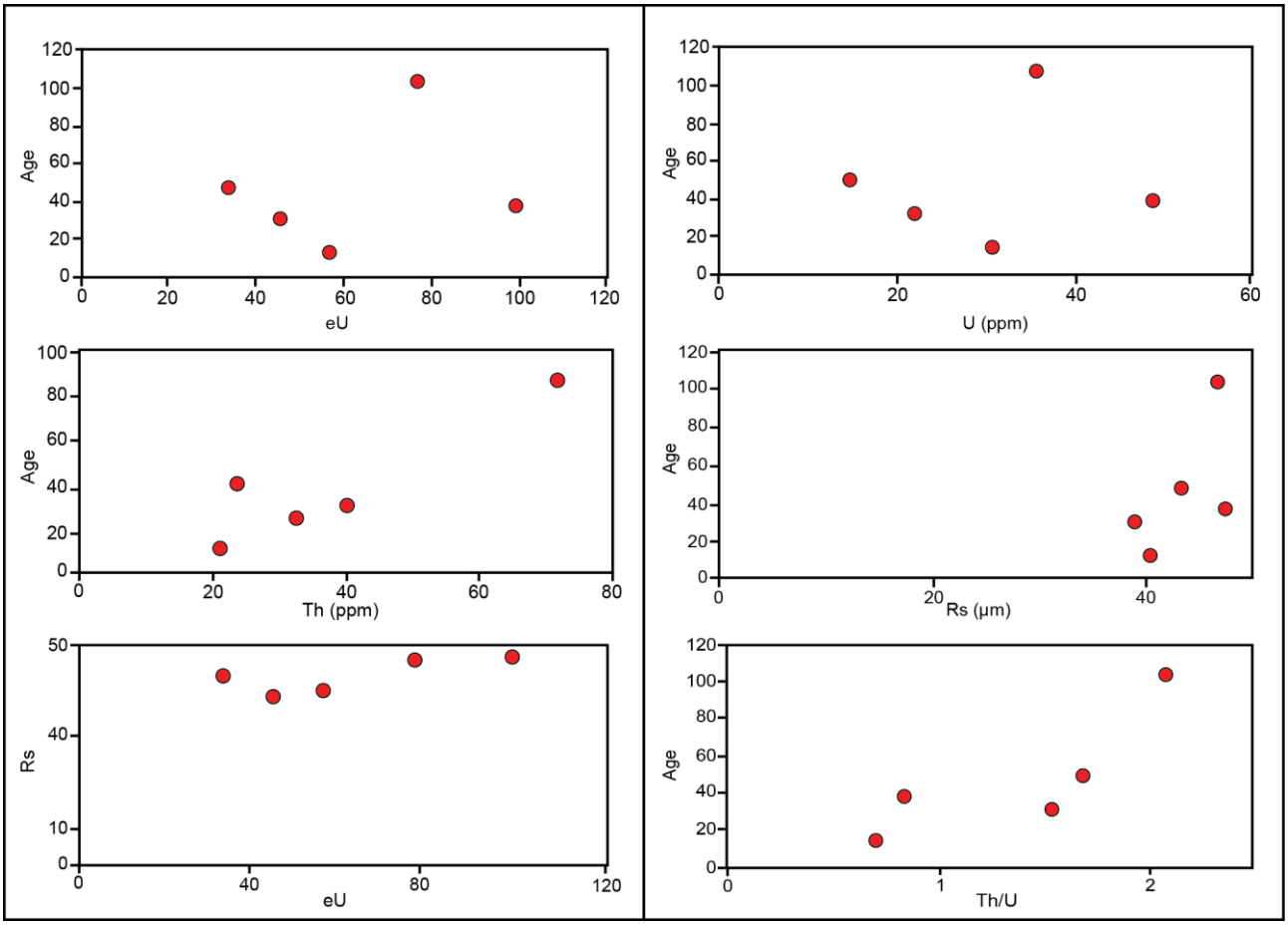

Figure S6- Plots related to apatite (U-Th)/He results of sample FT03

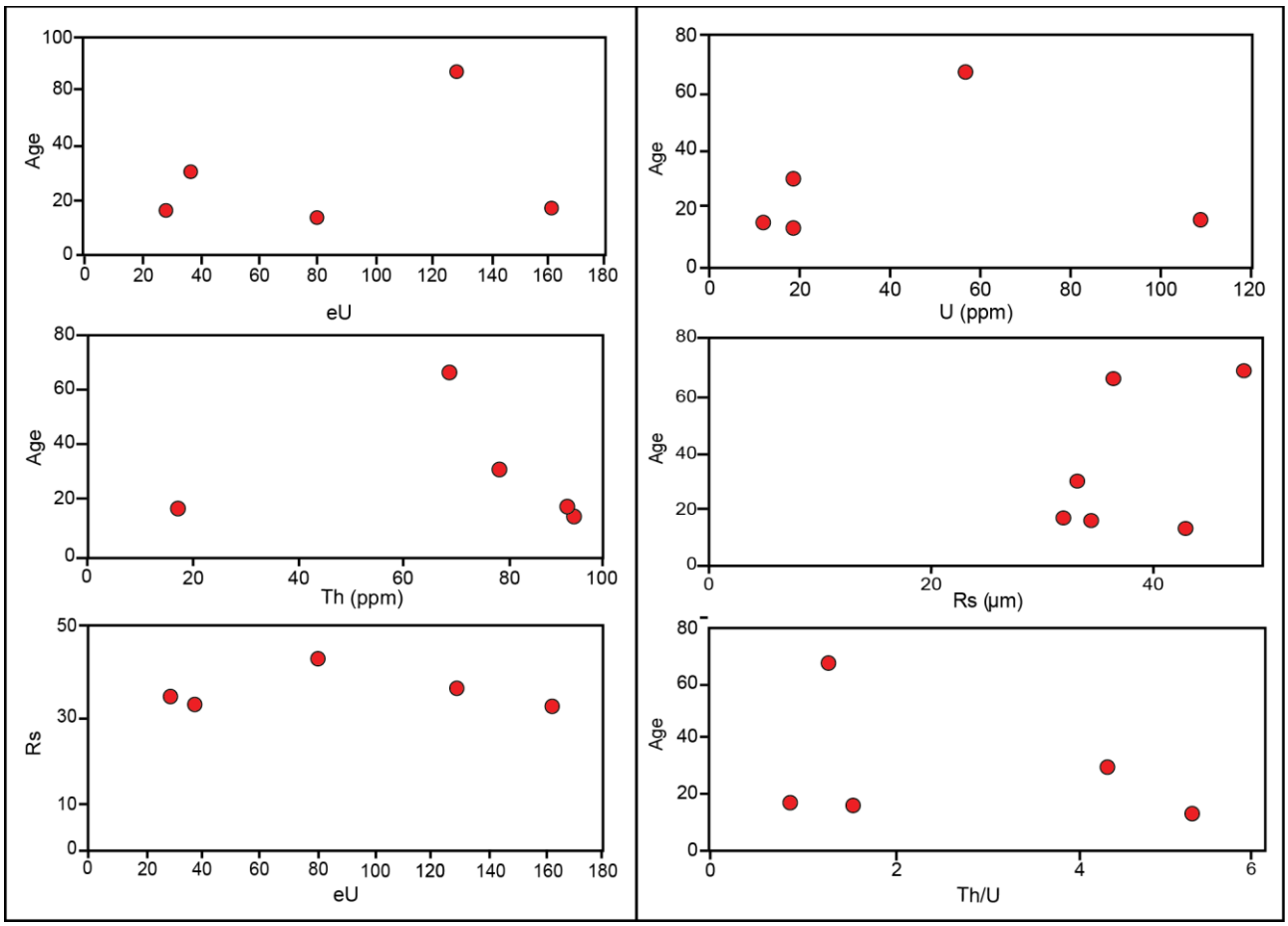

Figure S7- Plots related to apatite (U-Th)/He results of sample FT06

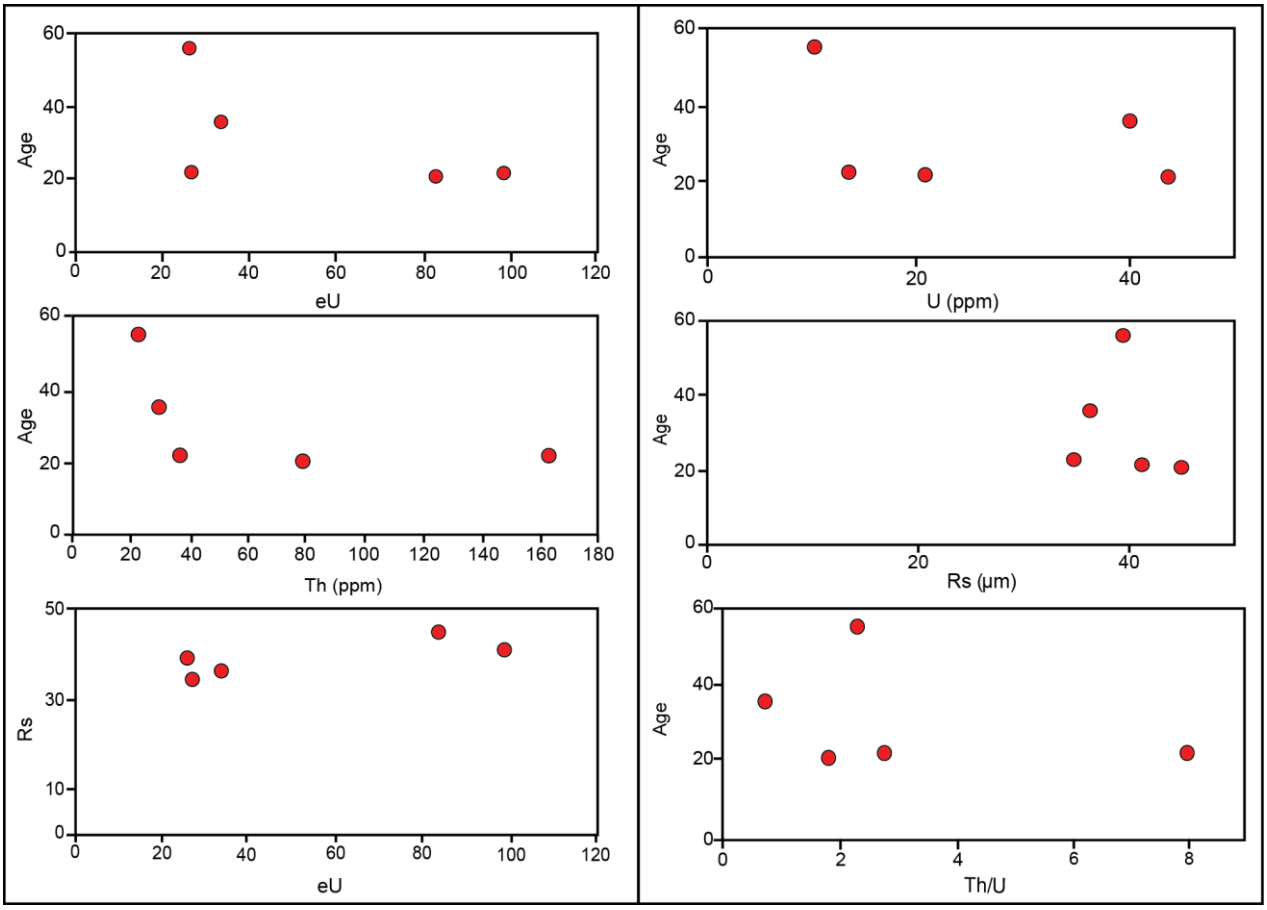

Figure S8- Plots related to apatite (U-Th)/He results of sample FT10

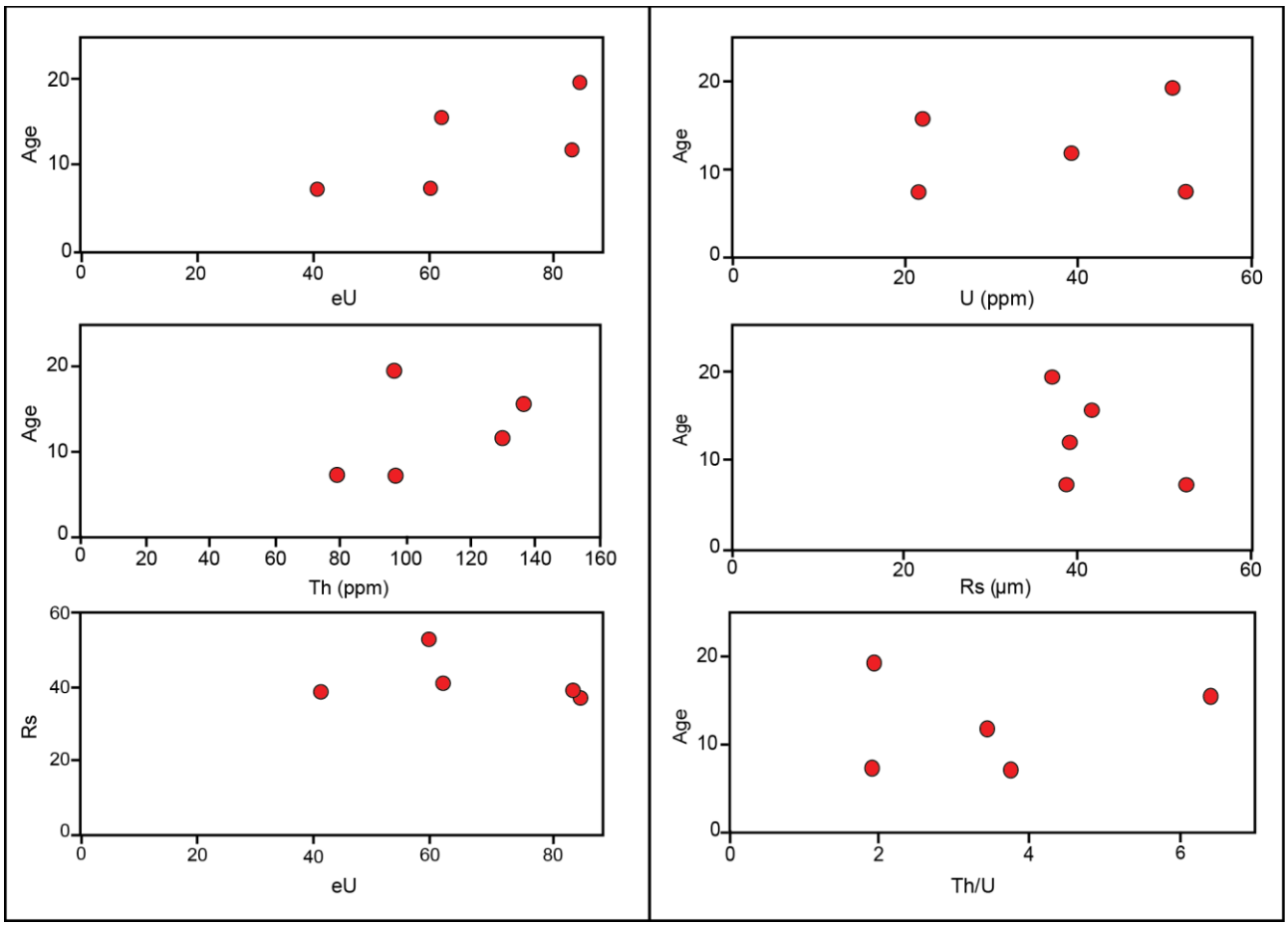

Figure S9- Plots related to apatite (U-Th)/He results of sample FT12

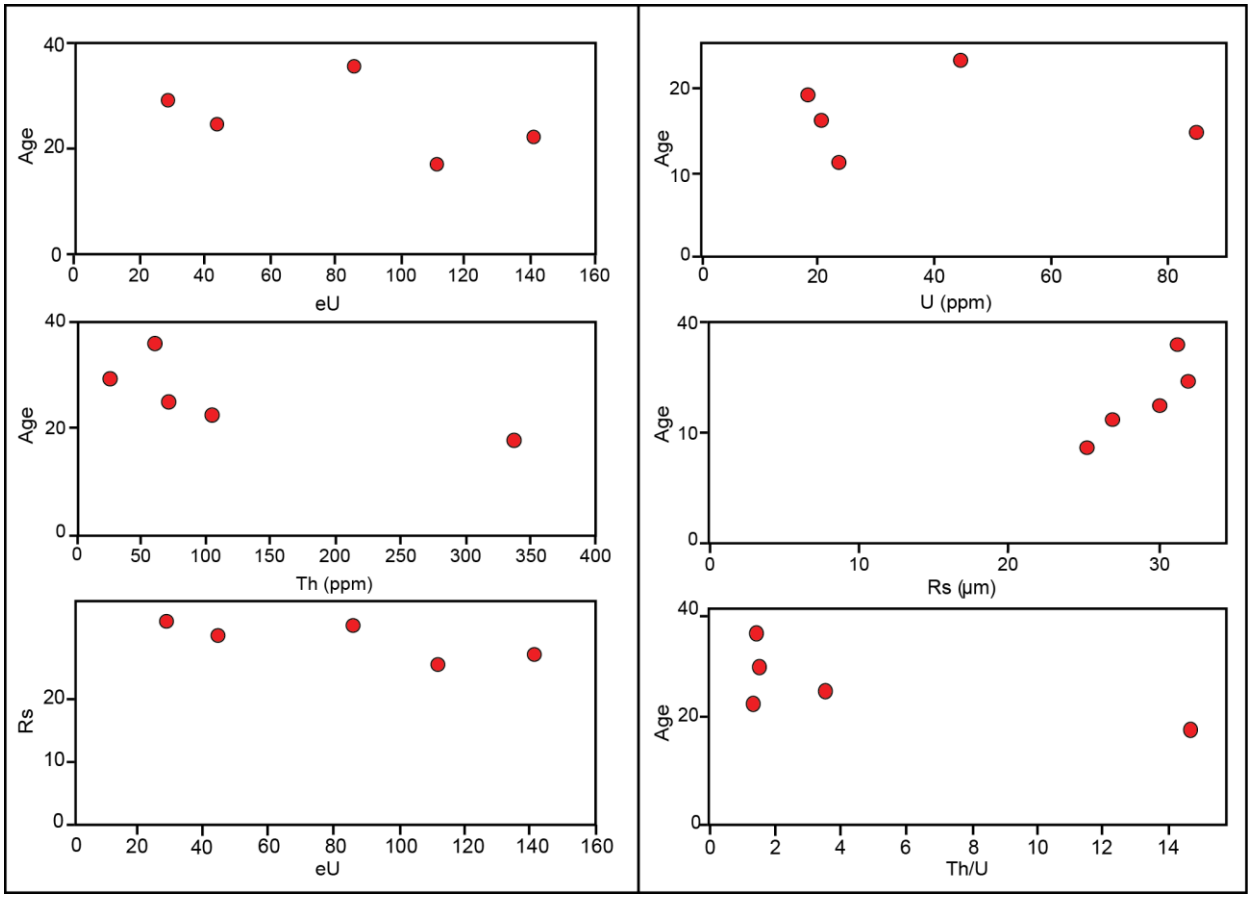

Thermal modelling

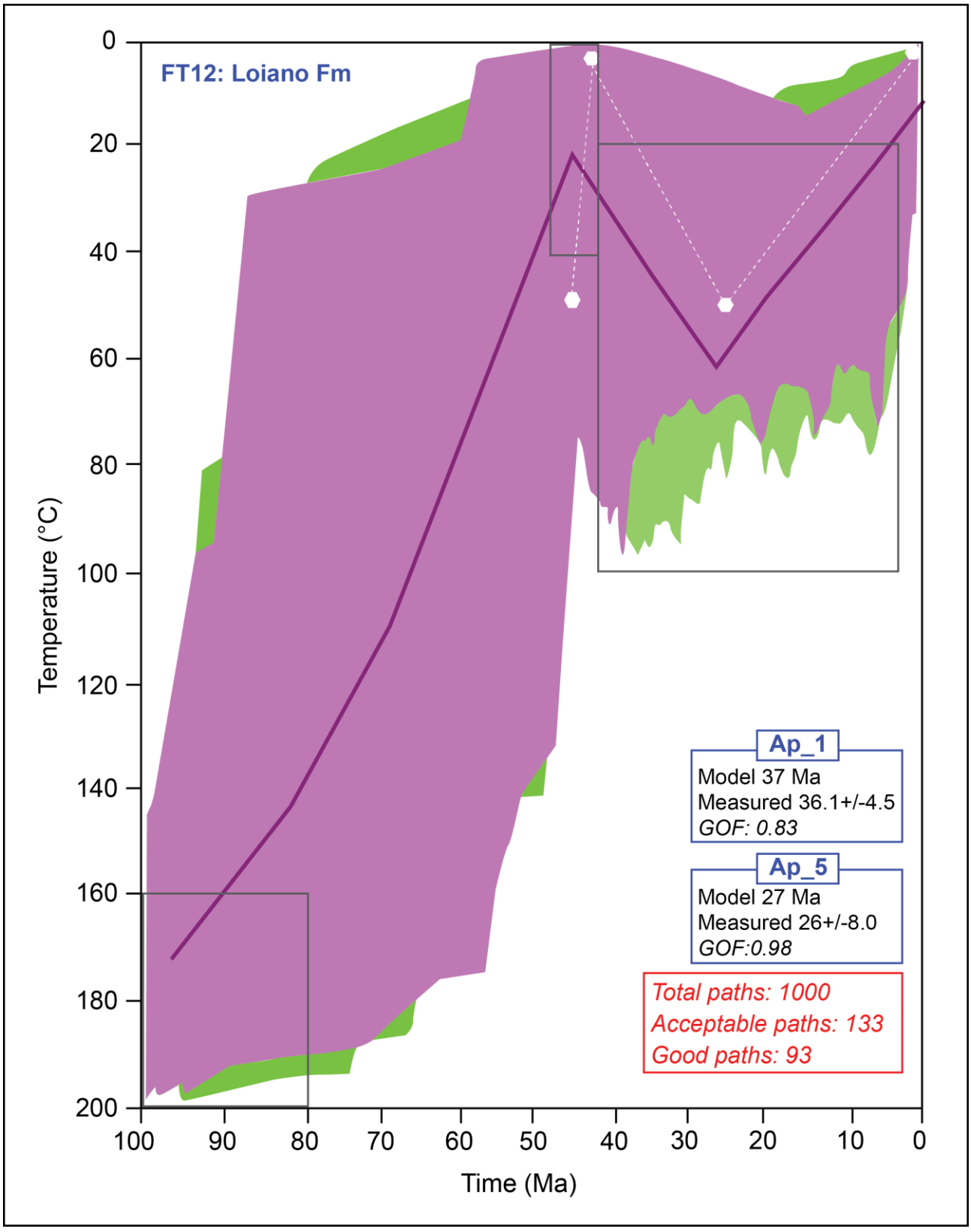

Figure S10- AHe inverse model of the FT12 showing the main constrains used (dark grey boxes), the good path interval (purple area) and the acceptable path interval (green area). The white dotted line represents the forward model (Ap_1: GOF=0.55; Ap_5: GOF=0.98).

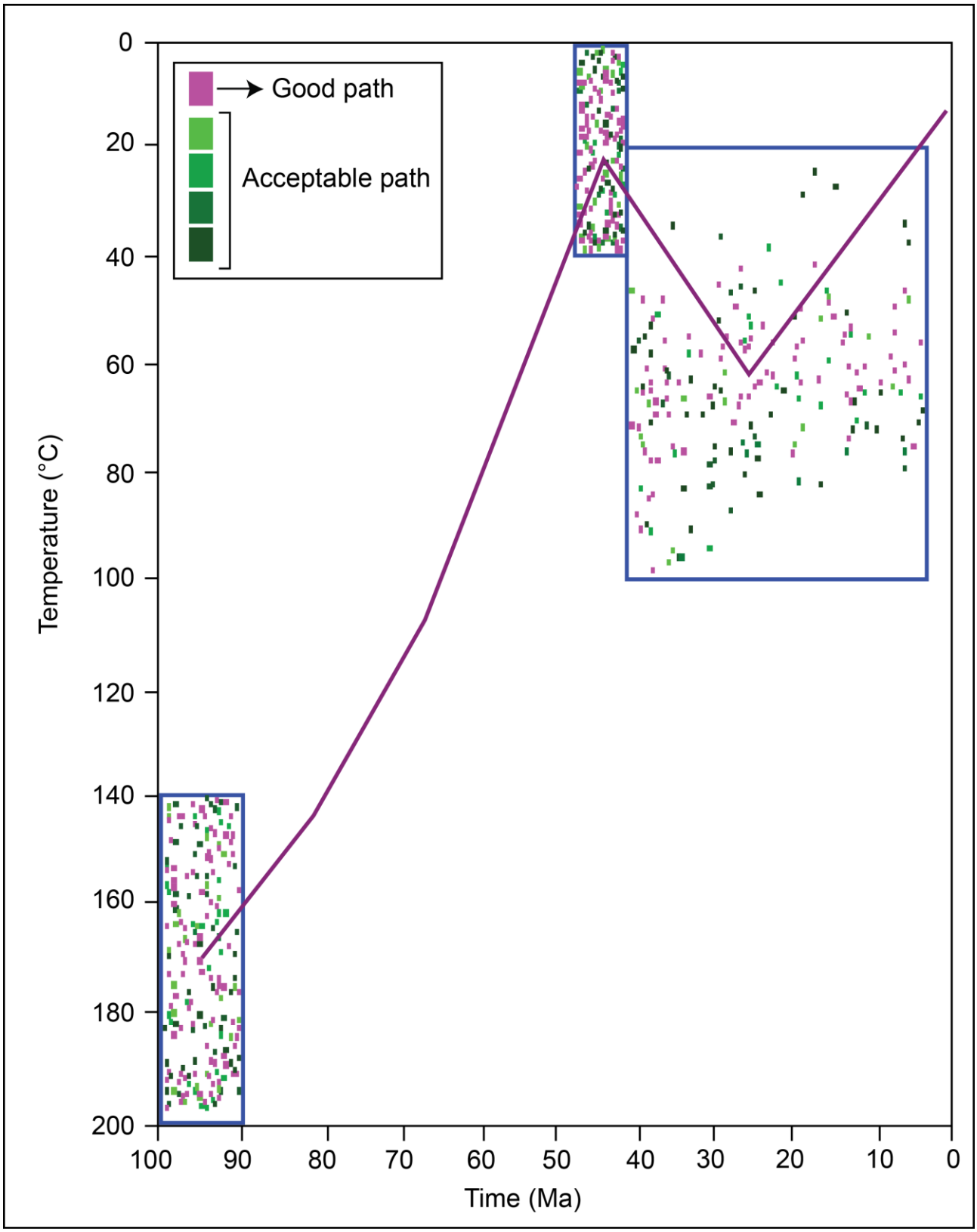

Figure S10- AHe inverse model of the FT12 showing the main constrains points obtained.

Chapter 5

Late Pleistocene deformation in the axial zone of the Northern Apennines, Italy: insights into the early stages of post-orogenic extension

Francesca Stendardi[1], Gianluca Vignaroli[1], Alberto Ceccato[2], Hsun-Ming Hu[4,5], Chuan-Chou Shen[4,5], Giulio Viola[1]

(This chapter is part of a paper that is in preparation to be submitted to Italian Journal of Geosciences)

1- Dipartimento di Scienze Biologiche, Geologiche e Ambientali - Università degli Studi di Bologna, Bologna, Italy (gianluca.vignaroli@unibo.it)

2 - Structural Geology and Tectonics Group, Geological Institute, Department of Earth Sciences, ETH Zurich, Sonneggstrasse 5, 8092, Zurich, Switzerland

3 - High-Precision Mass Spectrometry and Environment Change Laboratory (HISPEC), Department of Geosciences, National Taiwan University, Taipei 10617, Taiwan, ROC

4- Research Center for Future Earth, National Taiwan University, Taipei 10617, Taiwan, ROC

5.1 Introduction

Post-orogenic extension is a major mechanism operating after the build-up of a fold-and-thrust belt and thickened orogen (e.g., Dewey, 1988; Platt et al., 2003). In detail, it mostly drives deformation in the hinterland of fold-and-thrust belts, while concomitant crustal shortening deforms their frontal part, which propagates towards the foreland through major folding and thrusting (Malinverno and Ryan, 1986; Hodges et al., 1992; Vissers et al., 1995).

At brittle upper crustal levels, post-orogenic structures commonly rework the nappe stack, reshape the structural and morphological configuration of the belt, and create conditions for localised accumulation of stress-driven resources (fluid migration) and hazards (seismicity) (Sibson, 2000; Hayman, 2006; Collettini, 2011; Smeraglia et al., 2016). As the compressional front migrates towards the foreland, extension is first activated in the hinterland and may then propagate to the axial domain of the belt, i.e., the domain that links the hinterland and the frontal domains **(Fig. 5.1)**. In the belt axial domain, extension, coupled with active surface erosion, provides a suitable mechanism to restore the wedge from an overcritical mechanical configuration to a stable geometry (e.g., Platt, 1986; Woodward, 1987; Braathen et al., 1999).

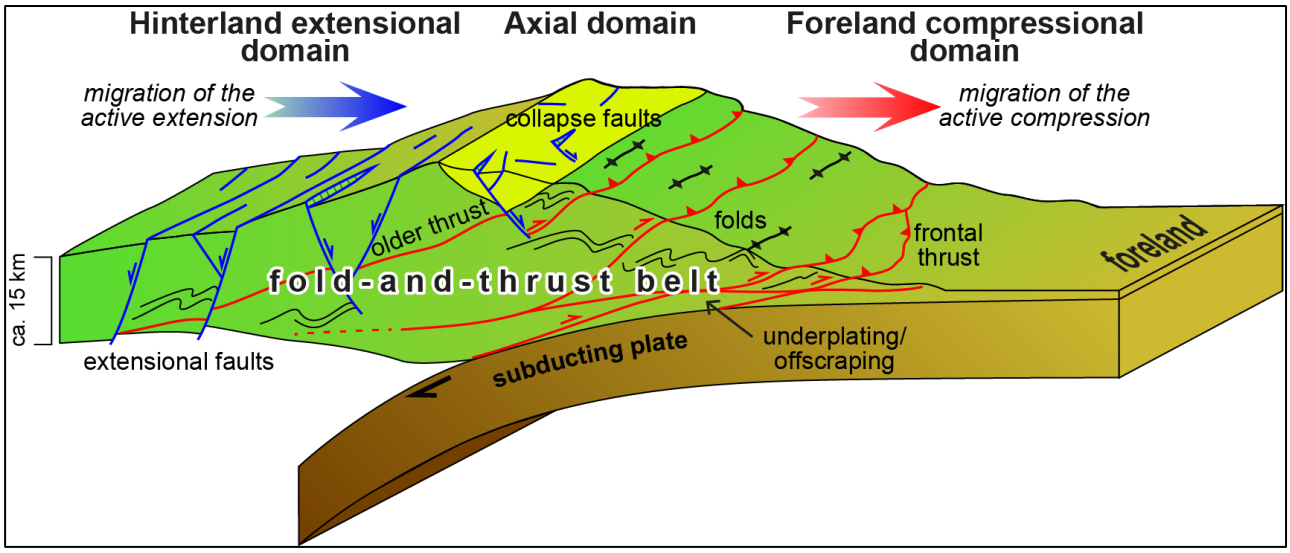

Figure 5.1- Conceptual evolutionary model of a fold-and-thrust belt (modified and redrawn after Platt, 1986).

Although the contemporaneous occurrence of compression and extension has been documented for several orogenic domains worldwide (e.g., Malavieille, 1993; Royden, 1993; Cavinato and DeCelles, 1999; Fassoulas, 1999; Martin-Rojas et al., 2023; Vignaroli et al., 2012), no firm structural constraints currently document the characteristics of the post-orogenic extensional framework that affects the axial portion of a mountain belt, where extensional structures formed in response to i) gravity-driven events related to the collapse as a consequence of local stress field variation through time that probably reflect structural adjustments to local taper instability conditions; ii) migration of the post-orogenic extensional front started in the hinterland side and related to the opening of the Tyrrhenian basin. However, the following key questions remain unanswered: What is the structural pattern of juvenile post-orogenic extensional faults occurring in belt axis? How

do these faults correlate with the regional-scale extensional structures operating in the hinterland of the orogen?

In this perspective, the Northern Apennines (NA) of Italy is a classic example of active fold-and-thrust belt characterised by progressive forward propagation of the frontal thrusts in the foreland domain (Po Plain and Adriatic Sea) and extension and crustal-scale thinning in the hinterland regions (e.g., Tyrrhenian Sea; **Fig. 5.2a)** (e.g., Malinverno and Ryan, 1986; Carmignani and Kligfield, 1990; Pauselli et al., 2006). Both geological and geophysical constraints indicate nearly cylindrical deformation at the front part of the belt, with in-sequence activation of NW-SE-striking (i.e., parallel to the belt axis) thrusts and folds (Toscani et al., 2006; Boccaletti et al., 2011; Bonini et al., 2014a), while extensional and transtensional faults presently bound NW-SE–trending Miocene-to-Quaternary sedimentary basins and host active seismicity on the Tyrrhenian side (e.g., Carmignani et al., 1994; Jolivet et al., 1998; Molli et al., 2018). The axial part of this belt, however, has been under-investigated from a structural perspective, with only few geological constraints available on the kinematics and timing of deformation. Such a lack of knowledge hinders our understanding of the transition from compression to extension during orogenesis and the impact of extensional faulting on the structural evolution of the belt at large. The axial domain of the NA is characterised by the occurrence of wedge-top basins (the Epiligurian units), which represent a useful stratigraphic-structural marker for deciphering the syn- to post-orogenic evolution of the belt (e.g., Beaumont, 1981; Ori & Friend, 1984; Stendardi et al., 2023). The Epiligurian units are therefore an

ideal target for studying the post-orogenic pattern of the NA because they were not affected by the accretionary phase that instead deformed the underlying wedge during underplating, and record phases of building and dismantling of the belt in their continuous stratigraphic succession (Middle Eocene-Upper Miocene).

In this work, we approach the pattern and the kinematics of the post-orogenic structural setting deforming the Epiligurian units of the NA through a multidisciplinary approach. Lineament detection on digital elevation models (DEMs) has been carried out on a selected Epiligurian basin (named the Marzabotto Basin; Stendardi et al., 2023) to unravel the general structural trends at the regional scale. Field structural investigations addressed the spatial distribution, geometry, and kinematics of the main post-orogenic faults cross cutting the entire Epiligurian succession. We then performed U-Th dating to constrain the age of syn-kinematic mineralisations (calcite veins, slickenlines and slickenfibers) decorating selected, representative faults and, therefore, to provide age constraints upon the activity of the extensional phase in the axial portion of the belt. Our data provide evidence of extensional deformation in the Marzabotto Basin during the Middle-Late Pleistocene. This is significant for reconstructing the mechanisms that control the origin of extensional faults in the NA axial domain and improving our knowledge on the structural-temporal evolution of the belt.

5.2 Geological setting

The Apennines fold-and-thrust belt derived from the Cenozoic Europe-Adria continental collision after the complete consumption of the intervening Liguro-Piedmont Ocean (e.g., Dewey et al., 1989; Boccaletti et al., 1990; Faccenna et al., 2001; Wortel and Spakman, 2002; Carminati et al., 2010; Mantovani et al., 2019; **Fig. 5.2a**). The Apennines are characterised by the Neogene-to-Quaternary foreland-ward migration of thrust fronts and foredeep basins coeval with the activation of a post-orogenic extensional regime at the rear (e.g., Elter et al., 1975; Malinverno and Ryan, 1986; Dewey, 1988; Boccaletti et al., 1990; Lavecchia et al., 1994; Cipollari and Cosentino, 1995; Cello et al., 1997; Jolivet et al., 1998; Cavinato and DeCelles, 1999; Casciello et al., 2006; Pauselli et al., 2006 Patacca et al., 2008), in response to the eastward rollback of the subducting Adria slab (Royden et al., 1987; Doglioni, 1991; Faccenna et al., 2004; Rosenbaum and Lister, 2004). Both compressional and extensional structures in the belt are mainly oriented parallel to the strike of the belt, thus trending ENE-WSW in the Northern Apennines, E-W in the Central Apennines, and ESE-WNW in the Southern Apennines.

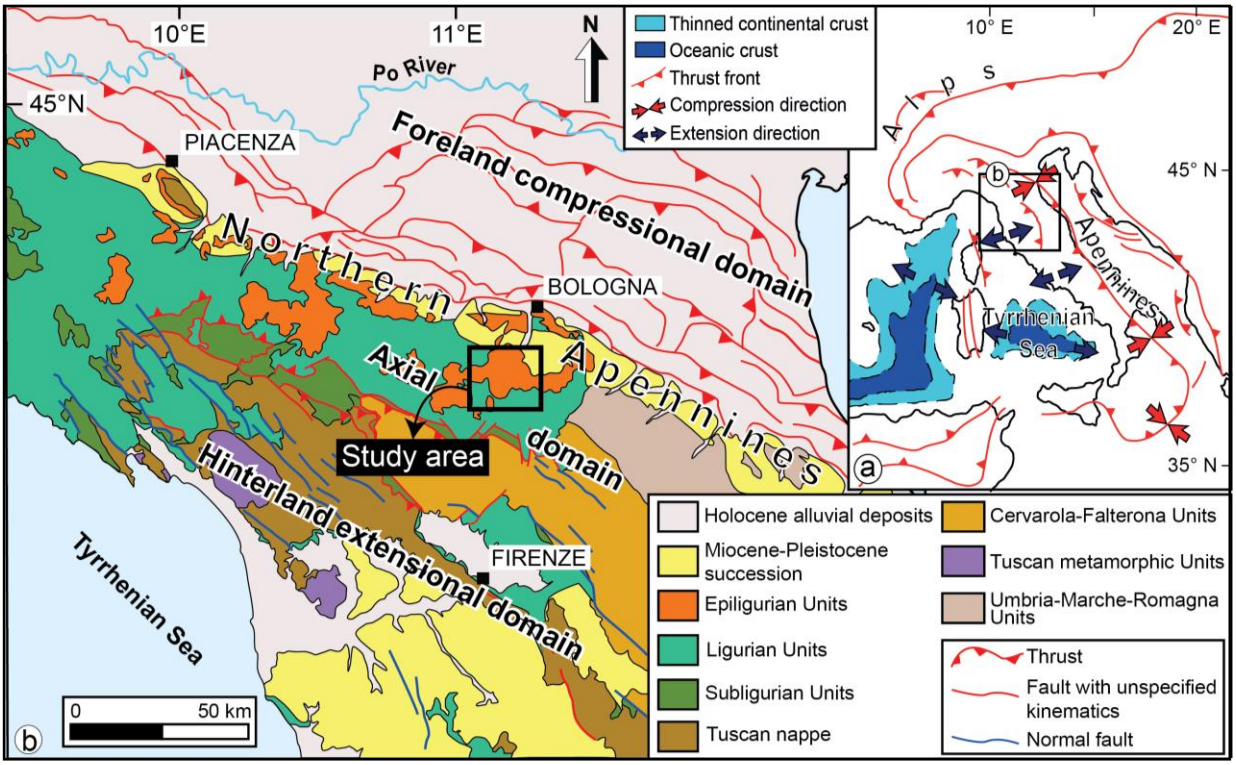

Figure 5.2- a) Schematic tectonic framework of the Northern Apennines also reporting the distribution of the thrust fronts and the active normal faults (modified and readapted after Conti et al., 2020); b) Geological map of the Northern Apennines.

Our study area is located in the NA **(Fig.5.2)**, which consist of a Cenozoic orogenic segment that experienced polyphase and prolonged tectonic deformation since the Oligocene. Earlier deformation ensued during the imbrication of tectonic slices scraped from the Liguro-Piedmont Ocean (Ligurian Domain) to form an accretionary wedge. These slices consist of Jurassic ophiolites and their Cretaceous to-Palaeocene sedimentary cover (e.g., Conti et al., 2020). Middle Eocene-Upper Miocene siliciclastic successions (named the Epiligurian Basins, the target of this study) unconformably overly the Ligurian Domain and are commonly considered to have escaped the major phase of

shortening of the wedge (e.g., Ori and Friend, 1984; Amorosi et al., 1996; Ricci Lucchi, 1987; Argnani and Ricci Lucchi, 2001).

Starting in the early Oligocene, the compressive front progressively migrated toward the east, (e.g., Carmignani et al., 1995; Bettelli et al., 2003; Elter et al. 2003; Rosenbaum and Lister, 2004; Boccaletti et al., 2011; Carminati and Doglioni, 2012). The Ligurian Domain and the Epiligurian Basins are imbricated over thrust sheets scraped off from the Adria continental margin. These sheets mainly consist of Paleocene-to-Lower Miocene deep marine sediments and turbidites (Sub-Ligurian Domain) and Triassic-to-Oligocene platform and basinal carbonate successions overlain by Miocene-Pliocene turbidites (Tuscan-Umbria-Marche Domain) (Boccaletti et al., 1990; Mantovani et al., 2019; Conti et al., 2020).

The post-orogenic extensional phase led to the development of orogen-parallel (i.e., NW-SE-striking) sedimentary basins dissected by NW-SE-striking normal faults at the rear of the eastward advancing belt (e.g., Carmignani et al., 1994; Keller et al., 1994; Collettini et al., 2006; Brogi, 2011; Rossetti et al., 2011; Brogi et al., 2014; Molli et al., 2018). Pulses of Miocene-Pliocene out-of-sequence thrusting have been also documented in the NA hinterland, producing the repeated polyphase compressive reactivation of low-angle extensional structures (e.g., Bonini et al., 2014b; Viola et al., 2018).

The present-day structural setting of the NA encompasses **(Fig. 5.3)** (i) a frontal domain, where shortening and deformation are accommodated by the development of arcuate thrusts and the associated WNW-ESE-striking Emilian and Ferrarese fold systems buried

beneath the Middle Pleistocene-Holocene of the Po Plain, and (ii) a hinterland domain where NW-SE extensional faults overprint the early nappe stack edifice accommodating subsidence and sedimentation in Pliocene-Quaternary grabens and half-grabens. Within this spatial partitioning of compression and extension in the NA, there is evidence of middle Pleistocene to Holocene extensional structures that deform continental deposits at the belt-Po Plain margin (Capozzi et al., 1991; Bertotti et al. 1997; Picotti and Pazzaglia, 2008; Picotti et al., 2009). These extensional structures are mainly NW-SE-striking normal faults that were activated in response to differential vertical movement between the uplifting belt in its southwestern sector and the subsiding Po Plain to the north-east. The present-day seimotectonic framework of the NA confirms the active and coexisting compression and extension **(Fig.5.3).** Hypocenters showing

compressive focal mechanisms occur at depth of ~50 to 30 km below the NA water divide and progressively localise at shallower depth (up to ~8 km) below the Emilian fold system. On the other hand, < 20 km hypocentres associated with extensional focal mechanisms occur in the Tyrrhenian side of the belt, together with a few transcurrent solutions (e.g., Pondrelli et al., 2020; Eva et al., 2022; Rovida et al., 2020). Noteworthy, the axial zone of the NA belt appears to be characterised by minor (or absent) seismicity at shallow (< 20 km) crustal depth (e.g., Ferretti et al., 2002; Eva et al., 2022).

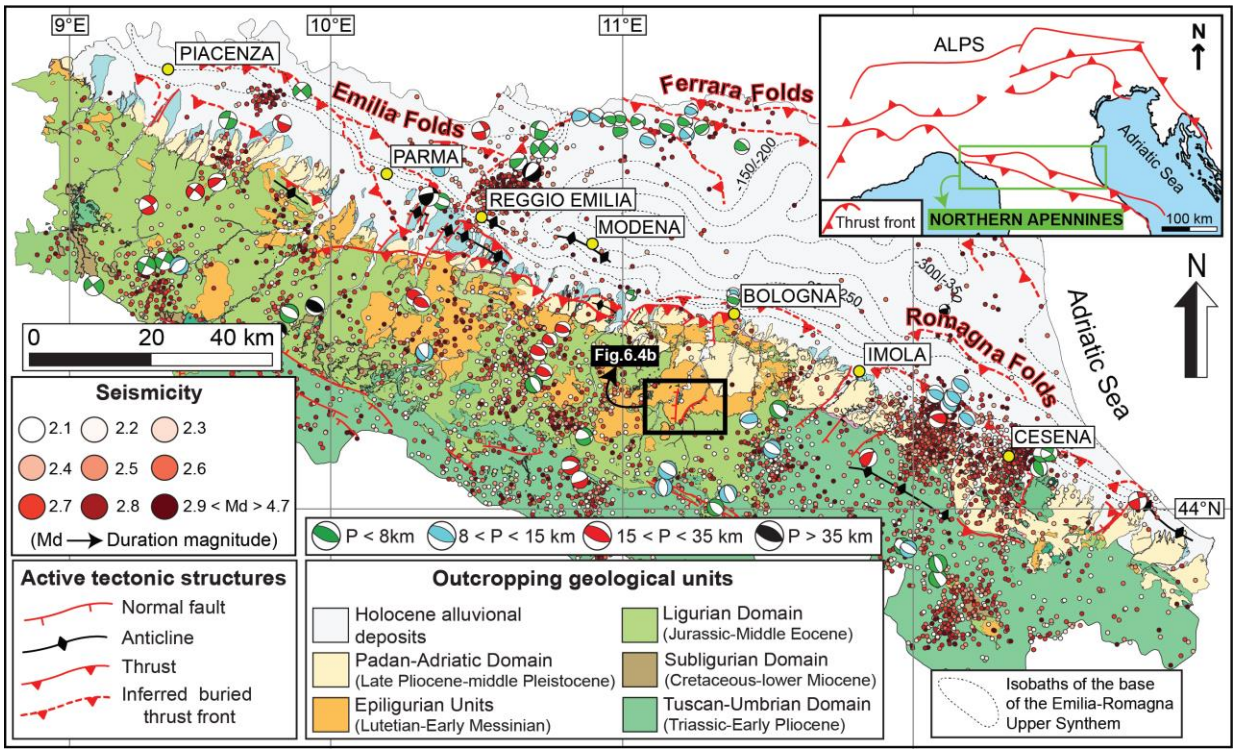

Figure 5.3 - Structural map of the Northern Apennines fold-and-thrust belt highlighting recent and active structures. Additionally, the subsurface geology in the Po Plain is documented by isobaths delineating the base of the Lower Pleistocene (Boccaletti et al., 2001). Seismicity data used in this study were sourced from the Italian Seismological Instrumental and Parametric Database (ISIDe) accessible at http://terremoti.ingv.it/en/iside. Focal mechanisms are reported from the Seismotectonic Map of the Emilia-Romagna and surrounding areas (Martelli et al., 2017).

The study area (the Marzabotto Basin) is located in the Epiligurian units, which are exposed in stratigraphic depressions along the axial domain of the NA belt. From a sedimentological point of view, the Epiligurian units exhibit an intense compositional variability characterized by arkosic sandstones and hemipelagic marls that vary upward to calcarenites and marly-sandy sandstones. The lower succession of the Epiligurian units is composed by five formations (from bottom to top: Loiano Fm., Marne di Monte Piano

Fm., Ranzano Fm., Antognola Fm., Contignaco Fm.) that deposited in a deep-sea depositional environment. The upper succession consists of three formations (from bottom to top): Pantano Fm., Cigarello Fm., Termina Fm.) that deposited in a shallow-sea-outer shelf depositional environment. The transition between the two environments is marked by an erosional unconformity of regional importance known as the Burdigalian Unconformity **(Fig. 5.4a).**

The Epiligurian units are characterised by a complex tectonic framework **(Fig. 5.4b)** that reflects the syn-to-post orogenic history of the belt. The structural setting of these units is characterised by several tectonic structures with different trends and kinematics: i) NE-SW and NW-SE striking thrusts; ii) NE-SW-striking left-lateral strike slip faults; iii) NNE-SSW and NW-SE-striking normal faults partly reactivating the strike-slip ones; iv) variably oriented normal faults associated with the late collapse of the belt (see Chapter 3 for details).

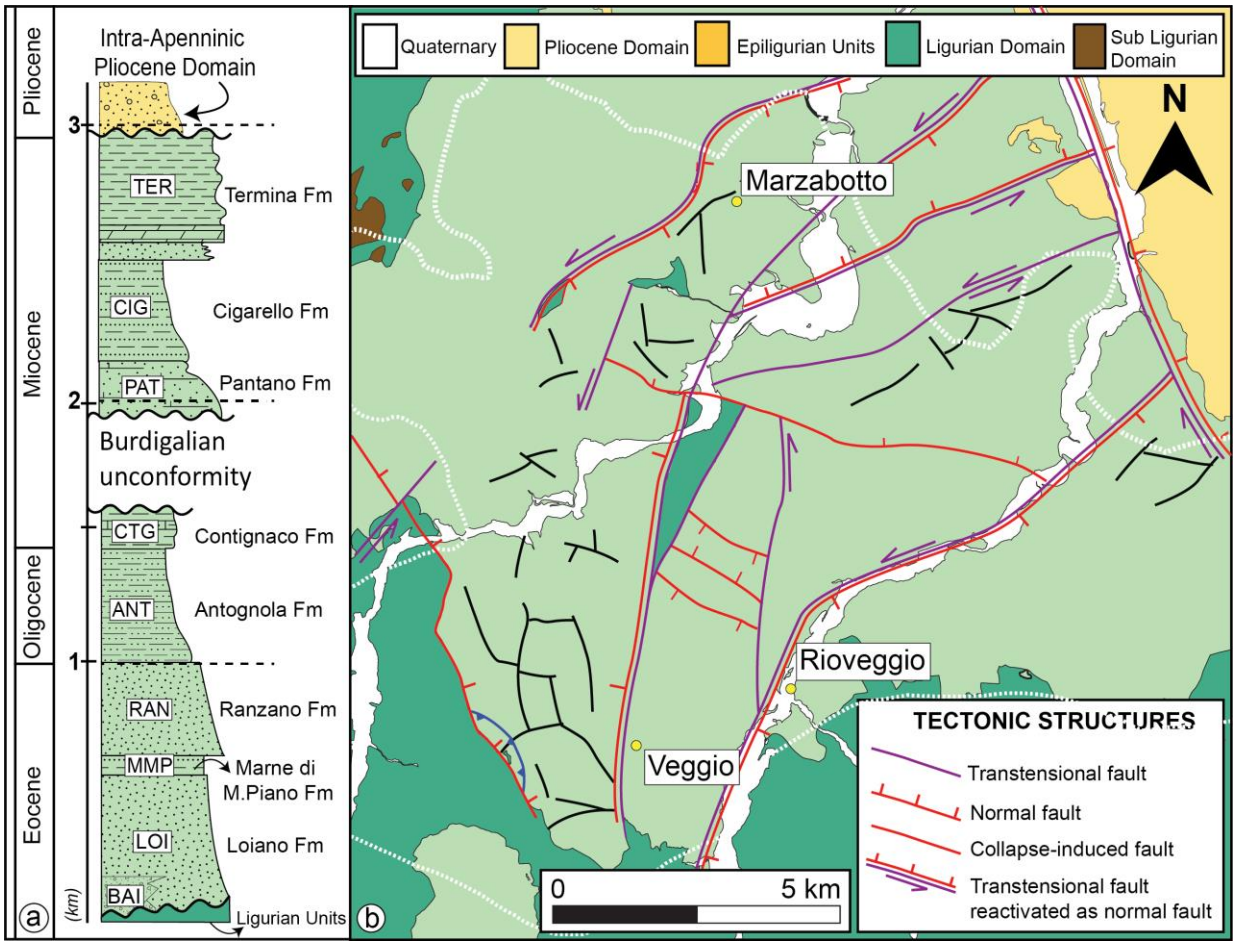

Figure 5.4- a) Stratigraphic column illustrating the Epiligurian Succession; b) Schematic representation of the main tectonic structures affecting the Epiligurian units in the study area (Marzabotto Basin) based on the geological map of the Emilia-Romagna Region (RER) website (https://datacatalog.regione.emilia-romagna.it/(PortaleminERva)) (Panini et al., 2002; Balocchi, 2011). The white dashed polygon represents the area investigated by remote sensing.

5.3 Methods and Materials

To unravel the post-orogenic structural style and architecture of the NA axial domain, we investigated the structural setting of the Epiligurian units by combining structural

surveys, remote sensing analysis of lineaments and U-Th dating of syn-kinematic mineralisations (for details about the analytical method see the Appendix, paragraph I.4).

The main purpose of the lineament analysis was to investigate the dominant trends of the morphostructures affecting the Epiligurian units exposed in the Marzabotto Basin to obtain regional-scale information on the general fracturing and faulting pattern, as well as the stress conditions in the upper structural levels of the belt. The analysis was performed on a 15 m resolution DEM, using different hill shadings with different illumination sources located at varying azimuths (45° from the north), with a height set at 45 m and at an observation scale varying from 1:50.000 to 1:1.000. We followed insights from Scheiber et al. (2015) to improve the reliability of remote sensing lineament interpretation. The analysis has been done to see if there occurs a change in the strike and density distribution of structures above and below the regional Burdigalian unconformity, which marks a major switch of the sedimentation environment and source feeding the Epiligurian basin under study (see Chapter 3 and 4 for details). The lineaments have been classified into pre- or post-Burdigalian groups based on the mapped stratigraphic units, rather than the age of the structures themselves. Field geology and structural analysis further expand the dataset by Stendardi et al., (2023) for the Marzabotto Basin.

Structural surveys aimed at providing constraints on the spatial distribution, geometry and kinematics of selected normal faults decorated by datable syn-kinematic mineralisations. Crosscutting and overprinting relationships between mapped fault

segments have been carefully investigated to generate constraints on the relative timing of multiple faulting events. The kinematics of each fault segment has been inferred through the analysis of stratigraphic offset at the fault surface, integrated with the interpretation of slickensides and synthetic shears (e.g., Petit, 1987; Doblas, 1998).

Carbonate mineralisations from the faults were collected for several analytical purposes. Thin sections of fault rocks cut parallel to the slip vector have been analysed to characterise the textural relationships between carbonate mineralisation and host rock. Optical microscopy analysis and cold cathodoluminescence imaging were used to constrain the internal properties of the mineralisation, in terms of its nature and textural overprinting of multiple generations of crystallisation.

Samples for geochronological analysis have been obtained by micro-drilling on mesoscale samples after microscopical characterisation. U-Th geochronological investigations have been performed on syn-kinematic mineralisations associated with fault rocks to provide a minimum age for the activity of the deformation structures themselves. We collected calcite fibres growing on fault surfaces, calcite aggregates on slickensides and calcite-filled veins that are structurally related to the fault segments. Analytical details for the U-Th method are reported in the Appendix.

5.4 Results

5.4.1 Lineament analysis

Hillshades with illumination from 90°, 180°, 270° and 360° show two lineaments main directions-oriented NW-SE and NE-SW) and one subordinate E-W trend **(Fig. 5.5 b, d, f, h)**. The length of lineaments ranges between 250 m and 1,6 km. Longer features are concentrated along the NE-SW trend.

Hillshades with illumination from 45°, 135°, 225°, 315° highlight two main (NW-SE and NE-SW) and two subordinate directions (E-W and N-S) **(Fig. 5.5 a, c, e, g)**. The length of lineaments ranges between 200 m and 2 km. Longer features are concentrated along the NW-SE direction.

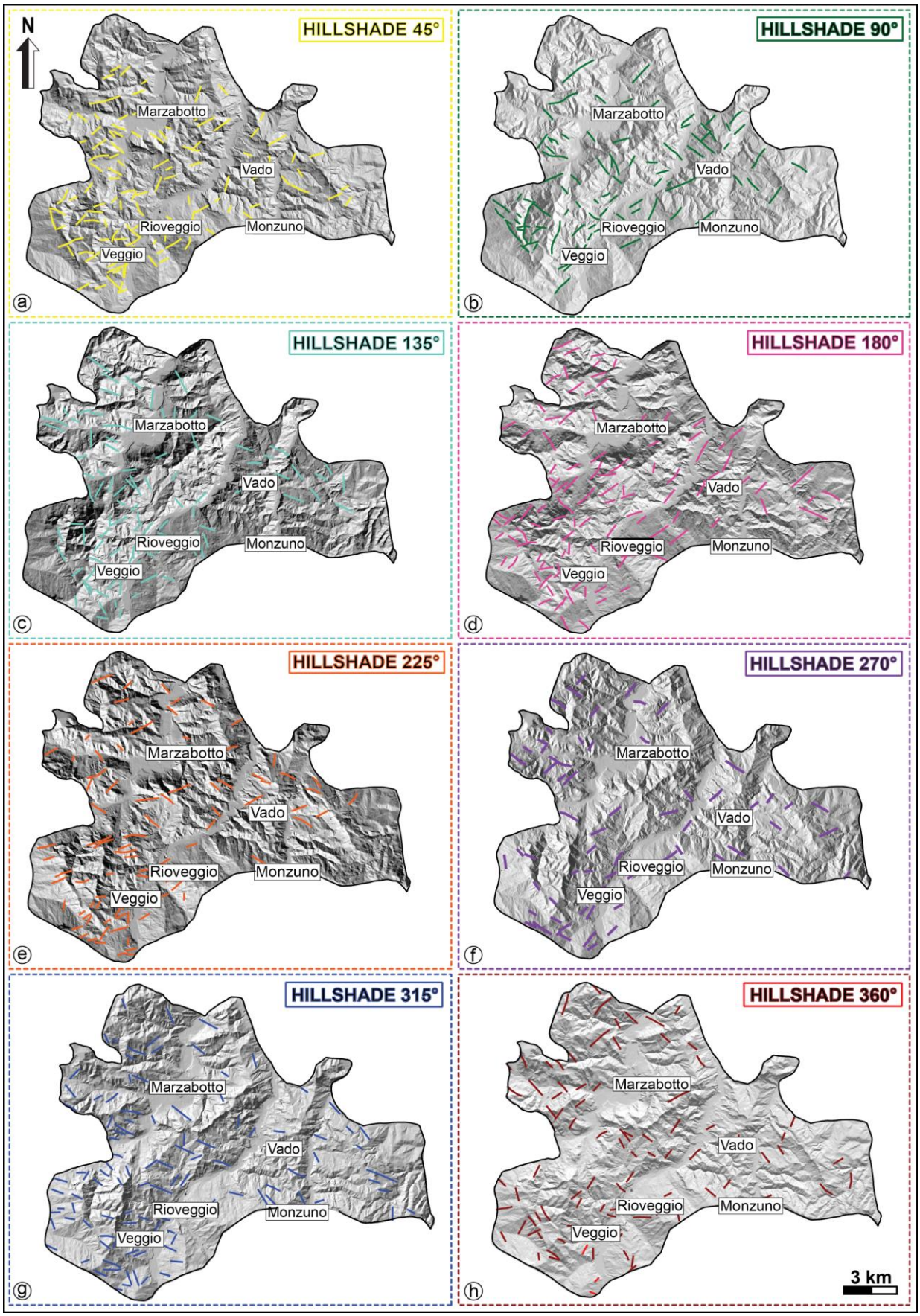
N
HILLSHADE 45°
Marzabotto
Vado
Rioveggio
Monzuno
Veggio
a
HILLSHADE 90°
Marzabotto
Vado
Rioveggio
Monzuno
Veggio
b
HILLSHADE 135°
Marzabotto
Vado
Rioveggio
Monzuno
Veggio
c
HILLSHADE 180°
Marzabotto
Vado
Rioveggio
Monzuno
Veggio
d
HILLSHADE 225°
Marzabotto
Vado
Rioveggio
Monzuno
Veggio
e
HILLSHADE 270°
Marzabotto
Vado
Rioveggio
Monzuno
Veggio
f
HILLSHADE 315°
Marzabotto
Vado
Rioveggio
Monzuno
Veggio
g
HILLSHADE 360°
Marzabotto
Vado
Rioveggio
Monzuno
Veggio
3 km
h

Figure 5.5 - Remote sensing analysis of lineaments from DEM images showing hillshades with illumination from 045°, 0,90°, 135°, 180°, 225°, 270°, 315° and 360° azimuths.

Collectively, lineaments have length between 200 m and 2 km (with 1000 m as a mean). Lineaments are characterised by a highly variable distribution of trends ranging from N-S to NE-SW, to E-W, NW-SE **(Fig. 5.6a)**. The trend distribution and density of the lineaments have been considered also in relationship with the tectono-stratigraphic units at the outcrop (pre-Burdigalian and post-Burdigalian; **Fig. 5.6b)**. The area covered by pre-Burdigalian units is characterised by the occurrence of 159 lineaments aligned along NW-SE, NE-SW and E-W main directions, while the N-S direction is subordinate. The area covered by post-Burdigalian units is characterised by the occurrence of 154 lineaments aligned along NW-SE and NE-SW main directions, while the N-S and E-W directions are subordinated.

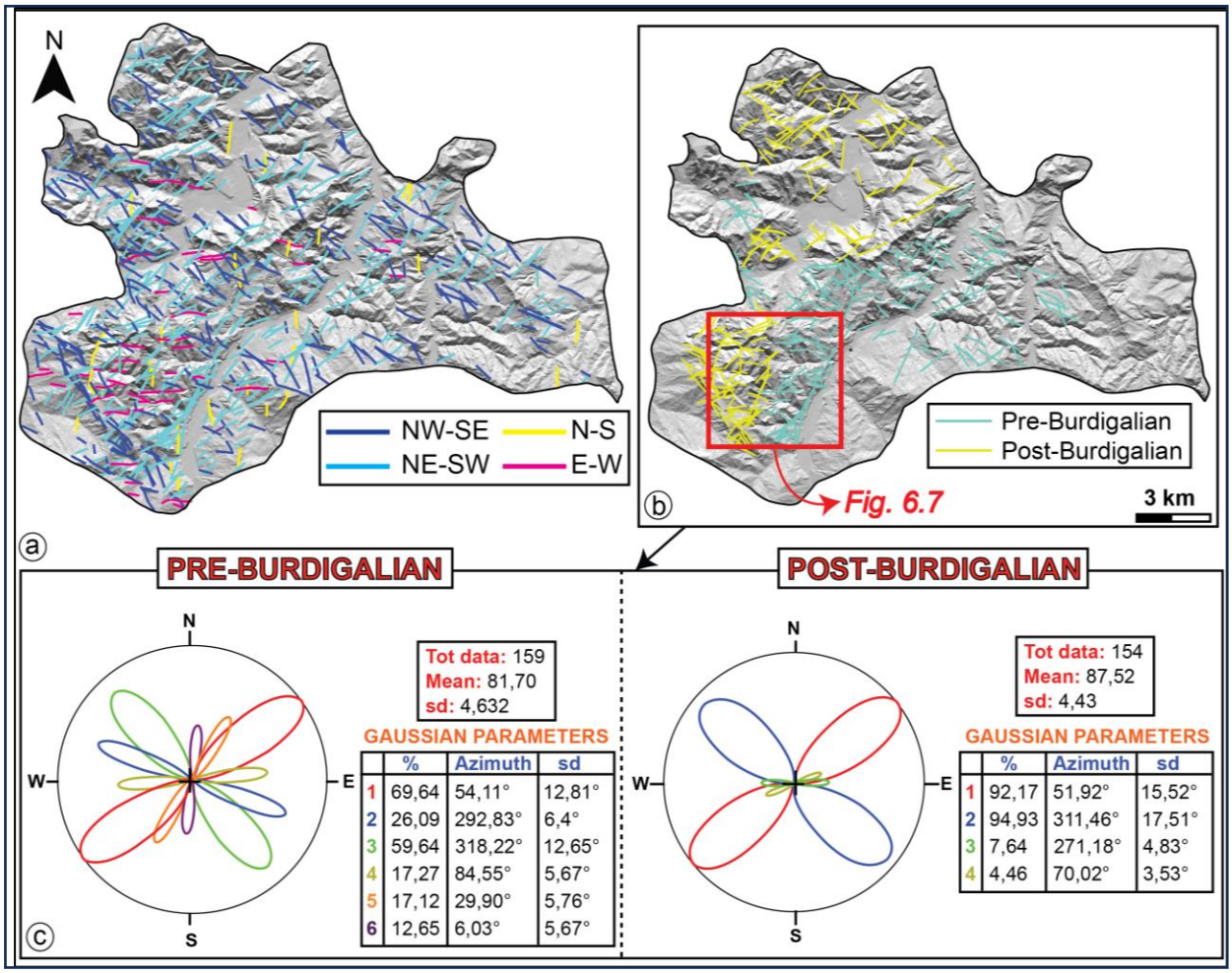

Figure 5.6- a) Map of the main trend distribution obtained from remote sensing analysis of lineaments; b) lineament trends unravelled for pre- and post-Burdigalian Epiligurian units; c) Cumulative rose diagram, representing the pre- and post-Burdigalian trend distribution of lineaments. Rose diagrams have been elaborated using the software Daisy 3 (Structural Data Integrated System) (version 5.40) (Salvini, 2002).

5.4.2 Mesoscale structures

Collectively, ca. 60 structural data of faults and fault-related joints have been collected in the southwestern portion of the Marzabotto Basin, where lineaments mapped in both pre- and post-Burdigalian units are densely distributed **(Fig. 5.7)**.

Overall, the collected data depict a complex structural architecture of dominant NNE-SSW-striking fault zones with subordinate trends-oriented NW-SE and E-W. Scattered orientations (i.e., N-S, WNW-ESE, NNW-SSE) define a complex geometrical mesh that variably offsets the Epiligurian stratigraphic sequence. In the pre-Burdigalian units, we mostly found and mapped NNE-SSW-striking fault zones defined by the alignment of subparallel normal fault segments hundreds of metres long **(Fig. 5.7)**.

Within the post-Burdigalian units, the NNW-SSE-striking set is commonly accompanied by subsidiary fault sets whose orientation varies between E-W and WNW-ESE **(Fig. 5.7)**. In map view, these subordinate faults commonly exhibit a planar-to-curvilinear geometry and terminate against a N-S-striking fault, which represents a tectonic contact between the pre- and post-Burdigalian Epiligurian units **(Fig. 5.7)**.

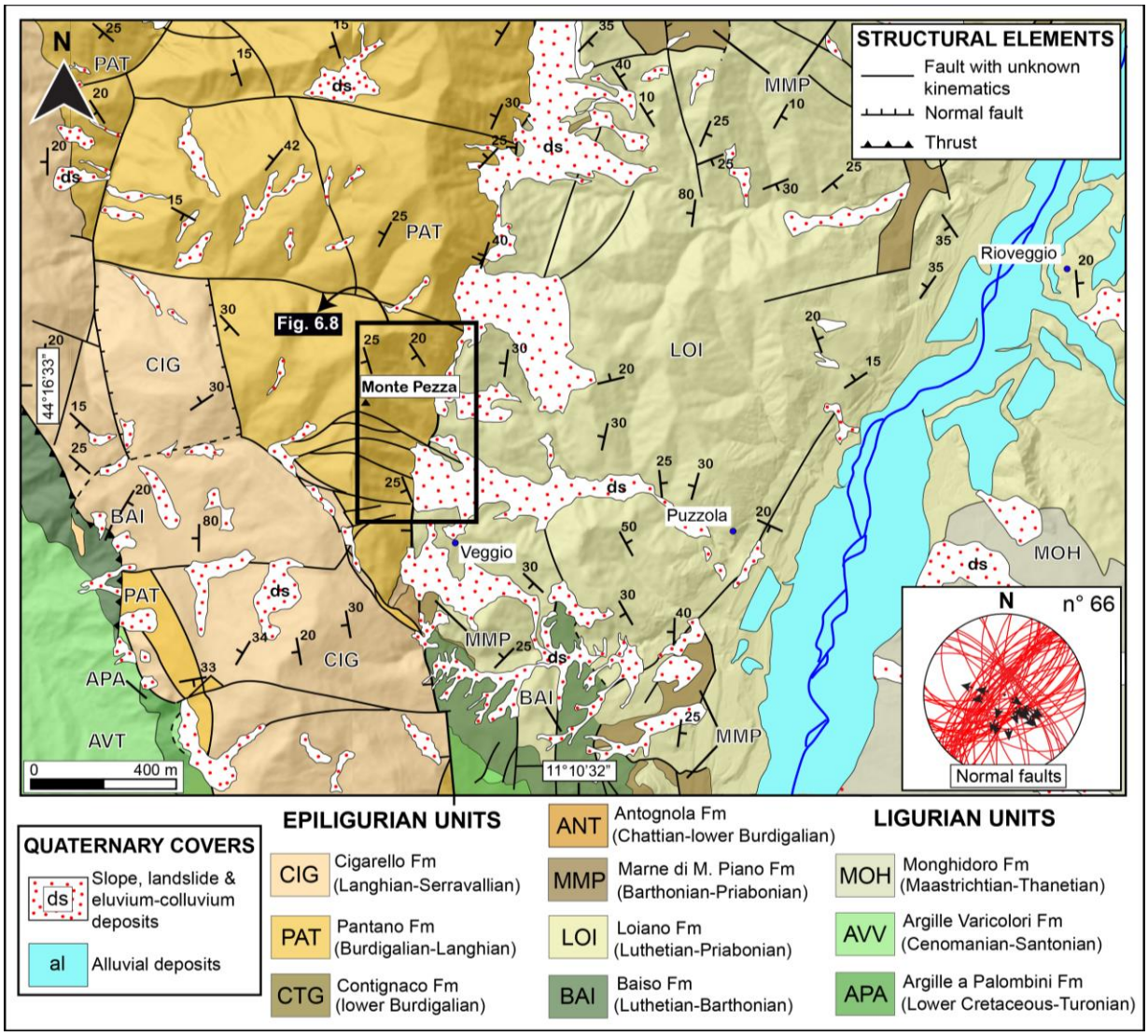

Figure 5.7- Structural map of the central part of the study area (Monte Pezza to Rioveggio) which show the main tectonic structure affecting the Epiligurian units.

Although normal and oblique faults can be commonly detected at different stratigraphic levels within the Epiligurian Succession, syn-kinematic mineralisations along their slip planes are scarce. The area around the Veggio village **(Fig. 5.8)** is an interesting case where to study Epiligurian units as controlled by the occurrence of multiple sets of normal faults that can be mapped continuously from the base to the top of the succession. There, a main NNE-SSW-striking fault system, steeply dipping (~75°) to the west occurs

in the eastern side of the area and controls the lateral contact between the Lutetian-Priabonian Loiano Fm., to the east, and the Burdigalian-Langhian Pantano Fm., to the west. A 20 m-thick sequence of Chattian-lower Burdigalian Antognola Fm. is sandwiched between these two formations, where there occurs a sulphur spring **(Fig. 5.8)**. The NNE-SSW-striking normal fault system systematically cuts and dislocates SE-dipping reverse faults (structural site 1; **Fig. 5.8**) and reworks NNE-SSW-striking, steeply dipping left- or right-lateral strike slip faults (structural sites 2 and 4**; Fig. 5.8**). The internal structural architecture changes in style passing from the footwall (Loiano Fm.) to the hanging wall (Pantano Fm.). At the footwall, the porous arenaceous layers of the Loiano Fm. are locally deformed by ~N-S-striking deformation bands dipping at high angle (> 80°). At the outcrop scale, these deformation bands cut across the bedding and accommodate a cumulative stratigraphic offset between a few mm and a maximum of c. 10 cm. The lack of continuous exposures prevents the observation of the geometry and spacing of the deformation bands when approaching the main fault.

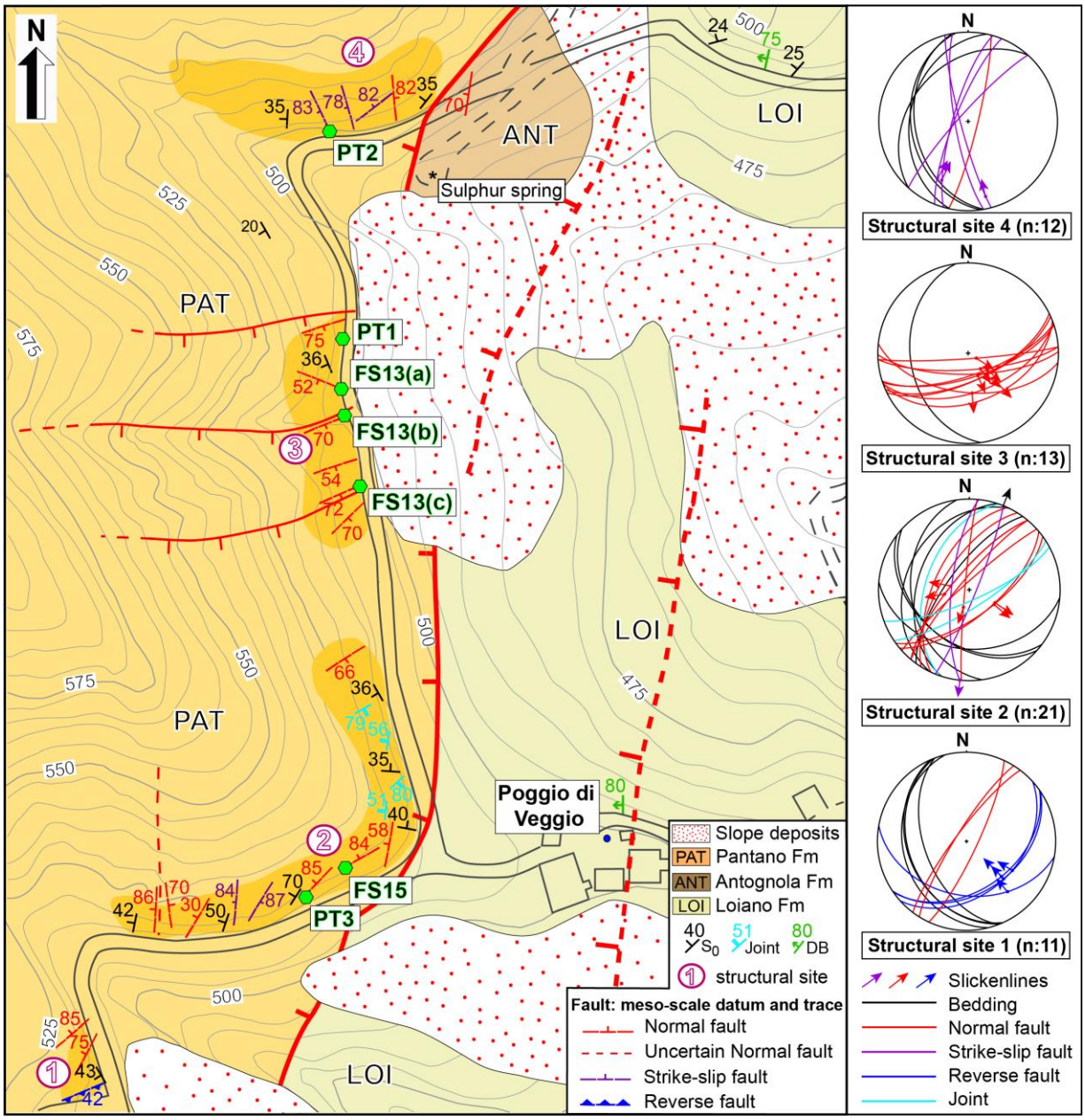

Figure 5.8- Zoom the southern central part of the Marzabotto Basin aiming at structural perspective.

In the hanging wall of the main fault, a set of ca. NNE-SSW-striking, metre-scale spaced fault segments produce centimetre-to-metre across-fault offset of the marly layers of the Pantano Fm. (structural sites 1, 2 and 4; **Fig. 5.8**). Fault surfaces have a general sub-planar geometry, high dip values (>50°) and dip either to WNW or ESE. These fault surfaces are

locally characterised by decimetre-thick damage zones in which sub-planar joints are aligned parallel to the fault surface and dip at higher angle than single fault surfaces. Slickenlines on fault surfaces are represented by abrasion striae or striated calcite slickefibres. The pitch of the slickenlines ranges between 60° and 125° (see stereographic projections for structural site 2 in **Fig. 5.8**), documenting dominant dip-slip kinematics. Calcite slickensides commonly occur on fault surfaces and indicate a normal sense of movement.

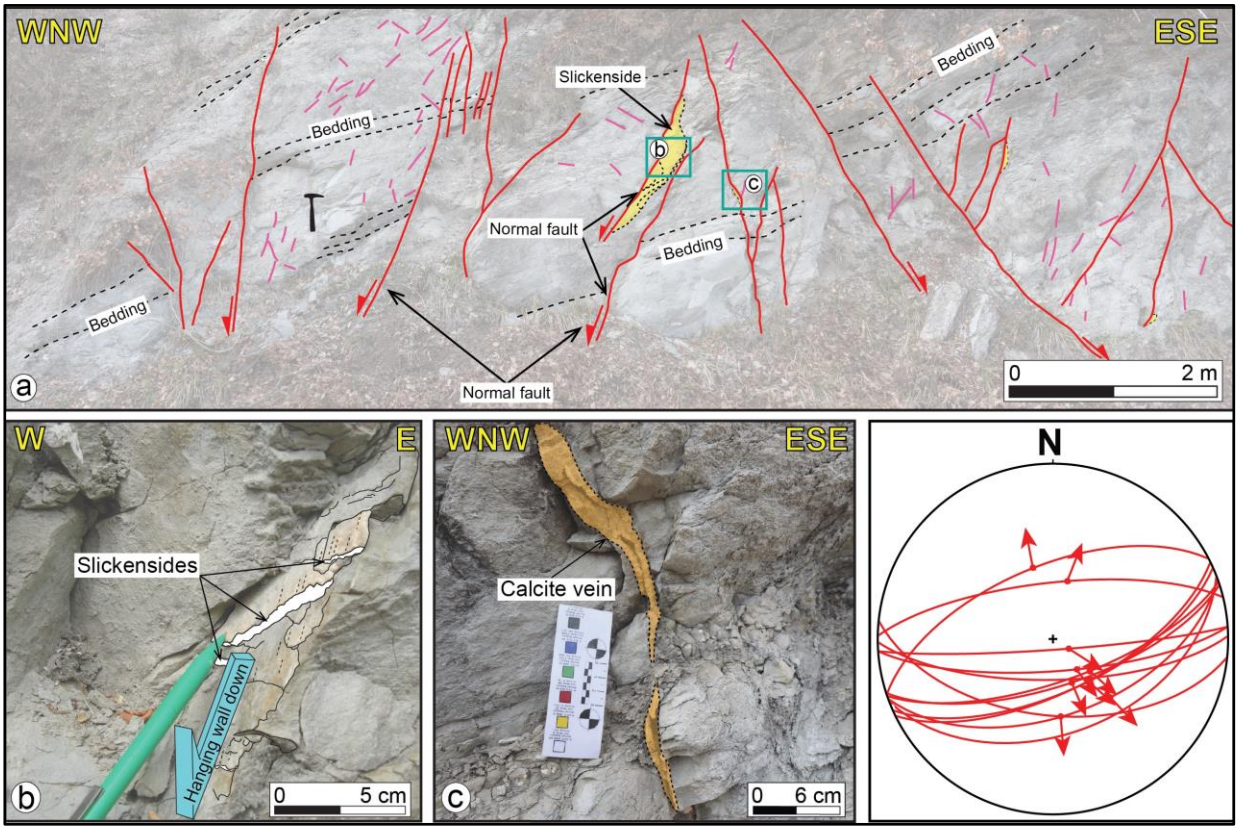

Figure 5.9- a) Pantano Fm. outcrop located in the central part of the study area. b) WNW and ESE-dipping normal faults which cut and deform the bedding with a centimetric offset. Syn-kinematic indicators are represented by well-developed slickensides and slickenlines (b) and calcite veins (c).

A set of E-W-striking faults (structural site 3; **Fig. 5.8**) is found in the hanging wall of the NNE-SSW fault system and clearly cuts across the Pantano Fm., while no evidence for their along-strike continuation is found in the Loiano Fm. They mainly dip to south, although some north-dipping structures also occur and are interpreted as conjugate structures. These E-W-striking fault surfaces are locally characterised by decimetre-thick damage zone in which sub-planar joints are aligned parallel to the fault surface and dip at higher angle with respect to that of the single fault surface. The normal sense of movement is indicated by the occurrence of widespread calcite slickensides **(Fig. 5.9b)** bearing striated calcite fibres with pitch between 75° to 100° (see stereographic projections in **Fig. 5.9**). Calcite also occurs as infilling material in curvilinear, cm-thick joints **(Fig. 5.9c)** running parallel to the E-W-striking faults and having sub-vertical attitude.

5.4.3 Syn-kinematic mineralisations

At the microscale, slickenside calcite mineralisations are characterised by variations in texture and grain size **(Fig. 5.10)**. A well-defined layering due to a change in size is appreciable both in the optical microscopy and the cathodoluminescence mode. Blocky textures consist in coarse-grained calcite crystals (up to 2 mm in diameter). Micro-twinning and straight narrow lamellae characterise the calcite grains, while the lack of undulate extinction suggests that grains are little internally deformed.

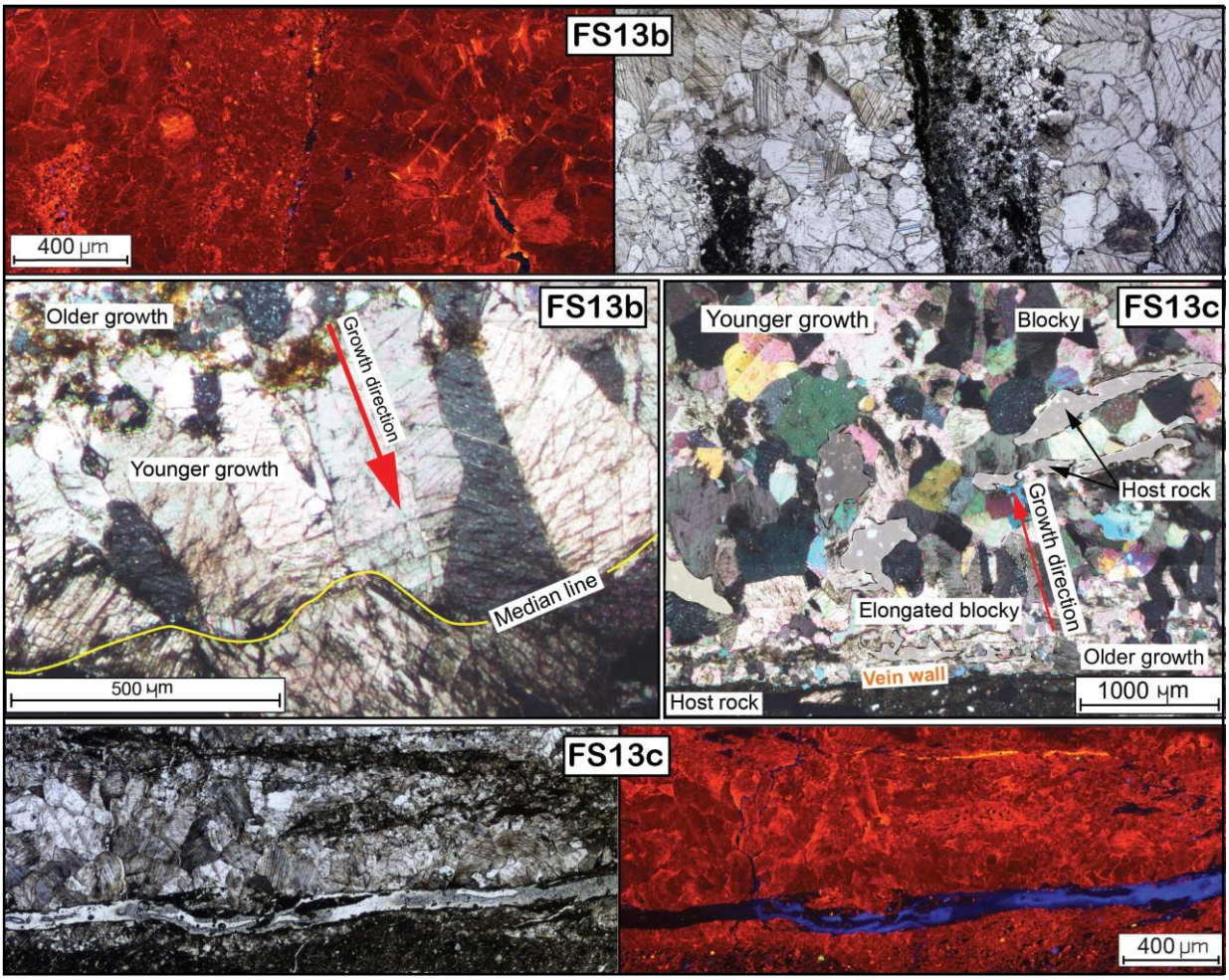

Figure 5.10- Microphotographs (including cathodoluminescence images) of the studied syn-kinematic mineralisations.

Grain boundaries among calcite crystals are generally rectilinear or gently curved, although twisting boundaries due to growing competition locally occur. Locally, blocky textures evolve into elongate blocky textures where finer-grained calcite grains show a growth direction roughly perpendicular to the attitude of the layering **(Fig. 5.10)**.

Slickenside mineralisations include a younger growth that is represented by finer-grained calcite (maximum diameter of 100 µm) along a layer parallel to the blocky calcite one. This fine-grained layer consists of dirty calcite mixed with clay particles.

Calcite crystals are sub-rounded with gently curved boundaries. The layer of fine-grained calcite often embeds sub-mm-thick lenses of the host rock, in which very fine-grained particles are organised to form a massive texture.

Calcite mineralisations infilling the veins result from a general antitaxial growth mechanism defined by an older growth of blocky crystals in the internal part of the vein and a younger growth of fine-grained crystals towards the vein walls **(Fig. 5.10)**.

Cathodoluminescence patterns of both blocky and fine-grained textures in slickensides and veins show a comparable sequence of intensity variations. Generally, two main intensity patterns can be observed, with a lighter one being progressively overprinted by a darker one. Thus, both the blocky texture and fine-grained layer are characterised by yellow-to-red or red-to dull brown patterns, in which the darker intensity pattern (red and dull brown, respectively) replaces the lighter one and is dominant in the texture.

5.4.4 U-Th geochronology

We dated calcites from four slickenlines and two veins (Table 1) collected along the fault zone in the Veggio area **(Fig. 5.8)**. The dated samples are characterised by a homogeneous $^{230}Th/^{238}U$ activity ratio (between 0.63 and 1.12), whereas the $^{230}Th/^{232}Th$ activity ratio, which indicates the extent of detrital contamination in the analysed samples, is varies slightly between 11.64 and 170.1 **(Table 1).** Collectively, we obtained four corrected ages between 65 and 280 kyr (with 2σ errors < 24 kyr) and two samples (PT1 and PT3) were older than the limit of the dating method (ca. 600 kyr). In particular, we obtained (i) two similar ages (138 ± 24 and 144 ± 2 kyr) and one out of the limit of the dating method from

samples FS15, PT2, and PT3, respectively, collected from slip surfaces of the NNE-SSW-striking fault zone (sites of measurement n°2 and 4 in **Fig. 5.8**); (ii) variable ages (65 ± 3 kyr; 280 ± 16 kyr; >600 kyr) from samples FS13c, FS13b2 and PT1, respectively, collected from slip surfaces of the E-W-striking faults (site of measurement n° 3 in **Fig. 5.8**).

Table 1- U-Th ages of the carbonate mineralisations from the fault systems at Veggio village. Sample was analysed through MC-ICP-MS at the HISPEC of the National Taiwan University (errors quoted as 2σ).

Sample ID	Structure	Latitude	Longitude	Weight g	^{238}U $10^{-9}g/g$ [a]	^{232}Th $10^{-12}g/g$	$d^{234}U$ measured[a]	$[^{230}Th/^{238}U]$ activity[c]	$^{230}Th/^{232}Th$ atomic (x 10^{-6})	Age (kyr ago) uncorrected	Age (kyr ago) corrected [c,d]	$d^{234}U_{initial}$ corrected[b]
FS13b2	slickenline	44°16′27.46′′	11°09′50.73′′	0.3304	64.475 ± 0.076	23624 ± 99	67.8 ± 1.4	1.012 ± 0.012	45.53 ± 0.59	289.256 ± 16.894	280.495 ± 16.281	149.6 ± 8.1
FS13c	slickenline	44°16′27.46′′	11°09′50.73′′	0.0816	61.42 ± 0.16	13583 ± 41	304.7 ± 9.1	0.6288 ± 0.0079	46.88 ± 0.59	69.568 ± 1.379	65.207 ± 2.585	366 ± 11
FS15	slickenline	44°16′17.59′′	11°09′47.54′′	0.6421	73.0 ± 2.2	76895 ± 467	-55 ± 15	0.744 ± 0.029	11.64 ± 0.29	173.749 ± 19.291	138.022 ± 24.817	-81 ± 23
PT1	slickenline	44°16′27.46′′	11°09′50.73′′	0.0726	165.92 ± 0.15	106600 ± 4900	-16.4 ± 1.3	1.0908 ± 0.0047	28.0 ± 1.3	>600	>600	-
PT2	vein	44°16′28.82′′	11°09′52.58′′	0.0834	94.83 ± 0.10	7145 ± 18	47.0 ± 1.5	0.7776 ± 0.0049	170.1 ± 1.1	145.5 ± 2	143.6 ± 2	70.4 ± 2.3
PT3	vein	44°16′20.88′′	11°09′49.98′′	0.0660	69.758 ± 0.061	12349 ± 36	4.2 ± 1.7	1.1169 ± 0.0098	104.03 ± 0.95	>600	>600	-

(a) $[^{238}U] = [^{235}U] \times 137.818$ (±0.65‰) (Hiess et al., 2012); $\circledcirc^{234}U = ([^{234}U/^{238}U]_{activity} - 1) \times 1000$.

(b) $\circledcirc^{234}U_{initial}$ corrected was calculated based on ^{230}Th age (T), i.e., $\circledcirc^{234}U_{initial} = \circledcirc^{234}U_{measured} \; X \; e^{\circledcirc 234 * T}$, and T is corrected age.

(c) $[^{230}Th/^{238}U]_{activity} = 1 - e^{-\circledcirc 230 T} + (\circledcirc^{234}U_{measured}/1000)[\circledcirc_{230}/(\circledcirc_{230} - \circledcirc_{234})](1 - e^{-(\circledcirc 230 - \circledcirc 234) T})$, where T is the age. Decay constants are 9.1705×10^{-6} yr^{-1} for ^{230}Th, 2.8221×10^{-6} yr^{-1} for ^{234}U (Cheng et al., 2013), and 1.55125×10^{-10} yr^{-1} for ^{238}U (Jaffey et al., 1971).

(d) Age corrections, relative to chemistry date on March 10th, 2022, were calculated using an estimated atomic $^{230}Th/^{232}Th$ ratio of $4 (\pm 2) \times 10^{-6}$. Those are the values for a material at secular equilibrium, with the crustal $^{232}Th/^{238}U$ value of 3.8. The errors are arbitrarily assumed to be 50%.

5.5 Discussion and Conclusions

5.5.1 Structural synthesis

Our multidisciplinary dataset provides insight into the pattern of the post-orogenic extensional setting deforming the Epiligurian units in the Marzabotto Basin.

1) The internal structural architecture of the Marzabotto Basin includes strike-slip faults and extensional tectonic structures. The latter can be grouped into two main types: i) normal faults developed as the result of the reactivation of the early (syn-orogenic) strike-slip faults; or ii) late normal faults characterised by variable strike distribution and mainly located at the basin margins. Structural details from this work reveal that brittle deformation structures in the study area show two dominant trends: NNE–SSW and WNW–ESE. Lineament analysis allows upscaling to the scale of the basin the importance of the tectonic structures detected in the field. Although there is no direct, one-to-one correspondence with specific faults mapped at the surface, we can distinguish dominant NE–SW and WNW–ESE alignments by comparing the spatial distribution of the features deduced from the remote sensing analysis with the main directions of tectonic features measured in the field. We also observed similar cross-cutting relationships at both the mesoscale and the remote sensing scale, reflecting the deformation state of the entire Epiligurian succession in response to recent stress conditions. This kinematic scenario offers a comparison term for evaluating the mechanisms of

nucleation and propagation of immature extensional structures in the axial zone of the NA with respect to the overall extensional setting operating in its hinterland.

2) Some of the extensional structures we mapped in the Marzabotto Basin are characterised by a well-defined damage zone that provides pathways for the ingress of calcite-rich fluids. Syn-kinematic mineralisations (calcite veins, slickenlines and slickenfibers) commonly occur within the fault damage zones. These features provide valuable insights into the timing of fluid flow during the fault activity, offering constraints on the extensional phase in the axial portion of the belt.

3) Our U-Th geochronological dataset is, to our knowledge, the first record of the absolute timing of extensional fault activity in the Epiligurian Basin and, also, in the axial portion of the NA. Apart from the samples that are older than the range of the U-Th method (> 600 kyr), both fault slickenlines and calcite-filled veins gave corrected ages spanning between 65 and 290 kyr. Noteworthy, the dated syn-kinematic mineralisations are associated with two sets of normal faults: E-W-striking (FS13b2: 290 kyr; FS13c: 70 kyr) and NNE-SSW-striking (FS15: 174 kyr; PT2: 146 kyr). Considering these time constraints and the mutual cross-cutting relationships between these fault systems (see discussion above), it is plausible to propose that both systems shared a common tectonic regime. Thus, our U-Th ages constrain the main phases of normal faulting activity in the Marzabotto Basin between the Middle Pleistocene and the Late Pleistocene.

We conclude that the Epiligurian units in the Marzabotto Basin accumulated deformation during normal faulting in the Pleistocene, revealing a structural architecture for this part of the Northern Apennines governed by an overall extensional regime. The data suggest a dominant NW-SE and a subordinate N-S as maximum extension directions since the Middle Pleistocene. Overall, this kinematic pattern is not compatible with the general NE-SW stretching direction constrained for the hinterland of the Northern Apennines belt (e.g., Montone et al., 2012). This suggests that local and sub-regional factors, rather than the regional tectonic field, primarily influence the nucleation and the development of normal faults in the axial portion of the belt. Interestingly, the orientation of the normal faults in our study area matches that of the older left-lateral faults, and they formed later on top of them. These left-lateral faults developed during the final stages of the compressional event. (Balocchi et al., 2011). We, therefore, propose that the localisation of Middle-Late Pleistocene normal faults in the study area was likely conditioned by the occurrence of inherited regional structures, which provided major structural breaks to accommodate normal-sense movements.

5.5.2 Post-orogenic extension in Northern Apennines axial zone

Extensional faulting represents the most recent deformation in Northern Apennines hinterland, playing a key role in controlling late Miocene-Quaternary magmatism, hydrothermal fluids circulation along the Tyrrhenian margin and, finally, active

seismicity (e.g., Barberi et al., 1994; Acocella and Rossetti, 2002; Annunziatellis et al., 2008; Liotta et al., 2010; Vignaroli et al., 2013; **Fig. 5.3**).

The extensional architecture is also documented in the frontal part of the emerged belt, near the Pedeapenninic Thrust Front, where NNE-dipping extensional faults are responsible of the down throwing of the northernmost portion of the belt buried below the Po Plain deposits (Bertotti et al., 1997; Picotti and Pazzaglia, 2008; Picotti et al., 2009). These kinds of faults cropping out at the front are typically steep, dipping to the NE and having a vertical throw up to a few hundred metres, with conjugate SW-dipping normal fault subordinate (Bertotti et al., 1997). These tectonic structures have been interpreted as the result of the stretching of the upper part of the crust that is folding at the mountain front due to the presence of a deep blind reverse fault (Picotti and Pazzaglia, 2008; Picotti et al., 2009).

Collectively, these published data and our original ones denote that the axial zone of the NA belt is experiencing an overall tectonic regime defined by the stretching at upper crustal levels. In particular, the results of our study allow us to state that the documented extensional wave in the NA hinterland is migrating toward the northeastern quadrants and affected the belt axis in the Middle Pleistocene. Therefore, we can use the recorded deformation in the Epiligurian units to test the structural pattern of early extension in the uppermost structural levels of the axial zone of the Northern Apennines as the advancing extensional front migrates from the hinterland of a belt.

Our view, schematised in Figure 5.11, frames the concomitance of compression and extension tectonics in the NA within the dynamics of the Tertiary eastward rollback of the Adria subducting plate and retreat of the trench system (Royden, 1993; Faccenna et al., 2004; Rosenbaum and Lister, 2004; Chiarabba et al., 2015). In this geodynamic model, the forelandward propagation of thrusts and crustal accretion are concomitant with crustal thinning starting from the Tyrrhenian margin.

In **Fig. 5.11** a schematic representation of the propagation of compressional and extensional front since the Miocene to the present-day is shown. In this context, the Epiligurian wedge-top basins are considered as coeval to an Eocene-Oligocene shortening tectonic phase, which strongly influence their sedimentary framework. More in general, with respect to the evolution of the NA, shortening culminated with the Oligo-Miocene overthrusting of the Ligurian units on the Tuscan Domain and, since the Miocene, the extensional tectonic regime started, expressed by the development of normal faults having a NE-direction of extension (parallel to the belt axis), which affect the most internal part of the belt **(Fig. 5.11a).**

Compressional and extensional waves migrated contemporaneously toward the foreland, reaching their current positions. Active compressional seismicity now occurs along buried thrusts below the Po Plain and in the Adriatic offshore, while active extensional seismicity occurs along the belt's morphological divide **(Fig. 5.3)**. Surface expression of the extensional deformation in the axial domain is represented by **(Fig. 5.11b)**: i) km-spaced NW-SE-striking (thus, oriented perpendicularly with respect to the

belt axis) normal faults that reactivated early transfer faults; and ii) Collapse-induced normal faults formed in response to local instabilities during overall thinning and leading to an overall polygonal architecture in the Epilugurian units (Stendardi et al., 2023). Within this scenario, the inherited transfer faults oriented transversally to the NW-SE extensional faults are interpreted as mechanical weaknesses where the earliest stages of extensional deformation localise in the belt axial domain. Many of these transverse faults, while only locally reactivated in normal movement, can accommodate hundreds of meters of stratigraphic offset, thus impacting on the present-day structural setting of the belt. We speculate that the normal faults nucleated and grew along these transfer zones are non-Andersonian structures restricted to shallow levels. These structures will likely cease to evolve when the ongoing extensional regime will develop mature (NW-SE-striking) faults that are kinematically compatible with the regional crustal stretching.

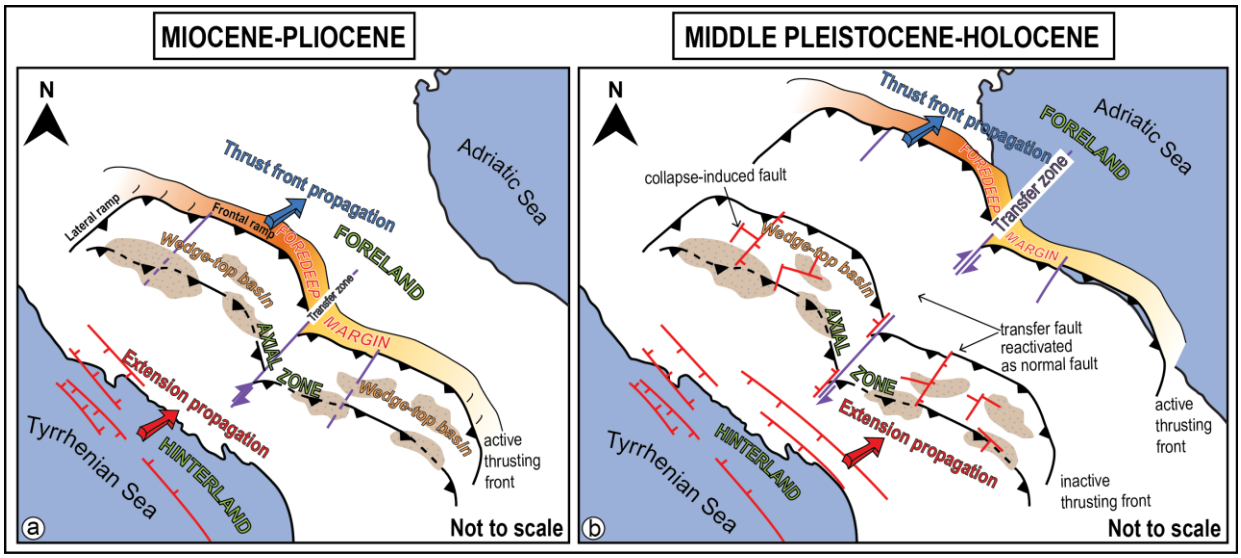

Figure 5.11- A two-stage schematic representation of the compressional and extensional front propagation within the Northern Apennines fold-and-thrust belt.

Chapter 6

Discussion and conclusions

Wedge-top basins have been studied worldwide to provide key clues about the deformation and sedimentary record within these basins, as well as to reconstruct the tectonic history of a given area. By analysing some specific case studies presented in the follows, the thesis aims to validate its methodological approach and demonstrate its applicability to diverse geological contexts.

Herail et al. (1996) conducted a study in the Cordillera Oriental (Colombian Andes) with the aim to reconstruct, through stratigraphic, structural and geochronological investigations, the tectonic history of two key Cenozoic wedge-top basins, the Nazareno and Estarca basins. These latter, which record detrital deposition in an alluvial fan environment, are set on a Miocene N-S-oriented and W-vergent thrust, which places Ordovician rocks on top of Cenozoic sedimentary strata. The results have been used to document the different tectonic steps which affected the wedge-top basins during the syn-orogenic history of the orogen. In particular, these basins are characterised by a shortening phase in the Miocene represented by N-S-striking thrusts, which stopped at around 10 Ma in the western area and jumped towards the foreland. However, uplift of the western part of the Cordillera Oriental continued, while being carried passively on the moving Main Andean Thrust.

Recently, Azizi et alii (2024) determined the age of deformation and tectonic history of the Seynane and El Mejel basins, located in Maghrebide range (northern Tunisia), and characterised by syn-tectonic Pliocene infill. In particular, structural fieldwork analysis and geomorphic studies (identification of topographic breaks and fault surfaces on DTM

images) on depositional systems from the Miocene-Quaternary succession provided new insights into the evolution of the tectono-sedimentary processes that governed the evolution of the wedge-top basins. The results have been used to determine the relative ages of thrust mobility and kinematics deformations during syn-orogenic compression in the Maghrebian belt. In fact, the tectonic history of the basins is characterized by the propagation of two major generations of out-of-sequence thrust, one Pliocene and one Quaternary in age, responsible for significant landscape alteration, and the development of local normal faults in the backlimbs and reverse forelimb faults of major structures.

Like this thesis, other studies based on detrital thermochronological allowed to understand the early stage of orogenic development of foreland basin systems, as reported and explained in the published work of Filleaudeau et al. (2011). The Authors made a correlation between the different cooling events and uplift in the Tremp wedge-top basin (south-central Pyrenees) consisting in an elongated E-W basin deepening northwards, sourced from the north-central Pyrenees, which is the site of deposition of Late Cretaceous-Palaeocene continental fluvial deposits and lacustrine limestones. Through the use of detrital thermochronology ((U-Th)/He analysis), the Authors provide insights reveal the long-term thermal and exhumation evolution of the northern Iberian continental margin from the pre-orogenic extensional tectonic setting in the Triassic and Early Cretaceous to the Cenozoic inversion and Pyrenean Mountain building. They individuated four main (U-Th)/He age peaks which, from the older to the younger are related to: i) a Triassic denudation event, associated with the propagation of Atlantic

rifting within the Variscan crystalline basement; ii) an Early Cretaceous rift-related erosion associated with extension: iii) a Late Cretaceous exhumation event due to a southward migration of thrust on the pro-wedge side of the Pyrenean orogen; iv) a Late Cretaceous- Middle Eocene decrease of thrust-related exhumation.

These studies of wedge-top basins demonstrate the importance of a multidisciplinary approach, combining fieldwork with multi-technique laboratory analyses. This approach yields insights into how these basins represent key elements of orogenic belts and how they assist when understanding the evolutionary steps that characterised the belt's complete syn-to-post orogenic evolution.

The analyses showed in this work of thesis were applied to the study of a representative example of Epiligurian basin (the Marzabotto Basin) to provide useful insights into the generally still poorly understood tectonic history of the wedge-top basins of the Northern Apennines. Specifically, mesoscale structural analysis (see Chapters 3 and 5) was crucial for the identification of multiple fault populations, each with different kinematics, and for deciphering cross-cutting relationships between structure sets that became activated during different tectonic stages of the belt evolution.

Remote sensing analyses (see Chapters 3 and 5) made it possible to investigate the geometric and kinematic pattern of the various recognised deformation structures affecting the Epiligurian units and to assess the significance of the results from mesoscopic observations upon the broader regional perspective. This was a novel approach to the structural characterisation of the Epiligurian units as it had never been

applied to such geological elements before. Lineament detection, mapping and characterisation provide useful information about the general fracturing and faulting pattern, which, in turn, can be used to infer the stress conditions in the upper structural levels of a belt during progressive deformation.

Detrital low-temperature thermochronology was fundamental to constrain the vertical movements of the studied basin during its tectonic evolution. Specifically, it was possible to obtain important insights into the spatial-temporal shift of the source regions that fed the Marzabotto Basin. The adopted approach relied on analysing apatite sub-populations from the stratigraphically oldest Loiano Fm. This provided additional information regarding the cooling history of the siliciclastic deposits source region as well as the basin burial and later exhumation. This thermochronological study represents a significant novelty, as there exist no other systematic thermochronological studies of the Epiligurian wedge-top basins.

Finally, for the first time, this study provided precise age constraints on post-orogenic tectonic activity within the axial domain of the Northern Apennines belt. Through the U/Th analyses of syn-kinematic tectonic carbonates associated with normal faults cutting across the Epiligurian units, it was possible to constrain the timing and duration of post-orogenic tectonic processes that have reshaped this tectonic region.

6.1 Main structural constraints of the Epiligurian wedge-top basins

Remote sensing made it easier to identify the faults that later became the direct target of fieldwork and ground truthing. Structural elements investigated show a spatial distribution consistent with that of regional features. A stated before, direct field observations permitted to define their kinematic characterisation and cross-cutting relationships, making it possible for a chronological reconstruction of tectonic events to be proposed.

In particular, moving from the chronologically older towards the younger tectonic phases, it was possible to discriminate: i) two distinct sets of thrusts constraining NE-SW and NW-SE shortening of the Epiligurian sedimentary succession. The NW-SE striking (with a NE-SW direction of shortening) compressional tectonic structures, lower-Oligocene-Lower Miocene in age, are linked to the structuring of the Northern Apennines. These structures have a regional scale significance and they also affected the frontal portion of the Northern Apennines fold-and-thrust belt as reported by Ottria (2000) and Balocchi and Santagata (2018) (see paragraph 3.6.1) and involve both the Cretaceous-Eocene Ligurian units and the pre-Burdigalian Epiligurian succession. The second set, represented by NE-SW striking thrust (NW-SE direction of shortening), is related to the post-Messinian compressional tectonic phase. In this case, thrusts exploit the presence of inherited structures with strike-slip kinematics, resulting in transpression events that have predominantly local significance. These tectonic structures controlled

the juxtaposition of tectonic slices of Ligurian units on top of the Epiligurian formations (Panini et al., 2002); ii) NE-SW left-lateral transtensional faults related to a strike-slip tectonic phase that led the lateral juxtaposition of Ligurian units and Epiligurian units; iii) three sets of extensional structures, all of which are rather pervasive in the entire study area, cutting across and displacing the thrusts of (i) (see paragraph 3.6.1 and 5.4.2 in Chapter 5).

Several published works have documented and characterised at the mesoscale the deformative structures and stress regimes within other Epiligurian basins in the Northern Apennines (e.g., Capitani and Sasso 1994; Ottria 2000; Antonellini and Mollema, 2002; Panini et al., 2002; Artoni et al., 2006; Balocchi, 2014; Piazza et al., 2016; Balocchi and Santagata, 2018; Del Sole et al. ,2020). In some cases, the deformation phases or the type of associated structures recorded in the study area are different with respect to these works. For example, Catanzariti et al., 2015, documented an Oligocene compressional phase which involved the basal portion of the Epiligurian succession (Marne di M. Piano and Ranzano fms.). In a regional tectonic framework, the Rupelian thrusting affecting the Epiligurian units is related to the closure of the innermost portion of the Subligurian basin and the field expression of this compressional phase is represented by the Enza Valley syncline. However, there is no evidence on the field of this tectonic phase in the study area object of this thesis, and this is probably related to the lack of suitable outcrops for the formations involved. However, in general, the results of this work of thesis are often consistent with those already documented in the other Epiligurian wedge-top basins,

both in terms of orientation and kinematic faults (even if some local variation of the deformation in different points of the axial zone of the belt). In Balocchi, 2014 was documented that the uppermost portion of the Epiligurian succession (Pantano and Cigarello fms.), is affected by NE-SW and NW-SE- striking mostly left transtensional faults, in which the former set cuts the latter, reactivated later as extensional faults. The same kinematic and cross-cutting relationships have been found in the study area and, indeed, these are the structures that played a major role in the present-day architectural conformation of the Marzabotto Basin.

6.2 Syn-to-post-orogenic evolution of the Northern Apennines: insights from the Epiligurian wedge-top basins

This study has shown that individual wedge-top basins, despite their shallow structural position, recorded a complex and long-lasting evolution that can be directly connected with that of the deeper structural levels of the belt.

Indeed, the thermochronological analyses presented in Chapter 4, when combined with existing published data on the underlying domains, aimed to: i) constrain the exhumation history of the Epiligurian units from a thermal perspective and ii) correlate it with that recorded by other tectonic domains of the Northern Apennines. My results indicate that the Epiligurian units recorded a cooling phase that began at ca. 30 Ma, while the basins were generally still subsiding, which is consistent with a similar pattern for the Ligurian units on which they rest.

Moreover, the thermochronology results provide important insights into an assessment of the cumulative uplift of the Northern Apennines during their syn-orogenic evolution. In particular, the study helped to better constrain the time of rock cooling in the belt, and to verify the maximum temperature reach by the wedge-top basins in relation to their vertical movement strictly linked to the evolution of the underlying fold-and-thrust belt. Moreover, it was possible to correlate this uplift phase to what is known about the time of shortening and the amount of the exhumation rates recorded by the underlying tectono-stratigraphic units. In fact, the work allowed to speculate, in relation to the thermal modelling obtained for the Epiligurian units, that the exhumation recorded was not steady-state and reflected the shortening phases which affected the Northern Apennines, characterised by the Ligurian overthrusting on the Umbria Marche Domain during the Eocene-early Miocene and frontal accretion with the development of out-of-sequence thrusts during the middle Miocene-Quaternary.

Systematic analysis of the deformation pattern provides first-order constraints on the post-orogenic extensional tectonic phase in the axial domain of the Northern Apennines (Chapter 5), which differs from the style of extensional deformation occurring in the hinterland of the belt (e.g., Carmignani et al., 1994; Keller et al., 1994; Collettini et al., 2006; Brogi, 2011; Rossetti et al., 2011; Brogi et al., 2014; Molli et al., 2018).

The new data document if, how, and when the advance of the Northern Apennines extensional wave was recorded by the Epiligurian wedge-top basins. In particular, for the first time it is shown that the axial domain of the Northern Apennines orogenic belt is

characterised by a complex pattern of normal faults exhibiting different orientation and amounts of offset. Extension in the axial domain of the belt is partly controlled by inherited structures such as strike-slip faults.

6.3 Conclusions

This thesis investigated the structural architecture and deformation history of the Epiligurian wedge-top basins by specifically focussing on the Marzabotto Basin as a representative case study.

By using a multidisciplinary approach that combined fieldwork and laboratory analyses at different observation scales, this thesis has provided insights into the progressive deformation that steered the evolution of the Epiligurian Basins of the Northern Apennines. This led to the proposal of a tectonic model that accounts for the syn-to-post orogenic evolution of the pellicular structural levels of the belt.

Wedge-top basins are shown to represent extremely useful tectonic elements for the characterization of the evolution of the underlying fold-and-thrust belt, both in space and time, as their final state of deformation sums up the bulk shortening and structural instability conditions of the belt.

Moreover, the conclusions of this thesis open new research avenues for studying and interpreting the significance of wedge-top basins in the tectonic evolution of the fold-and-thrust belts worldwide. For example, future studies could focus on:

- Correlating the burial and exhumation history of other wedge-top basins with that of the underlying fold-and-thrust belt to better understand the timing and spatial distribution of deformation events during continental collision.
- Using wedge-top basins to constrain the deformation style and the structural pattern of the upper structural levels of a fold-and-thrust belt.
- Applying the multidisciplinary approach used in this thesis to other wedge-top basins worldwide to compare their evolution and develop a more general understanding of the deformation processes that act in the axial domain of a fold-and-thrust belt.

References

Abbate, E., Balestrieri, M.L., Bigazzi, G., Norelli, P., and Quercioli, C. (1994). Fission-track datings and recent rapid denudation in northern Apennines, Italy. *Memorie delle Società Geologica Italiana, 48:* 579-585.

Abbate, E., Balestrieri, M.L., Bigazzi, G., Ventura, B., Zattin, M., Zuffa, G.G. (1999). An extensive apatite fission-track study throughout the Northern Apennines nappe belt. *Radiation Measurements, 31*: 673-676.

Abbate, E., and Bruni, P. (1987). Modino-Cervarola o Modino e Cervarola? Torbiditi oligo-mioceniche ed evoluzione del margine nord-appenninico. *Mem. Soc. Geol. Ital., 39*: 19-33.

Acocella, V., and Rossetti, F. (2002). The role of extensional structures on pluton ascent and emplacement: the case of southern Tuscany (Italy). *Tectonophysics, 354*: 71-83.

Amorosi, A. (1995). Glaucony and sequence stratigraphy; a conceptual framework of distribution in siliciclastic sequences. *Journal of sedimentary research, 65(4b)*: 419-425.

Amato, A., Azzara, R., Chiarabba, C., Cimini, G.B., Cocco, M., Di Bona, M., Margheriti, S., Mazza, F., Mele, G., Basili, E., Boschi, F., Courboulex, A., Deschamps, S., Gaffet, A., Bittarelli, L., Chiaraluce, D., Piccinini, M., and Ripepe, M. (1998). The 1997 Umbria-Marche, Italy, earthquake sequence: A first look at the main shocks and aftershocks. *Geophysical Research Letters, 25(15),* 2861-2864.

Ambrosi, A., Colalongo, M.L., and Vaiani, S.C. (1996). Revisione litostratigrafica dell'unità Bismantova (Miocene epiligure, Appennino settentrionale*). Bollettino della Società Geologica Italiana, 115*: 355-368.

Amorosi, A. (1995). Glaucony and sequence stratigraphy; a conceptual framework of distribution in siliciclastic sequences. *Journal of sedimentary research, 65(4b)*: 419-425.

Amorosi, A. Colalongo, M.L., and Vaiani, S.C. (1996). Detecting a sequence boundary across different tectonic domains: an example from the middle Miocene of the northern Apennines (Italy). *Terra Nova,8 (4)*: 334-346.

Amorosi, A., Scarponi, D., and Lucchi, F.R. (2002). Palaeoenvironmental changes in the Pliocene Intra-Apenninic Basin, near Bologna (Northern Italy). *Geobios, 35*: 7-18.

Andreucci, B. (2013). Thermochronology of the Polish and Ukrainian Carpathians. PhD thesis.

Annunziatellis, A., Beaubien, S.E., Bigi, S., Ciotoli, G., Coltella, M., Lombardi, S. (2008). Gas migration along fault systems and through the vadose zone in the Latera caldera (central Italy): implications for CO2 geological storage. *International Journal of Greenhouse Gas Control, 2*: 353-372.

Antonellini, M.A., Aydin, A., and Pollard, D.D. (1994). Microstructure of deformation bands in porous sandstones at Arches National Park, Utah. *Journal of structural geology, 16(7)*: 941-959.

Antonellini, M., and Mollema, P. (2002). Cataclastic faults in the Loiano sandstones; northern Apennines, Italy. *Bollettino della Società Geologica Italiana, 121(2):* 163-178.

Argnani, A., and Ricci Lucchi, F. (2001). Tertiary silicoclastic turbidite systems of the Northern Apennines. In: G.B. Vai and I.P. Martini (Eds.), *Anatomy of an Orogen: the Apennines and Adjacent Mediterranean Basins*: 327–350. Kluwer Academic Publishers, Dordrecht.

Artoni, A., Bernini, M., Vescovi, P., Lorenzi, U., Missorini, E. (2006). Estensione alla sommità del cuneo orogenico appenninico: contatti tettonici elisionali nella successione epiligure di M. Barigazzo (Appennino settentrionale, prov. Parma)**.** *Rend. Soc. Geol. It., 2*: 69-72.

Ascione, A., Capalbo, A., Capolongo, D., Mazzoli, S., Pazzaglia, F., Valente, E., and Zattin, M. (2012). Uplift vs. denudation in the southern Apennines: geomorphologic evidence

and constraints from terrestrial cosmogenic nuclides and apatite (U-Th)/He data. *Rend Online Soc. Geol. Ital., (21)*: 1102-1104.

Aydin, A., and Johnson, A.M. (1978). Development of faults as zones of deformation bands and as slip surfaces in sandstone. *Pure and applied Geophysics, 116(4)*: 931-942.

Aydin, A., and Johnson, A.M. (1983). Analysis of faulting in porous sandstones. *Journal of structural Geology, 5(1)*:19-31.

Aydin, A., Borja, R.I., and Eichhubl, P. (2006). Geological and mathematical framework for failure modes in granular rock. *Journal of Structural Geology, 28(1)*: 83-98.

Azizi, R., Barhoumi, A., and Mancini, A. (2024). New insight on the structural architecture of northern Tunisia with a multidisciplinary approach: Association of Miocene piggy-back basin and active Plio-quaternary out-of-sequence thrusts. *Marine and Petroleum Geology, 160*: 106639.

Balestrieri, M.L., Abbate, E., and Bigazzi, G. (1996). Insigths on the thermal evolution of the Ligurian Apennines (Italy) through fission-track analysis. *Journal of the Geological Society of London, 153:* 419-425.

Balestrieri, M.L., Bernet, M., Brandon, M.T., Picotti, V., Reiners, P., and Zattin, M. (2003). Pliocene and Pleistocene exhumation and uplift of two key areas of the Northern Apennines. *Quaternary International, 101:* 67-73.

Balocchi, P. (2012). Analisi della deformazione tettonica inerente alla sinclinale Canossa-Viano-Castellarano (Appennino Settentrionale). *GeoResearch Center Italy-GeoBlog, 2*: 2-12.

Balocchi, P. (2014). Analisi macrostrutturale e mesostrutturale del Gruppo di Bismantova affiorante tra Zocca e Castel d'Aiano (Appennino modenese e bolognese). *Atti della Società dei Naturalisti e Matematici di Modena, 145*: 27-42.

Balocchi, P., and Santagata, T. (2018). The transpressive deformation zone of the Ranzano Formation along the River Secchia near Castellarano (Northern Apennines). *Atti Soc. Nat. Mat. di Modena, 149*: 57-67.

Balocchi, P., and Little, W. W. (2020). Influence of the Canossa-San Romano fault system on the development of the River Secchia fluvial terraces (Northern Apennines, Italy). *Atti della Societa dei Naturalisti e Matematici di Modena, 151*.

Barberi, F., Buonasorte, G., Cioni, R., Fiordelisi, A., Foresi, L., Iaccarino, S., Laurenzi, M.A., Sbrana, A., Vernia, L., Villa, I.M. (1994). Plio-Pleistocene geological evolution of the geothermal area of Tuscany and Latium. *Memorie Descrittive della Carta Geologica Italiana, 49:* 77-133.

Barbero, E., Festa, A., Fioraso, G., and Catanzariti, R. (2017). Geology of the Curone and Staffora Valleys (NW Italy): field constraints for the Late Cretaceous–Pliocene tectono-stratigraphic evolution of Northern Apennines. *Journal of Maps, 13(2)*: 879-891

Barchi, M.R, Landuzzi, A., Minelli, G., and Pialli, G. (2001). Outer Northern Apennines. *Anatomy of an orogen: the Apennines and Adjacent Mediterranean Basins,* 215-253.

Barchi, M.R, Pauselli C, Chiarabba C, Di Stefano R, Federico C, and Minelli G. (2006). Crustal structure, tectonic evolution and seismogenesis in the Northern Apennines (Italy). *Bollettino di Geofisica teorica e Applicata, 47*: 249-270.

Barchi, M.R. (2010). The Neogene-Quaternary evolution of the Northern Apennines: crustal structure, style of deformation and seismicity. *Journal of the Virtual Explorer*, *36*.

Bartole, R. (1995). The North Tyrrhenian-Northern Apennines post-collisional system: constraints for geodynamic model. *Terra Nova, 7:* 7-30.

Bartolini, C., Bemini, M., Carloni, G.C., Castaldini, P., Costantini, A., Federici, P.R., Francavilla, F., Gasperi, G., Lazzarotto, G., Mazzanti, A., Papani, G., Pranzini, G., Rau, A., Sandrelli, F., and Vercesi, P.L. (1983). Carta neotettonica dell'Appennino Settentrionale. *Note illustrative, Boll. Sot. Geol. Ital.*

Beaumont, C. (1981). Foreland basins. *Geophysical Journal International, 65(2)*: 291-329.

Bertotti, G., Capozzi, R., and Picotti, V. (1997). Extension controls Quaternary tectonics, geomorphology and sedimentation of the N-Appennies foothills and adjacent Po Plain (Italy). *Tectonophysics, 282(1-4)*: 291-301.

Bettelli G., Bonazzi U., Fazzini P., Panini F., (1987a). Schema introduttivo alla geologia delle Epiliguridi dell'Appennino modenese e delle aree limitrofe. *Mem. Soc. Geol. It., 39*: 215-246.

Bettelli G., Bonazzi U., Fazzini P., Panini F., (1987b). Schema introduttivo alla geologia delle Epiliguridi dell'Appennino modenese e delle aree limitrofe. *Mem. Soc. Geol. It., 39*: 91-126.

Bettelli, G., and Vannucchi, P. (2003). Structural style of the offscraped Ligurian oceanic sequences of the Northern Apennines: new hypothesis concerning the development of mélange block-in-matrix fabric. *Journal of Structural Geology, 25(3)*: 371-388.

Bernet, M., and Spiegel, C. (Eds.). (2004). Detrital thermochronology: Provenance analysis, exhumation, and landscape evolution of mountain belts, *378*. Geological Society of America.

Bernet, M., Brandon, M.T., Garver, J. I., Balestrieri, M.L., Ventura B., and Zattin, M. (2009). Exhuming the Alps through tie: Clues from detrital zircon fission-track ages. *Basin Res., 21:* 781–798.

Boccaletti, M., Elter, P., and Guazzone, G. (1971). Plate tectonic models for the development of the Western Alps and Northern Apennines. *Nature Physical Science*, *234*(49), 108-111.

Boccaletti, M., Coli, M., Eva, C., Ferrari, G., Giglia, G., Lazzarotto, A., Merlanti, F., Nicolich, R., Papani, G., and Postpischl D. (1985). Considerations on the seismotectonics of the Northern Apennines. *Tectonophysics, 117(1-2):* 7-38.

Boccaletti M, Calamita F, Deiana G, Gelati R, Massari F, Moratti G, Ricci Lucchi F. (1990). Migrating foredeep-thrust belt systems in the northern Apennines and southern Alps: Palaeogeography, Palaeoclimatology, Palaeoecology, *v.77*: 3-14.

Boccaletti, M., Corti, G., and Martelli, L. (2011). Recent and active tectonics of the external zone of the Northern Apennines (Italy). *International Journal of Earth Sciences, 100(6)*: 1331-1348.

Boettcher, S.S., and McBride, E.F. (1993). Thermal histories of piggy-back and foreland basins in the northern Apennines, Italy, derived from apatite fission track thermochronology. *EOS, 74(43)*: 547.

Bonini, M., and Sani, F. (2002). Extension and compression in the Northern Apennines (Italy) hinterland: Evidence from the late Miocene-Pliocene Siena-Radicofani Basin and relations with basement structures. *Tectonics*, *21*(3): 1-1.

Bonini, M. (2007). Interrelations of mud volcanism, fluid venting, and thrust-anticline folding: Examples from the external northern Apennines (Emilia-Romagna, Italy). *Journal of Geophysical Research: Solid Earth, 112*(B8).

Bonini, L., Toscani, G., Seno, S. (2014a). Three-dimensional segmentation and different rupture behavior during the 2012 Emilia seismic sequence (Northern Italy). *Tectonophysics, 630:* 33-42, http://dx.doi.org/10.1016/j.tecto.2014.05.006.

Bonini, M., Sani, F., Stucchi, E.M., Moratti, G., Benvenuti, M., Menanno, G., Tanini, C., (2014b). Late Miocene shortening of the Northern Apennines back-arc. *Journal of Geodynamics, 74*: 1-31.

Bortolotti, V., Principi, G., and Treves, B. (2001). Ophiolites, Ligurides and the tectonic evolution from spreading to convergence of a Mesozoic Western Tethys segment. In *Anatomy of an orogen: The Apennines and adjacent Mediterranean basins* (pp. 151-164). Dordrecht: Springer Netherlands.

Botti, F., Aldega, L., and Corrado, S. (2004). Sedimentary and tectonic burial evolution of the Northern Apennines in the Modena-Bologna area: constraints from combined stratigraphic, structural, organic matter and clay mineral data of Neogene thrust-top basins. *Geodinamica Acta*, *17*(3), 185-203. https://doi.org/10.3166/ga.17.185-203

Boyer, S.E., and Elliot, D. (1982). Thrust systems: *Bulletin American Association of Petroleum Geologists, v. 66*.

Braathen, A., Bergh, S.G., Maher, H.D. (1999). Application of a critical wedge taper model to the Tertiary transpressional fold-thrust belt on Spitsbergen, Svalbard. *GSA Bulletin, 111*: 1468-1485.

Braun, J., Van Der Beek, P., and Batt, G. (2006). Quantitative thermochronology: numerical
methods for the interpretation of thermochronological data: 1–258

Brogi, A. (2011). Bowl-shaped basin related to low-angle detachment during continental extension: The case of the controversial Neogene Siena Basin (central Italy, Northern Apennines). *Tectonophysics, 499*: 54-76.

Brogi, A., Capezzuoli, E., Martini, I., Picozzi, M., Sandrelli, F. (2014). Late Quaternary tectonics in the inner Northern Apennines (Siena Basin, southern Tuscany, Italy) and their seismotectonic implication. *Journal of Geodynamics, 76*: 25-45.

Capitani, M., and Sasso, F. (1994). Analisi mesostrutturale della Formazione di Bismantova di Pavullo nel Frignano (Appennino modenese). *Atti Tic. Sc. Terra, 37*: 99-110.

Capozzi, R., Landuzzi, A., Negri, A., Vai, G.B. (1991). Stili deformativi ed evoluzione tettonica della successione neogenica romagnola. *Studi Geologici Camerti, vol. spec. 1991/1*: 261-278.

Caricchi C., Aldega L., and Corrado S. (2015). Reconstruction of maximum burial along the Northern Apennines thrust wedge (Italy) by indicators of thermal exposure and modeling. *Bulletin, 127(3-4)*: 428-442.

Carlini, M., Artoni, A., Aldega, L., Balestrieri, M.L., Corrado, S., Vescovi, P., Bernini, M. and Torelli, L. (2013). Exhumation and reshaping of far-travelled/allochthonous tectonic units in mountain belts. New insights for the relationships between shortening and coeval extension in the western Northern Apennines (Italy). *Tectonophysics, 608*: 267-287.

Carmignani, L., and Kligfield, R. (1990). Crustal extension in the Northern Apennines: the transition from compression to extension in the Alpi Apuane core complex. *Tectonics, 9(6)*: 1275-1303.

Carmignani, L., Decandia F.A., Fantozzi, P.L., Lazzarotto, A., Lotta, D., Meccheri, M. (1994). Tertiary extensional tectonics in Tuscany (Northern Apennines, Italy). *Tectonophysics, 238*: 295-315.

Carmignani, L., Decandia, F.A., Disperati, L., Fantozzi, P.L., Lazzarotto, A., Liotta, D., and Oggiano, G. (1995). Relationships between the Tertiary structural evolution of the Sardinia-Corsica-Provençal Domain and the Northern Apennines. *Terra Nova, 7(2)*: 128-137.

Carminati, E., Lustrino, M., Cuffaro, M., and Doglioni, C. (2010). Tectonics, magmatism and geodynamics of Italy: what we know and what we imagine. *J. Virtual Explor., 36(8)*: 10-3809.

Carminati, E., and Doglioni, C. (2012). Alps vs. Apennines: the paradigm of a tectonically asymmetric Earth. *Earth-Science Reviews, 112(1-2)*: 67-96.

Carminati, E., Lustrino, M., and Doglioni, C. (2012). Geodynamic evolution of the central and western Mediterranean: Tectonics vs. igneous petrology constraints. *Tectonophysics*, *579*: 173-192.

Carrapa, B., and DeCelles, P.G. (2008). Eocene exhumation and basin development in the Puna of northwestern Argentina. *Tectonics, 27(1).*

Carrapa, B. (2009). Tracing exhumation and orogenic wedge dynamics in the European Alps with detrital thermochronology. *Geology, 37(12):* 1127-1130.

Carrapa, B., Bywater-Reyes, S., DeCelles, P.G., Mortimer, E., and Gehrels, G.E. (2012). Late Eocene–Pliocene basin evolution in the Eastern Cordillera of northwestern Argentina (25–26 S): Regional implications for Andean orogenic wedge development. *Basin Research, 24(3):* 249-268.

Carrapa, B., Di Giulio, A., Mancin, N., Stockli, D., Fantoni, R., Hughes, A., and Gupta, S. (2016). Tectonic significance of Cenozoic exhumation and foreland basin evolution in the Western Alps. *Tectonics*, *35*(8): 1892-1912.

Cartwright, J., James, D., and Bolton, A. (2003). The genesis of polygonal fault systems: a review. *Geological Society, London, Special Publications, 216(1)*: 223-243.

Casciello, E., Cesarano, M., Pappone, G. (2006). Extensional detachment faulting on the Tyrrhenian margin of the Southern Apennines contractional belt (Italy). *Journal of the Geological Society of London, 163*: 617-629.

Castellarin, A. (2001). Alps-Apennines and Po Plain-frontal Apennines relations. *Anatomy of an Orogen: the Apennines and adjacent Mediterranean Basins,* 177-195. Vai GB and Martini IP (eds).

Catanzariti, R., Cerrina Feroni, A., Ottria, G., and Vescovi, P. (1999). Lower Oligocene thrust-system in the epi-Ligurian succession: evidence from the Enza Valley (northern Apennines, Italy). *Geodinamica acta, 12(2)*: 81-96.

Cavinato, G. P.,and Celles, P.D. (1999). Extensional basins in the tectonically bimodal central Apennines fold-thrust belt, Italy: response to corner flow above a subducting slab in retrograde motion. *Geology, 27(10)*: 955-958.

Cavinato, G.P., Carusi, C., Dall'Asta, M., Miccadei, E., and Piacentini, T. (2002). Sedimentary and tectonic evolution of Plio-Pleistocene alluvial and lacustrine deposits of Fucino Basin (central Italy). *Sedimentary Geology, 148*: 29-59, doi: 10.1016/S0037-0738(01)00209-3

Cawood, P.A., Kröner, A., Collins, W.J., Kusky, T.M., Mooney, W.D., and Windley, B.F. (2009). Accretionary orogens through Earth history. Geological Society, London, Special Publications, 318(1): 1-36.

Cello, G., Mazzoli, S., Tondi, E., Turco, E. (1997). Active tectonics in the central Apennines and possible implications for seismic hazard analysis in peninsular Italy. *Tectonophysics, 272*: 43-68, doi:10.1016/S0040-1951(96)00275-2

Cheng, H., Edwards, R. L., Shen, C.-C., Polyak, V.J., Asmerom, Y., Woodhead, J., Hellstrom, J., Wang, Y., Kong, X., and Spötl, C. (2013). Improvements in ^{230}Th dating, ^{230}Th and ^{234}U half-life values, and U-Th isotopic measurements by multi-collector inductively coupled plasma mass spectroscopy. *Earth Planet. Sc. Lett.*, 371-372, 82-91, 10.1016/j.epsl.2013.04.006.

Chiang, C.S., Yu, H.S., and Chou, Y.W. (2004). Characteristics of the wedge-top depozone of the southern Taiwan foreland basin system. *Basin Research, 16(1)*: 65-78.

Chiarabba, C., Jovane, L., and DiStefano, R. (2005). A new view of Italian seismicity using 20 years of instrumental recordings. *Tectonophysics*, *395(3-4)*, 251-268.

Chiarabba, C., De Gori, P., and Mele, F. M. (2015). Recent seismicity of Italy: Active tectonics of the central Mediterranean region and seismicity rate changes after the Mw 6.3 L'Aquila earthquake. *Tectonophysics*, *638*, 82-93.

Chiaraluce, L., Ellsworth W.L., Chiarabba C., and Cocco, M. (2003). Imaging the complexity of an active normal fault system: The 1997 Colfiorito (central Italy) case study, *J. Geophys. Res*, *108(B6)*: 2294, doi:10.1029/2002JB002166.

Chiaraluce, L., Chiarabba, C., Collettini, C., Piccinini, D., and Cocco, M. (2007). Architecture and mechanics of an active low-angle normal fault: Alto Tiberina fault, northern Apennines, Italy. *Journal of Geophysical Research: Solid Earth, 112(B10).*

Chiaraluce, L., Amato, A., Carannante, S., Castelli, V., Cattaneo, M., Cocco, M., Collettini, C., D'Alema, E., Di Stefano, R., Latorre, D., Marzorati, S., Mirabella, F., Monachesi, G., Piccinini D., Nardi, A., Piersanti, A., Stramondo, S., and Valoroso, L. (2014). The Alto Tiberina Near Fault Observatory (northern Apennines, Itay). *Annals of Geophysics.*

Ciarcia, S., and Vitale, S. (2013). Sedimentology, stratigraphy and tectonics of evolving wedge-top depozone: Ariano Basin, southern Apennines, Italy. *Sedimentary Geology, 290*: 27-46.

Cibin, U., Spadafora, E., Zuffa, G.G., and Castellarin, A. (2001). Continental collision history from arenites of episutural basins in the Northern Apennines, Italy. *Geological Society of America Bulletin, 113 (1)*: 4-19.

Cipollari, P., and Cosentino, D. (1995). Miocene unconformities in the Central Apennines: geodynamic significance and sedimentary basin evolution. *Tectonophysics, 252*: 375-389.

Cloos, M. (1984). Flow melanges and the structural evolution of accretionary wedges. *Geological Society of America Special Paper*, *198*: 71-79.

Cloos, M., and Shreve, R.L. (1988a). Subduction-channel model of prism accretion, melange formation, sediment subduction, and subduction erosion at convergent plate margins: 1. Background and description. *Pure and Applied Geophysics, 128(3)*: 455-500.

Cloos, M., and Shreve, R.L. (1988b). Subduction-channel model of prism accretion, melange formation, sediment subduction, and subduction erosion at convergent plate margins: 1. Background and description. *Pure and Applied Geophysics, 128(3):* 501-545.

Collettini, C. (2011). The mechanical paradox of low-angle normal faults: Current understanding and open questions. *Tectonophysics, 510*: 253-268.

Collettini, C., De Paola, N., Holdsworth, R.E., Barchi, M.R. (2006). The development and behavior of low-angle normal faults during Cenozoic asymmetric extension in the Northern Apennines, Italy. *Journal of Structural Geology*, *28*: 333-352.

Coltorti, M., Consoli, M., Dramis, F., Gentili, B., and Pambianchi, G. (1991). Evoluzione geomorfologica delle piane alluvionali delle Marche centro-meridionali. *Geografia Fisica e Dinamica Quaternaria*, *14*(1), 87-100.

Coogan, J.C., Link, P.K., Kuntz, M.A., and Platt, L.B. (1992). Structural evolution of piggyback basins in the Wyoming-Idaho-Utah thrust belt. Regional geology of eastern Idaho and western Wyoming: *Geological Society of America Memoir, 179*: 55-81.

Conti, P., Cornamusini, G., and Carmignani, L. (2020). An outline of the geology of the Northern Apennines (Italy), with geological map at 1: 250,000 scale. *Italian Journal of Geosciences, 139 (2)*: 149-194.

Corrado, S., Aldega, L., Zattin, M. (2010). Sedimentary vs. tectonic burial and exhumation along the Apennines (Italy). *Journal of Virtual Explorer, 36*.

Cuffaro, M., Riguzzi, F., Scrocca, D., Antonioli, F., Carminati, E., Livani, M., and Doglioni, C. (2010). On the geodynamics of the northern Adriatic plate. *Rendiconti Lincei*, *21*: 253-279.

D'Agostino, N., Mantenuto, S., D'Anastasio, E., Avallone, A., Barchi, M., Collettini, C., Radicioni, F., Stoppini, A., and Fastellini, G. (2009). Contemporary crustal extension in the Umbria–Marche Apennines from regional CGPS networks and comparison between geodetic and seismic deformation. *Tectonophysics*, *476(1-2)*, 3-12.

Dahlen, F.A. (1984). Non-cohesive critical Coulomb wedges: An exact solution. Journal of Geophysical Research: *Solid Earth, 89(B12)*: 10125-10133.

Dahlen, F.A. (1990). Critical taper model of fold-and-thrust belts and accretionary wedges. *Annual Review of Earth and Planetary Sciences:* 18-55.

Davis, D., Suppe, J., and Dahlen, F.A. (1983). Mechanics of fold-and-thrust belts and accretionary wedges. *Journal of Geophysical Research: Solid Earth, 88(B2)*: 1153-1172.

Decandia, F.A., Lazzarotto, A., Liotra, D., Cernobori, L. and Nicholic, R. (1998). The CROP 03 traverse: insights on post-collisional evolution of the northern Apennines. *Memorie della Societfi Geologica Italiana, 52:* 427-439.

DeCelles, P.G-, and Mitra, G. (1995). History of the Sevier orogenic wedge in terms of critical taper models, northeast Utah and southwest *Wyoming. Geological Society of America Bulletin, 107(4)*: 454-462.

DeCelles, P.G., and Giles, K.A. (1996). Foreland basin systems. *Basin research, 8(2)*: 105-123.

DeCelles, P.G. (2011). Foreland basin systems revisited: Variations in response to tectonic settings. *Tectonics of sedimentary basins: Recent advances*, 405-426.

Del Sole, L., and Antonellini, M. (2019). Microstructural, petrophysical, and mechanical properties of compactive shear bands associated to calcite cement concretions in arkose sandstone. *Journal of Structural Geology, 126*: 51-68.

Del Sole, L., Antonellini, M., Soliva, R., Ballas, G., Balsamo, F., and Viola, G. (2020). Structural control on fluid flow and shallow diagenesis: insights from calcite cementation along deformation bands in porous sandstones. *Solid Earth, 11(6)*: 2169-2195.

Dewey, J.F., and Bird, J.M. (1970). Mountain belts and the new global tectonics. *Journal of geophysical Research, 75(14)*: 2625-2647.

Dewey, J.F. (1988). Extensional collapse of orogens. *Tectonics, 7*: 1123–1139, doi:10.1029/TC007i006p01123

Di Naccio, D., Boncio, P., Brozzetti, F., Pazzaglia, F.J., and Lavecchia, G. (2013). Morphotectonic analysis of the Lunigiana and Garfagnana grabens (northern Apennines, Italy): Implications for active normal faulting. *Geomorphology, 201*: 293-311.

Doblas, M. (1998). Slickenside kinematic indicators. *Tectonophysics 295*: 187–197.

Doglioni, C. (1991). A proposal for the kinematic modelling of W-dipping subductions-possible applications to the Tyrrhenian-Apennines system. *Terra Nova, 3(4)*: 423-434.

Doglioni, C. (1992). Main differences between thrust belts. *Terra Nova, 4(2)*: 152-164.

Doglioni, C., Harabaglia, P., Merlini, S., Mongelli, F., Peccerillo, A.T., and Piromallo, C. (1999). Orogens and slabs vs. their direction of subduction. *Earth-Science Reviews, 45(3-4)*: 167-208.

Doglioni, C., Carminati, E., and Cuffaro, M. (2006). Simple kinematics of subduction zones. *International geology review, 48(6)*: 479-493.

Donelick, R.A., O'Sullivan, P.B., and Ketcham, R.A. (2005). Apatite Fission-Track Analysis: Reviews in Mineralogy and Geochemistry, v. 58, p. 49–94, doi:10.2138/rmg.2005.58.3.

Dumitru, T.A. (1993). A new computer-automated microscope stage system for fission-track analysis. *Nuclear Tracks and Radiation Measurements, 21(4)*: 575-580.

Dunkl, I. (2002). TRACKKEY: a Windows program for calculation and graphical presentation of fission track data. *Computers & Geosciences, 28(1)*: 3-12.

Ehlers, T.A., and Farley, K.A. (2003). Apatite (U–Th)/He thermochronometry: methods and applications to problems in tectonic and surface processes. *Earth and Planetary Science Letters, 206*: 1–14.

Elter, P., Grasso, M., Parotto, M., and Vezzani, L. (2003). Structural setting of the Apennine-Maghrebian thrust belt. *Episodes, 26(3)*: 205-211.

England, P., and Molnar, P. (1990). Surface uplift, uplift of rocks, and exhumation of rocks. *Geology, 18*: 1173-1177.

Erlanger, E.D., Fellin, M.G., and Willett, S.D. (2022). Exhumation and erosion of the Northern Apennines, Italy: new insights from low-temperature thermochronometers. *Solid Earth, 13(2)*: 347-365.

Eva, E., Pettenati, F., Solarino, S., Sirovich, L. (2022). The focal mechanism of the 7 September 1920, Mw 6.5 earthquake: insights into the seismotectonics of the Lunigiana–Garfagnana area, Tuscany, Italy. *Geophysical Journal International, 228*: 1465–1477, https://doi.org/10.1093/gji/ggab411.

Faccenna, C., Mattei, M., Funiciello, R., and Jolivet, L. (1997). Styles of back-arc extension in the central Mediterranean. *Terra Nova, 9*(*3*): 126-130.

Faccenna, C., Becker, T.W., Lucente, F.P., Jolivet, L., and Rossetti, F. (2001). History of subduction and back-arc extension in the Central Mediterranean. *Geophysical Journal International, 145(3)*: 809-820.

Faccenna, C., Piromallo, C., Crespo-Blanc, A., Jolivet, L., and Rossetti, F. (2004). Lateral slab deformation and the origin of the western Mediterranean arcs. *Tectonics, 23(1).*

Farley, K.A., Wolf, R.A., Silver, L.T. (1996). The effects of long alpha-stopping distances on (U-Th)/He dates. *Geochim Cosmochim Acta, 60*:1–7.

Farley, K.A. (2002). (U-Th)/He dating: techniques, calibrations, and applications. Rev. Mineral. *Geochem. 47*: 819–844. https://doi.org/10.2138/rmg.2002.47.18

Fassoulas, C. (1999). The structural evolution of central Crete: insight into the tectonic evolution of the south Aegean (Greece). *Journal of Geodynamics, 27*: 23–43.

Fellin, M.G., Reiners, P.W., Brandon, M.T., Wüthrich, E., Balestrieri, M.L., and Molli. G. (2007). Thermochronologic evidence for the exhumational history of the Alpi Apuane metamorphic core complex, northern Apennines, Italy. *Tectonics, 26(6).*

Ferretti, G., Solarino, S. and Eva, E. (2002). Crustal structure of the Lunignana-Garfagnana area (Tuscany, Italy): seismicity, fault-plane solutions, and seismic tomography. *Bollettino di Geofisica Teorica e Applicata, 43(3-4)*: 221-238.

Ferrière, J., Reynaud, J.Y., Pavlopoulos, A., Bonneau, M., Migiros, G., Chanier, F., Proust, J.N., and Gardin, S. (2004). Geologic evolution and geodynamic controls of the Tertiary intramontane piggyback Meso-Hellenic basin, Greece. *Bulletin de la Société géologique de France, 175(4)*: 361-381.

Festa, A., Ogata, K., Pini, G. A., Dilek, Y., and Codegone, G. (2015). Late Oligocene–early Miocene olistostromes (sedimentary mélanges) as tectono-stratigraphic constraints to the geodynamic evolution of the exhumed Ligurian accretionary complex (Northern Apennines, NW Italy). *International Geology Review, 57(5-8)*: 540-562.

Filleaudeau, P. Y., Mouthereau, F., and Pik, R. (2012). Thermo-tectonic evolution of the south-central Pyrenees from rifting to orogeny: Insights from detrital zircon U/Pb and (U-Th)/He thermochronometry. *Basin Research*, *24*(4): 401-417.

Fleischer, R.L., Price, P.B., and Walker, R.M. (1975). Nuclear tracks in solids: principles and applications: University of California Press.

Flowers, R.M., Ketcham, R.A., Shuster, D.L., Farley, K.A. (2009). Apatite (U-Th)/He thermochronometry using a radiation damage accumulation and annealing model. *Geochim. Cosmochim. Acta 73*: 2347–2365. https://doi.org/10.1016/j.gca.2009.01.015.

Ford, M. (2004). Depositional wedge tops: interaction between low basal friction external orogenic wedges and flexural foreland basins. *Basin Research, 16(3)*: 361-375.

Fossen, H., and Bale, A. (2007). Deformation bands and their influence on fluid flow. *AAPG bulletin, 91(12)*: 1685-1700.

Fossen, H., and Hesthammer, J. (1998.) Deformation bands and their significance in porous sandstone reservoirs. *First Break, 16(1).*

Fossen, H., Schultz, R.A., Shipton, Z.K., and Mair, K. (2007). Deformation bands in sandstone: a review. *Journal of the Geological Society, 164(4)*: 755-769.

Fugenschuh, B., and Schmid, S.M. (2003). Late stages of deformation and exhumation of an orogen constrained by fission-track data: A case study in the Western Alps. *Geological Society of America Bulletin, 115(11)*: 1425-1440.

Galbraith R.F. and Green P.F., 1990. Estimating the component ages in a finite mixture. *Nucl. Tracks. Radiat. Meas*. *17*, 197–206.

Galbraith, R.F., and Laslett, G.M., 1993. Statistical models for mixed fission track ages. Nuclear tracks and radiation measurements, *21*(4), 459-470.

Gallagher, K., Brown, R., and Johnson, C. (1998). Fission track analysis and its applications to geological problems. *Annual Review of Earth and Planetary Sciences*, *26*(1), 519-572.

Garver, J.I., Brandon, M.T., Roden-Tice, M., and Kamp, P.J. (1999). Exhumation history of orogenic highlands determined by detrital fission-track thermochronology. *Geological Society, London, Special Publications, 154(1)*: 283-304.

Gautheron, C., Tassan-Got, L., Barbarand, J., and Pagel, M. (2009). Effect of alpha-damage annealing on apatite (U-Th)/He thermochronology. *Chemical Geology, 266*: 157–170.

Gleadow, A.J.W., and Duddy, I.R. (1981). A natural long-term track annealing experiment for apatite. *Nuclear Tracks, 5*: 169–174.

Gleadow, A.J.W., Duddy, I.R., Green, P.F., and Lovering, J.F. (1986). Confined fission track lengths in apatite: a diagnostic tool for thermal history analysis. *Contribution to Mineralogy and Petrology, 94*: 405–415.

Glotzbach, C., Bernet, M., and Van Der Beek, P. (2011). Detrital thermochronology records changing source areas and steady exhumation in the Western European Alps. *Geology, 39(3)*: 239-242.

Green, P.F., Duddy, I.R., Gleadow, A.J.W., Tingate, P.R., and Laslett, G.M. (1985). Fission track annealing in apatite: track length measurements and the form of the Arrhenius plot. *Nuclear Tracks and Radiation Measurements, 10*: 323–328

Gugliotta, C., and Morticelli, M.G. (2012). Using high-resolution stratigraphy and structural analysis to constrain polyphase tectonics in wedge-top basins: Inferences from the late Tortonian Scillato Basin (central-northern Sicily). *Sedimentary Geology*, *273*: 30-47.

Hayman, N.W. (2006). Shallow crustal rocks from the Black Mountains detachments, Death Valley, CA. *Journal of Structural Geology 28*: 1767–1784.

Hérail, G., Oller, J., Baby, P., Bonhomme, M., and Soler, P. (1996). Strike-slip faulting, thrusting and related basins in the Cenozoic evolution of the southern branch of the Bolivian Orocline. *Tectonophysics*, *259*(1-3): 201-212.

Hiess, J., Condon, D. J., McLean, N. and Noble, S. R. (2012). $^{238}U/^{235}U$ systematics in terrestrial uranium-bearing minerals. Science, 355, 1610-1614.

Hill, R.E. (1990). Analysis of deformation bands in the Aztec sandstone, Valley of Fire State Park, Nevada (Doctoral dissertation, University of Nevada, Las Vegas).

Hippolyte, J.C., Angelier, J., Roure, F., and Casero, P. (1994). Piggyback basin development and thrust belt evolution: structural and palaeostress analyses of Plio-Quaternary basins in the Southern Apennines. *Journal of Structural Geology, 16(2)*: 159-173.

Hodges, K.V., Parrish, R.R., Housh, T.B., Lux, D.R., Burchfiel, B.C., Royden, L.H., Chen, Z. (1992). Simultaneous Miocene extension and shortening in the Himalayan orogen. *Science, 258*: 1466-1470.

Horton, B.K. (1998). Sediment accumulation on top of the Andean orogenic wedge: Oligocene to late Miocene basins of the Eastern Cordillera, southern Bolivia. *Geological Society of America Bulletin, 110(9)*: 1174-1192.

Hülscher, J., Sobel, E. R., Verwater, V., Groß, P., Chew, D., and Bernhardt, A. (2021). Detrital apatite geochemistry and thermochronology from the Oligocene/Miocene Alpine

foreland record the early exhumation of the Tauern Window. *Basin Research*, *33*(6), 3021-3044.

Hurford, A.J., and Green, P.F. (1982). A users' guide to fission track dating calibration. *Earth and Planetary Science Letters, 59*: 343–354.

Hurford, A.J. and Green, P.F. (1983). The zeta age calibration of fission-track dating. Chemical *Geology, 41*: 285-317.

Hurford, A.J., Fitch, F.J., and Clarke, A. (1984). Resolution of the age structure of the detrital zircon populations of two Lower Cretaceous sandstones from the Weald of England by fission track dating. *Geological Magazine, 121(4)*: 269-277.

Hurford, A.J. (1990). Standardization of fission track dating calibration: Recommendation by the Fission Track Working Group of the I.U.G.S. *Subcommission on Geochronology: Chemical Geology, 80:*171–178.

Hurford, A.J. (2019). An Historical Perspective on Fission-Track Thermochronology, *in* Malusà, M.G. and Fitzgerald, P.G. eds., *Fission-Track Thermochronology and its Application to Geology, Springer Berlin Heidelberg:* 3–23.

Jolivet, L., Daniel, J.M., Truffert, C. and Goffe, B. (1994). Exhumation of deepcrustal metamorphic rocks and crustalextension in arc and back-arc regions. *Lithos,33,* 3-30.

Jolivet, L., B. Goffé, P. Monié, C. Truffert-Luxey, M. Patriat, M., and M. Bonneau (1996). Miocene detachment in Crete and exhumation P–T–t paths of high-pressure metamorphic rocks, *Tectonics (15):* 1129–1153.

Jolivet, L., Faccenna, C., Goffé, B., Mattei, M., Rossetti, F., Brunet, C., Storti, F., Funiciello R., Cadet, J.P., D'agostino, N., and Parra, T. (1998). Midcrustal shear zones in postorogenic extension: example from the northern Tyrrhenian Sea. *Journal of Geophysical Research: Solid Earth*, *103(B6):* 12123-12160.

Jolivet, L., and Patriat, P. (1999). Ductile extension and the formation of the Aegean Sea, in *The Mediterranean Basins: Tertiary Extension Within the Alpine Orogene*, *Spec. Publ.*, edited

by B. Durand, A. Mascle, L. Jolivet, F. Horvàth, and M. Séranne, pp. 427–456, *Geological Society, London*.

Jolivet, L., Faccenna, C., Goffé, B., Burov, E., and Agard, P. (2003). Subduction tectonics and exhumation of high-pressure metamorphic rocks in the Mediterranean orogens. *American Journal of Science*, *303*(5), 353-409.

Jordan, T.E. (1981). Thrust loads and foreland basin evolution, Cretaceous, western United States. *AAPG bulletin*, *65(12):* 2506-2520.

Keller, J.V.A., Minelli, G., Pialli, G. (1994). Anatomy of a late orogenic extension: the Northern Apennines case. *Tectonophysics, 238*: 275-294, doi.org/10.1016/0040-1951(94)90060-4.

Ketcham, R. A., Donelick, R. A., and Donelick, M. B. (2000). AFTSolve: A program for multi-kinetic modeling of apatite fission-track data. *Geological Materials Research, 2(1)*: 1-32.

Ketcham, R.A. (2005). Forward and inverse modeling of low-temperature thermochronometry data. Rev. Mineral. *Geochem. 58*: 275–314. https://doi.org/10.2138/rmg.2005.58.11.

Ketcham, R.A., Carter, A., Donelick, R.A., Barbarand, J., Hurford, A.J. (2007). Improved modeling of fission-track annealing in apatite. *Am. Mineral. 92*: 799–810. https://doi.org/10.2138/am.2007.2281.

Ketcham, R.A., Donelick, R.A., Balestrieri, M.L., and Zattin, M. (2009). Reproducibility of apatite fission-track length data and thermal history reconstruction. *Earth and Planetary Science Letters, 284(3-4)*: 504-515.

Ketcham, R.A., Gautheron, C., Tassan-Got, L. (2011). Accounting for long alpha-particle stopping distances in (U-Th-Sm)/He geochronology: Refinement of the baseline case.

Kohn, B., Chung, L., and Gleadow, A., 2019, Fission-Track Analysis: Filed Collection, Sample Preparation and Data Acquisition, *in* Malusà, M.G. and Fitzgerald, P.G. eds.,

Fission-Track Thermochronology and its Application to Geology, Springer International Publishing, p. 25–48, doi:10.1007/978-3-319-89421-8_3

Lanari, R., Reitano, R., Faccenna, C., Agostinetti, N.P., and Ballato, P. (2023). Surface and crustal response to deep subduction dynamics: Insights from the Apennines, Italy. *Tectonics, 42*, e2022TC007461. https://doi.org/10.1029/2022TC007461.

Lavecchia, G., Minelli, G. and Pialli, G. (1984). L'Appennino umbra-marchigiano: tettonica distensiva ed ipotesi di sismogenesi. *Boll. Sot. Geol. Ital. 103*: 467-476.

Liotta, D., Ruggieri, G., Brogi, A., Fulignati, P., Dini, A., Cardini, I. (2010). Migration of geothermal fluids in extensional terrains: the ore deposits of the Boccheggiano-Montieri area (southern Tuscany, Italy). *International Journal of Earth Sciences, 99*: 623-644.

Lucchi, F.R. (1986). The Oligocene to Recent foreland basins of the northern Apennines. In Foreland basins (Vol. 8: 105-139). Blackwell Scientific Oxford.

Lucchi, F.R. (1990). Turbidites in foreland and on-thrust basins of the northern Apennines. *Palaeogeography, Palaeoclimatology, Palaeoecology, 77(1)*: 51-66.

Lucente, C.C., and Pini, G.A. (2008). Basin-wide mass-wasting complexes as markers of the Oligo-Miocene foredeep-accretionary wedge evolution in the northern Apennines, Italy. *Basin Research*, *20*(1), 49-71.

Malavieille, J. (1993). Late Orogenic extension in mountain belts: Insights from the basin and range and the Late Paleozoic Variscan Belt, *Tectonics, 12(5)*: 1115–1130, doi:10.1029/93TC01129.

Malinverno, A., and Ryan, W.B. (1986). Extension in the Tyrrhenian Sea and shortening in the Apennines as result of arc migration driven by sinking of the lithosphere. *Tectonics, 5(2)*: 227-245.

Malusà, M.G., Polino, R., Zattin, M., Bigazzi, G., Martin, S., and Piana, F. (2005). Miocene to Present differential exhumation in the Western Alps: Insights from fission track thermochronology. *Tectonics, 24(3)*.

Malusà, M.G., and Balestrieri, M.L. (2012). Burial and exhumation across the Alps–Apennines junction zone constrained by fission-track analysis on modern river sands. *Terra Nova, 24(3)*: 221-226.

Malusà, M.G., and Fitzgerald, P.G. (Eds.). (2019). Fission-track thermochronology and its application to geology. Switzerland: Springer International Publishing.

Malusà, M.G., and Fitzgerald, P.G. (2020). The geologic interpretation of the detrital thermochronology record within a stratigraphic framework, with examples from the European Alps, Taiwan and the Himalayas. *Earth-Science Reviews, 201*: 103074.

Mantovani, E., Viti, M., Babbucci, D., Tamburelli, C., Vannucchi, A., Falciani, F., and Cenni, N. (2014). Assetto tettonico e potenzialità sismogenetica dell'Appennino Tosco-Umbro-Marchigiano. Università di Siena: Siena, Italy.

Mantovani, E., Viti, M., Babbucci, D., Tamburelli, C., and Cenni, N. (2019). How and why the present tectonic setting in the Apennine belt has developed. *Journal of the Geological Society, 176(6)*: 1291-1302.

Marroni, M., Molli, G., Montanini, A., Ottria, G., Pandolfi, L., and Tribuzio, R. (2002). The External Ligurian units (Northern Apennine, Italy): from rifting to convergence of a fossil ocean-continent transition zone. *Ofioliti, 27(2)*: 119-131.

Martelli, L., Bonini, M., Calabrese, L., Corti, G., Ercolessi, G., Molinari, F.C., Calabrese, L., and Severi, P. (2017). Note illustrative della carta sismotettonica della Regione Emilia Romagna ed aree limitrofe. Carta sismotettonica della Regione Emilia-Romagna e aree limitrofe; Regione Emilia Romagna, Ed, 94.

Martin-Rojas, I., Alfaro, P., Galindo-Zaldivar, J., Borque-Arancón, M. J., García-Tortosa, F. J., de Sanz, G. C., Avilès, M., Sanchez-Alzola, A., Gonzales-Castillo, L., Ruano, P., Medina-Cascales, I., Tendero-Salmeròn, V., Madarieta-Txurruka, A., Pedrosa-Gonzalez, M.T., and Gil-Cruz, A.J. (2023). Insights of active extension within a collisional orogen from GNSS (Central Betic Cordillera, S Spain). *Tectonics*, e2022TC007723.

Martini, I.P., and Sagri, M. (1993). Tectono-sedimentary characteristics of Late Miocene-Quaternary extensional basins of the Northern Apennines, Italy. *Earth-Science Reviews, 34(3)*: 197-233.

Massoli, D., Koyi, H.A., and Barchi, M.R. (2006). Structural evolution of a fold and thrust belt generated by multiple décollements: analogue models and natural examples from the Northern Apennines (Italy). *Journal of Structural Geology, 28(2)*: 185-199.

McClay, K.R. (2012). *Thrust tectonics*. Springer Science & Business Media.

Mirabella, F., Brozzetti, F., Lupattelli, A., and Barchi, M.R. (2011). Tectonic evolution of a low-angle extensional fault system from restored cross-sections in the Northern Apennines (Italy). *Tectonics, 30(6).*

McDannell, K.T., Issler, D.R., and O'Sullivan, P.B. (2019). Radiation-enhanced fission track annealing revisited and consequences for apatite thermochronometry. *Geochimica et Cosmochimica Acta, 252*: 213–239, doi:10.1016/j.gca.2019.03.006.

Mitra, G. (1997). Evolution of salients in a fold-and-thrust belt: The effects of sedimentary basin geometry, strain distribution and critical taper. In Evolution of geological structures in micro-to macro-scales. *Springer, Dordrecht*: 59-90.

Molli, G. (2008). Northern Apennine–Corsica orogenic system: an updated overview. *Geological Society, London, Special Publications, 298(1)*: 413-442.

Molli, G., Cortecci, G., Vaselli, L., Ottria, G., Cortopassi, A., Dinelli, E., Mussi, M., and Barbieri, M. (2010). Fault zone structure and fluid–rock interaction of a high angle normal fault in Carrara marble (NW Tuscany, Italy). *Journal of Structural Geology*, *32*(9): 1334-1348.

Molli, G., Carlini, M., Vescovi, P., Artoni, A., Balsamo, F., Camurri, F., Clemenzi, L., Storti, F., Torelli, L. (2018). Neogene 3-D structural architecture of the north-west Apennines: The role of the low-angle normal faults and basement thrusts. *Tectonics, 37*: 2165-2196, https://doi.org/10.1029/2018TC005057.

Montone, P., Mariucci, M.T., and Pierdominici, S. (2012). The Italian present-day stress map. *Geophysical Journal International*, 189: 705-716, doi: 10.1111/j.1365-246X.2012.05391.x.

Morley, C.K., King, R., Hillis, R., Tingay, M., and Backe, G. (2011). Deepwater fold and thrust belt classification, tectonics, structure and hydrocarbon prospectivity: A review. *Earth-Science Reviews, 104 (1-3)*: 41-91.

Mutti, E., Tinterri, R., Benevelli, G., di Biase, D., and Cavanna, G. (2003). Deltaic, mixed and turbidite sedimentation of ancient foreland basins. *Marine and Petroleum Geology, 20(6-8)*: 733-755.

Nemcok, M., Stuart, C., Segall, M., Allen, R. B., Christensen, C., Hermeston, S. A., and Davison, I. (2005). Structural development of southern Morocco: Interaction of tectonics and deposition. *Petroleum System of Divergent Continental Margins Basins, 25.*

Nirta, G., Principi, G., and Vannucchi, P. (2007). The Ligurian units of Western Tuscany (Northern Apennines): insight on the influence of pre-existing weakness zones during ocean closure. *Geodinamica Acta, 20(1-2)*: 71-97.

Ori, G.G., and Friend, P.F. (1984). Sedimentary basins formed and carried piggyback on active thrust sheets. *Geology, 12(8)*: 475-478.

Ogata, K., Festa, A., Pini, G. A., Pogačnik, Ž.,and Lucente, C.C. (2019). Substrate deformation and incorporation in sedimentary mélanges (olistostromes): Examples from the northern Apennines (Italy) and northwestern Dinarides (Slovenia). *Gondwana Research*, *74*: 101-125.

Ottria, G. (2000). Polyphase thrusting in piggy-back deposits: the example of epi-Ligurian Succession (northern Apennines, Italy). Comptes Rendus de l'Académie des Sciences-Series IIA-*Earth and Planetary Science, 330(12)* : 845-852.

Panini, F., Bettelli, G., Pizziolo, M., Bonazzi, U., Capitani, M., Gasperi, G., Fioroni, C., and Fregni, P. (2002). Note illustrative alla Carta Geologica d'Italia a scala 1: 50.000. Foglio N. 237 "Sasso Marconi".

Papeschi, S., Vannucchi, P., Hirose, T., and Okazaki, K. (2022). Deformation and material transfer in a fossil subduction channel: Evidence from the Island of Elba (Italy). *Tectonics*, e2021TC007164.

Patacca, E., Sartoti, R., and Scandone, P. (1990). Tyrrhenian basin and Apenninic arcs: Kinematic relations since late tortonian time. *Mem. Soc. Geol. It. (45):* 425-451.

Patacca, E., Scandone, P., Di Luzio, E., Cavinato, G.P., and Parotto, M., (2008). Structural architectures of the Central Apennines: Interpretation of the CROP 11 seismic profile from the Adriatic coast to the orographic divide. *Tectonics, 27*: TC3006, doi:10.1029/2005TC001917.

Pauselli, C., Barchi, M.R., Federico, C., Magnani, M.B., and Minelli, G. (2006). The crustal structure of the Northern Apennines (Central Italy): an insight by the CROP03 seismic line. *American Journal of Science, 306(6)*: 428-450.

Peper, T., and de Boer, P.L. (1995). Intrabasinal thrust-tectonic versus climate control on rhythmicities in the Eocene South Pyrenean Tremp-Graus foreland basin: inferences from forward modelling. *Tectonophysics, 249(1-2)*: 93-107.

Petit, J.P. (1987). Criteria for the sense of movement on fault surfaces in brittle rocks. *Journal of Structural Geology, 9(5-6)*: 597-608.

Petracchini, L., Antonellini, M., Billi, A., and Scrocca, D. (2015). Syn-thrusting polygonal normal faults exposed in the hinge of the Cingoli anticline, northern Apennines, Italy. *Frontiers in Earth Science (3)*: 67.

Peyton, S.L., and Carrapa, B. (2013). An overview of low-temperature thermochronology in the Rocky Mountains and its application to petroleum system analysis.

Pialli, G., and Alvarez, W. (1995). Chapter B2 Tectonic setting of the miocene northern apennines: The problem of contemporaneous compression and extension. *In Developments in Palaeontology and Stratigraphy (15)*: 167-185.

Piazza, A., Artoni, A., and Ogata, K. (2016). The Epiligurian wedge-top succession in the Enza Valley (Northern Apennines): evidence of a syn-depositional transpressive system. *Swiss Journal of Geosciences, 109(1)*: 17-36.

Picotti, V., and Pazzaglia, F.J. (2008). A new active tectonic model for the construction of the Northern Apennines Mountain front near Bologna (Italy). *Journal of Geophysical Research: Solid Earth*, *113*(B8).

Picotti, V., Ponza, A., Pazzaglia, F.J. (2009). Topographic expression of active faults in the foothills of the Northern Apennines. *Tectonophysics, 474*: 285-294, doi:10.1016/j.tecto.2009.01.009

Pieri, M., and Groppi, G. (1981). Subsurface geological structure of the Po Plain, Italy

Pieri, M. (1983). 3.4 Detached Sediments: 3.4. 1 Decollement Tectonics (A-Subduction): Three Seismic Profiles Through the Po Plain.

Pizzi, A., and Scisciani, V. (2012). The May 2012 Emilia (Italy) earthquakes: preliminary interpretations on the seismogenic source and the origin of the coseismic ground effects. *Annals of Geophysics*, *55*(4).

Platt, J.P. (1986). Dynamics of orogenic wedges and the uplift of high-pressure metamorphic rocks. *Geological society of America bulletin, 97(9)*: 1037-1053.

Platt, J.P., Whitehouse, M.J., Kelley, S.P., Carter, A., Hollick, L. (2003). Simultaneous extensional exhumation across the Alboran Basin: implications for the causes of late orogenic extension. *Geology, 31*: 251–254.

Pondrelli, S., Salimbeni, S., Perfetti, P., Danecek, P. (2012). Quick regional centroid moment tensor solutions for the Emilia 2012 (northern Italy) seismic sequence. *Annals of Geophysics, 55 (4).*

Rahl, J.M., Ehlers, T.A., and van der Pluijm, B.A. (2007). Quantifying transient erosion of orogens with detrital thermochronology from syntectonic basin deposits. *Earth and Planetary Science Letters, 256(1-2)*: 147-161.

Reiners, P.W., Ehlers, T.A., eds. (2005). Low-Temperature Thermochronology: Techniques, Interpretations, Applications. *Reviews in Mineralogy and Geochemistry, 58*: 622. Chantilly, VA: Mineral. Soc. Am., Geochem. Soc.

Reiners, P.W., and Brandon, M.T. (2006). Using Thermochronology To Understand Orogenic Erosion. *Annual Review of Earth and Planetary Sciences, 34*: 419–466, doi:10.1146/annurev.earth.34.031405.125202.

Remitti, F., Vannucchi, P., Bettelli, G., Fantoni, L., Panini, F., and Vescovi, P. (2011). Tectonic and sedimentary evolution of the frontal part of an ancient subduction complex at the transition from accretion to erosion: The case of the Ligurian wedge of the northern Apennines, Italy. *Bulletin*, *123*(1-2): 51-70.

Ricci Lucchi, F. (1986). The Oligocene to Recent foreland basins of the northern Apennines. *Foreland basins:* 103-139.

Ricci Lucchi, F. (1987). Semi-allochthonous sedimentation in the Apenninic thrust belt. *Sedimentary Geology, 50(1)*: 119-134.

Rosenbaum, G., and Lister, G.S. (2004). Neogene and Quaternary rollback evolution of the Tyrrhenian Sea, the Apennines, and the Sicilian Maghrebides. *Tectonics (23).*

Rossetti, F., Aldega, L., Tecce, F., Balsamo, F., Billi, A., Brilli, M. (2011). Fluid flow within the damage zone of the Boccheggiano extensional fault (Larderello–Travale geothermal field, central Italy): structures, alteration and implications for hydrothermal mineralization in extensional settings. *Geological Magazine, 148 (4)*: 558-578.

Rovida, A., Locati, M., Camassi, R., Lolli, B., Gasperini, P. (2020). The Italian earthquake catalogue CPTI15. B. *Earthq. Eng., 18(7)*: 2953-2984, https://doi.org/10.1007/s10518-020-00818-y

Royden, L., Patacca, E., Scandone, P. (1987). Segmentation and configuration of subducted lithosphere in Italy: an important control on thrust belt and foredeep-basins evolution. *Geology, 15:* 714-717.

Royden, L.H. (1993). The tectonic expression slab pull at continental convergent boundaries. *Tectonics*, *12(2):* 303-325.

Royden, L.H. (1993). Evolution of retreating subduction boundaries formed during continental collision: *Tectonics*, 12 (3): 629–638, doi: 10.1029/92TC02641

Ruh, J.B. (2020). Numerical modeling of tectonic underplating in accretionary wedge systems. *Geosphere*, *16*(6): 1385-1407.

Salvini, F. (2002). Daisy 3, the Structural Data Integrated Analyser. Dipartimento di Scienze Geologiche, Università di "Roma Tre", Roma.

Scheiber, T., Fredin, O., Viola, G., Jarna, A., Gasser, D., and Łapińska-Viola, R. (2015). Manual extraction of bedrock lineaments from high-resolution LiDAR data: methodological bias and human perception. *Gff*, *137*(4): 362-372.

Scisciani, V., and Pizzi, A. (2012). The Seismogenic sources of the 2012 Emilia eartyhquakes (Northern Italy): Some preliminary results. *Tectonophysics, 243*: 37-55.

Scrocca, D., Carminati, E., Doglioni, C., and Marcantoni, D. (2007). Slab retreat and active shortening along the central-northern Apennines. *In Thrust belts and foreland basins. Springer, Berlin, Heidelberg*: 471-487.

Sempere, T. (2000). Discussion: Sediment accumulation on top of the Andean orogenic wedge: Oligocene to late Miocene basins of the Eastern Cordillera, southern Bolivia Discussion. *Geological Society of America Bulletin, 112(11)*: 1752-1755.

Shen, C.-C., Cheng, H., Edwards, R.L., Moran, S.B., Edmonds, H.N., Hoff, J.A., and Thomas, R.B. (2003). Measurement of attogram quantities of ^{231}Pa in dissolved and

particulate fractions of seawater by isotope dilution thermal ionization mass spectroscopy. *Anal. Chem., 75:* 1075–1079.

Shen, C.-C., Wu, C.-C., Cheng, H., Edwards, R.L., Hsieh, Y.-T., Gallet, S., Chang, C.-C., Li, T.-Y., Lam, D.D., Kano, A., Hori, M., and Spötl, C. (2012). High-precision and high-resolution carbonate ^{230}Th dating by MC-ICP-MS with SEM protocols. *Geochim. Cosmochim. Acta, 99*: 71–86.

Shreve, R. L., and Cloos, M. (1986). Dynamics of sediment subduction, melange formation, and prism accretion. *Journal of Geophysical Research: Solid Earth*, *91*(B10), 10229-10245.

Sinclair, H.D., and Allen, P.A. (1992). Vertical versus horizontal motions in the Alpine orogenic wedge: stratigraphic response in the foreland basin. *Basin Research*, *4*(3-4): 215-232.

Smeraglia, L., Berra, F., Billi, A., Boschi, C., Carminati, E., Doglioni, C. (2016). Origin and role of fluids involved in the seismic cycle of extensional faults in carbonate rocks. *Earth Planet. Sc. Lett. 450*: 292–305, http://dx.doi.org/10.1016/j.epsl.2016.06.042.

Sobel, E. R., and Seward, D. (2010). Influence of etching conditions on apatite fission-track etch pit diameter. *Chemical Geology, 271(1-2)*: 59-69.

Spotila, J.A. (2005). Applications of low-temperature thermochronometry to quantification of recent exhumation in mountain belts. *Reviews in Mineralogy and Geochemistry, 58(1)*: 449-466.

Stendardi, F., Viola, G., and Vignaroli, G. (2023). Multiscale structural analysis of an Epiligurian wedge-top basin: insights into the syn-to post-orogenic evolution of the Northern Apennines accretionary wedge (Italy). *International Journal of Earth Sciences*, 1-23.

Suppe, J. (1983). Geometry and kinematics of fault-bend folding. *American Journal of Science, 283(7)*: 684–721.

Suppe, J., and Connors, C. (1992). Critical taper wedge mechanics of fold-and-thrust belts on Venus: Initial results from Magellan. *Journal of Geophysical Research: Planets*, *97*(E8): 13545-13561.

Tagami, T., and O′ Sullivan, P., (2005). Fundamentals of Fission-Track Thermochronology. *Reviews in Mineralogy and Geochemistry*, *58*: 19–47, doi:10.2138/rmg.2005.58.2

Tavani, S., Storti, F., Lacombe, O., Corradetti, A., Muñoz, J.A., and Mazzoli, S. (2015). A review of deformation pattern templates in foreland basin systems and fold-and-thrust belts: Implications for the state of stress in the frontal regions of thrust wedges. *Earth-Science Reviews, 141*: 82-104.

ter Voorde, M., de Bruijne, C.H., Cloething, S.A.P.L., Andriessen, P.A.M. (2004). Thermal consequences of thrust faulting: simultaneous versus successive fault activation and exhumation. *Earth and Planetary Science Letters, 223*: 395-413, doi:10.1016/j.epsl.2004.04.026.

Thomson, S.N., Brandon, M.T., Reiners, P.W., Zattin, M., Isaacson, P.J., and Balestrieri, M.L. (2010). Thermochronologic evidence for orogen-parallel variability in wedge kinematics during extending convergent orogenesis of the northern Apennines, Italy. *Bulletin, 122(7-8):* 1160-1179.

Tinterri, R., and Muzzi Magalhaes, P. (2011). Synsedimentary structural control on foredeep turbidites: An example from Miocene Marnoso-arenacea Formation, Northern Apennines, Italy. *Marine and Petroleum Geology, 28*: 629-657 https://doi.org/10.1016/j.marpetgeo.2010.07.007.

Toscani, G., Seno, S., Fantoni, R., Rogledi, S. (2006). Geometry and timing of deformation inside a structural arc: the case of the western Emilian folds (Northern Apennine front, Italy). *Bollettino della Società Geologica Italiana, 125*: 59–65.

Turcotte, D. L., and Schubert, G. (2002). *Geodynamics*. Cambridge university pressTwiss, R.J., and Moores, E.M. (1992). Structural geology. Macmillan

Vai, G.B., and Martini, P. (2001). Anatomy of an orogen: the Apennines and adjacent Mediterranean basins. Springer Science & Business Media.

Vannucchi, P., Remitti, F., and Bettelli, G. (2012). Lateral variability of the erosive plate boundary in the Northern Apennines, Italy. *Italian Journal of Geosciences, 131(2)*: 215-227.

Ventura, B., Pini, G.A., and Zuffa, G.G. (2001). Thermal history and exhumation of the Northern Apennines (Italy): evidence from combined apatite fission track and vitrinite reflectance data from foreland basin sediments. *Basin Research, 13(4):* 435-448.

Vera, E.R., Mescua, J., Folguera, A., Becker, T.P., Sagripanti, L., Fennell, L., Orts, D., and Ramos, V.A. (2015). Evolution of the Chos Malal and Agrio fold and thrust belts, Andes of Neuquén: Insights from structural analysis and apatite fission track dating. *Journal of South American Earth Sciences, 64*: 418-433.

Vermeesch, P. (2009). RadialPlotter: A Java application for fission track, luminescence and other radial plots. *Radiation Measurements, 44(4)*: 409-410.

Vermeesch, P., and Tian, Y. (2014). Thermal history modelling: HeFTy vs. QTQt. *Earth-Science Reviews, 139*: 279-290.

Vignaroli, G., Minelli, L., Rossetti, F., Balestrieri, M.L., and Faccenna, C. (2012). Miocene thrusting in the eastern Sila Massif: Implication for the evolution of the Calabria-Peloritani orogenic wedge (southern Italy). *Tectonophysics, 538*: 105-119.

Vignaroli, G., Pinton, A., De Benedetti, A.A., Giordano, G., Rossetti, F., Soligo, M., Berardi, G. (2013). Structural compartmentalisation of a geothermal system, the Torre Alfina field (central Italy). *Tectonophysics, 608*: 482-498, http://dx.doi.org/10.1016/j.tecto.2013.08.040

Viola, G., Mancktelow, N.S., and Seward, D. (2001). Late Oligocene-Neogene evolution of Europe-Adria collision: New structural and geochronological evidence from the Giudicarie fault system (Italian Eastern Alps). *Tectonics, 20(6)*: 999-1020.

Viola, G., Mancktelow, N. S., Seward, D., Meier, A., and Martin, S. (2003). The Pejo fault system: an example of multiple tectonic activity in the Italian Eastern Alps. *Geological Society of America Bulletin, 115(5)*: 515-532. https://doi.org/10.1130/0016-7606(2003)115%3C0515:TPFSAE%3E2.0.CO;2

Viola, G., Torgersen, E., Mazzarini, F., Musumeci, G., van der Lelij, R., Schönenberger, J., and Garofalo, P.S. (2018). New constraints on the evolution of the inner Northern Apennines by K-Ar dating of Late Miocene-Early Pliocene compression on the Island of Elba, Italy. *Tectonics, 37*: 3229-3243, https://doi.org/10.1029/2018TC00518.

Vissers, R.L.M., Platt, J.P., van der Wal, D. (1995). Late orogenic extension of the Betic Cordillera and the Alboran Domain: A lithospheric view. *Tectonics 14:* 786–803.

Wedepohl, K.H. (1995). The composition of the continental crust. *Geochimica et Cosmochimica Acta, 59*: 1217–1239.

Weltje, G. (1992). Oligocene to Early Miocene sedimentation and tectonics in the southern part of the Calabrian-Peloritan Arc (Aspromonte, southern Italy): a record of mixed-mode piggy-back basin evolution. *Basin Research, 4(1)*: 37-68.

Willett, S.D. (1992). Dynamic and kinematic growth and change of a Coulomb wedge, in McClay, K.R., ed., *Thrust Tectonics*: London, Chapman and Hall: 19-31.

Woodward, N.B. (1987). Geological applicability of critical wedge thrust-belt models. *Geological Society of America Bulletin, 99*: 827-832.

Wortel, M.J.R., and Spakman, W. (2000). Subduction and slab detachment in the Mediterranean-Carpathian region. *Science, 290:* 1910-1917.

Zattin, M., Landuzzi, A., Picotti, V., and Zuffa G.G. (2000). Discriminating between tectonic and sedimentary burial in a foredeep succession, Northern Apennines. *Journal of the Geological Society, 157(3):* 629-633.

Zattin, M., Picotti, V., and Zuffa, G.G. (2002). Fission-track reconstruction of the front of the Northern Apennine thrust wedge and overlying Ligurian unit. *American Journal of Science, 302(4)*: 346-379.

Zattin, M., and Zuffa, G.G. (2004). Unravelling the source rocks of Late Eocene-Miocene orogenic wedge and foredeep arenites of the northern Apennines and southern Alps. *Bollettino della Società Geologica Italiana, 123(1)*: 67-76.

Zoetemeijer, R., Cloetingh, S., Sassi, W., and Roure, F. (1993). Modelling of piggyback-basin stratigraphy: record of tectonic evolution. *Tectonophysics, 226(1-4)*: 253-269.

APPENDIX I

(Chapters 4 and 5)

Analytical methods

In this Appendix, the fundamental of the methods applied for the geochronological and thermochronological reconstruction are briefly described. In particular, I report: i) low-temperature detrital thermochronology applied on apatite grains and including (U-Th)/He and fission-track (AFT) analyses **(Fig.I.1)** and ii) U-Th dating applied on calcite veins.

I.1 Principle of thermochronometry

Low-temperature thermochronology has the aim to reconstruct the cooling/exhumation history of rocks during time considering the main tectonic evolution of the study area. The methods described comprise a brief explanation of the principles of thermochronometry, sampling techniques, sample processing and analytical procedure while the interpretation of the data is described in the Supplementary Materials.

Thermochronometry is a quantitative study of the thermal history of rocks using temperature-sensitive radiometric dating methods based on the comparison between the abundance of radioactive isotopes in nature and its decay product. The ages obtained are based on the ratio of parent and daughter isotopes.

With the term "thermochronometer" we define an isotopic system consisting in: a) radioactive parent; b) radiogenic daughter; c) the mineral in which they are found (Reiners et al., 2005). Each isotopic system is characterised by a particular thermal sensitivity and closure temperature (Tc) which is defined as the temperature of the isotopic system at the time of its cooling age, with the assumption of a steady monotonic

cooling history. In particular, the closure thermochronometer occurs in a range of temperature that varies from 0% (maximum temperature) to 100% (minimum temperature).

This temperature interval is known as Partial Annealing Zone (PAZ) for the fission-tracks dating and Partial Retention Zone (PRZ) for the (U-Th)/He dating. These intervals are related to many factors including chemical composition and morphology of the analysed grain, hold time and cooling rate (Peyton and Carrapa, 2013). The thermochronometric age given by a particular thermochronometer represents the latest time of cooling of a sample above the Tc (or above the top of the PAZ/PRZ). Conversely, when sample is heated under the Tc (or under the base of the PAZ/PRZ) the system re-opens and the previous thermochronometric age is obliterated; this process is called reset of the sample.

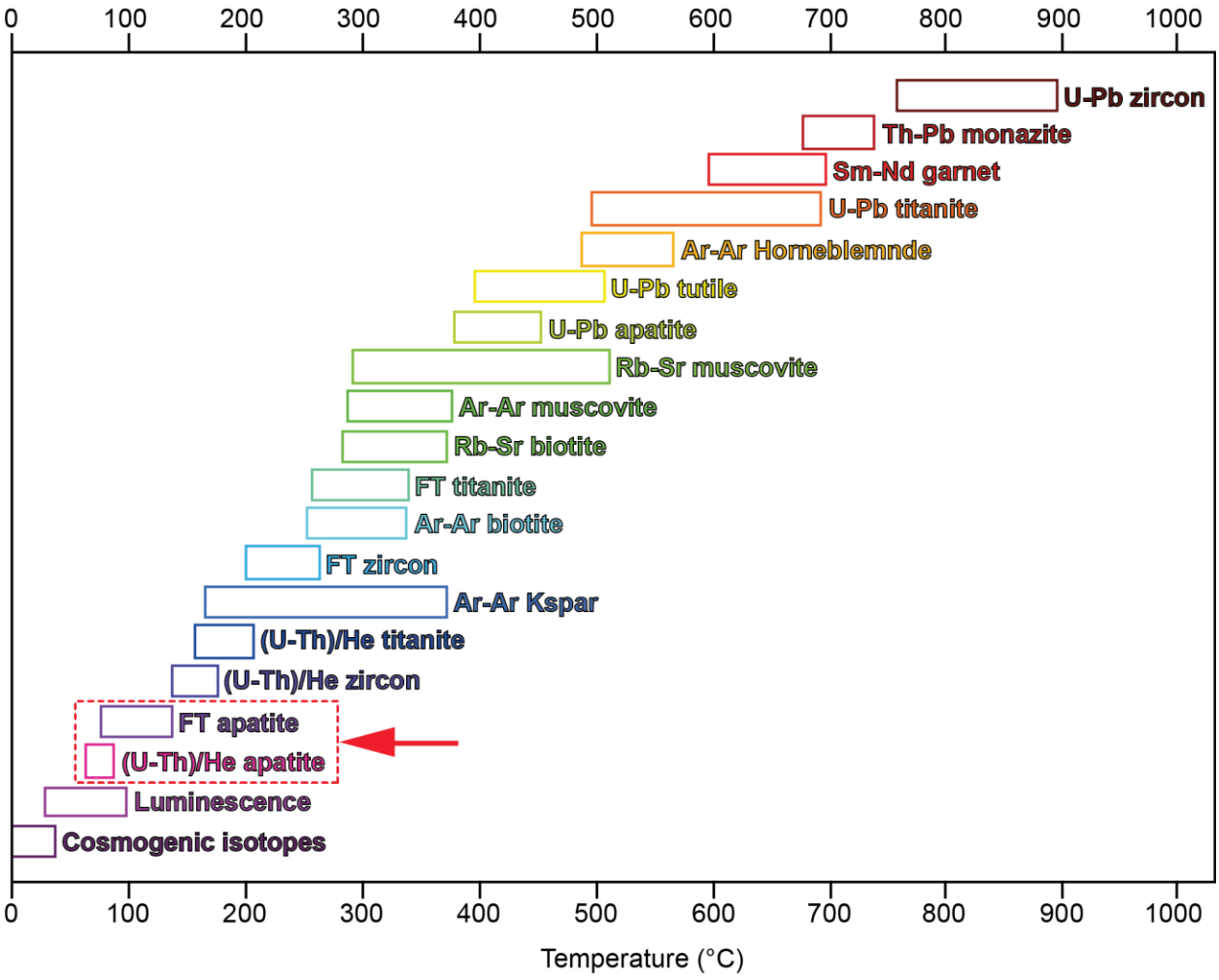

Figure I.1- Closure temperatures of different thermochronometers and geochronometers (modified from P. Fitzgerald, S. Baldwin, G. Gehrels, P. Reiners, and M. Ducea).

A vast array of thermochronometers is known nowadays. The ones I used in this work of thesis are sensitive to low-temperature (Fig.I.1, red-dashed rectangle), typically between 40°C and 120°C and are typically used to investigate the thermal evolution of tectonic-stratigraphic units within the upper part of the Earth's crust (< 5 km).

I.1.1 Fission-track thermochronology

Fission-tracks dating method is based on the decay of an unstable parent to a stable daughter atom and, as in the other isotopic methods, the age is function of the proportion between the abundance of the new stable isotope (^{235}U) and the parent unstable atom (^{238}U). More specifically, concerning this method, the decay product is not an isotope, but a trail of physical damage of the crystal lattice resulting from the spontaneous decay of parent nucleus that, after irradiation with low-energy neutron induce the formation of a second generation of induced tracks which are revealed and counted in the apatite itself or, more usually, in a detector held against the mineral. The number of spontaneous tracks depends on the amount of uranium in the apatite grains, which is determined by irradiation with low-energy neutrons (e.g., Malusà and Fitgerald, 2019).

In particular, during the spontaneous decay of the unstable nucleus, it splits into two positively charged nuclear fragments, which are pushed away from each other by Coulomb repulsion forces. Then, the energy released by the nuclear fission travel through the crystal affecting the electrostatic charge of the region they crossed by nuclear fragments. Electrons are ripped off from the atoms of the lattice and the ionized particles dislocated with respect to their original positions due to repulsive forces. Consequently, the stressed region relaxed elastically, straining the undamaged matrix ("Ion Explosion Spike" model for fission-track formation by Fleischer et al., (1975); **Fig. I.2**).

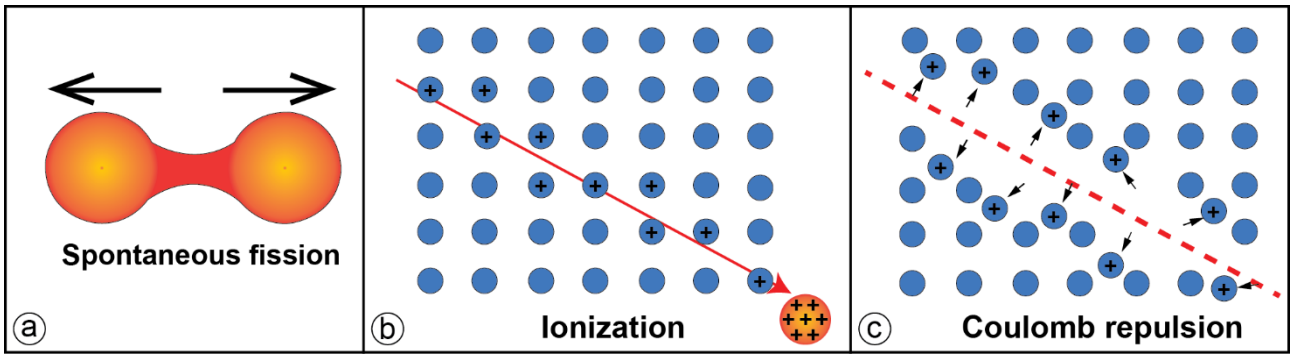

Figure I.2- The "Ion Explosion Spike" model for FT formation: a) Heavy nucleus splits in two nuclear fragments; b) the two positively charged fragments are pushed away from each other and along their tracks they tear off electrons from the atoms of the lattice; c) the positively charged atoms along the track dislocate from their lattice position due to repulsive electrostatic forces (redrawn after Fleischer et al., 1975).

The length of the new fission-tracks is specific for the mineral involved; in particular, for the apatite grains, fission-tracks have an initial width of ~10 nm and a length of ~16 μm (Reiners and Brandon, 2006). The determination of fission-tracks age is made using the same general equation of any radioactive decay scheme, modified considering that ^{238}U decays not only by spontaneous fission but also by α-decay (Tagami and O' Sullivan, 2005).

The technique can be applied to minerals which contain sufficient U (typically>10 ppm) to generate a statistically constraining quantity of fission-tracks over geological time. In this work of thesis apatite was the only mineral used of the dating, and the following equation is specific for this thermochronometer:

$$N_s = \lambda_f / \lambda_\alpha \, ^{238}N \, (e^{\lambda \alpha t} - 1)$$

where:

N_s = number of spontaneous fission-tracks per unit volume;

λ_f = spontaneous fission decay constant ($8.5 * 10^{-17}$ yr-1);

λ_α = α- decay constant ($1.5 * 10^{-10}$ yr-1);

^{238}N= number of ^{238}U atoms per unit volume;

t = time

The most common technique used with the aim to infer AFT single grain ages is the External Detector Method (EDM) (the main stages are indicated in **Fig. I.3**).

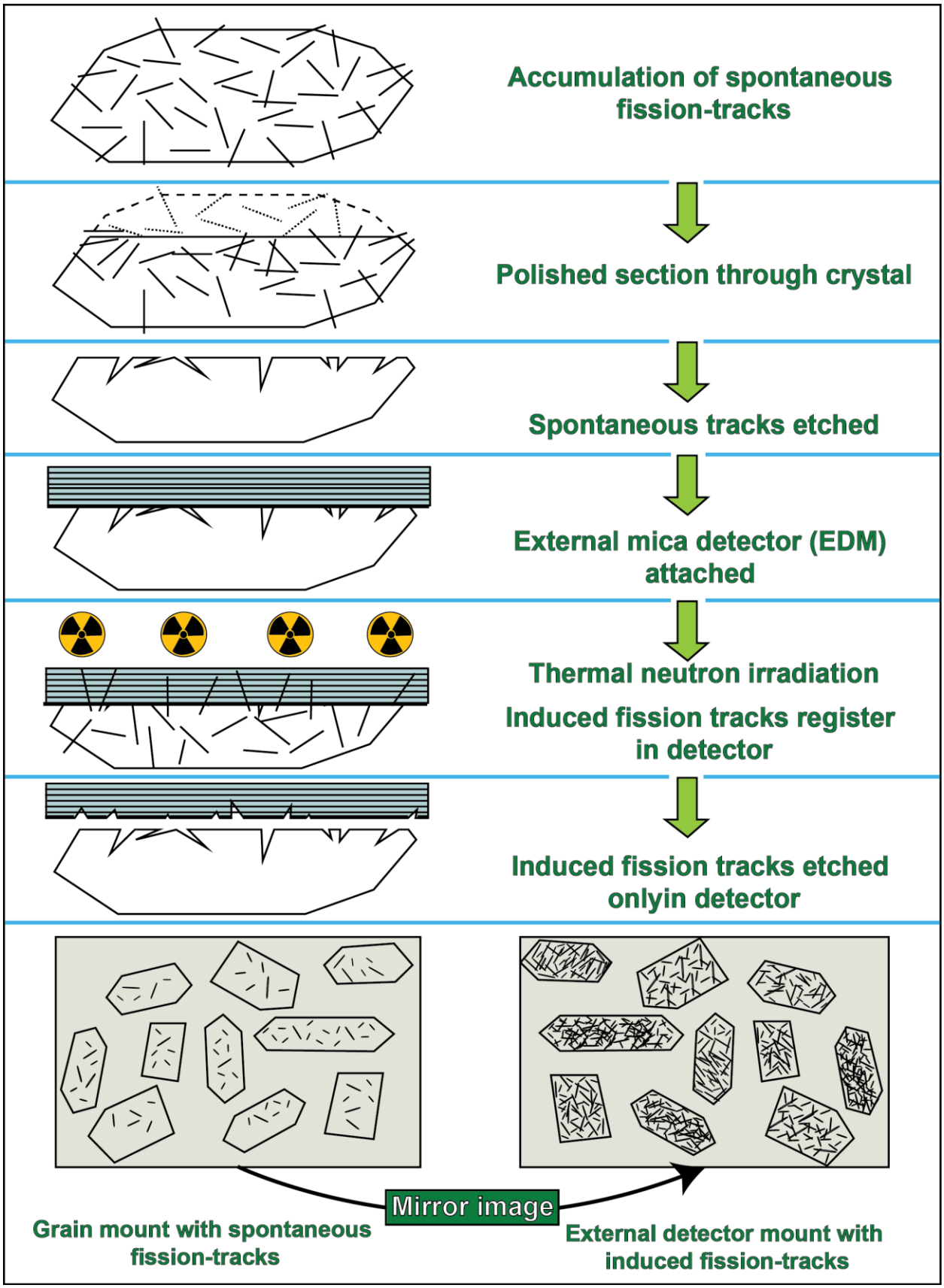

Figure I.3- Schematic procedure for AFT analysis with the ED method (modified and redrawn after Gallagher et al., 1998).

A detailed description about the method procedure is reported in previous published works (Gleadow and Duddy, 1981; Hurford and Green, 1982; 1983; Green et al., 1985; Gleadow et al., 1986; Hurford, 1990; Donelick et al., 2005; Peyton and Carrapa, 2013).

After sampling, samples have been crushed, sieved and then the apatire grains were separated using hydrodynamic, magnetic and heavy liquid density procedures (details about sample preparation are reported in the next paragraph).

Then the mineral grains are mounted in epoxy resin, polished and chemically etched. By doing so, latent fission-tracks are revealed and can be counted under an optical microscope, thus determining the spontaneous tracks density of the single mineral grain.

In order to determine the ^{238}U initial concentration a sheet of U-free mica is placed over the polished mount, then the mount-mica package is sent for neutron irradiation in a nuclear reactor. The mica records the fission tracks produced by the ^{235}U decay and, when properly etched, provides the number of induced fission tracks (N_i).

The spontaneous and induced track densities are counted with an optical microscope implemented with a sliding table and a dedicated software. Then knowing the natural $^{235}U/^{238}U$ ratio, the initial ^{238}U content can be determined. The equation used to date the single apatite grains is:

$$\mathbf{t_i = 1/\lambda_D \ln (1+ \lambda_D \zeta g \varrho_d \varrho_{s,i} / \varrho_{i,i})}$$

where:

t_i = fission track age of the grain i;

λ_D = total decay constant of ^{238}U;

ζ= calibration factor, different for each counting operator (Hurford and Green, 1982, 1983);

g = geometry factor for spontaneous fission tracks registration;

ϱ_d = induced fission track density for an uranium standard corresponding to the sample position during neutron irradiation;

$\varrho_{s,i}$ = spontaneous track density for grain i;

$\varrho_{i,i}$ = induced track density for grain i.

Visible tracks considered for track-length investigations can be divided into two groups. The first one is given by the tracks which directly intersect the crystal surface and which are also for age determinations (TINT = Tracks IN Tracks); the second one represented the confined tracks localized in the interior of the crystal and can be revealed by the etchant only if they intersect another track, a cleavage or a fracture that emerge at the crystal surface (TINCLE= Tracks IN CLEavage) **(Fig.I.4)**.

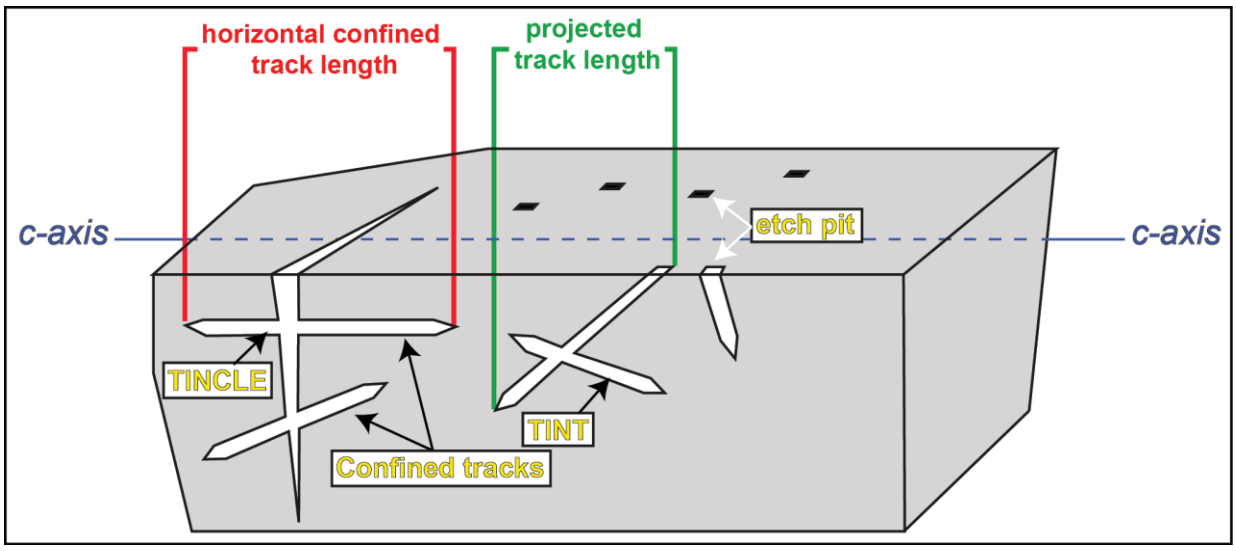

Figure I.4- Schematic illustration for the revelation of fission-tracks by chemical etching. It includes tracks-in-tracks (TINTs) and tracks-in-cleavage (TINCLEa) (redrawn after Hurford, 2019).

I.1.2 Fission-track annealing

Fission-tracks annealing models have thus been developed using a completely empirical approach, looking at what form of the annealing relationship best fit the data statistically (Braun et al., 2006). Fission-tracks are characterised by a semi-stable nature: all newly formed tracks in apatite have a length of ~ 16 μm but they significantly shorten when heated within the PAZ. FT annealing behaviour is independent on grain size, but it is demonstrated its variation with: a) apatite chemistry; b) retention increasing with increasing Cl/(F+Cl) ratio. The annealing behaviour also depends on the crystallographic orientation of the tracks, with higher annealing rate for tracks orthogonal than tracks parallel to the c-axis of the crystal (Green et al., 1986; Donelick et al., 1999; Ketcham et al., 2007). The Dpar, i.e., the mean width of fission-track etch pits, is a commonly used proxy for track retentivity of single crystals, first proposed by Ketcham et al. (1999). The effects of annealing can be quantified by measuring the lengths of horizontal confined tracks (Gleadow et al., 1986). This depends on the fact that tracks form continuously, and thus each track experiences a different portion of the integrated thermal history (Braun et al., 2006). Therefore, the tracks length distribution obtained by measuring a sufficient number of horizontal confined tracks (usually at least 50) contains information on the thermal history experienced by the sample (Braun et al., 2006; **Fig. I.5**).

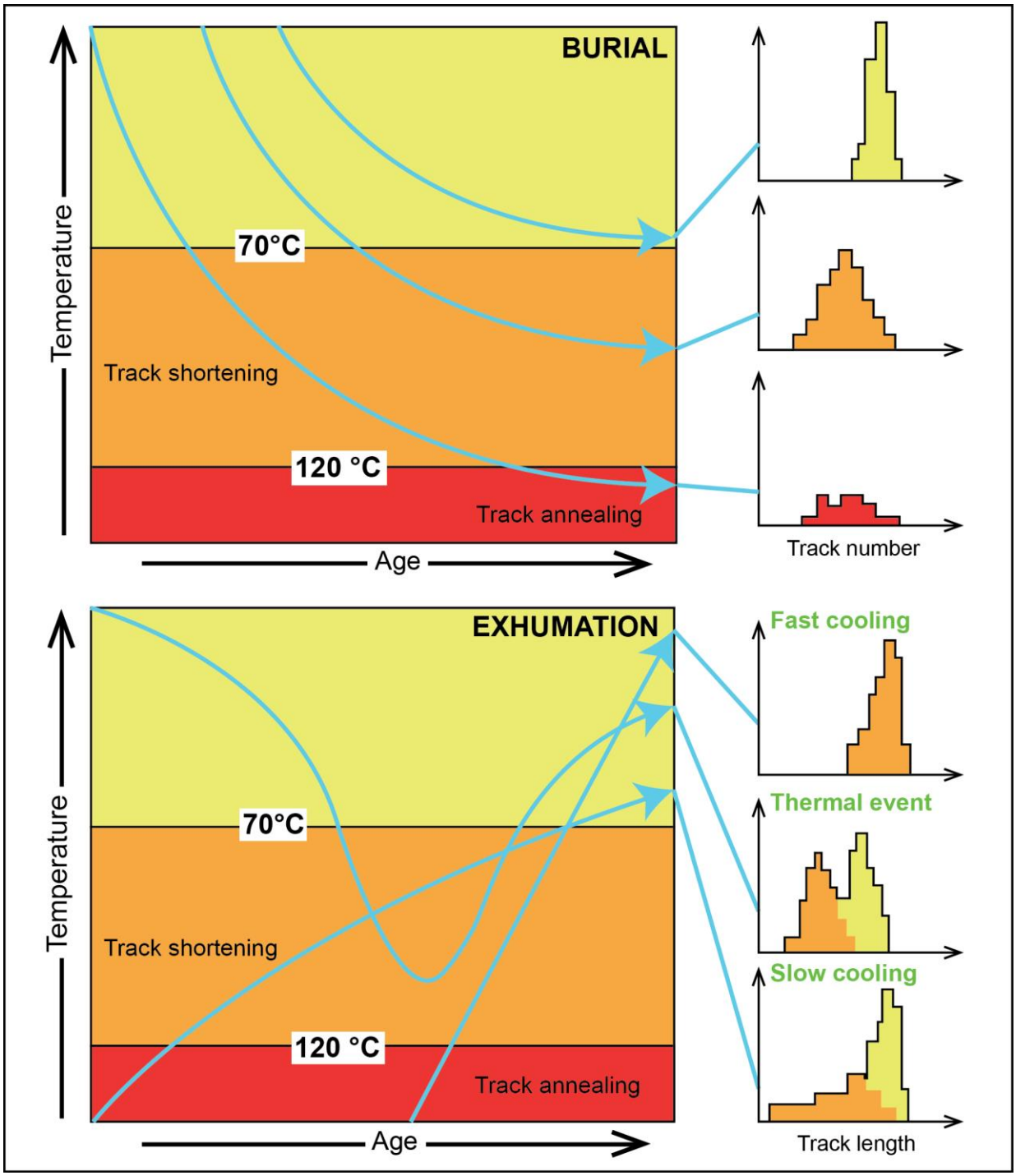

Figure I.5- Correlation of thermal history and track length distribution (redrawn after Gleadow et al., 1983).

The lower and upper temperature limits of AFT PAZ are usually comprised between 60 and 120°C (that are found between ~2 and 4 km below Earth's surface, assuming a 30 °C/km geothermal gradient), but can be significantly different depending on cooling rate and apatite chemistry. AFT closure temperatures generally vary between ca. 80 and 120°C but are largely affected by apatite composition; an apatite grain of "average" composition (Ketcham et al., 1999) has Tc=116 °C for cooling rates of 10 °C/Ma.

I.1.3 Fission-track data analysis

AFT thermochronometric age is achieved measuring the number of spontaneous and induced tracks, the relative areas and the mean Dpar for usually 20-30 apatite grains from the same rock sample. Measured data were put into the Trackkey software (Dunkl, 2000), which calculates the central age, tests the homogeneity of age populations, and generates radial plots for every analysed sample. The Y axis of a radial plot represents the standard error ((ag-ac)/ σ) of the single grain age (ag) with respect to the central age of the whole population (ac) and the X axis represents the relative error (1/σ) decreasing toward the radial scale **(Fig. I.6)**.

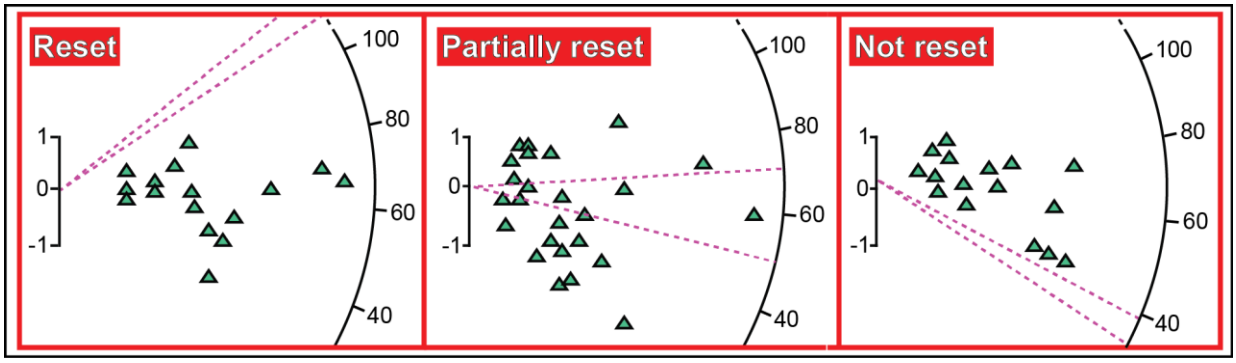

Figure I.6- 3 examples of radial plots referred to the apatite fission-tracks resetting stages (modified and redrawn after Andreucci, 2013).

Single grain ages are read on the intercept with the radial axis (plotted on logarithmic scale) of the line drawn through the single grain point at the origin. The χ^2 statistical test (Galbraith, 1981) is used to define the probability that all the grains counted belong to a single population of ages. A probability of less than 5% is the evidence of an asymmetric spread of grain ages, indicating the presence of different populations due to the inheritance from mixed detrital source areas (as in the case analysed in this thesis), or differential annealing in grains with different compositions (Green et al., 1989). If the sample pass the χ^2 (probability > 5%) the central age, which consist in a weighted mean on the single grain ages, represents the AFT age of the sample, which can be modelled.

Moreover, the thermal modelling is also constrained by the measuring of confined fission-tracks. These latter have to be possibly more than 50 in order to have enough statistical confidence. In suitable samples confined track lengths are measured, if possible, along their orientation with respect to the C-axis and mean Dpar (more information about the thermal modelling process in provide in paragraph I.3).

I.1.4 (U-Th)/He thermochronology

(U-Th)/He dating is based on the production of He nuclei (α particles) consequently the U and Th decay series and, to a minor extent, Sm. The equation which explains the He ingrowth through time in apatite grains is:

$$^{4}He = 8\ ^{238}U\ (e^{\lambda 238t} - 1) + 7\ ^{235}U\ (e^{\lambda 235t} - 1) + ^{232}UTh\ (e^{\lambda 232t} - 1)$$

where:

λ= decay constant ($\lambda_{238} = 1.551*10^{-10}\ yr^{-1}$; $\lambda_{235} = 9.849*10^{-10}\ yr^{-1}$; $\lambda_{232} = 4.948*10^{-11}\ yr^{-1}$);

U,Th and He are the number of atoms of each isotope;

t = (U-Th)/He age

In particular, He thermochronology relies on the accumulation of ^{4}He during the α disintegration of ^{238}U, ^{232}Th and their daughter products. The He ingrowth equation assumes the absence of ^{4}He both initial and produced by external sources. However, low content of U-Th is typically yielded by apatites and for such mineral phases the presence of external sources of He can be represented by U-Th rich inclusions or coating. In this case a most careful selection of grains for the analysis is required. Below the closure temperature in crystalline apatite and zircon, ~70°C and 180°C respectively, He is largely retained in the crystal and calculated apatite and zircon He ages will record the cooling age of samples. Above this closure temperature, He escapes from crystal through diffusion and the calculated age will be zero (e.g., Peyton and Carrapa, 2013). In general, He ages are typically younger with respect to the ones obtained with the FT method, because the closure temperature and the PRZ range are lower (i.e., shallower in the upper crust).

I.1.5 Diffusion behaviour

The He diffusivity in apatite grains is affected by several factors: i) grains size; ii) composition; iii) crystallographic features; iv) vacancy damage; v) radiation damage; vi) strain-induced dislocation traps (e.g., Farley, 2002; Ehlers and Farley, 2003).

Many factors, such as the size of a crystal, may affect how much He is lost to diffusion, with larger crystals which lose proportionally less He then the smaller ones. When cooling through the PRZ has been slow enough for the occurrence of He diffusion, larger apatite crystals will record older He then the smaller apatite grains belonging to the same samples. Moreover, radiation damage may have significant effects on He diffusion and it is caused by the recoil of a parent nuclide (U or Th) as it decays by ejecting an α particle.

In apatites, these radiation-induced damages in the crystal lattice have an effect on the diffusion parameters which are impeded in He. These damage sites may form traps for He and result in a range of AHe ages from the same sample that are proportional to the effective U concentration of the apatite crystals, defined as eU = [U] + 0.235[Th]. Apatites with higher eU will accumulate more damage traps and so will develop a higher closure temperature that apatites with lower eU, that accumulate fewer damage traps (Peyton and Carrapa, 2013 and refs. therein). The effect of radiation damage on He diffusivity is quite large, corresponding to a variation of up to tens of degrees in Tc, across the range of typical apatite eU. Radiation damages evolve as a function of time, temperature and eU concentration (Flowers et al., 2009; Gautheron et al., 2009; McDannell et al., 2019).

I.1.6 (U-Th)/He data analysis

Usually, three to five grains from the same sample (called replicates) are used for the analysis and comparing each single grain ages of replicates gives useful information about the thermal history of the sample. The first stage necessary is to check the age reproducibility, in particular; if the age dispersion is low and the single grain ages cluster strictly the weighted mean of ages can be used for assumed a "classical" thermal interpretation; if the age dispersion is high, it means the presence of more complex thermal history (i.e., slow cooling and long permanence within the PRZ. The extent of the impact of factors which control He diffusion (such as zonation, crystal size, kinetic parameters) increases as the cooling rate decreases (Ehlers and Farley, 2003). The correlation between grain age and crystal size (radius) is particularly evident under slow cooling, since crystal size affects both α ejection and He diffusion kinetics; in this case, age dispersion adds additional information about the evolution of the samples and can be used to model the thermal history.

I.2 Sample processing and analytical procedures

In order to perform low-temperature thermochronological analyses 2 kg for each sample have been collected. In this study, rocks are constituted by medium to course-grained polygenic sandstones and calcarenites. Apatite grains had to be separated through different stages performed at the Laboratory of Sedimentary Petrography of the University of Bologna (Italy). All the passages necessary for the rock separation have been

sketched in the figure below **(Fig. I.7)** and they will be deeply explained in the next paragraphs.

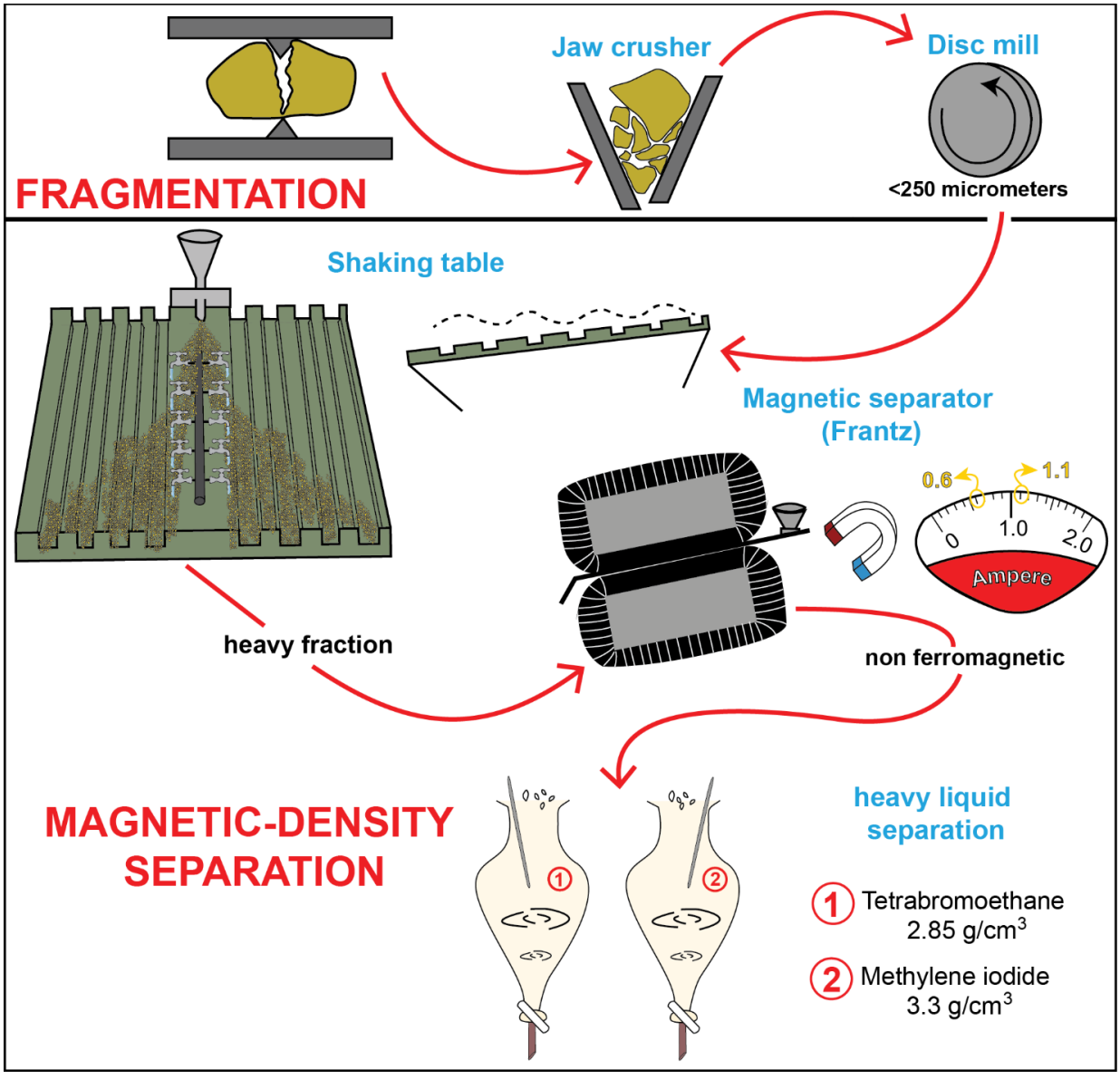

Figure I.7- Flow chart illustrating different steps for the preparation of apatite grains for thermochronological (AFT and AHe) analysis (modified and redrawn after Kohn et al., 2019).

I.2.1 Sample preparation

First of all, the 1.5 kg of rock have been chrushed using a jaw crusher first and a roller mill successively. Then, the crushed samples were sieved with the aim to obtain a rock powder of <250 μm grain size. During the second phase heavy and light minerals were separated from the <250 μm powder through hydrodynamic separation, using a Wilfley water table. The heavy minerals fraction was then passed in the magnetic separator to eliminate ferromagnetic minerals and maintain only diamagnetic ones. Then, the diamagnetic fraction was further separated with two heavy liquids density methods under a fume hood, involving Tetrabromoethane and Methylene Iodide, which have the function of separating the apatite grains from other minerals.

Separated apatites have been seen in both reflected and transmitted light microscopy, aiming to the selection of the best grains in terms of size, shape and quantity.

I.2.1.1 AFT analysis

Then, apatites have been mounted in epoxy resin (10:3 proportion), making one mount for each sample. Every mount was first hand-ground using 800 and 1200 μm alumina powders and then polished with two different grain-size of diamond crystals (6 to 1 μm respectively), in order to expose grain surfaces. Each lapping cycle consisted in 5 min at 250 r.p.m in a Buhler machine.

Polished mounts have been etched in nitric acid (HNO3 5M) for 20 seconds. Etched mounts were then cut into thin (~1.3/1.4 mm thick) discs and again lapped to obtain little

squares of about 1.2 cm2. In the end, a square of U free muscovite mica sheet was attached to every mount containing the apatites etched, and all the so constructed packages were put into appropriate holders **(Fig.I.8)**, together with dosimeters (standard glass CN-5) which have the function of controlling the neutron fluence during irradiation.

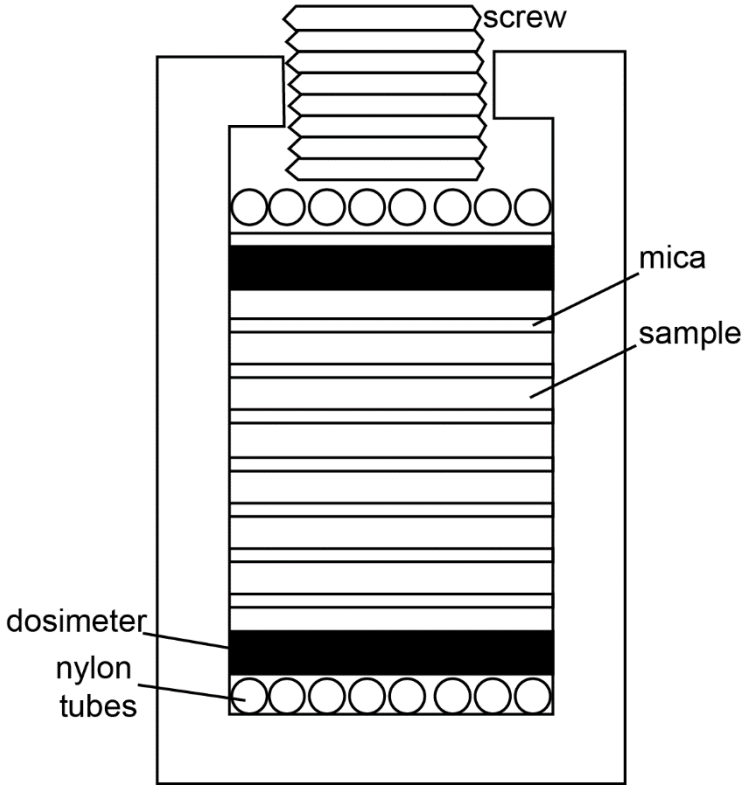

Figure I.8- Representation of a holder used for irradiation and position of mounts, micas and dosimeters.

These holders were then sent to the nuclear reactor at Radiation Center of Oregon State University, where mounts were irradiated with a nominal neutron fluence of 9 *1015 n/cm2. After irradiation, induced fission tracks in the U-free muscovite sheets that covered apatite grain mounts were etched in 40% HF at 20 °C for one hour.

As said before, AFT ages have been calculated using the EDM and the zeta-calibration methods (Hurford and Green, 1983). Neutron fluences is measured counting neutron-

induced tracks in the Corning glass dosimeter CN-5 (U concentration: 2-17±0.62 ppm; ^{235}U atom %: 0.720). Age standard used is Durango apatites (IUGS age standards) and the mean value obtained for the zeta-factor is 342.61±10.74. According to the EDM the spontaneous ϱs and the induce ϱi, tracks densities have been calculated on the mount and the mica respectively. Counting of tracks has been carried out using a computer-automated stage and tablet system running the FTStage software of Trevor Dumitru. Before counting, the stage was calibrated to automatically pass from the apatite to the corresponding image on the mica. Where possible, at least 20 crystals with the proper characteristics (section parallel to the c-axis; no fracture or inclusion and no zoning) have been selected. The recognition of the proper section is facilitated by the reflected light since the etch pit are all parallel.

I.2.1.2 AHe analysis

For the AHe analysis apatite grains were not mounted in epoxy resin, but grain selection (3-to 5 grains) and packing have been made under optical stereoscope. Only the most beautiful (> 60 μm) intact, euhedral, unabraded and inclusion free grains, have been selected for analysis. Selected grains are then digitally photographed and geometrically characterized by measuring each grain for its prism length (parallel to the c axis) and prism width in at least two different orientations (perpendicular to the c axis). Then, apatite grains have been packed in Nb tubes **(Fig I.9)**.

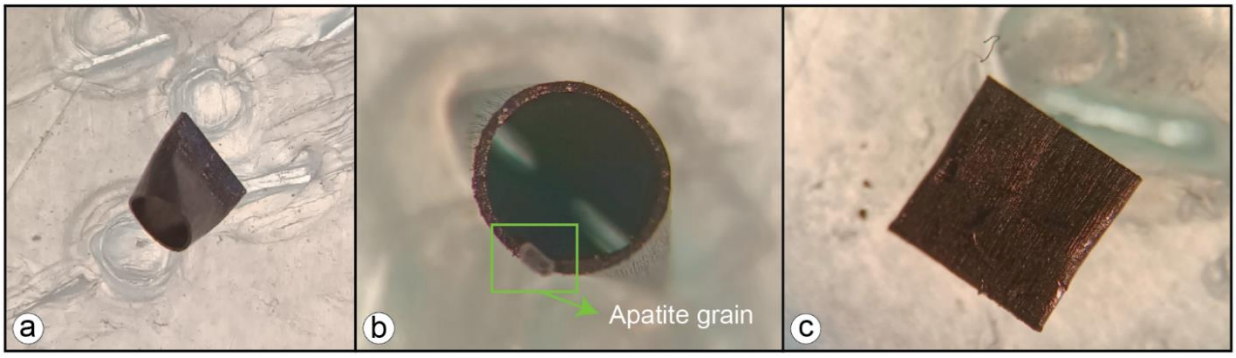

Figure I.9- Steps of packing procedure of an apatite grain into a Nb tube.

A two-stage analytical procedure is commonly used to measure 4He, U, Th and Sm. In the first stage the crystal is degassed by heating and 4He is measured by gas-source mass spectrometry. In the second stage, after chemical dissolution of the crystal, U, Th and Sm contents are measured by inductively coupled plasma mass spectrometry.

I.3 t-T modelling

Inverse modelling procedure has been performed to calculate time-temperature paths that match certain thermochronometric data and ages, within a specified amount of statistical error, assuming a starting time and temperature. Track-length distribution, AFT and AHe ages and a kinetic parameter such as Dpar, represent the entire thermal history of an apatite grain from cooling through the PAZ to the present-day temperature and provide significant constraints on possible thermal histories. Modelling is thus the only way to gain understanding of the thermal histories of slowly cooled samples, or of samples that have experienced complex t-T paths, residing in the PAZ or PRZ for a

significant time (relative to their age) and so being partially reset (e.g., Peyton and Carrapa, 2013).

Inverse modelling of track-length data was performed using HeFTy software (Ketcham, 2005) **(Fig.I.10)** with the aim to obtain realistic thermal modelling for the analysed samples. Time temperature paths (T-t paths) have been generated using constrained Monte Carlo algorithm that allows to specify time and temperature regions through which paths are forced to pass. In particular, each path must also pass some statistical criteria, on the basis of which they are distinct in "good" or "acceptable" respect to the data (Ketcham, 2009).

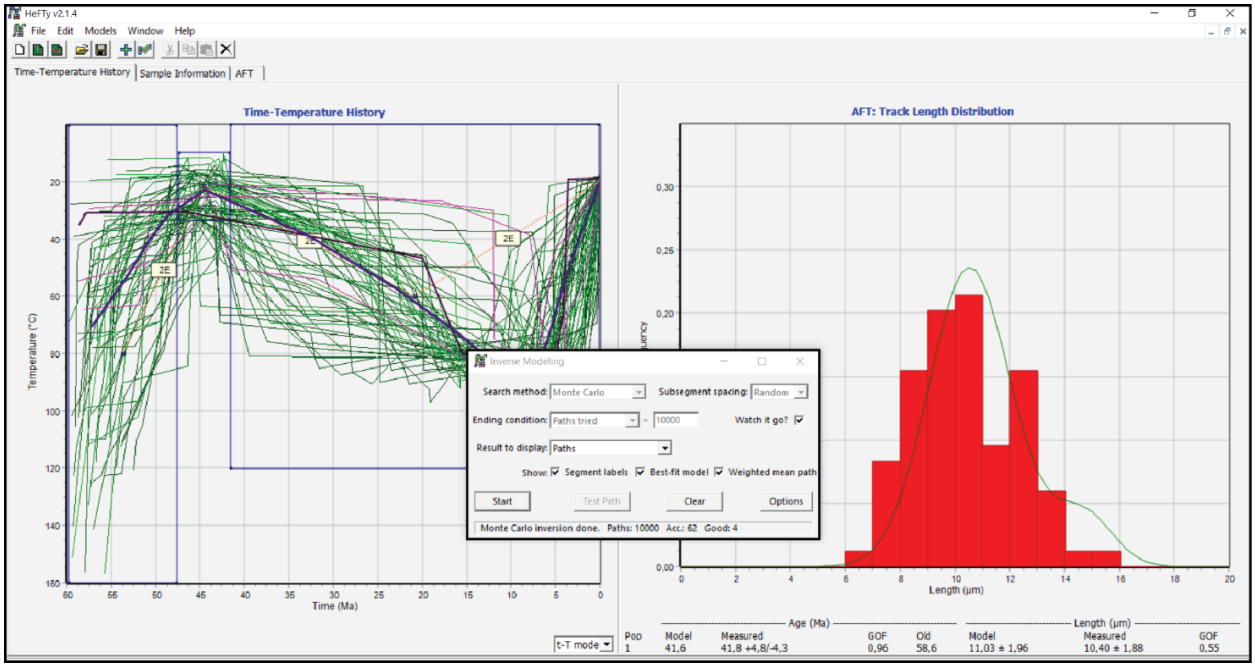

Figure I.10- HeFTy inverse modelling example.

The imput parameters for AFT are single grain ages and confined fission-track length orientation and mean Dpar. Modelling was based on the fission-track annealing model

of Ketcham et al., (2007), and the diffusion kinetics of apatites after Ehlers and Farley (2003) and Flowers et al., (2009). For apatites, a homogeneous distribution of U and Th was assumed. The gauge of the match between the modelled thermal history and the experimental data is given by the goodness-offit parameter (GOF), which indicates the probability of failing the null hypothesis that the model and data are different. In general, a value of 0.05 or higher is considered not to fail the null hypothesis, and thus reflects an acceptable fit between model and data (Ketcham, 2009). Furthermore, GOF values give an indication about the fit between observed and predicted data (values close to 1 indicate a high degree of fit, while on the contrary values close to 0 indicate a poor degree of fit). GOF values higher than 0.5 are considered good and the closer the GOF gets to 1, the more the modelled T–t paths fit the data.

I.4 U/Th dating

U-Th dating was carried out on a Thermo Electron Neptune multi-collector inductively coupled mass spectrometer (MC-ICP-MS) (Shen et al., 2012) at the High-Precision Mass Spectrometry and Environment Change Laboratory (HISPEC), National Taiwan University. We covered about 0.05 g of each sample with H_2O and dissolved it gradually with double distilled 14 N HNO_3. After dissolution, we added a ^{229}Th–^{233}U–^{236}U spike (Shen et al., 2003) to the sample, followed by 10 drops of $HClO_4$ to decompose organic matter. We followed the chemical procedure described in Shen et al., (2003) for the separation of uranium and thorium. Detailed instrumental analysis is given in Shen et al., (2012). Age correction was calculated using an estimated atomic $^{230}Th/^{232}Th$ ratio of

$4\pm2 \times 10^{-6}$. The value is the one typical for a material at secular equilibrium with the crustal $^{232}Th/^{238}U$ value of 3.8 and an arbitrarily assumed 50% error. Half-lives of U-Th nuclides used for age calculation with 2-sigma uncertainty are from Cheng et al. (2013). For samples with a $^{230}Th/^{232}Th$ activity ratio higher than 80 (with insignificant non-radiogenic ^{230}Th), ages were determined using the measured $^{230}Th/^{234}U$ and $^{234}U/^{238}U$ activity ratio. Sample ages characterized by a $^{230}Th/^{232}Th$ activity ratio less than or equal to 80 indicating the presence of non-radiogenic (detrital) ^{230}Th required a correction based on the assumption of an average $^{230}Th/^{232}Th$ activity ratio of 0.85 ± 0.36 for all detrital Th (Wedepohl, 1995).